

**Molecular Mechanisms of Synaptic Composition and Function:
From CNS Regeneration Inhibitors to Off-Target Effects,
Underscoring the Importance of microRNAs**

by

Rafi Kohen

A dissertation submitted in partial fulfillment
of the requirements for the degree of
Doctor of Philosophy
(Neuroscience)
in the University of Michigan
2020

Doctoral Committee:

Professor Roman J. Giger, Chair
Associate Professor Catherine A. Collins
Professor Gabriel Corfas
Associate Professor Shigeki Iwase
Professor Edward L. Stuenkel
Professor Michael A. Sutton

Rafi Kohen

kohen@umich.edu

ORCID iD: [0000-0001-5651-712X](https://orcid.org/0000-0001-5651-712X)

© Rafi Kohen 2020

DEDICATION

This dissertation is whole-heartedly dedicated to my role model in life:
my loving, brave, and inquisitive grandfather Refael Kohen.

No matter where he roams,
I will forever share his name with pride,
cherish our memories with joy,
and follow his teachings with respect.

ACKNOWLEDGEMENTS

I have not exactly had the easiest time throughout my doctoral training. From the first moment I was introduced to Katie, I knew this project was going to be challenging. On the other hand, it was love at first sight all around! I had hours-long discussions with Roman, where one could hear a harmonious *mélange* of his Swiss-German and my Turkish accent. In the lab, I felt instantly welcomed by all members. The lab quickly became a shelter, where I could escape from time-consuming coursework. In just about two months, I read a considerable volume of primary literature, learned how to prepare primary hippocampal cultures at a glacial pace due to lack of any prior experience, ran my first solo Western blots of which I am currently embarrassed, and gave a quasi-impressive primary data meeting according to those days' standards. I was so hooked that I used this project in my grant-writing course, even though I was rotating in another lab at the time, and I knew I could never submit the proposed grant to an NSF/NIH-funded agency due to my citizenship. I did it solely for the experience, practice, and fun. While people's eyes looked puzzled and half-closed, mine were shining with excitement.

The courting period typically seen between a principal investigator and the rotating first-year student extended to the classroom, since Roman was teaching and administering exams for the Neuroscience Graduate Program (NGP). I was inspired and humbled by how intelligent, passionate, and academically rigorous Roman was

throughout these courses, in addition to the weekly primary data and journal club meetings. It was both motivating and daunting at the same time; I was still referring to him as Dr. Giger, profusely dehydrating as I was answering his interrogative questions, and making a conscious effort to impress him with my skills and intellect. To cut a very long story short, I am so very grateful to my mentor, Dr. Roman Giger, for seeing a potential in me, even when I had my own doubts about previous research experience and abilities. Over the course of the past six years, Roman made a serious investment despite my ineligibility to apply for my own grants, did day-long bench-work experiments right alongside me, supported me when I wanted to take business or French classes on the side, and did not completely dismiss me or my future when my project went awry. Instead he showed, not only by words, but also by actions, that he had complete confidence in my training and abilities by encouraging and allowing me to present this controversial work in a nanosymposium at the annual Society for Neuroscience conference. Even if our writing styles could not be any more discordant, I see a lot of Roman's positive influence when I read journal articles, think of complicated experimental designs, or train my undergraduate research assistants. For that, and much more, I will be forever grateful, even if I do not show it as often as I should.

Going along the lines of academic excellence, scientific rigor, and emotional support when experiments do not go as intended, I want to thank my committee members, Drs. Catherine Collins, Gabriel Corfas, Shigeki Iwase, Edward Stuenkel, and Michael Sutton. When I chose my dissertation committee, I paid close attention to individual research background and expertise, as much as personality and harmony. Judging from our committee meetings, I could say that I was honored to be amongst

such stellar scientists. At times the discussions got heated, since they shared their opinions, and I became defensive and protective of my work. However, this level of perfectionism and passion proved to be only beneficial for my training, and for that I feel indebted to this team of supportive scientists, both individually and collectively. Furthermore, our meetings yielded fruitful collaborations that helped advance my projects: the initial BrU-seq and mRNA-seq experiments were done with help from Tricia Garay in the Iwase Lab, the electrophysiological recordings were done by Alex Chen and Takao Tsukahara in the Sutton Lab, and my side-project on post-injury axonal regeneration/degeneration was heavily advised by the members of the Collins Lab.

The next line of support came from administrative offices of both NGP and Department of Cell and Developmental Biology (CDB). I feel connected to both entities in very different, but equally important ways. Thanks to the summer boot camp, NGP became my first home in Michigan, even before I joined my peers at the Program in Biomedical Sciences. I am therefore grateful that NGP welcomed me with open arms, helped me get through the transition into grad school, and ensured that I maintain my sanity over preliminary exams. Once I joined Roman's lab, I also became a permanent member of the CDB family, which extended invitations to much-needed social events, while making every effort to make me feel supported and included. Overall, I would like to express my gratitude to both entities' leadership (Ed, Audrey, Les, Pierre) and administrative teams (Rachel, Valerie, Karen, Kristen, Brittney and Rebecca).

What sculpted my time in Michigan the most was my daily interactions with the members of the Giger Lab, also known as the Gigerites. I am forever indebted to Katie, who laid the foundation of my dissertation project, trained me in techniques I had

absolutely no prior experience with, showed me the ropes while never scolding me for having failed an experiment, and shared a constant stream of funny anecdotes all along. Upon Katie's departure, I turned to Yevgeniya for help with failing experiments, and quickly realized that she was not as scary and distant as she had initially appeared. Later on, we bonded over our undying and quite expensive passion for hipster coffee, gourmet dining, and frequent travelling. She was my partner-in-crime in our sacred mission to convince Roman to buy an espresso machine for the lab, which continuously brings joy to past, present, and future members. Ever since her departure, Yev still manages to instantly respond to my paragraphs of messages, and serves as a counselor, a colleague, and a friend. The next lab member who left a big mark in my life was without doubt Jing-Ping. She was the first to call me an energy vampire, for my constant quest for social interaction and attention in an otherwise anti-social scientific community. Through constant troubleshooting efforts and questioning of my scientific rationale, she quickly became my go-to person. Jing-Ping really is one of the most creative scientists I have known, who can think alternatively and quickly on her feet, and generously devote her precious time to help you figure out the next logical step. Once her snarky comments can be masterfully neutralized, she is also a great confidant, whose vision and advice I valued and appreciated during tough times in and out of the lab. Speaking of, it is a known fact that Ashley and I did not get along well at first, and even sometimes nowadays. We both have so much passion about our science and such strong opinions on all matters. Over time, maybe we did not, but circumstances definitely changed. We bonded over our proclivity to spend all of our earnings on expensive coffee shipped from different states and roasters, supported each other

through common weaknesses about good food and more often than not a stiff drink. We learned to habituate to each other's way of communication, decided to fight together and not against each other, and ended up working collectively on the same project. This journey was definitely tumultuous for the both of us, but I think we made it to the other side in one piece and looking pretty sharp, too. I hope we continue this frenemy beyond the constraints of science or the Giger Lab. With such strong personalities, the Giger Lab would have been a complete chaos without Xiaofeng and Choya, who constantly maintained peace and showed compassion. I am genuinely thankful for their emotional and mental support throughout my time in the lab. Whenever I talk to either one of them, I am instantly filled with serenity and peace, as their soft and gentle voice penetrates my frustrations and anxiety. Despite her relatively short tenure in the lab, Dao left behind a legacy as a concurrent lab manager, research assistant, *in situ* hybridization wizard, and dependable point-person for Maxi Preps. But more importantly, she was the life of any party or happy hour, exuded joy to anyone she talked to, interacted with, or laughed around, and was the creative mastermind behind our departmental Halloween costumes. She left the Giger Lab, not only as any alumna, but also as one of my dearest friends. Dao's shoes were partially filled by Corey, who joined the lab initially as my undergraduate research assistant, and later on acted as interim lab manager for the longest time. Corey showed great potential even from her first day on, acquired and mastered technically challenging skills in tissue culture preparation and Western blotting, and quickly became my replacement for when I was out of town, drowned in other work, or writing my dissertation. Needless to say, she was the first undergraduate student in this lab to have attended to a national conference, and proved to be a fun

traveller as well. Corey also motivated us all with her vibrant energy, unexpected dance moves or consecutive sneezes, excitement about science, and equally sassy comebacks. Of course, the lab would not be complete without our in-house Michigander boys: Ryan and Lucas. Since Ryan and I rotated in and joined the Giger lab at the same time, he has always been my rival, colleague, and companion all throughout this journey. I hope he no longer feels like a plastic bag drifting through the wind. Joined us a year later, Lucas seemed to share my passion for cooking, eating, and learning about food – even though I can never prepare as meticulous dishes as his, in the limited space of the BSRB kitchenettes. Outside of the lab, we traveled to Toronto for a fun and spontaneous get-away, explored mixology at cocktail workshops, assembled my living room's IKEA furniture, and shopped for hours for the perfect outfit. Lastly, I want to thank all of our undergraduate assistants and lab managers, but particularly: Sarah for her strong advocacy, Isabel for her inquisitive mind, Colin for his dance moves and catchy phrases, Nadine for her sense of fashion, Olivia for her knowledge in hip street lingo, Kim for her extremely funny and witty commentary, Kevin for his incredibly logical mind, and Riley for his inspiringly adventurous travel anecdotes.

Above all mentors, colleagues, and trainees, I feel privileged to have received the emotional and mental support and endless motivation from my friends. My dearest friends from Istanbul, Turkey proved that geographical distances and time-zone differences matter very little when it comes to feeling together. Fortunately, my twelve years in the Ulus Private Jewish Schools not only offered me strong mentorship by and long-lasting connections with excellent teachers, but also bestowed upon me some of my best friends still. I am whole-heartedly thankful to Roksan, Feyza, Wendy, Sindy and

Aylin for being available to receive my WhatsApp calls whenever they are not at work or asleep, especially if I need to vent or go on a rant. I am also blessed with childhood friends, such as Sarita and Leysi, who went through life alongside me for more than twenty years. I am grateful to my fellow Brandeisians who not only made my college years bearable and fun, but also kept in touch and became close friends over collected time and shared memories. I knew I could reach out and get calming support from Lesli in Istanbul, Rozi in Jerusalem, Selen and Arielle in Boston, Missy in Washington, and Sigrid in New Jersey. Lastly, my Ann Arborite friends provided the biggest level of day-to-day support, shared frustrations, and celebrated joyous occasions. From the NGP cohort, I want to thank Christina for our Northern Michigan trips, concert outings, and Passover cook-offs; Tricia for our hour-long therapy sessions and infectious laughs during around-the-block walks; Jessica for our deep philosophical conversations; and Daria for constantly finding ways to provide entertainment. Whenever I needed a break from neuroscientists, PhD students or post-docs from different walks of life helped me forget about my project and reset my mind. I am forever grateful for the friendship of my resident art historian and excellent mathematician Isabelle, my French mistress with a secret garden Typhanie, my distinguished Ottoman architects Seda, Maja, and Dicle. Lastly, I feel obligated to thank the Turkish-Jewish community in Michigan, who had become my second family especially over the high holidays, my friends on the dance floor, my sous-chefs or partners-in-crime in the kitchen. I will miss lengthy conversation over celebratory dinners, which are graciously hosted by powerful matriarchs Suzet and Gina, counterbalanced by patriarchs Izak and Yuksel, and greatly livened up by the youthfulness of Aksel, Derin, Ece, Enis, and Eray.

Lastly, I want to thank my core and extended family in Istanbul and Israel, with special recognition to my uncle Izzet, my grandfather Refael, and my mother Luset. My uncle has always been like a father to me, even since my earliest memories from infancy. Simply knowing how much he loves me, cares for me, supports me, and feels proud of me is sufficient; but he always ends up doing more. My grandfather Refael is my idol, my hero, and my inspiration in this life. Even though he passed away without having witnessed the completion of my Ph.D., I know that he has always been extremely and explicitly proud of my accomplishments. After all, he proved to me that new knowledge, languages, or skills could be acquired through internal dedication, conscious effort, and a curious mind, regardless of socioeconomic status, societal expectations, and age. I will forever be honored to share his name, cherish our memories together, strive to be the best version of myself, and respect and follow his teachings. Last but not least, I want to deeply, whole-heartedly, and genuinely thank my mother Luset. She is the most generous woman and mother that I have ever come across. She sacrificed a lot from her own needs, devoted everything she had and more to my health, success, and happiness. She always knew how to penetrate through my non-expressive and aloof demeanor, and shower me with love and affection. I can say without a single shred of doubt that I owe who and where I am to my mother's single-handed efforts, which overwhelmingly outweighed her limited means. I know that whatever I do, wherever I end up, she will still be the proudest mother in the world. However, I know that I will always strive to exceed her expectations, support her in return, and prove worthy of her unconditional love.

TABLE OF CONTENTS

DEDICATION	ii
ACKNOWLEDGEMENTS	iii
LIST OF FIGURES	xvii
LIST OF TABLES	xix
LIST OF ABBREVIATIONS	xx
ABSTRACT	xxv

CHAPTER 1: Introduction to the Interplay of Regeneration, NogoA, and Synaptic

Plasticity	1
1.1 Abstract	1
1.2 Introduction	2
1.2.1 CNS Regeneration or the Undeniable Lack There-of	2
1.2.2 Introduction to NogoA: Beginning of a 32-Year Long Journey	5
1.2.3 Controversial Reports on Genomic Nogo Deletion	8
1.2.4 Neutralization of NogoA Signaling and Function	10
1.2.5 RNA Interference (RNAi)-Mediated Knockdown of NogoA	12
1.2.6 Activity-Dependent and Homeostatic Synaptic Plasticity	14
1.2.7 Biogenesis of and Master Regulation by Synaptic miRNAs	16

1.3 Conclusions	19
1.4 Figures	22
1.5 References	23
 CHAPTER 2: Activity-Dependent Regulation of the Neuronal Phospho-Protein	
NogoA	32
2.1 Abstract	32
2.2 Introduction	33
2.3 Results	37
2.3.1 NogoA Expression is Highly Neuronal and Localizes to Somatodendritic Synapses	37
2.3.2 Surface NogoA is Bidirectionally Regulated by Global Changes in Neuronal Network Activity	41
2.3.3 Intracellular Neuronal NogoA is Phosphorylated at Ser-343	44
2.4 Discussion	55
2.5 Materials and Methods	59
2.5.1 Animals	59
2.5.2 Primary Neuronal Cultures	59
2.5.3 Primary Astroglial Cultures	61
2.5.4 Pharmacological Treatments	63
2.5.5 Transient and Sparse Transfection	63
2.5.6 Lentiviral Transduction	64
2.5.7 Immunofluorescence Labeling	65

2.5.8 Cell Surface Biotinylation	66
2.5.9 Crude Fractionation of Myelin, Synaptosomes, and PSD	67
2.5.10 Lambda Phosphatase Treatment	69
2.5.11 NogoA Immunoprecipitation	69
2.5.12 Development of anti-Rat NogoA p-343 Antibody	70
2.5.13 Western Blot Analysis	71
2.5.14 Mass Spectroscopy for Phospho-Proteomics	73
2.5.15 Statistical Analysis	73
2.6 Acknowledgements	75
2.7 Author Contribution	75
2.8 Figures	76
2.9 Tables	86
2.10 References	96

CHAPTER 3: shRNA in Neurons: Robust Synaptic Regulations Independent of

Primary Target	102
3.1 Abstract	102
3.2 Introduction	103
3.3 Results	106
3.3.1 NogoA shRNA Reduces Baseline Excitatory Synaptic Transmission and Blocks Homeostatic Scaling	106
3.3.2 shNogoA Alters the Landscape of the Immediate-Early Synaptic Gene Expression	111

3.3.3 Global shNogoA Transduction Upregulates Npas4 via L-Type VGCC Activation	114
3.3.4 NogoA Interacts with and/or Modulates L-type VGCC Auxiliary Subunit $\text{Ca}_v\alpha 2\delta 1$	118
3.3.5 shNogoA Impairs Homeostatic Scaling Through Immediate-Early Gene Induction	122
3.3.6 shNogoA Transduction Impairs Inhibitory Synaptogenesis	124
3.3.7 Observed Synaptic Phenotypes are NogoA-Independent	126
3.3.8 Step-wise Mutated shNogoA Still Replicates Regulation of Excitatory and Inhibitory Synapse Formation and Strength	128
3.3.9 mRNA Sequencing Experiments with Step-wise Mutated shNogoA Constructs Shed Light onto NogoA-Independent Regulations	132
3.3.10 Small RNA Sequencing Identifies shNogoA-Regulated miRNA Expression	138
3.4 Discussion	142
3.5 Materials and Methods	150
3.5.1 Animals	150
3.5.2 Primary Neuronal Cultures	150
3.5.3 Pharmacological Treatments	151
3.5.4 Transient and Sparse Transfection	151
3.5.5 Lentiviral Transduction	152
3.5.6 Immunofluorescence Labeling	153
3.5.7 Crude Brain Membrane Isolation	155

3.5.8 NogoA Immunoprecipitation	155
3.5.9 Western Blot Analysis	156
3.5.10 Electrophysiological Recordings	157
3.5.11 Reverse Transcription PCR (RT-qPCR)	158
3.5.12 RNA Sequencing	159
3.5.12 Statistical Analysis	163
3.6 Acknowledgements	165
3.7 Author Contribution	160
3.8 Figures	166
3.9 References	194
CHAPTER 4: Discussion and Future Directions	204
4.1 Abstract	204
4.2 Key Findings and Future Directions for the Regulation of NogoA	205
4.2.1 Neuronal NogoA Expression is Regulated by Membrane Depolarization	205
4.2.2 Surface NogoA is Bidirectionally Regulated by Homeostatic Synaptic Plasticity	206
4.2.3 Neuronal NogoA is Intracellularly Phosphorylated in a Context- Dependent Manner	208
4.2.4 Future Directions	211
4.3 Key Findings and Future Directions for the shNogoA-Mediated Regulation of Synapse Formation and Strength	214

4.3.1 shNogoA Permanently Downscales Baseline Excitatory Synaptic	
Transmission	214
4.3.2 shNogoA Transduction Causes a Robust Reduction in Inhibitory	
Synaptogenesis	218
4.3.3 shNogoA Transduction Manifests Synaptic Phenotypes	
Independently of NogoA	219
4.3.4 shNogoA Transduction Concurrently Regulates mRNA and miRNA	
Expression Important for Synapse Formation and Strength	222
4.3.5 Future Directions	226
4.4 Concluding Remarks	230
4.5 References	231

LIST OF FIGURES

Figure 1-1: microRNA biogenesis pathway is shared by short hairpin RNA processing machinery	22
Figure 2-1: <i>In vitro</i> primary cultures offer extremely powerful, albeit impure systems to study	76
Figure 2-2: NogoA is expressed at the neuronal somatodendritic regions and synaptosomes more strongly than on neuronal cell surface, crude CNS myelin, and astrocytes	78
Figure 2-3: Surface expression of neuronal NogoA is under the bidirectional regulation of network activity states	80
Figure 2-4: Intracellular and synaptosomal neuronal NogoA is phosphorylated at serine 343	82
Figure 2-5: NogoA phosphorylation is regulated by network activity <i>in vitro</i> , with an unknown physiological relevance and kinase/phosphatase pair	84
Figure 3-1: NogoA shRNA reduces baseline excitatory synaptic transmission and blocks homeostatic scaling	166
Figure 3-2: shNogoA alters the landscape of the immediate-early synaptic gene expression	168

Figure 3-3: Global shNogoA transduction upregulates Npas4 via L-Type VGCC activation	170
Figure 3-4: NogoA interacts with and/or modulates L-type VGCC auxiliary subunit Ca _v α2δ1	172
Figure 3-5: shNogoA impairs homeostatic scaling through immediate-early gene induction	174
Figure 3-6: shNogoA transduction drastically impairs inhibitory synaptogenesis	176
Figure 3-7: Observed synaptic phenotypes are NogoA-independent	178
Figure 3-8: shNogoA seed region was mutated with two or five basepairs to study the target-specificity of observed regulations	180
Figure 3-9: Step-wise mutated shNogoA still replicates regulation of excitatory and inhibitory synapse formation and strength	182
Figure 3-10: mRNA sequencing experiments with step-wise mutated shNogoA constructs demonstrate robust transcript regulation	184
Figure 3-11: mRNA sequencing reveals NogoA-independent regulation of synaptically important gene products	186
Figure 3-12: Analysis of NogoA-independent differentially expressed genes reveals synaptic protein-protein interactions	188
Figure 3-13: Small RNA sequencing identifies shNogoA-regulated miRNA expression	190
Figure 3-14: Small RNA sequencing reveals NogoA-independent regulation of activity- dependent miRNAs	192

LIST OF TABLES

Table 2-1: Neuronal NogoA is post-translationally modified in baseline conditions	86
Table 2-2: Post-translationally modifications on neuronal NogoA do not significantly change following chronic TTX treatment	91

LIST OF ABBREVIATIONS

A

AAV	Adeno-associated virus
ACM	Astrocyte-Conditioned Media
AGM	Astrocyte Growth Medium
AKT	Protein Kinase B
AMPA	α -Amino-3-hydroxy-5-methyl-4-isoxazolepropionic Acid
AnkG	Ankyrin G
AraC	Cytosine Arabinoside
Arc	Activity-Regulated Cytoskeleton-Associated Protein

B

BAR	Biotinylation by Antibody Recognition
BDNF	Brain-Derived Neurotrophic Factor
BGP	β -Glycerophosphate
BIC	Bicuculline
BLB	Brij Lysis Buffer
BME	β -Mercaptoethanol
BrdU	Bromodeoxyuridine
BrU	Bromouridine
BrU-seq	Bromouridine-Incorporated RNA Sequencing
BSA	Bovine Serum Albumin

C

CaMKII	Calcium/Calmodulin-Dependent Protein Kinase II
cDNA	Complementary DNA
Cer	Cerebellum
CID	Collision-Induced Dissociation
CNS	Central Nervous System
CPM	Counts Per Million
CREB	cAMP Response Element-Binding Protein
CSPG	Chondroitin Sulphate Proteoglycan
CST	Corticospinal Tract
Ctx	Neocortex

D

DAPI	4',6-Diamidino-2-Phenylindole
DEG	Differentially Expressed Genes
Dgcr8	DiGeorge Syndrome Critical Region 8
DIV	Days <i>in vitro</i>
DMSO	Dimethyl Sulfoxide
DPBS	Dulbecco's Phosphate-Buffered Saline
DRG	Dorsal Root Ganglion
dsRNA	Double Stranded RNA

E

EGTA	Ethylene Glycol-bis(β -aminoethyl ether)-N,N,N',N'-tetraacetic Acid
ER	Endoplasmic Reticulum
EV	Empty Vector

F

FBS	Fetal Bovine Serum
Fsk	Forskolin
FTO	Fat Mass and Obesity-associated Protein

G

GABA	γ -Aminobutyric Acid
GAD-65	Glutamate Decarboxylase 65
GAD-67	Glutamate Decarboxylase 67
GAPDH	Glyceraldehyde 3-Phosphate Dehydrogenase
GFP	Green Fluorescent Protein
GluA1	Glutamate Ionotropic Receptor AMPA Type Subunit 1
GluA2	Glutamate Ionotropic Receptor AMPA Type Subunit 2
GluN2B	Glutamate Ionotropic Receptor NMDA Type Subunit 2B
GFAP	Glial Fibrillary Acidic Protein
GPCR	G Protein-Coupled Receptor

H

Hom	Homogenate
HBS	HEPES-Buffered Saline
HBSS	Hanks' Balanced Salt Solution
HCD	Higher-Energy Collisional Dissociation

HEK-293T	Human Embryonic Kidney 293 with SV40 T Antigen
Hip	Hippocampus
HRP	Horseradish Peroxide
HSP	Homeostatic Synaptic Plasticity

I

IEG	Immediate-Early Gene
IgG	Immunoglobulin
IP	Immunoprecipitation

L

LC-MS/MS	Liquid Chromatography Tandem Mass Spectrometry
lncRNA	Long Noncoding RNA
LTP	Long-Term Potentiation
LV	Lentiviral Vector

M

MAG	Myelin-Associated Glycoprotein
MAI	Myelin-Associated Inhibitor
MAP2	Microtubule-Associated Protein 2
mEPSC	Miniature Excitatory Post-Synaptic Current
mGluR1	Metabotropic Glutamate Receptor 1
mIPSC	Miniature Inhibitory Post-Synaptic Current
miRNA	Micro RNA
mRNA	Messenger RNA
mTOR	Mammalian Target of Rapamycin
Mye	Myelin

N

NCM	Neuronal Conditioned Media
NeuN	Neuronal Nuclei
NGM	Neuronal Growth Medium
NgR1	Nogo-66 Receptor 1
Nim	Nimodipine
Npas4	Neuronal Pas Domain 4

O

Olig2	Oligodendrocyte Transcription Factor 2
OMgp	Oligodendrocyte Myelin Glycoprotein
OPC	Oligodendrocyte Precursor Cell

P

P/S	Penicillin/Streptomycin
PBS	Phosphate-Buffered Saline
PCA	Principle Component Analysis
PIC	Protease Inhibitor Cocktail
PirB	Paired Immunoglobulin-Like Receptor B
PKA	Protein Kinase A
PKC	Protein Kinase C
pLL3.7	pLentilox 3.7
PNS	Peripheral Nervous System
PPI	Protein-Protein Interaction
pre-miRNA	Precursor Micro RNA
pri-miRNA	Primary Micro RNA
PSD	Post-synaptic Density
PSD-95	Post-synaptic Density 95
PTM	Post-translational Modification
Pvalb	Parvalbumin

R

RAG	Regeneration-Associated Gene
RhoGEF	Rho Guanine Exchange Factor
RISC	RNA-Induced Silencing Complex
RNAi	RNA Interference
ROCK	Rho-Associated Protein Kinase
rRNA	Ribosomal RNA
Rtn4	Reticulon-4
RT-qPCR	Quantitative Reverse Transcription Polymerase Chain Reaction

S

S1PR2	Sphingosine-1-Phosphate Receptor 2
S6K	Ribosomal Protein p70 S6 Kinase Beta-1
Sc	Spinal Cord
Scr	Scrambled shRNA
sgRNA	Single Guide RNA

shNogoA	shRNA directed against NogoA
shNogoA-2pMt	shNogoA with 2 Point Mutations
shNogoA-5pMt	shNogoA with 5 Point Mutations
shRNA	Small Hairpin RNA
SHY	Synaptic Homeostasis Hypothesis
siRNA	Small Interfering RNA
Sst	Somatostatin
StCx	Somatosensory Cortex
Synap	Synaptosome

T

TBS	Tris-Buffered Saline
TfR	Transferrin Receptor
TMM	Trimmed Mean
TTX	Tetrodotoxin
TUJ1	β -III Tubulin

U

UTR	Untranslated Regions
-----	----------------------

V

Veh	Vehicle
VGCC	Voltage-Gated Calcium Channel

#

λ -PP	Lambda Phosphatase
---------------	--------------------

ABSTRACT

Myelin-associated inhibitor NogoA exerts an inhibitory effect on CNS axonal regeneration and synaptic plasticity. Studies have shown that neutralization of NogoA signaling enhanced long-term potentiation, increased dendritic branching complexity and spine immaturity. However, upstream regulators of NogoA and downstream molecular signaling still remain largely unknown. Here, I demonstrate that neuronal NogoA levels and surface trafficking are under the regulation of membrane depolarization and chronic changes in network activity, respectively. I also identify intracellular and neuron-specific phosphorylation of NogoA as a possible mechanism for surface trafficking and signaling. Since NogoA knockout mouse models were shown to have compensatory upregulation of axon guidance inhibitors, I employ a previously published shRNA-mediated NogoA knockdown to study the downstream molecular mechanisms, I demonstrate that following shNogoA transduction, hippocampal neurons display permanently downscaled excitatory synaptic transmission, impaired homeostatic synaptic scaling, and reduced functional inhibitory synaptogenesis. Having verified NogoA target-specificity by using commercial shNogoAs, I conduct biochemical and RNA sequencing experiments to identify synaptogenic molecules regulated by shNogoA transduction. However, combining shNogoA-mediated knockdown and Cre-mediated knockout of *NogoA* revealed that the observed synaptic gene and protein regulations

are largely NogoA-independent. Concurrent mRNA and miRNA sequencing experiments following transduction with step-wise mutated shNogoA constructs confirmed that these complementary regulations were NogoA-independent. Comparison of transcriptomes following transduction with two scrambled shRNAs revealed a sequence-dependent, but not sequence-specific off-target regulation of synaptic gene expressions. In conclusion, the findings that I hereby report strongly implicate shRNA overexpression-mediated saturation and/or off-target dysregulation of the miRNA processing machinery as a possible mechanism.

CHAPTER 1:

Introduction to the Interplay of Regeneration, NogoA, and Synaptic Plasticity

1.1 Abstract

The adult mammalian central nervous system (CNS) differs from the peripheral nervous system (PNS) in its inability to spontaneously regenerate axons post-injury. In addition to the reduced intrinsic growth-promoting programs, the environmental micromillieu of the CNS is quite hostile for injured axons to re-grow, find original targets, and re-establish synapses. One such contributor is the myelin-associated inhibitor (MAI) NogoA, which is a negative regulator of neurite outgrowth and axonal regeneration. Expressed by both oligodendrocytes and neurons, NogoA not only maintains a multi-faceted brake system on the regenerative capacity of the injured adult mammalian CNS, but also exerts a negative regulation on activity-dependent synaptic plasticity. In fact, even in baseline and health, NogoA locks in highly plastic processes, such as dynamic re-sculpturing of neuronal morphology and bidirectional modulation of synaptic strength, which collectively form the basis of learning and memory formation. Therefore, it is paramount to thoroughly investigate and precisely describe the function of NogoA, especially by way of studying receptor partners and downstream signaling. In this chapter, I review key characteristics of CNS axon regeneration, discovery and inhibitory function of NogoA, and involvement in the regulation of synaptic plasticity.

1.2 Introduction

1.2.1 CNS Regeneration or the Undeniable Lack There-of

The central nervous system (CNS) development requires harmonious execution of a multitude of processes, possible with a concerted effort between attractive and repulsive signals. In fact, numerous inhibitory molecules are expressed all throughout development, providing sufficient negative cues to direct otherwise lost neuronal cell bodies or processes. Overall, CNS development depends on a fine balance between positive and inhibitory molecules for the timely order and proper execution of cell proliferation, migration, initial synaptic connectivity, synaptic pruning, and maturation (1-3). However, once these complex circuitries are formed and stabilized following developmental stage and closure of the critical period, the now-adult CNS neurons lose their plastic ability (4-7). This is certainly true in healthy baseline, where sensory exploration of the surrounding space, immediate response to external stimuli, consequent active learning and long-lasting memory formation take place on a regular basis. An example of this is seen with cellular regenerative capacity being highly limited to only two select sites of the entire CNS: the olfactory bulb and the hippocampus (8-10). Perhaps more detrimental to the human health is the CNS neurons' near-complete inability to self-renew, regenerate, or functionally recover following injury (11-13).

After a trauma or injury to the CNS, while all non-neuronal (or glial) cells can self-populate, neurons remain least resilient and mostly incapable to regenerate (12, 13). Resident microglia can rapidly proliferate, migrate to the damaged area to phagocytose

cell debris, and trigger initial intercellular communication, which ultimately helps mount an immune response (14, 15). One such target of this signaling, astrocytes can assume a reactive polarization profile, migrate to and proliferate at the damaged area to form an isolating glial scar, which was shown to actually facilitate regeneration (16, 17). Finally, oligodendrocyte precursor cells (OPCs) can also proliferate, and fully differentiate into myelinating oligodendrocytes, so that the newly regenerated axons, if any, could be re-myelinated for faster action potential conduction, as well as mechanical and metabolic support (18, 19). So what makes neurons, the principal cells of the nervous system, so resilient to spontaneous regeneration, either on a cellular or subcompartmental level?

First of all, mature neurons of the adult CNS have limited cell-intrinsic capacity to entrain axonal regeneration. Having both peripheral and central branches, sensory dorsal root ganglion (DRG) neurons historically provided the ideal platform to study the differential activation of regeneration-associated gene (RAG) expression following either CNS or PNS injury. A nerve crush or complete transection injury to the sciatic nerve, which constitutes the peripheral axonal branch of sensory and motoneurons, robustly upregulates multitude of RAGs that ultimately facilitate spontaneous axonal regeneration (20-22). However, without prior injury to the sciatic nerve (referred to as conditioning injury), a hemisection of the dorsal column in the spinal cord, which contains the central branch, fails to upregulate expression of RAGs (23). In fact, manipulations to epigenetically upregulate these RAGs (24), remove the transcriptional inhibition on the Jak-STAT pathway (25), or constitutively activate the mTOR pathway (26) can dramatically increase regenerative capacity of the CNS neurons. Taken together, these findings demonstrate that the DRG neurons can enter a regenerative

state following injury to the PNS, remain completely vulnerable following injury to the CNS, but can be primed to regenerate with conditioning injury or genetic manipulations.

Secondly, the microenvironment of the adult, mammalian CNS is far more restrictive and hostile for regeneration than the PNS. This was elegantly demonstrated by nerve grafting experiments, where CNS neurons could overcome their cell-intrinsic negative regulation and sustain axonal regeneration in the presence of PNS nerve transplantation. Conversely, optic nerve segments grafted onto the sciatic nerve were bypassed by regenerating axons due to the hostile CNS environment (27, 28). In addition to a drastic lack of sufficient neurotrophic support (29, 30), there are also various negative regulators of growth within the extracellular milieu. In addition to the chondroitin sulfate proteoglycans (CSPGs) secreted by reactive astrocytes within the glial scar to inhibit regenerative growth and plasticity (31, 32), oligodendrocytic myelin encapsulates expression of numerous inhibitory molecules, collectively referred to as myelin-associated inhibitors (MAIs). For instance, enriched in Schmidt-Lanterman incisures and the periaxonal membrane of myelin sheath (33), myelin-associated glycoprotein (MAG) regulates the axonal cytoskeleton and caliber (34), post-translational modification of microtubules (35, 36), phosphorylation of MAP2 (37), and activation of the RhoA/ROCK signaling pathway. Another commonly studied MAI is the oligodendrocyte myelin glycoprotein (OMgp), which is enriched near the nodes of Ranvier, and shown to negatively regulate axon collateral sprouting (38) and activity-dependent synaptic plasticity (39). The final component of the MAIs is the reticulon family member RTN4A/NogoA, which will constitute the main focus of our work described here, and therefore will be introduced in greater detail.

Taken together, neurons of the adult, mammalian CNS are at a double-faceted disadvantage in terms of responding to an external injury, recovering from the negative regulations of the extracellular milieu, and mounting growth-promoting cell-intrinsic programs in order to sustain axonal regeneration, target pathfinding, and functional synaptogenesis. As such, further mechanistic investigations on both individual components and their complex interactions are required before we could gain a deeper understanding of the pathophysiology of currently untreatable spinal cord injury, as it sharply contrasts impressive PNS regeneration and functional recovery.

1.2.2 Introduction to NogoA: Beginning of a 32-Year Long Journey

Twelve years after the identification of membrane-bound molecules relaying the inhibitory nature of the CNS myelin (40, 41), NogoA was first fully discovered and characterized from spinal cord myelin extract. In fact, that very study identified that neutralization of NogoA with the function-blocking antibodies (AS Bruna, AS 472 or mAb IN-1) could negate the inhibitory influence of the CNS myelin, and consequently allow for cultured DRG neurites to grow into the optic nerve explants (42). Identified as a reticulon family member with an endoplasmic reticulum retention signal (42, 43), Nogo has three splice isoforms with different molecular weights, shared domains, expression pattern, and consequent function. NogoA (1163aa, 190kDa) was expressed most strongly by the oligodendrocytes and neurons of the brain and spinal cord, and to a lesser extent by testis and heart. NogoB (360aa, 55kDa) was also strongly expressed within the brain and spinal cord tissues, but almost equally within the testis, heart,

spleen, and kidney, and most strongly within the lung. Lastly, NogoC (25kDa) was expressed in small fraction within the brain tissue, but nowhere as strongly as within the skeletal muscle (42, 44). When this expression profile (44) was combined with complete and efficient neutralization of inhibitory function with NogoA-specific antibody AS Bruna 472 (42), the field mostly focused on the signaling mechanism and associated physiological roles of the NogoA isoform.

NogoA has three discrete regions, where only two were shown to exert a robust, yet varying inhibitory functions on growth cone collapse, neurite outgrowth, and activity-dependent synaptic plasticity. The extracellular and C-terminal Nogo-66 domain (rat aa 1026-1091) was identified first as commonly shared amongst all Nogo splice isoforms. The dimeric Nogo-66 relays the strongest degree of growth cone collapse through the neuronally expressed Nogo-66 Receptor 1 (NgR1) (45, 46). In fact, receptor-binding partner for other MAIs such as MAG and OMgp, NgR1 activation was shown to drive actomyosin contraction as well as microtubule and F-actin disassembly downstream of RhoA/ROCK-dependent signaling (45-48). Later studies collectively demonstrated that the Nogo-66 binding event with synaptic NgR1 exerted a strong negative regulation on dendritic spine morphology and activity-dependent synaptic plasticity (39, 49, 50). Moreover, either genomic deletion of *NgR1* (39, 49) or treatment with the anti-NgR1 function-blocking antibody (50) resulted in enhanced induction of hippocampal long-term potentiation. Lastly, Nogo-66 domain was also shown to directly bind to the paired immunoglobulin-like receptor B (PirB) (51), which is partially responsible for relaying inhibitory function of CNS myelin due to concurrent OMgp binding (39).

More recently, the focus of the field has shifted onto the NogoA-specific NogoA- Δ 20 region (rat aa 544-725), which was discovered to exert a strong inhibition of neurite outgrowth as well as growth cone collapse capability (45). The NogoA- Δ 20 region has so far only one well-characterized and reproducibly identified receptor partner: the G protein-coupled receptor (GPCR) sphingosine 1 receptor 2 (SP1PR2). As soon as 15 minutes following binding, the NogoA- Δ 20-SP1PR2 complex is internalized in a pincher- and rac-dependent, but clathrin- and dynamin-independent manner. Once endocytosed into the neurites, this NogoA- Δ 20-containing signalosome is retrogradely transported to the cell body, all the meanwhile leading to the activation of the G protein G₁₃, leukemia-associated Rho guanine exchange factor (RhoGEF) LARG, and RhoA (52, 53). Lastly, it is through interaction with S1PR2 that the NogoA- Δ 20 region negatively regulates activity-dependent synaptic plasticity within the hippocampus or motor cortex. Indeed, disruption of the NogoA- Δ 20 signaling via treatment with function-blocking anti-NogoA-specific antibody (11C7) or pharmacological S1PR2 antagonist (JTE-013) releases the inhibitory influence, and induces enhanced LTP. Lastly, JTE-013 treatment of hippocampal slices from *NogoA*^{-/-} mouse does not lead to any change in LTP induction, suggesting that S1PR2-mediated negative regulation of synaptic plasticity is solely through NogoA binding (52).

Taken together, an impressive collection of biochemical and electrophysiological *in vitro* studies helped characterize NogoA topology, expression pattern, binding partners, and multi-faceted inhibitory function. As NogoA is at least in part responsible for the CNS myelin's powerful inhibition on growth cone maintenance, neurite outgrowth, and activity-dependent synaptic plasticity, the possibility of blockade of this

complex signaling gained increasing popularity as a way to recover function following injury. Consequently, further studies were carried out with NogoA and its identified receptor partners, particularly using *in vivo* models with RNA interference as well as genomic and conditional knockouts.

1.2.3 Controversial Reports on Genomic Nogo Deletion

The field's first attempt to block the inhibitory function of complex NogoA signaling was through genomic knockout of *NogoABC*. In 2003, Simonen *et al.* genetically removed *NogoA* from the mouse genome, and assessed neurite outgrowth and corticospinal tract (CST) regeneration following spinal cord injury. They found that the spinal cord extract from the *NogoA* KO mice was less inhibitory to neurite outgrowth *in vitro*. Moreover, axonal regeneration or sprouting past the lesion site following dorsal column hemisection was increased upon NogoA depletion. However, this was at the expense of the robust upregulation of NogoB protein as a compensatory mechanism (54). To avoid the concurrent upregulation of NogoB upon *NogoA* deletion, Kim *et al.* genetically deleted both *NogoA* and *NogoB* from the mouse genome, and reported increased sprouting and CST fiber regeneration, and enhanced locomotor function (55).

On the other hand, there were studies that reported lack of enhanced injured CNS regeneration with the *Nogo* genomic deletion mouse models. Indeed, Zheng *et al.* produced both *NogoAB* and *NogoABC*-deficient mice, and studied CST fiber regeneration following dorsal column hemisection. Although they did report *NogoAB*-

deficient myelin's reduced inhibitory regulation on neurite outgrowth *in vitro*, their results demonstrated no significant improvement in axonal regeneration in either mouse model (56). In line with this evidence, Lee *et al.* generated a *NogoAB* gene-trap knockout mouse model, and replicated lack of CST regeneration following spinal cord injury (57). Altogether, this further corroborated the conclusion that *Nogo* deletion alone is not sufficient for enhanced axonal regeneration of adult CNS mammalian neurons

These differences in observations were explained by presence of one or more isoforms of *Nogo* (54, 55, 57), strain-dependent differences between mouse knockout models (58), as well as compensatory upregulation of numerous inhibitory axon guidance molecules upon *NogoA* deletion (59). As such, efforts refocused on conditional knockout of *NogoA* in oligodendrocytes or neurons only to delineate cell-specific function of the inhibitory role of NogoA signaling. Upon oligodendrocyte-specific depletion of *NogoA* (*Cnp-Cre^{+/-}; Rtn4A^{fl/fl}*), Vajda *et al.* reported increased both spontaneous and inflammation-mediated axonal outgrowth following complete intraorbital optic nerve crush. In contrast, they reported that the neuron-specific depletion of *NogoA* (*Thy1-Cre^{tg}; Rtn4A^{fl/fl}*) decreased axon sprouting in the injured optic nerve (60). Follow-up studies by Zemmar *et al.* demonstrate that both *NogoA* conditional knockout models show enhanced dendritic spine remodeling of the adult motor cortex, while neuronal and oligodendrocytic *NogoA* affect dendritic branching complexity, length, and spine density at proximal and distal regions, respectively (61). Most recently, Meves *et al.* independently confirmed that only the oligodendrocyte-specific deletion of all *Rtn4* isoforms (*PLP-Cre-ER^T; Rtn4^{fl/fl}*) enhances compensatory sprouting of injured CST axons without any significant functional recovery. On the other

hand, the neuron-specific deletion of *Rtn4* via cortical adeno-associated virus (AAV2)-Cre injection into the *Rtn4^{fl/fl}* mouse brain failed to show any significant change in compensatory sprouting following unilateral pyramidotomy (62).

Given the contradictory results obtained from various approaches to genetically deleting *Nogo* alone, the field has not so far reached a consensus about whether the removal of NogoA's inhibitory effect was sufficient on enhancing axonal sprouting, regeneration, or synaptic plasticity. As such, alternative methods of NogoA depletion or NogoA signaling blockade were employed to better study its physiological function without serious ramifications of compensation, strains, and cell-specificity.

1.2.4 Neutralization of NogoA Signaling and Function

Especially since the genomic knockout of *Rtn4/Nogo* caused a plethora of complexities, including strain differences, targeting isoform, compensatory upregulations, functional studies investigating the physiologically relevant inhibitory role of NogoA have more heavily used the acute treatment with the function-blocking anti-NogoA antibodies. First described in 1988 to neutralize the newly discovered non-permissive substrate properties of the CNS myelin (40, 41), IN-1 antibody was later on found to bind to the NogoA-Δ20 (42, 45), induce internalization (53), and blocks NogoA inhibitory signaling on cell surface and therefore function. Since as early as 1998, treatment of injured adult rat CST with the IN-1 or 11C7 function-blocking antibodies were demonstrated to increase axonal sprouting with a consequent improvement in functional recovery in motor and sensory tests (63, 64). In fact, studies with 11C7

showed similar results with non-human primates subjected to unilateral cervical lesions (65, 66). Moreover, this treatment was extended to clinical trials with relatively tolerable adverse effects (67), and is currently in the Phase II clinical trial stage (NCT03935321).

Of more importance for our studies was anti-NogoA function blocking-antibody treatments in the context of regulation of activity-dependent synaptic plasticity and dendrospinal morphology. In 2010, Zagrebelsky *et al.* treated days *in vitro* (DIV) 21 organotypic neonatal mouse hippocampal slices with the 11C7 anti-NogoA function-blocking antibody for 4 days, and assessed dendrite and spine structure. Neutralization of NogoA increased dendritic intersections in both CA1 and CA3 regions of the hippocampus, and shifted dendritic spines to a more immature state, while sparing axonal complexity and length (68). Delekate *et al.* used hippocampal slices acutely treated with anti-NogoA (11C7) and anti-NgR1 function-blocking antibodies, and found enhanced LTP induction at a fast and immediate time scale, which once again demonstrated the negative regulatory function of NogoA (50). These experiments formed the foundation of *in vivo* studies, where Zemmar *et al.* replicated blockade of either NogoA or NgR1 leading to enhanced LTP induction in rat motor cortex slices. The investigators took these results one step further, and demonstrated that 6 day continuous intrathecal application of the anti-NogoA function-blocking antibody increased dendritic spine density of layer 5 cortical pyramidal neurons with a consequent improved motor learning (69).

Taken together, results from these and many other studies suggest a strong and physiological role for NogoA-mediated inhibition, which can be negated both immediately, functionally, and morphologically via treatments with anti-NogoA or anti-

NgR1 function-blocking antibodies. Nonetheless, since NogoA is ubiquitously expressed within the developing and adult rodent CNS, the target(s) of these antibodies or the cell autonomy of these neutralization experiments are still unanswered, key questions.

1.2.5 RNA Interference (RNAi)-Mediated Knockdown of NogoA

Unlike acute NogoA neutralization, genomic deletion of *NogoA* does not lead to a significant morphological change in dendrite and spine structure (68) or activity-dependent synaptic plasticity (50). To circumvent unwanted compensatory upregulation of other isoforms and inhibitory molecules (59) and to decipher cell-autonomous nature of phenotypes seen with the targeted cells, studies have used various RNA interference (RNAi)-mediated approaches to selectively and acutely knock down NogoA expression. In the same study mentioned above, Zagrebelsky *et al.* used a short hairpin (RNA)-mediated NogoA knockdown on acute hippocampal slices, and reproduced similar results in dendritic morphology and spine maturity (68). Moreover, Pradhan *et al.* delivered another shRNA against NogoA, packaged into an AAV2/8, to pyramidal neurons of the neonatal rat primary sensorimotor cortex to study morphology and density of dendritic spines *in vivo*. Results showed that the cell-autonomous knockdown of neuronal NogoA led to a decrease in spine density, and an increase in filopodia-like spine immaturity (70). Especially the findings with the immature dendritic spine morphology was in line with previous studies using NogoA neutralization, as well as conceptually meaningful in the sense that upon the release of the inhibitory brakes, cytoskeletal structures of the spines become more dynamic than stable.

Last two mechanistic studies used either NogoA micro RNA (miRNA)-mediated transgenic rat or small interfering RNA (siRNA)-mediated NogoA knockdown to study its function in synaptic electrophysiology and receptor expression pattern. Tews *et al.* generated L2 line rats with constitutively active NogoA miRNA expression, demonstrated NogoA-specific knockdown without an upregulation of the NogoB isoform or apparent repercussion on the global miRNA machinery. Moreover, they showed an enhanced LTP induction in both hippocampus and cortex, which could be correlated to the manifestation of schizophrenia-like behaviors (71). Peng *et al.* used yet another siRNA to specifically knock down NogoA or NgR1 in primary hippocampal neurons. Despite incomplete depletion of either expression, they showed a robust increase in GluA1/2, GluN2A/B, and PSD-95 protein levels, which were regulated upon the activation of the mTOR signaling pathway (72). These observations were certainly consistent and complementary with previous studies.

Taken together, neutralization of the NogoA function or knockdown of NogoA expression was repeatedly studied with various different antibodies and RNAi approaches to harmoniously demonstrate the negative regulatory influence of NogoA on axonal growth and activity-dependent synaptic plasticity. However, because each small RNA-mediated knockdown and model system employed by these studies was entirely different, observed findings failed to build up on one another, strengthening our conceptual and mechanistic understanding of the physiological role of NogoA expression and signaling. Collectively, these observations and the forthcoming open questions ultimately formed the basis of our investigations.

1.2.6 Activity-Dependent and Homeostatic Synaptic Plasticity

When action potentials are propagated to the presynaptic axon terminal, voltage gated calcium channels (VGCCs) change conformation, lead to an increase of intracellular calcium, which then triggers fusion of primed and docked synaptic vesicles packed with neurotransmitters. In an excitatory synapse, glutamate reaches the post-synaptic densities, mostly located in dendritic spines, bind to ionotropic glutamate receptors such as AMPA receptors, which allow in cations such as sodium and calcium. The membrane potential depolarizes, and the influx of calcium triggers a host of intracellular signaling cascade including activation of calcium/calmodulin-dependent protein kinase II (CaMKII). Activating stepwise transcriptional mechanisms as well as immediate local protein translation, this signaling cascade ultimately monitors successive trafficking of more AMPA receptors both to the directly activated synaptic site and to the nearby silent synapses, which contained mostly NMDA receptors that were blocked by magnesium in the absence of nearby depolarization. Consequently, the next time the post-synaptic neuron is stimulated, the cation influx, the calcium signaling, the consequent increase in glutamatergic receptor production and trafficking would be of a higher magnitude. This mechanistic cycle, in essence and simplistic terms, constitute the long-term potentiation (LTP) as a form of activity-dependent Hebbian synaptic plasticity. As such, the synaptic connection between a pre- and post-synaptic neuron pair firing temporally proximally to one another is strengthened over time, which constitutes the basis of learning and memory formation (73-75).

When pairs of neurons are stimulated back and forth, they start firing action potentials at a higher than normal target rate, and the network they belong to will become more and more activated over time. As such, the excitatory-inhibitory balance of network activity gets disrupted, and the uncontrolled over-activation could lead to excitotoxicity or epileptic seizures. One mechanism to avoid such positive feedback loops and sustain maintenance of target firing rate is termed homeostatic synaptic plasticity. Accordingly, when neuronal activity is chronically silenced by lack of external stimuli, for example, neurons activate a somewhat shared signaling mechanism to produce more glutamatergic receptors, and more importantly increase their trafficking into or stabilization at synaptic sites. By so doing, the post-synaptic neuron is essentially increasing its synaptic drive, or in other words, sensitivity to a forthcoming external stimulus. This particular set of events are referred to as homeostatic up-scaling. In *in vitro* primary hippocampal or cortical neuronal cultures, chronic treatment with tetrodotoxin is a common way to block voltage-gated sodium channels to inhibit action potential propagation. As such, if the global neuronal network is silenced for 24-48 hours, individual neurons increase total production and surface/synaptic trafficking of AMPA receptors. Moreover, AMPA receptors present at the synapse would be post-translationally modified for better anchoring or retention. Consequently, electrophysiological recordings demonstrate an increase in miniature excitatory post-synaptic current (mEPSC) amplitude but not frequency, since the post-synaptic response to each pre-synaptic neurotransmitter-filled vesicle fusion event is going to be higher. Conversely, when global neuronal networks are over-activated for a prolonged period of time, individual neurons reduce synaptic drive by decreasing AMPA receptor

content from synaptic sites by endocytosis-mediated internalization or lateral diffusion into extra-synaptic sites. This set of events are referred to as homeostatic down-scaling. In primary neuronal cultures, bicuculline is a commonly used pharmacological reagent to chronically block GABA_AR receptors, reduce inhibitory tone, and consequently lead to over-excitation. In response, global neuronal networks reduce surface and synaptic AMPA receptors, and mEPSC amplitude for each vesicle fusion event (76-83).

Taken together, both activity-dependent and homeostatic synaptic plasticity use converging signaling mechanisms, and therefore must exist in synergy to maintain proper excitatory-inhibitory balance. Overall, the interplay between the two mechanisms have been conceptualized by the synaptic homeostasis hypothesis (SHY), which postulates the requirement and importance of sleep as a stage of homeostatic down-scaling of neuronal network drive following activation during learning and memory formation (84-87). As such, investigations of underlying mechanisms both individual to and shared between each form of synaptic plasticity are of importance. Lastly, we are particularly interested in the interplay between MIAs such as NogoA and regulation of synaptic plasticity, especially since both an important role in the discovery of a novel therapeutic intervention to sustain axonal regeneration, re-innervation, and functional recovery following CNS injury.

1.2.7 Biogenesis of and Master Regulation by Synaptic miRNAs

Once transcribed, mRNAs can be stably expressed and translated for an extended time (88, 89). One mechanism to dictate context-dependent translation of

mRNA expression is through endogenous miRNAs. Through association with the 3' untranslated region (UTR) of target mRNAs, these small RNAs can act as master regulators of local translation in response to acute and dynamic external stimuli (90). Owing to long axonal projections that could span more than a meter in larger organisms such as humans, neurons switch on or off local translation of distally trafficked mRNAs by regulating miRNA expression, trafficking, and processing. This is especially important for fast responses to axonal injury, which would otherwise be stalled by generation and trafficking of nascent mRNAs (91). Similarly, the synaptic sites for the majority of excitatory synaptic transmission, dendritic spines could reside on highly arborized dendritic branches located long distances away from cell soma. As such, an immediate and robust transcriptional regulation is especially important for fast-scale mechanisms such as activity-dependent synaptic plasticity (92). Consequently, there have been a lot of studies on how miRNAs are regulated in a synaptic activity-dependent manner (93, 94).

In an elegant study, Sambandan *et al.* posed and explored the possibility that the miRNA-mediated master regulation of mRNAs could immediately follow local synaptic activity in individual dendritic spines by local processing and maturation of miRNAs (95). Moreover, mRNAs are overwhelmingly more abundant than miRNAs, and can be targeted by the same mature miRNA. As such, one way to efficiently and specifically repress expression of an activity-dependent mRNA could become possible through on-demand miRNA processing in close proximity to the targeted mRNAs. A mature miRNA is generated after two steps of enzymatic processing: first, a primary miRNA (pri-miRNA) is transcribed and gets processed within the nucleus by Drosha and Dgcr8 to

generate a pre-miRNA (96-98). Then, the pre-miRNA is transported to the cytoplasm, where it is locally processed by Dicer to generate a mature miRNA (Figure 1-1) (98, 99). Since both Dicer and pre-miRNAs were observed in dendrites and near synapses (100-103), and Dicer activity is known to be calcium-dependent (103), Sambandan *et al.* investigated this intricate interplay between the two. First, they evaluated expression and abundance of miRNAs within the hippocampal neuropil, and their possible mRNA targets within the context of synaptic stimulation. At the top of the list was miR-181a (95), which was previously identified as a neuronal miRNA with high hippocampal expression (102, 104, 105). Pre-miR-181a was abundantly found in the cell soma and dendrites, and was processed in a Dicer-dependent manner as soon as 10 minutes following evoked action potential firing. In fact, pre-miR-181a at the dendritic shaft or spine was found to be processed into mature miRNA as soon as 10 seconds following local glutamate uncaging. Moreover, since one of the known targets of miR-181a is the master regulator *CaMKII α* , Sambandan *et al.* found a significant reduction in local synthesis of CaMKII α following dendrite-specific glutamate uncaging and consequent miR-181a maturation (95). Taken together with numerous studies studying regulation of synaptic miRNAs (93, 94, 106-109), these results clearly demonstrate an important role for tightly regulated miRNA expression and processing machinery. Consequently, dynamic miRNA-mRNA interactions at synaptic sites dictate regulation of local protein synthesis, required for the induction and maintenance of synaptic plasticity.

1.3 Conclusions

Neurons of the adult mammalian CNS fail to support axonal regeneration following injury due to intrinsically turned off growth programs and extrinsically hostile environment without sufficient neurotrophic factors. One of the strongest inhibitory regulators of the CNS neurons is the MAI NogoA, which negative regulates neurite outgrowth *in vitro*, axonal sprouting *in vivo*, and activity-dependent synaptic plasticity. To date, only three receptor partners have been well established and characterized, with poor understanding of the complex signaling mechanism. Moreover, the cell autonomy and the cell-type origin of these inhibitory cues are still not well understood. Curiously, the germline knockout of either *NogoA/B/C* or *NgR1* does not manifest a significant alleviation of the inhibitory brakes on regeneration or synaptic plasticity. As such, studies have so far employed various approaches to neutralize NogoA function within the context of injury or synaptic plasticity, using cell-type conditional knockouts, function-blocking antibody treatments, pharmacological reagents, or RNA interference.

In Chapter 2, we took an alternative approach and set out to fill the gaps in knowledge on physiological conditions or contexts that modulate NogoA protein expression. First, we lay out the foundation of our studies by describing our primary neuronal and astroglial culture systems and characterizing cell type- and subcellular compartment-specific NogoA protein expression patterns. Next, we demonstrate that total NogoA protein expression was robustly downregulated following chemically induced membrane depolarization on synaptically immature neurons. We also show that upon synaptic maturity, NogoA levels at the neuronal cell surface, but not within

intracellular pools, are bidirectionally regulated with homeostatic synaptic plasticity, in an opposite fashion to surface GluA1 expression. Lastly, we generate and characterize a phospho-specific anti-NogoA ser-343 antibody. We show this NogoA phosphorylation event was restricted to neuronal populations, since expression was not seen with either primary astroglial cultures or oligodendrocytic myelin membranes from rat brains. Moreover, since NogoA p-S343 was also absent from the neuronal surface, we hypothesize that this phosphorylation mark might be associated with the regulation of NogoA endo-/exocytosis. Future investigations should build on these findings to identify the kinase/phosphatase pair(s) responsible for NogoA phosphorylation and consequent regulation of subcompartmental trafficking.

In Chapter 3, we switch gears, and follow a conciliatory approach, where we combine previously reported culture systems (72) and NogoA-specific shRNA (68). Unlike previous findings, however, we detect a robust downregulation of synaptically important key genes and their protein products, namely GluA1/2, GAD-65/67, and S6K. We link the functional outcome of these regulations to a drastic reduction in mEPSC amplitude and an inability to drive homeostatic scaling in either direction. Following expansive RNA sequencing experiments and complementary biochemical analyses, we conclude that shNogoA transduction causes activation of L-type VGCCs, consequent elevated levels of intracellular calcium at a global network level, and a concurrent upregulation of immediate-early genes, such as *Npas4*, *Arc*, and *Fos*. Despite multiple facets of verification, we rigorously demonstrate that the shNogoA relayed manifestation of these phenotypes through non-specific, secondary targets. Small and total RNA sequencing experiments following step-wise mutations of the shNogoA seed region

corroborate NogoA-independent nature of these observations, and heavily implicate the dysfunctional miRNA machinery. Current investigations are exploring the involvement of miRNA processing enzymes in relaying shNogoA's off-target effects

In conclusion, the first portion of our work addresses some of the open questions within the domain of physiological role of NogoA function, and provides novel tools to study NogoA as a neuron-specific phospho-protein. The second portion of our work addresses a larger audience, and communicates important findings that would collectively advise rigorous scrutiny on miRNA machinery when using RNAi methods, especially with highly specialized and complex cell-types such as post-mitotic neurons. We therefore recommend that RNAi findings be verified with null tissue, and replicated through alternative acute depletion approaches such as CRISPR-Cas9 systems.

1.4 Figures

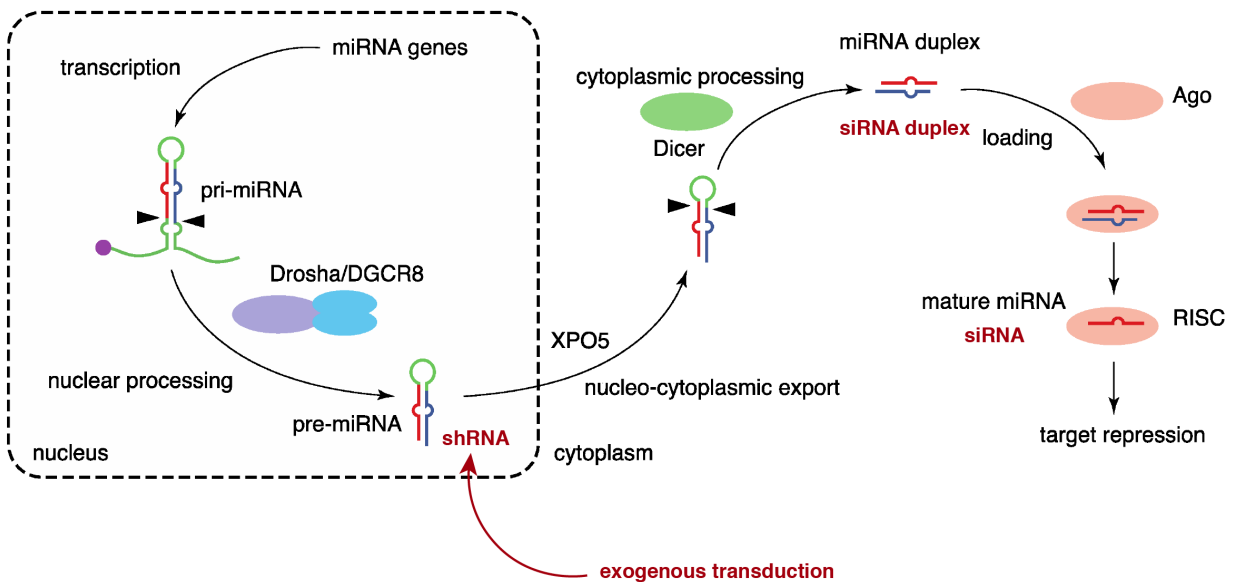


Figure 1-1: microRNA biogenesis pathway is shared by short hairpin RNA processing machinery.

Newly transcribed primary miRNA (pri-miRNA) is processed in the nucleus by Drosha/Dgcr8 complex into precursor miRNA (pre-miRNA). Exogenously transduced short hairpin RNA (shRNA) structurally and functionally resembles pre-miRNA. Both are then exported from the nucleus by exportin-5 (XPO5). In the cytoplasm, Dicer processes pre-miRNA and shRNA into corresponding miRNA and short interfering RNA (siRNA) duplexes. Argonuate (Ago) proteins load these duplexes into the RNA-induced silencing complex (RISC) for messenger RNA (mRNA) repression Adapted with permission from Matsuyama and Suzuki, 2019 (98).

1.5 References

1. B. J. Dickson, Molecular Mechanisms of Axon Guidance. *Science* **298**, 1959-1964 (2002).
2. K.-L. Guan, Y. Rao, Signalling mechanisms mediating neuronal responses to guidance cues. *Nature Reviews Neuroscience* **4**, 941-956 (2003).
3. M. M. Riccomagno, A. L. Kolodkin, Sculpting Neural Circuits by Axon and Dendrite Pruning. *Annual Review of Cell and Developmental Biology* **31**, 779-805 (2015).
4. D. H. Hubel, T. N. Wiesel, S. LeVay, H. B. Barlow, R. M. Gaze, Plasticity of ocular dominance columns in monkey striate cortex. *Philosophical Transactions of the Royal Society of London. B, Biological Sciences* **278**, 377-409 (1977).
5. T. Pizzorusso *et al.*, Reactivation of Ocular Dominance Plasticity in the Adult Visual Cortex. *Science* **298**, 1248-1251 (2002).
6. T. K. Hensch, Critical Period Regulation. *Annual Review of Neuroscience* **27**, 549-579 (2004).
7. T. K. Hensch, Critical period plasticity in local cortical circuits. *Nature Reviews Neuroscience* **6**, 877-888 (2005).
8. G.-I. Ming, H. Song, Adult Neurogenesis in the Mammalian Central Nervous System. *Annual Review of Neuroscience* **28**, 223-250 (2005).
9. P.-M. Lledo, M. Alonso, M. S. Grubb, Adult neurogenesis and functional plasticity in neuronal circuits. *Nature Reviews Neuroscience* **7**, 179-193 (2006).
10. C. Zhao, W. Deng, F. H. Gage, Mechanisms and Functional Implications of Adult Neurogenesis. *Cell* **132**, 645-660 (2008).
11. M. T. Fitch, J. Silver, CNS injury, glial scars, and inflammation: Inhibitory extracellular matrices and regeneration failure. *Experimental Neurology* **209**, 294-301 (2008).
12. S. G. Kernie, J. M. Parent, Forebrain neurogenesis after focal Ischemic and traumatic brain injury. *Neurobiology of Disease* **37**, 267-274 (2010).
13. J. M. Parent, Z. S. Vexler, C. Gong, N. Derugin, D. M. Ferriero, Rat forebrain neurogenesis and striatal neuron replacement after focal stroke. *Annals of neurology* **52**, 802-813 (2002).

14. H. Neumann, M. R. Kotter, R. J. M. Franklin, Debris clearance by microglia: an essential link between degeneration and regeneration. *Brain* **132**, 288-295 (2008).
15. G. A. Garden, T. Möller, Microglia Biology in Health and Disease. *Journal of Neuroimmune Pharmacology* **1**, 127-137 (2006).
16. S. A. Liddelow *et al.*, Neurotoxic reactive astrocytes are induced by activated microglia. *Nature* **541**, 481-487 (2017).
17. M. A. Anderson *et al.*, Astrocyte scar formation aids central nervous system axon regeneration. *Nature* **532**, 195-200 (2016).
18. A. Almad, F. R. Sahinkaya, D. M. McTigue, Oligodendrocyte Fate after Spinal Cord Injury. *Neurotherapeutics* **8**, 262-273 (2011).
19. Z. C. Hesp, E. A. Goldstein, C. J. Miranda, B. K. Kaspar, D. M. McTigue, Chronic Oligodendrogenesis and Remyelination after Spinal Cord Injury in Mice and Rats. *The Journal of Neuroscience* **35**, 1274-1290 (2015).
20. K. Tanabe, I. Bonilla, J. A. Winkles, S. M. Strittmatter, Fibroblast growth factor-inducible-14 is induced in axotomized neurons and promotes neurite outgrowth. *The Journal of neuroscience : the official journal of the Society for Neuroscience* **23**, 9675-9686 (2003).
21. R. Seijffers, A. J. Allchorne, C. J. Woolf, The transcription factor ATF-3 promotes neurite outgrowth. *Molecular and cellular neurosciences* **32**, 143-154 (2006).
22. A. Blesch *et al.*, Conditioning lesions before or after spinal cord injury recruit broad genetic mechanisms that sustain axonal regeneration: superiority to camp-mediated effects. *Exp Neurol* **235**, 162-173 (2012).
23. V. Chandran *et al.*, A Systems-Level Analysis of the Peripheral Nerve Intrinsic Axonal Growth Program. *Neuron* **89**, 956-970 (2016).
24. R. Puttagunta *et al.*, PCAF-dependent epigenetic changes promote axonal regeneration in the central nervous system. *Nature communications* **5**, 3527 (2014).
25. F. Sun *et al.*, Sustained axon regeneration induced by co-deletion of PTEN and SOCS3. *Nature* **480**, 372-375 (2011).
26. K. K. Park *et al.*, Promoting axon regeneration in the adult CNS by modulation of the PTEN/mTOR pathway. *Science* **322**, 963-966 (2008).
27. A. J. Aguayo *et al.*, Ensheatment and myelination of regenerating PNS fibres by transplanted optic nerve glia. *Neurosci Lett* **9**, 97-104 (1978).

28. A. J. Aguayo, S. David, G. M. Bray, Influences of the glial environment on the elongation of axons after injury: transplantation studies in adult rodents. *The Journal of experimental biology* **95**, 231-240 (1981).
29. A. Logan, Z. Ahmed, A. Baird, A. M. Gonzalez, M. Berry, Neurotrophic factor synergy is required for neuronal survival and disinhibited axon regeneration after CNS injury. *Brain* **129**, 490-502 (2005).
30. L. L. Jones, M. Oudega, M. B. Bunge, M. H. Tuszynski, Neurotrophic factors, cellular bridges and gene therapy for spinal cord injury. *The Journal of Physiology* **533**, 83-89 (2001).
31. M. L. Lemons, D. R. Howland, D. K. Anderson, Chondroitin Sulfate Proteoglycan Immunoreactivity Increases Following Spinal Cord Injury and Transplantation. *Experimental Neurology* **160**, 51-65 (1999).
32. E. J. Bradbury *et al.*, Chondroitinase ABC promotes functional recovery after spinal cord injury. *Nature* **416**, 636-640 (2002).
33. B. D. Trapp, S. B. Andrews, C. Cootauco, R. Quarles, The myelin-associated glycoprotein is enriched in multivesicular bodies and periaxonal membranes of actively myelinating oligodendrocytes. *J Cell Biol* **109**, 2417-2426 (1989).
34. X. Yin *et al.*, Myelin-associated glycoprotein is a myelin signal that modulates the caliber of myelinated axons. *The Journal of neuroscience : the official journal of the Society for Neuroscience* **18**, 1953-1962 (1998).
35. S. T. Hsieh *et al.*, Regional modulation of neurofilament organization by myelination in normal axons. *The Journal of neuroscience : the official journal of the Society for Neuroscience* **14**, 6392-6401 (1994).
36. T. Nguyen *et al.*, Axonal protective effects of the myelin-associated glycoprotein. *The Journal of neuroscience : the official journal of the Society for Neuroscience* **29**, 630-637 (2009).
37. S. M. Dashiell, S. L. Tanner, H. C. Pant, R. H. Quarles, Myelin-associated glycoprotein modulates expression and phosphorylation of neuronal cytoskeletal elements and their associated kinases. *J Neurochem* **81**, 1263-1272 (2002).
38. J. K. Huang *et al.*, Glial membranes at the node of Ranvier prevent neurite outgrowth. *Science* **310**, 1813-1817 (2005).
39. S. J. Raiker *et al.*, Oligodendrocyte-Myelin Glycoprotein and Nogo Negatively Regulate Activity-Dependent Synaptic Plasticity. *The Journal of Neuroscience* **30**, 12432-12445 (2010).
40. M. E. Schwab, P. Caroni, Oligodendrocytes and CNS myelin are nonpermissive substrates for neurite growth and fibroblast spreading in vitro. *The Journal of*

- neuroscience : the official journal of the Society for Neuroscience* **8**, 2381-2393 (1988).
41. P. Caroni, M. E. Schwab, Antibody against myelin-associated inhibitor of neurite growth neutralizes nonpermissive substrate properties of CNS white matter. *Neuron* **1**, 85-96 (1988).
 42. M. S. Chen *et al.*, Nogo-A is a myelin-associated neurite outgrowth inhibitor and an antigen for monoclonal antibody IN-1. *Nature* **403**, 434-439 (2000).
 43. T. GrandPré, F. Nakamura, T. Vartanian, S. M. Strittmatter, Identification of the Nogo inhibitor of axon regeneration as a Reticulon protein. *Nature* **403**, 439-444 (2000).
 44. A. B. Huber, O. Weinmann, C. Brosamle, T. Oertle, M. E. Schwab, Patterns of Nogo mRNA and protein expression in the developing and adult rat and after CNS lesions. *The Journal of neuroscience : the official journal of the Society for Neuroscience* **22**, 3553-3567 (2002).
 45. T. Oertle *et al.*, Nogo-A inhibits neurite outgrowth and cell spreading with three discrete regions. *The Journal of neuroscience : the official journal of the Society for Neuroscience* **23**, 5393-5406 (2003).
 46. A. E. Fournier, T. GrandPre, S. M. Strittmatter, Identification of a receptor mediating Nogo-66 inhibition of axonal regeneration. *Nature* **409**, 341-346 (2001).
 47. B. Niederost, T. Oertle, J. Fritsche, R. A. McKinney, C. E. Bandtlow, Nogo-A and myelin-associated glycoprotein mediate neurite growth inhibition by antagonistic regulation of RhoA and Rac1. *The Journal of neuroscience : the official journal of the Society for Neuroscience* **22**, 10368-10376 (2002).
 48. A. Kempf, M. E. Schwab, Nogo-A Represses Anatomical and Synaptic Plasticity in the Central Nervous System. *Physiology* **28**, 151-163 (2013).
 49. H. Lee *et al.*, Synaptic function for the Nogo-66 receptor NgR1: regulation of dendritic spine morphology and activity-dependent synaptic strength. *The Journal of neuroscience : the official journal of the Society for Neuroscience* **28**, 2753-2765 (2008).
 50. A. Delekate, M. Zagrebelsky, S. Kramer, M. E. Schwab, M. Korte, NogoA restricts synaptic plasticity in the adult hippocampus on a fast time scale. *Proceedings of the National Academy of Sciences* **108**, 2569-2574 (2011).
 51. J. K. Atwal *et al.*, PirB is a Functional Receptor for Myelin Inhibitors of Axonal Regeneration. *Science* **322**, 967-970 (2008).

52. A. Kempf *et al.*, The Sphingolipid Receptor S1PR2 Is a Receptor for Nogo-A Repressing Synaptic Plasticity. *PLOS Biology* **12**, e1001763 (2014).
53. A. Joset, D. A. Dodd, S. Halegoua, M. E. Schwab, Pincher-generated Nogo-A endosomes mediate growth cone collapse and retrograde signaling. *The Journal of cell biology* **188**, 271-285 (2010).
54. M. Simonen *et al.*, Systemic Deletion of the Myelin-Associated Outgrowth Inhibitor Nogo-A Improves Regenerative and Plastic Responses after Spinal Cord Injury. *Neuron* **38**, 201-211 (2003).
55. J.-E. Kim, S. Li, T. GrandPré, D. Qiu, S. M. Strittmatter, Axon Regeneration in Young Adult Mice Lacking Nogo-A/B. *Neuron* **38**, 187-199 (2003).
56. B. Zheng *et al.*, Lack of enhanced spinal regeneration in Nogo-deficient mice. *Neuron* **38**, 213-224 (2003).
57. J. K. Lee *et al.*, Reassessment of Corticospinal Tract Regeneration in Nogo-Deficient Mice. *The Journal of Neuroscience* **29**, 8649-8654 (2009).
58. L. Dimou *et al.*, Nogo-A-deficient mice reveal strain-dependent differences in axonal regeneration. *The Journal of neuroscience : the official journal of the Society for Neuroscience* **26**, 5591-5603 (2006).
59. A. Kempf *et al.*, Upregulation of axon guidance molecules in the adult central nervous system of Nogo-A knockout mice restricts neuronal growth and regeneration. *European Journal of Neuroscience* **38**, 3567-3579 (2013).
60. F. Vajda *et al.*, Cell type-specific Nogo-A gene ablation promotes axonal regeneration in the injured adult optic nerve. *Cell death and differentiation* **22**, 323-335 (2015).
61. A. Zemmar *et al.*, Oligodendrocyte- and Neuron-Specific Nogo-A Restrict Dendritic Branching and Spine Density in the Adult Mouse Motor Cortex. *Cereb Cortex*, 1-9 (2017).
62. J. M. Meves, C. G. Geoffroy, N. D. Kim, J. J. Kim, B. Zheng, Oligodendrocytic but not neuronal Nogo restricts corticospinal axon sprouting after CNS injury. *Experimental Neurology* **309**, 32-43 (2018).
63. M. Thallmair *et al.*, Neurite growth inhibitors restrict plasticity and functional recovery following corticospinal tract lesions. *Nat Neurosci* **1**, 124-131 (1998).
64. T. Liebscher *et al.*, Nogo-A antibody improves regeneration and locomotion of spinal cord-injured rats. *Annals of neurology* **58**, 706-719 (2005).

65. P. Freund *et al.*, Anti-Nogo-A antibody treatment promotes recovery of manual dexterity after unilateral cervical lesion in adult primates--re-examination and extension of behavioral data. *Eur J Neurosci* **29**, 983-996 (2009).
66. P. Freund *et al.*, Nogo-A-specific antibody treatment enhances sprouting and functional recovery after cervical lesion in adult primates. *Nature medicine* **12**, 790-792 (2006).
67. K. Kucher *et al.*, First-in-Man Intrathecal Application of Neurite Growth-Promoting Anti-Nogo-A Antibodies in Acute Spinal Cord Injury. *Neurorehabilitation and neural repair* **32**, 578-589 (2018).
68. M. Zagrebelsky, R. Schweigreiter, C. E. Bandtlow, M. E. Schwab, M. Korte, Nogo-A stabilizes the architecture of hippocampal neurons. *The Journal of neuroscience : the official journal of the Society for Neuroscience* **30**, 13220-13234 (2010).
69. A. Zemmar *et al.*, Neutralization of Nogo-A Enhances Synaptic Plasticity in the Rodent Motor Cortex and Improves Motor Learning in Vivo. *The Journal of Neuroscience* **34**, 8685-8698 (2014).
70. A. D. Pradhan *et al.*, Dendritic spine alterations in neocortical pyramidal neurons following postnatal neuronal Nogo-A knockdown. *Developmental neuroscience* **32**, 313-320 (2010).
71. B. Tews *et al.*, Synthetic microRNA-mediated downregulation of Nogo-A in transgenic rats reveals its role as regulator of synaptic plasticity and cognitive function. *Proceedings of the National Academy of Sciences* **110**, 6583-6588 (2013).
72. X. Peng, J. Kim, Z. Zhou, D. J. Fink, M. Mata, Neuronal Nogo-A regulates glutamate receptor subunit expression in hippocampal neurons. *Journal of Neurochemistry* **119**, 1183-1193 (2011).
73. T. V. P. Bliss, G. L. Collingridge, A synaptic model of memory: long-term potentiation in the hippocampus. *Nature* **361**, 31-39 (1993).
74. M. A. Lynch, Long-Term Potentiation and Memory. *Physiological Reviews* **84**, 87-136 (2004).
75. J. Lisman, R. Yasuda, S. Raghavachari, Mechanisms of CaMKII action in long-term potentiation. *Nat Rev Neurosci* **13**, 169-182 (2012).
76. G. G. Turrigiano, K. R. Leslie, N. S. Desai, L. C. Rutherford, S. B. Nelson, Activity-dependent scaling of quantal amplitude in neocortical neurons. *Nature* **391**, 892-896 (1998).

77. G. G. Turrigiano, S. B. Nelson, Homeostatic plasticity in the developing nervous system. *Nat Rev Neurosci* **5**, 97-107 (2004).
78. M. A. Sutton *et al.*, Miniature Neurotransmission Stabilizes Synaptic Function via Tonic Suppression of Local Dendritic Protein Synthesis. *Cell* **125**, 785-799 (2006).
79. J. D. Shepherd *et al.*, Arc/Arg3.1 Mediates Homeostatic Synaptic Scaling of AMPA Receptors. *Neuron* **52**, 475-484 (2006).
80. M. C. Guzman-Karlsson, J. P. Meadows, C. F. Gavin, J. J. Hablitz, J. D. Sweatt, Transcriptional and epigenetic regulation of Hebbian and non-Hebbian plasticity. *Neuropharmacology* **80**, 3-17 (2014).
81. Graham H. Diering, Ahleah S. Gustina, Richard L. Huganir, PKA-GluA1 Coupling via AKAP5 Controls AMPA Receptor Phosphorylation and Cell-Surface Targeting during Bidirectional Homeostatic Plasticity. *Neuron* **84**, 790-805 (2014).
82. J. Barral, A. D. Reyes, Synaptic scaling rule preserves excitatory–inhibitory balance and salient neuronal network dynamics. *Nature Neuroscience* **19**, 1690-1696 (2016).
83. G. H. Diering, R. L. Huganir, The AMPA Receptor Code of Synaptic Plasticity. *Neuron* **100**, 314-329 (2018).
84. S. Diekelmann, J. Born, The memory function of sleep. *Nat Rev Neurosci* **11**, 114-126 (2010).
85. G. Wang, B. Grone, D. Colas, L. Appelbaum, P. Murrain, Synaptic plasticity in sleep: learning, homeostasis and disease. *Trends in Neurosciences* **34**, 452-463 (2011).
86. G. H. Diering *et al.*, Homer1a drives homeostatic scaling-down of excitatory synapses during sleep. *Science* **355**, 511-515 (2017).
87. G. Tononi, C. Cirelli, Sleep function and synaptic homeostasis. *Sleep Medicine Reviews* **10**, 49-62 (2006).
88. J. Ross, mRNA stability in mammalian cells. *Microbiological Reviews* **59**, 423-450 (1995).
89. J. Guhaniyogi, G. Brewer, Regulation of mRNA stability in mammalian cells. *Gene* **265**, 11-23 (2001).
90. D. P. Bartel, MicroRNAs: target recognition and regulatory functions. *Cell* **136**, 215-233 (2009).

91. H. Jung, B. C. Yoon, C. E. Holt, Axonal mRNA localization and local protein synthesis in nervous system assembly, maintenance and repair. *Nature Reviews Neuroscience* **13**, 308-324 (2012).
92. M. A. Sutton, E. M. Schuman, Dendritic Protein Synthesis, Synaptic Plasticity, and Memory. *Cell* **127**, 49-58 (2006).
93. Z. Hu, Z. Li, miRNAs in synapse development and synaptic plasticity. *Current Opinion in Neurobiology* **45**, 24-31 (2017).
94. G. Schratt, microRNAs at the synapse. *Nat Rev Neurosci* **10**, 842-849 (2009).
95. S. Sambandan *et al.*, Activity-dependent spatially localized miRNA maturation in neuronal dendrites. *Science* **355**, 634-637 (2017).
96. Y. Lee *et al.*, The nuclear RNase III Drosha initiates microRNA processing. *Nature* **425**, 415-419 (2003).
97. J. Han *et al.*, The Drosha-DGCR8 complex in primary microRNA processing. *Genes & Development* **18**, 3016-3027 (2004).
98. H. Matsuyama, H. I. Suzuki, Systems and Synthetic microRNA Biology: From Biogenesis to Disease Pathogenesis. *International Journal of Molecular Sciences* **21**, 132 (2019).
99. E. Bernstein, A. A. Caudy, S. M. Hammond, G. J. Hannon, Role for a bidentate ribonuclease in the initiation step of RNA interference. *Nature* **409**, 363-366 (2001).
100. G. Lugli, J. Larson, M. E. Martone, Y. Jones, N. R. Smalheiser, Dicer and eIF2c are enriched at postsynaptic densities in adult mouse brain and are modified by neuronal activity in a calpain-dependent manner. *J Neurochem* **94**, 896-905 (2005).
101. S. Bicker *et al.*, The DEAH-box helicase DHX36 mediates dendritic localization of the neuronal precursor-microRNA-134. *Genes & Development* **27**, 991-996 (2013).
102. R. Saba *et al.*, Dopamine-Regulated MicroRNA MiR-181a Controls GluA2 Surface Expression in Hippocampal Neurons. *Molecular and Cellular Biology* **32**, 619-632 (2012).
103. G. Lugli, V. I. Torvik, J. Larson, N. R. Smalheiser, Expression of microRNAs and their precursors in synaptic fractions of adult mouse forebrain. *Journal of Neurochemistry* **106**, 650-661 (2008).
104. M. J. Kye *et al.*, Somatodendritic microRNAs identified by laser capture and multiplex RT-PCR. *RNA (New York, N.Y.)* **13**, 1224-1234 (2007).

105. M. van Spronsen *et al.*, Developmental and Activity-Dependent miRNA Expression Profiling in Primary Hippocampal Neuron Cultures. *PLOS ONE* **8**, e74907 (2013).
106. J. E. Cohen, P. R. Lee, S. Chen, W. Li, R. D. Fields, MicroRNA regulation of homeostatic synaptic plasticity. *Proceedings of the National Academy of Sciences* **108**, 11650-11655 (2011).
107. N. M. Sosanya *et al.*, Degradation of high affinity HuD targets releases Kv1.1 mRNA from miR-129 repression by mTORC1. *Journal of Cell Biology* **202**, 53-69 (2013).
108. J. Remenyi *et al.*, miR-132/212 Knockout Mice Reveal Roles for These miRNAs in Regulating Cortical Synaptic Transmission and Plasticity. *PLOS ONE* **8**, e62509 (2013).
109. H. L. Scott *et al.*, MicroRNA-132 regulates recognition memory and synaptic plasticity in the perirhinal cortex. *European Journal of Neuroscience* **36**, 2941-2948 (2012).

CHAPTER 2:

Activity-Dependent Regulation of the Neuronal Phospho-Protein NogoA

2.1 Abstract

Identified as an inhibitor of axonal outgrowth, NogoA has also been shown to negatively regulate synaptic strength, including long-term potentiation of transmission. However, the underlying mechanisms and whether NogoA itself is regulated by neuronal activity still remain unknown. Here, we employ primary hippocampal cultures to study NogoA expression, surface trafficking, and post-translational modifications under the regulation of synaptic activity. We demonstrate that synaptically immature neurons downregulate NogoA expression upon sustained depolarization; however, once fully matured, total NogoA levels are largely stable regardless of network activity. In contrast, surface levels of NogoA are under bidirectional and homeostatic regulation. We show that chronic treatment with tetrodotoxin or bicuculline induces homeostatic scaling, and regulates surface NogoA in an opposite manner to GluA1. To elucidate the mechanism underlying such regulation, we identified phosphorylation sites on the rat NogoA, and characterized a neuron-specific, intracellular phosphorylation at NogoA serine-343. Future experiments should investigate the activity-dependent physiological contexts and identify the molecular players that modulate NogoA phosphorylation.

2.2 Introduction

NogoA was originally discovered in the central nervous system (CNS) myelin, formed by a glial subtype called oligodendrocytes (1). A later study showed that NogoA was expressed in high levels within the brain, spinal cord, and optic nerve. Moreover, NogoA expression was not only restricted to oligodendrocytes, but also seen with various subtypes of neurons, including glutamatergic, excitatory pyramidal neurons of the hippocampus and neocortex, as well as parvalbumin- and calbindin-expressing inhibitory interneurons. The same study also showed that GFAP-expressing astrocytes within the CNS white matter did not express NogoA protein (2). In stark contrast, brain RNA-seq transcriptome studies strongly demonstrated that *Rtn4* transcripts were detected with considerable abundance in all cell types of the CNS, including astrocytes, microglia, oligodendrocyte lineages from mouse and human origins (3, 4).

The physiological function of oligodendrocytic NogoA in preventing axonal sprouting and outgrowth has been well-studied and characterized. In these studies, cultured cells were treated with bath applied myelin extracts or recombinant NogoA fragments, and their cytoskeleton retraction, growth cone collapse, and lack of neurite outgrowth were observed (1, 2, 5-9). Moreover, receptor partners of NogoA were found to exert a restrictive influence on the ocular dominance plasticity of the visual system (10, 11). As such, when this negative regulation was removed by genomic knockout of *Nogo-66 Receptor 1 (NgR1)* (12) or *Paired immunoglobulin-like receptor B (PirB)* (13), ocular dominance plasticity continues after the end of the critical period, reminiscent of the experimental degradation of the inhibitory chondroitin sulphate proteoglycans

(CSPGs) (14). This led to the discovery that NogoA exert a negative regulation on the induction and maintenance of activity-dependent, morphological, and functional synaptic plasticity. For instance, acute hippocampal slices were treated with function blocking antibodies against the NogoA- Δ 20 domain or the Nogo66 Receptor 1 (NgR1), and the ability to sustain tetanus-induced long-term potentiation (LTP) was assessed (15-24). In both paradigms, the functional role of NogoA signaling was modulated: in the former case, exogenous NogoA was supplied to increase signaling, and in the latter scenario, endogenous NogoA was prevented from binding receptor partners. Although this shed some light onto the function of NogoA, the field still has some knowledge gaps in addressing the complex interactome of this signaling cascade besides cytoskeletal regulation. Moreover, the issue of how NogoA expression, trafficking, and signaling are modulated under more physiological conditions left untouched.

Until very recently, the focus of the field has been on the functional outcomes when NogoA signaling was experimentally overexpressed or interrupted. In 2019, Fricke *et al.* contributed a novel perspective, by treating synaptosomes isolated from acute hippocampal cultures with KCl, and assessing NogoA expression. They found that upon increased and sustained depolarization, not only the glutamatergic AMPA receptor subunit GluA1, but also the NogoA protein expression in the synaptosomes was robustly reduced (25). This was suggestive of neuronal NogoA's involvement in the maintenance of homeostatic synaptic plasticity.

The term homeostatic synaptic plasticity (HSP) refers to the set of complex mechanisms that maintain neuronal network firing rate at a set, pre-determined range. In other words, when a network of neurons is silenced or over-stimulated for an

extended period of time, the response of each individual neuron in the network is to increase (scale-up) or decrease (scale-down) the amplitude of the miniature excitatory post-synaptic current (mEPSC) derived from each stimulus. One way to do so is by mobilizing glutamatergic receptors to and from synapses, by means of lateral diffusion, endocytosis, or exocytosis (26-32). However, this is merely the functional outcome, assessed at static snapshots throughout chronic silencing or over-activation. We therefore reasoned that transmembrane proteins known to inhibit Hebbian forms of synaptic plasticity, such as NogoA and NgR1, could also be involved upstream of GluA1 surface expression, synaptic trafficking, or stabilized anchoring.

Mechanisms of activity-dependent LTP and HSP can converge on the same functional terminal step, which is the highly dynamic and regulated trafficking of the AMPA receptor subunits responsible for excitatory glutamatergic transmission. Many groups have so far identified labile post-translational modifications (PTMs) as an effective means to shuttle membrane-bound proteins to and from the cell surface (32-34). For instance, calcium permeable AMPA receptor subunit GluA1 can be phosphorylated by α -calcium-calmodulin-dependent protein kinase II (CaMKII) at serine-831 residue (35-37) and by protein kinase C (PKC) at serine-816/818 residues (38) to increase conductance and insertion during the induction of long-term potentiation. Similarly, GluA1 can also be phosphorylated by protein kinase A (PKA) at serine-845 residue, which enables better anchoring and retention at the post-synaptic density (PSD) following homeostatic scaling up. Conversely, recruitment of phosphatases that remove these phosphorylation marks will aid in the endocytosis or lateral diffusion of GluA1 subunits to extra-synaptic sites (28). As such, we reasoned that even when total

NogoA expression remained stable, network activity states could deposit various post-translational modifications, including but not limited to phosphorylation, in order to mobilize NogoA to various subcellular compartments, thereby modulating its function.

Here, we address these questions by employing primary neuronal and astroglial cultures isolated from the rodent hippocampus. Using a cohort of pharmacological reagents, we modulated neuronal network activity states, intracellular signaling pathways, and known NogoA interactors. By so doing, we assessed how total expression, surface trafficking, and post-translational modifications of neuronal NogoA are regulated in relationship to different network activity states. Our findings demonstrate that the total expression of NogoA is quite static, resistant to most manipulations except for acute and global membrane depolarization. However, NogoA on the neuronal cell surface is much more malleable, decreasing with sustained blockade of action potentials, and increasing with chronic decrease in inhibitory tone. Moreover, we identified and characterized a novel phosphorylation site (ser-343) on the rat NogoA that was absent from surface expression, restricted to neuronal NogoA, and showed regulation only following KCl-induced membrane depolarization. On the other hand, pharmacological manipulations that promote neuronal growth, such as activation of PKA or inhibition of Rho-associated protein kinase (ROCK) and myosin II ATPase, do not alter NogoA ser-343 phosphorylation. Overall, we demonstrate that endogenous neuronal NogoA expression and phosphorylation are regulated as a function of synaptic activity. These findings form the foundation for future investigations on various post-translational modifications deposited on NogoA as a way to modulate its total expression, localization, and function.

2.3 Results

2.3.1 NogoA Expression is Highly Neuronal and Localizes to Somatodendritic Synapses

Before we moved forward with the characterization of neuronal NogoA function in different physiological contexts, it was imperative that we investigate and reconcile contradictory reports on NogoA expression pattern (2-4).

For most of the studies reported here, we employed embryonic or perinatal rodent primary cultures, isolated from the hippocampus alone, or in conjunction with the neocortex (forebrain). Experiments investigating synaptic formation and plasticity were conducted with primary neuronal cultures, supplemented with primary astroglial culture conditioned media to facilitate structurally intact and functionally unsilenced synaptogenesis (39-42). Because neither culture preparation is pure in cell type composition, we took large, multi-tiled images from neuronal (Figure 2-1A) and astroglial cultures (Figure 2-1B), and qualitatively assessed differential cell type abundance. Neuronal cultures were stained with GFAP (Figure 2-1A) to demonstrate abundant presence of astrocytes. GFAP⁺ astrocytes (green) had long, thick extensions that spanned large surface areas compared to their GFAP⁻, Hoechst⁺ neighbors (blue). These cells are of presumptively neuronal origin, and in clearly dominant abundance compared to astrocytes. On the other hand, astroglial cultures isolated from perinatal rat neocortex were occupied mostly by GFAP⁺ astrocytes (magenta) with much wider and flatter morphology compared to those observed in neuronal cultures (Figure 2-1). There were also trace numbers of Olig2⁺ oligodendrocyte-lineage cells (cyan), as well as

TUJ1⁺ cells (yellow) that resembled more fibroblasts than neurons (Figure 2-1C-C'). Overall, we concluded that in each type of primary culture preparation, the principal cell type also constituted the majority.

We then wondered about the NogoA expression pattern between different cell types within the same culture, as well as between different culture preparations. To address these questions, we used immunofluorescent staining to assess NogoA expression within primary neuronal cultures, and found that GFAP⁻, Hoechst⁺ cells with neuronal morphology expressed NogoA (magenta) to much greater extents than GFAP⁺ astrocytes (green) (Figure 2-2A). To compare NogoA expression between neuronal and astroglial cultures, total cell lysates isolated from perinatal neocortical astroglial cultures and embryonic hippocampal neuronal cultures were analyzed by Western blotting. Firstly, neuron-specific β -III Tubulin (TUJ1) was exclusively detected from the neuronal cultures, whereas astrocyte-specific GFAP signal was greatly enriched in the astroglial culture. Gaining confidence in the composition of these culture preparations, we observed qualitatively higher NogoA expression detected from the neuronal lysates, thereby increasing confidence in immunofluorescent observations (Figure 2-2B).

We were then curious about the intracellular expression pattern of neuronal NogoA. To address that question, we carried out immunofluorescence staining under non-permeabilized and permeabilized conditions to detect NogoA expression on the cell surface and throughout the entire cell, respectively (Figure 2-2C). In addition to previous publications (24, 43, 44), the anti-NogoA or anti-NogoAB antibodies were initially verified by immunofluorescence staining following sparse neuronal transfection with the NogoA-specific small hairpin RNA (shRNA) (Figure 2-4H). Antibodies were also verified

by Western Blot analysis following global neuronal transduction with the same shRNA (Figure 2-4B) or following Cre-mediated deletion of *NogoABC^{fl/fl}* from primary hippocampal neurons (Figures 3-4E and 3-7). Delineating the neuronal morphology with somatodendritic MAP2 staining (green), we observed discrete and discontinuous patches of strong NogoA expression at the neuronal cell surface (45) and along MAP2⁺ dendrites. A weaker NogoA signal was observed on the surface of MAP2⁻ axons, marked with the axon initial segment protein Ankyrin-G staining. Staining under permeabilized conditions revealed an altogether distinct pattern of total NogoA expression: strongest signal was detected from the peri-nuclear regions, which was presumably due to the strong NogoA expression within the endoplasmic reticulum (ER) continuous with the nuclear envelope (7). NogoA was also strongly and uniformly expressed along MAP2⁺ dendrites, and to a lesser extent by MAP2⁻ axons. In order to biochemically verify this expression pattern, we employed cell surface biotinylation of primary hippocampal neurons, followed by Western blot analysis (Figure 2-2D). We first verified that intracellular proteins, such as AKT, are not biotinylated, whereas known neuronal cell surface proteins, such as the transferrin receptor (TfR), can be detected by cell surface biotinylation. Also worthy of note is the reduction of TfR within the intracellular fraction, which was obtained following streptavidin-coated agarose bead precipitation of biotinylated surface proteins. Resident to the ER, NogoA was indeed most abundant within the intracellular compartments. In comparison to total NogoA expression, we also detected significantly lower ($\leq 10\%$) levels of NogoA at the neuronal cell surface. These observations are in line with previously reported findings that an ER-resident transmembrane protein can be found at the plasma membrane, and give

confidence in our experimental methodology, as well as lead the way to answering important biological questions pertaining to the surface trafficking of NogoA under different physiological conditions (7, 45).

Next, we were curious whether NogoA signaling takes place in the synapses as much as within the crude myelin. To answer this question, adult rat hippocampi and neocortices were subjected to mechanical homogenization and subsequent subcellular fractionation. We verified correct fractionation by qualitatively assessing enrichment of post-synaptic density (PSD) proteins such as PSD-95 and Homer-1 (46). Moreover, isolated crude myelin fractions were heavily enriched for myelin-associated glycoprotein (MAG), which is typically found in the peri-axonal myelin sheath and Schmidt-Lanterman incisures (47) (Figure 2-2E). As previously described, NogoA localizes to synapses with higher abundance in the PSD (21), inner- and outer-loop of the CNS myelin sheath (2). As expected, we detected robust enrichment of NogoA expression within the PSD-95⁺, Homer-1⁺ synaptosomal fraction; but surprisingly, only very low levels within the MAG⁺ myelin fraction (Figure 2-2E). Finally, we were curious whether NogoA distribution follows a similar pattern in different regions of the CNS. To address that question, we used adult male C3H mice, dissected the spinal cords, hippocampi, somatosensory cortices, and cerebelli, and followed the same homogenization and subcellular fractionation protocol as before. In adult brain tissue, NogoA shows highest protein expression in the plastic-most regions of the CNS, namely the somatosensory cortex and the hippocampus, whereas spinal cord and cerebellum demonstrated modest levels. Consistent with our previous findings with rat hippocampus and neocortex (Figure 2-2E), mouse NogoA expression is highly enriched in the PSD-95⁺

synaptosomal fractions isolated from most of these CNS regions, and shows weaker levels in the MAG⁺ myelin fractions (Figure 2-2F). This confirms abundance of NogoA in various myelin compartments of the CNS, as well as in highly specialized synaptic sites with a hitherto undercharacterized function.

2.3.2 Surface NogoA is Bidirectionally Regulated by Global Changes in Neuronal Network Activity

In physiological conditions where neuronal growth and synaptic drive need to be continuously monitored and adjusted to maintain homeostasis (27), it is conceivable that expression or activity of NogoA can be regulated by fluctuations in network activity. To date, there has been only one very recent study that investigated endogenous NogoA expression as a function of neuronal activity: Frickle *et al.* found that when synaptosomes isolated from acute hippocampal slices were continuously depolarized with KCl treatments, NogoA expression was robustly reduced (25). The fact that this observation was in parallel with a reduction in glutamatergic AMPA receptor subunit GluA1 signaled to the maintenance of excitatory-inhibitory homeostasis (48).

First, we were curious whether fully intact, physiologically developing embryonic neuronal cultures were capable of modulating NogoA expression upon sustained membrane depolarization. To that end, we treated embryonic (E) 17.5 rat hippocampal cultures on days *in vitro* (DIV) 7 with 55mM KCl for 2 hours of continuous membrane depolarization, with or without a 10 minute pre-treatment with 5mM of extracellular

calcium chelator EGTA (Figure 2-3A). We verified the physiological response to KCl-induced neuronal membrane depolarization by assessing protein expression of the immediate-early transcription factor neuronal PAS domain 4 (Npas4) (49) by Western blot analysis. Two hours of KCl treatment increased Npas4 protein expression 1.8-fold compared to vehicle-treated cultures ($n=8$, $p=0.0008$). Induction of Npas4 was completely abolished by a 10 minute EGTA pre-treatment ($n=8$, $p<0.0001$). We then investigated NogoA, and found that in addition to a small (~ 5 kDa) reduction in molecular weight, total NogoA was reduced 0.7-fold compared to vehicle-treated cultures ($n=13$, $p=0.0129$). The KCl-induced reduction in molecular weight and protein abundance was no longer observed when cultures were pre-treated with EGTA ($n=13$, $p=0.0009$) (Figure 2-3A'). Strikingly, when same cultures were maintained until DIV14, where synaptic maturity has been demonstrated (50-52), KCl treatment no longer upregulated Npas4 or altered NogoA protein expression (data not shown; $n=3-4$, $p>0.1$). Interestingly, synaptically mature DIV14 cultures showed elevated levels of NogoA, when compared to more immature DIV7 cultures (data not shown). Nevertheless, it is worthwhile to point out that the increased mobility of the NogoA band could still be observed with bath applied KCl, and restored with EGTA pre-treatment (Figure 2-3A).

While continuous neuronal membrane depolarization with KCl still provides some insight into over-activated physiological state, we were curious more specifically about the bidirectional modulation of synaptic activity, and how it affects NogoA. To that end, we took advantage of neuronal networks' ability to globally scale synaptic drive at an individual unit neuron level to counteract chronic changes in external stimuli (26, 27). In more detail, we allowed formation and maintenance of structurally intact and functional

synapses (39-42), and treated DIV14 neurons for 24 or 48 hours with the following pharmacological reagents to induce homeostatic synaptic scaling: 2 μ M tetrodotoxin (TTX), which competitively blocks voltage-gated sodium channels and prevents action potential propagation, or 40 μ M bicuculline (BIC), which competitively blocks GABA_A receptors and significantly reduces inhibitory tone (26). Following drug treatments, cultures were subjected to cell surface biotinylation to label surface proteome, which can be precipitated with streptavidin-beads and analyzed by Western blotting in conjunction with total cell extracts. We first verified that these cultures were synaptically mature to sufficient levels to induce synaptic scaling. Consistent with previous reports (26, 28), in our studies, total GluA1 levels increased by ~15% after 48 hours of TTX treatment ($n=5$, $p=0.0015$), and decreased by ~30% after 48 hours of BIC treatment ($n=7$, $p=0.0106$). Surface GluA1 levels increased by ~17% after 48 hours of TTX treatment ($n=6$, $p=0.0377$), and showed a strong (~36%) but not statistically significant decrease with 48 hours of BIC treatment ($n=6$, $p=0.1223$). In the same cultures, total levels of NogoA did not significantly change following TTX or BIC treatments ($n=6-7$, $p>0.17$). However, NogoA at the cell surface was significantly and bidirectionally regulated in an opposite manner to that of GluA1: decreased by ~45% following 48 hours of TTX ($n=7$, $p=0.0001$), and increased by ~70% after 24 hours of BIC treatment ($n=5$, $p<0.0001$) (Figure 2-3B). This was the first demonstration that NogoA trafficked to and from the cell surface can be regulated with changes in neuronal network activity.

As an independent assessment for activity-dependent regulation of neuronal NogoA at the cell surface, we employed immunofluorescence staining of primary hippocampal neurons under permeabilized and non-permeabilized conditions. We

qualitatively assessed total and surface levels of GluA1 and NogoAB expression. In both conditions, GluA1 staining co-localized exclusively with somatodendritic marker MAP2, delineated dendritic spines, and showed a robust increase with 48 hours of TTX treatment. Under permeabilized conditions following 48 hours of TTX, whereas perinuclear and dendritic NogoAB staining showed modest decrease, axonal NogoAB intensity remained unchanged. Under non-permeabilized conditions, discrete and discontinuous patches of surface NogoAB signal were reduced with 48 hours of TTX treatment (Figure 2-3C). Altogether, these findings suggest that NogoA at the neuronal cell surface is regulated by network synaptic activity, in opposite direction to GluA1.

2.3.3 Intracellular Neuronal NogoA is Phosphorylated at Ser-343

Given how PTMs have been shown to dictate receptor localization, conformation, and function (32-34), we investigated how NogoA might be differentially phosphorylated at baseline, homeostatic scaling up and down (Figure 2-3B-C). Previous studies from our laboratory have affinity-purified NogoA from untreated and chronically TTX-treated primary rat hippocampal cultures, and analyzed PTMs by mass spectrometry. Under basal conditions, with ~68-72% coverage of the entire protein, this analysis revealed a plethora of post-translational modifications, including numerous phosphorylation sites (Table 2-1). Comparison between untreated and TTX-treated NogoA revealed no significant differences in phosphorylation site occupancy or ubiquitination (Table 2-2) (53). This was our first indication that NogoA surface trafficking and/or band separation might in fact due to multiple, concurrent post-translational modifications.

In 2017, Diering *et al.* published an interesting study, using tandem mass tag spectrometry to investigate differential phospho-proteome in the post-synaptic densities of the mouse forebrain isolated at either sleep (10AM) or wake (10PM) states. They found that GluA1 phosphorylation at ser-845 and ser-831 increased by ~50% in PSD proteome between wake and sleep forebrains (29). This further verified that these PTMs initially identified in *in vitro* settings under different pharmacological reagents and artificial physiological states (28, 35-37) do indeed translate to some learning and behavior function *in vivo* (29). Studying the whole list of identified proteins, phosphorylation of which showed significant change between wake and sleep states, we noticed Rtn4 phosphorylation sites that increased by a factor anywhere from 50% to 450% between wake and sleep states. The greatest change in mouse NogoA between wake and sleep states was phosphorylation at ser-344 with 450% increase (29). This phosphorylation site is evolutionarily conserved (Figure 2-4A), and was independently identified in hippocampal neurons at baseline neuronal activity state (Table 2-1) (53). We therefore decided to investigate this NogoA phosphorylation site in greater detail.

We raised and characterized a polyclonal antibody against the rat NogoA, phospho-ser-343 (Figure 2-4A). We then tested the specificity of this antibody by analyzing cell lysates that express endogenous levels of NogoA following control lentiviral infection with Empty-Vector-GFP (LV-EV), or undetectable levels of NogoA following lentiviral infection with the previously characterized and published NogoA-shRNA-GFP (LV-shNogoA) (24). Loading was duplicated, and the entire blots were probed with two different antibodies: one was α -NogoAB Bianca antibody that recognizes both ~200kDa and ~50kDa bands corresponding to NogoA and NogoB

isoforms respectively (2, 9), and the other was our custom-made α -NogoA p-S343 antibody. As reported previously, α -NogoAB antibody revealed that the LV-shNogoA depleted all detectable NogoA expression while retaining NogoB expression to control levels (24, 53). On the other hand, our α -NogoA p-S343 antibody strongly and specifically detected NogoA around the ~200kDa molecular weight, along with some minor, non-specific bands at lower molecular weight that did not disappear in cultures transduced with the LV-shNogoA (Figure 2-4B). Next, we wanted to verify whether our custom α -NogoA p-S343 antibody specifically detected a phosphorylation site within NogoA itself, and not any other phospho-protein with a molecular weight of ~200kDa. We immunoprecipitated NogoA with a mouse monoclonal antibody directed against the NogoA- Δ 20 domain (11C7) (9) from an E18.5 rat whole brain, and subjected samples to Western blotting, probed blots with anti-NogoAB and anti-NogoA p-S343 custom antibodies. Compared to the isotype-matched control α -BrdU antibody or empty beads, 11C7 successfully immunoprecipitated NogoA around ~200kDa molecular weight. While our α -NogoA p-S343 antibody revealed nonspecific bands around ~100 and ~150kDa, only the band around ~200kDa was heavily enriched by the NogoA immunoprecipitation (Figure 2-4C). Our final verification was to check if the antibody really detects a specific phosphorylation mark on NogoA. To address that question, solubilized neuronal lysates were treated with lambda phosphatase (λ -PP) *in vitro*, and analyzed by Western blotting. Signal obtained with α -AKT p-S473 or α -NogoA p-S343 antibodies was completely abolished with the λ -PP treatment, demonstrating strong phospho-specificity. When these blots were consecutively probed with the α -pan-AKT and α -NogoAB antibodies, signal was successfully recovered, albeit at a significantly lowered

molecular weight and signal intensity than that of the input due to robust dephosphorylation reaction (Figure 2-4D). Overall, this was sufficient evidence to indicate target-specificity of our custom-made α -NogoA p-S343 antibody.

Since our studies were so far carried out with neuronal hippocampal culture or whole brain lysates, we were curious whether NogoA phosphorylation was restricted to a specific cell type. So we investigated NogoA p-S343 expression within direct comparison of culture lysates obtained from perinatal rat neocortical astroglia and embryonic rat hippocampal neurons (Figure 2-2B). Neuronal cultures had specific, strong, but variable signals for NogoA phosphorylation. Strikingly, even the astroglial culture with the strongest NogoA expression showed no detectable NogoA phosphorylation with our custom antibody (Figure 2-4E). We were then curious whether alternate NogoA phosphorylation levels could be correlated with differential NogoA expression on the cell surface. We then revisited lysates from Figure 2-2D, where neurons were treated with 2 μ M TTX, 10 μ M AMPA, and 200nM K252a. Previous studies from our laboratory had demonstrated that acute treatment with a low dose of K252a inhibits TrkB in neuronal cultures, and causes a small, but persistent increase in NogoA band mobility, which could be interpreted as a downward shift in NogoA molecular weight. On the other hand, treatment with TTX or AMPA was shown to reveal a double band separation of NogoA, which was abolished with λ -PP treatment. However, neither observation could be definitively explained (53). Since we here demonstrated that TTX also reduces surface NogoA expression, this was an opportune moment to investigate NogoA phosphorylation as a function of surface trafficking. To that end, we subjected total, intracellular, and surface protein lysates to Western blot analysis, once again

verified correct compartmentalization, and assessed NogoA p-S343 levels. Whereas baseline and K252a treatment revealed a singular band with higher p-NogoA mobility, TTX and AMPA treatments revealed a singular band with lower p-NogoA mobility (Figure 2-4F). This was the first evidence that collective rat NogoA phosphorylation events could account for the observed molecular weight shift. Strikingly, however, NogoA S343 phosphorylation was completely undetectable from the surface proteome, even if NogoA itself was expressed at low levels. In fact, when the same blot was consecutively probed with α -pan-NogoAB antibody, the missing second bands from the total and intracellular pool, as well as the surface expression of NogoA could be recovered (Figure 2-4F). This suggested that the cell surface trafficking of neuronal NogoA was dependent on the dephosphorylation of the ser-343 residue.

In order to claim that NogoA S343 phosphorylation was specific to neurons, we wanted to exclude another glial type that heavily expressed NogoA: myelinating oligodendrocytes. We also wanted to investigate if NogoA localizing to the synaptic sites could retain phosphorylation before or after being trafficked to the cell surface. To address both questions, we analyzed previous samples from the adult female rat hippocampus or neocortex subcellular fractionation (Figure 2-2E), but probed for NogoA p-S343 expression. Interestingly, NogoA localized to the synaptosomes did express considerable levels of S343 phosphorylation, albeit without a visible enrichment as seen with pan NogoA expression (Figure 2-4G). What was more striking were the undetectable levels of NogoA S343 phosphorylation from the crude myelin (Figure 2-4G). Before we made further claims, we wanted to check whether the lack of NogoA S343 phosphorylation was a technical impediment instead of a biological phenomenon.

We reasoned that perhaps the detection of the α -NogoA p-S343 antibody was blocked by biotinylation itself, or overlooked due to the already lower NogoA expression within the crude myelin. To address these issues, we used 10-15 μ g of the crude myelin isolated from the cortex, treated the precipitates with PBS or the biotinylation reagent *in vitro*, and analyzed NogoA expression and phosphorylation by Western blotting. Even with higher amount of myelin membranes and NogoA expression, there was still no detectable NogoA p-S343 signal. As a result, treatment with the biotinylation reagent could not offer more information (Figure 2-4G').

We intended to verify our understanding of the NogoA p-S343 expression pattern and subcellular localization by supplementing our biochemical data with immunofluorescent visualization. To that end, we cultured embryonic rat hippocampal neurons, and transiently transfected them with the NogoA-shRNA-GFP at low efficiency. We then studied GFP⁺, NogoA-depleted neurons in comparison to the GFP⁻, NogoA-expressing neighbors. Whereas the strong perinuclear NogoA signal was almost completely abolished in the shRNA-transfected, GFP⁺ cells, signal retrieved from the α -NogoA p-S343 antibody remained unchanged. In fact, the expression pattern of this mostly nuclear signal did not overlap with NogoA expression altogether. This unfortunately suggested that this custom-made antibody did not work well or specifically for immunofluorescent staining, at least under these stereotypical conditions (Fig 4H). Consequently, the rest of the NogoA phosphorylation studies will henceforth be dependent on Western blot analysis.

We then wanted to recapitulate the findings of the initial study by Diering *et al.*, and show fluctuation of NogoA phosphorylation within the forebrain PSD as a function

of neuronal activity in wake and sleep states (29). Despite the highly similar sequence homology, our custom-made α -NogoA p-S343 antibody did not cross-react with the mouse NogoA (data not shown). Hence, subcellular fractionation from the CNS regions of the C3H mice (Figure 2-2F) could not be used to study NogoA S343 phosphorylation. As a result, we switched to carrying out these experiments with adult male Sprague-Dawley rats, which have been reported to entrain intact circadian rhythmicity (54). Rats were euthanized at 10AM (sleep) or 10PM (wake) regardless of the current sleep state at the time, tissue were flash frozen, homogenized, and fractioned in a discontinuous sucrose gradient for synaptosome isolation and PSD enrichment. We probed these samples for pan and p-S845 GluA1, as well as pan and p-S343 NogoA (Figure 2-5A). Surprisingly GluA1 expression or phosphorylation did not increase between wake and sleep states. As expected, however, total NogoA levels remained pretty stable across both compartments and timepoints. Interestingly, phosphorylated NogoA ratio seemed to have slightly decreased from sleep to wake states ($n=3$, $p=0.2382$ for Syn, $p=0.7790$ for PSD) (Figure 2-5A'). Overall, these *in vivo* studies proved inconclusive, possibly due to a failed entrainment of circadian rhythm in our shared animal facilities, as opposed to specialized light- and motion-controlled compartments used for these studies.

Before tackling the complex physiological relevance of this singular phosphorylation event, we wondered whether simplistic manipulations over neuronal activity states would change NogoA phosphorylation. We acutely treated forebrain or hippocampal neurons with 55mM KCl, 2 μ M TTX, or 50 μ M BIC, and assessed protein expression by Western blot analysis (Figure 2-5B). TTX reduced the baseline expression of the immediate-early transcription factor Npas4, whereas KCl on DIV7 and

BIC on DIV14 induced robust upregulation (49). As we also demonstrated earlier (Figure 2-3A), KCl significantly reduced the molecular weight of pan-NogoA band (Figure 2-5B). More importantly, NogoA p-S343 molecular weight as well as expression signal intensity also reduced statistically significantly with both timepoints of KCl treatment ($n=3$, $p<0.0002$) (Figure 2-5B'). TTX caused a band separation of the NogoA signal, while not changing total expression level as we have shown before (Figure 2-3B-4F). When we assessed NogoA phosphorylation, we could see a clear increase in molecular weight with TTX treatment, and a slight decrease with BIC. However, interestingly enough, neither TTX or BIC treatment on DIV14 changed the relative or absolute phosphorylated NogoA expression (Figure 2-5B). Altogether, these data suggest that while different neuronal activity states do indeed induce deposition or removal of phosphate groups on NogoA as inferred from molecular weight shifts, once synaptogenesis is nearly complete, the turnover is so highly regulated that the total levels remain similar at various snapshots. This is evident by the TTX timecourse: by short timepoints such as 30 minutes, change in NogoA mobility or molecular weight shift does not occur yet. However, longer acute treatments (Figure 2-5B) or chronic treatments (Figure 2-3B-4F) all induce a clear NogoA band separation. Moreover, NogoA phosphorylation is clearly affected by neuronal development and synaptogenesis *in vitro*. Whereas TTX and BIC only change phosphorylated NogoA mobility, KCl treatment leads to the removal of enough phosphate groups to cause both a downward molecular weight shift and reduced expression (Figure 2-5B). This implicates the signaling mechanism divergent between membrane depolarization and synaptic transmission modulation. Lastly, phosphorylated NogoA being completely

absent from the cell surface (Figure 2-4F) signals physiological importance for balance between endocytosis and exocytosis.

As phosphorylation events serve transitory physiological function and are therefore often labile, we were curious about the reversibility of the phosphorylation mark deposited on rat NogoA ser-343. Because we demonstrated that TTX and K252a changes NogoA mobility via the addition or removal of phosphate groups on NogoA, we wondered whether the combinatorial treatment of these two pharmacological reagents would override the effect of one. To address that question, we chronically pre-treated cultures with TTX, and combined with a low dose of acute K252a treatment. Interestingly enough, the differential mobility as well as the slight reduction of expression of NogoA p-S343 induced by TTX treatment alone could no longer be sustained in the presence of K252a (Figure 2-5B’). In order to increase our confidence, we also verified the bioreactivity of K252a by detecting the robust and consistent increase in AKT phosphorylation at ser-473, as reported previously (55). Altogether, these findings suggested that the phosphorylation induced by chronic TTX treatment can be negated by an acutely activated mechanism, implicating a dynamic and labile signaling imposed upon NogoA.

At this point, we wanted to describe the molecular players or a signaling cascade leading to the phosphorylation of NogoA at ser-343. We were initially curious whether NogoA-NgR1 complex signaling might be involved in regulating NogoA phosphorylation. To that end, we treated cultures with 20 μ M ROCK inhibitor Y27632 ($n=2$) or 30 μ M myosin II ATPase inhibitor blebbistatin ($n=3$), thereby counterbalancing this signaling cascade’s inhibitory effects on neuronal growth (56-58). Neither treatment significantly

altered pan or phosphorylated NogoA expression (Figure 2-5D''-E). We then shifted our balance to PKA, since it has been implicated to phosphorylate an E3 ubiquitin ligase that marks NogoA for degradation in heterologous systems (59). However, neither activation with 10 μ M forskolin ($n=1$) nor inhibition with 2 μ M KT5720 ($n=1$) changed showed any change (Figure 2-5D''-E). Then we completely shifted gears, and focused on the mTOR pathway, since inhibition of the upstream BDNF-TrkB signaling by K252a revealed molecular weight shifts (Figure 2-4F-5B''). Additionally, mTOR pathway is especially important for local protein synthesis required for the induction of LTP and many other forms of synaptic plasticity (60-62). Therefore, we treated cultures with 20ng/mL rapamycin ($n=1$), and assessed mTOR and S6K phosphorylation for verification, as well as NogoA expression and phosphorylation. Even when these two kinases were drastically shut off with this treatment, NogoA remained completely unaffected (Figure 2-5D'-E). Lastly, we investigated the possibility of calcium-dependent signaling, since this complex signaling cascade plays an important role for synaptic transmission and most forms of plasticity (63-65). We initially looked at CaMKII, as it interacts directly with F-actin (66), or translocates to the synapse to activate RAS-ERK signaling, leads to the phosphorylation of the GluA1-anchoring protein stargazin, or directly phosphorylates GluA1 to increase calcium conductance (67). So, we inhibited CaMKII activity with 1 μ M KN-93 ($n=10$) or blocked L-type voltage-gated calcium channels (VGCC) with 10 μ M nifedipine ($n=9$), respectively. KN-93 treatment induced a double band NogoA formation, and led to a slight increase of phosphorylated NogoA ratio, albeit not statistically significant ($n=10$; $p=0.0678$ for 30m, $p=0.1242$ for 2h) (Figure 2-5E). On the other hand, L-Type VGCC inhibition showed absolutely no

change in NogoA expression or phosphorylation. For our last target, we chose the Ca^{2+} /CaM-dependent serine/threonine protein phosphatase calcineurin, as it is heavily implicated in many forms of synaptic plasticity, especially including homeostatic synaptic plasticity (68). We treated cultures with 5 μM cyclosporin-A ($n=3$) to inhibit calcineurin, and assessed protein expression and phosphorylation by Western blotting. Upon verifying bioreactivity and dosing by observing increased GluA1 phosphorylation at ser-845 (68), we assessed NogoA expression and phosphorylation. Even though longer treatments with cyclosporin-A induced a greater separation of NogoA bands, neither total expression nor phosphorylation significantly changed even by 48 hours of treatment (Figure 2-5D'''-5E). Overall, we are still left with an unknown mechanism or kinase-phosphatase pair responsible for NogoA phosphorylation at ser-343 residue. Future investigations could incorporate techniques like biotinylation by antibody recognition (BAR) (69) or BioID (70) to study direct and dynamic protein-protein interactome in an unbiased fashion to identify possible kinase or phosphatase partners.

2.4 Discussion

Here, we detail a thorough initial characterization of NogoA, for the first time as a protein that is affected by other physiological events or signaling, and not as the one responsible for entraining them. Firstly, we describe our current system, its cell-type composition, and the limitations this impurity might bring onto the conclusions drawn from these findings. Next, we characterize NogoA expression as principally of a neuronal origin, localizing to the somatodendritic regions in high levels, to axons to a lesser extent, and to the cell surface at a ~5-10% fraction of total expression. Given that expression pattern, we successfully replicated previous findings that discovered strong NogoA expression within synaptosomes as well as post-synaptic densities (21), while extending this knowledge to different CNS regions to offer a deeper understanding of relative NogoA expression. Moreover, we offer an expression comparison between synaptosomes and crude myelin, despite the oligodendrocytic origins of NogoA's initial discovery. Finally, we demonstrate that despite being a resident ER protein, NogoA does localize to the neuronal cell surface, and that expression pattern is much more malleable than the intricate balance between NogoA production and degradation.

Since blocking NogoA function has already been shown to release the inhibitory brakes on activity-dependent synaptic plasticity, we were wondering whether or not neuronal activity was regulating NogoA expression, thereby closing the feedback loop. After we defined our system and characterized NogoA expression pattern, we tested this hypothesis by continuously depolarizing neuronal membranes as well as chronically modulating synaptic activity. We found that early on in culture development and

synaptogenesis, total NogoA expression can be downregulated by sustained membrane depolarization, while the mechanism in charge becomes stunted later on. At that fully mature and functional stage, different neuronal network activity states become in charge of modulating surface expression of NogoA in a bidirectional manner. All of this complex mechanism of action can be conceptualized as maintaining synaptic homeostasis. For instance, when neuronal networks are chronically silenced or deprived of external stimuli, disruption of inhibitory signaling by endocytosis of NogoA could either be sufficient alone to release pronounced synaptic inhibitory tone, or lead the way to exocytosis, synaptic diffusion, or anchoring of GluA1 for higher levels excitatory synaptic transmission.

In an attempt to elucidate how an ER-resident, principally intracellular protein such as NogoA can be trafficked onto the cell surface, we turned to post-translational modifications. Inspired by a recent report investigating total and phosphorylated proteome within the mouse PSD at wake and sleep states (29), we identified a phosphorylation site at ser-343 of the rat NogoA as a possible candidate for relaying activity-dependent, physiologically-relevant PTM in charge of regulating NogoA localization and function. We created a custom-designed polyclonal antibody against this NogoA phospho-site, and thoroughly characterized its detection pattern and specificity via Western blot analysis. First of all, we discovered that this phosphorylation event is unique to neurons – or at least nearly absent from astroglia and crude myelin. Next, we found that NogoA phosphorylated at this site is removed from the neuronal cell surface. This was an exciting finding, namely because these data might be interpreted as phosphorylation mark deposited by a specific kinase being somehow translated as a

signal for NogoA endocytosis. Alternatively, NogoA might be trafficked to the cell surface only when the phosphorylation mark is removed by a responsible phosphatase. This question itself yields an interesting problem to be tackled by future investigations.

Lastly, we modestly attempted to explore the physiological role of the NogoA phosphorylation *in vivo*, by studying rat synaptosomes and PSD fractions isolated from wake and sleep forebrain. Even though we failed at obtaining conclusive evidence, possibly due to lack of proper equipment to entrain a robust and well-controlled circadian rhythm onto male rats, there were trends of regulation of phosphorylated NogoA. When we turned back to our neuronal culture system, we discovered that KCl-induced, sustained membrane depolarization at early stages of *in vitro* development significantly reduced molecular weight, expression, and phosphorylation of NogoA. What is more intriguing was that not the molecular weight change, but the robust downregulation of phosphorylated NogoA expression disappeared as neurons underwent synaptic maturation. In other words, as neurons morphologically grew and synaptically matured, as network circuitry is stably molted, levels of total NogoA expression and phosphorylation became less sensitive or responsive to network activity changes, reminiscent of the closure of the critical period within the visual pathway (10, 11). We also tried a cohort of pharmacological inhibitors to identify the kinase/phosphatase partners responsible for NogoA ser-343 phosphorylation. To our surprise, when we pharmacologically inhibited neuronal growth-restrictive proteins particularly implicated downstream of NogoA-NgR1 signaling, such as ROCK or myosin II ATPase, we did not observe any significant change in total NogoA expression or phosphorylation level. Although this limited and biased search did not lead any fruitful

conclusions, we learned that the inhibition of BDNF-TrkB signaling could override NogoA phosphorylation. However, direct inhibition of mTOR or S6K phosphorylation by application of rapamycin was not sufficient to reduce molecular weight or expression of phosphorylated NogoA. These two findings alone significantly narrow down the list for future investigations. Overall, this body of work is a first step to acknowledge the gaps of knowledge within the literature on NogoA expression, localization, and function.

2.5 Materials and Methods

2.5.1 Animals

All procedures and experiments were approved by the University of Michigan Institutional Committee on the Use and Care of Animals (ICUCA) and were performed in accordance with guidelines developed by the National Institutes of Health (NIH). Time-pregnant adult Sprague-Dawley female rats were purchased from Charles River Laboratories, MA, USA. Adult male C3H/HeNTac mice were purchased from Taconic Biosciences, NY, USA. Adult Sprague-Dawley male rats were donated from the University of Michigan's Unit for Laboratory Animal Medicine (ULAM) Rodent Recycling Program.

2.5.2 Primary Neuronal Cultures

Time-pregnant female rat was euthanized, first by flow-controlled CO₂ influx, then by cervical dislocation. The abdomen was disinfected consecutive application of 70% ethanol and povidone-iodine solution. Surgical scissors and forceps were sterilized with 70% ethanol. Uterus was exposed with a wide bilateral incision, E18.5 rat embryos were extracted and placed into a sterile 10-cm petri dish (Fisher Scientific FB0875712) filled with Leibovitz's L-15 solution (Gibco 21083-027) supplemented with 1:100 Penicillin/Streptomycin (P/S) (Gibco 15140-122). Embryos were removed out of the amniotic sacs and transferred into fresh L-15 with P/S, heads were decapitated, brains

were exposed and cleaned of meningeal membranes. Either hippocampus alone or hippocampus combined with the neocortex (forebrain) was microdissected under a standard dissecting scope. Tissue was collected in conical test tubes, washed with Hanks' Balanced Salt Solution (HBSS) free of Ca^{2+} , Mg^{2+} , and phenol red (Gibco 14175-095). Tissue was digested fresh HBSS supplemented 1:1 with 0.5% Trypsin-EDTA (Gibco 15400-054) and 1:10 with DNase I dissolved in 10mL solution (Roche 10104159001) for 15-20 minutes in 37°C water bath with gentle agitation. Digestion was halted by 5 minute incubation with ice-cold 10% fetal bovine serum (FBS) (Gibco 16000-036) in 1x Dulbecco's Modified Eagle Medium (DMEM) with high glucose and no glutamine (Gibco 11960-044). Following another wash with the same solution, tissue was washed two more times with Neuronal Growth Medium (NGM): Neurobasal (Gibco 21103-049) with 25mM D(+)-glucose (Sigma G6152), 2mM Glutamax I (Gibco 35050-061), 50 units/mL penicillin and 50µg/mL streptomycin (Gibco 15140-122), and 2% B-27 supplement (Gibco 17504-044). Tissue was initially triturated with one pass through a P1000 pipet tip in 1mL NGM, then triturated approximately 10x times through flame-polished Pasteur pipette (VWR 14673-010) to fully dissociate into single cell suspension. After cell count with Trypan blue solution (Gibco 15250-061) and a hemacytometer, approximately 700000-800000 cells were plated per well of 100µg/mL poly-D-lysine (Sigma P7886) coated 6-well plate (TPP TP92006) containing 2mL of NGM. Alternatively, 50000-70000 cells were seeded onto a 12-mm coverslip (Carolina Biological Supply 633029) coated with 500µg/mL poly-L-lysine (Sigma P2636) in 30-50µL NGM, then supplemented with 500µL pre-warmed NGM after cells were observed to adhere. Cells were maintained *in vitro* with half-media changes every 2-3 days with

equal volume of pre-warmed fresh NGM and neuronal conditioned media (NCM). For cultures that required advanced synaptic formation and maturity, cells were fed with a 1:1:1 mix pre-warmed NGM, NCM, and astrocyte-conditioned media (ACM) supplemented with B-27, P/S, and 2 μ M cytosine arabinoside (AraC) (Sigma C1768). Due to empirical observation of B-27 lot-to-lot variability, a system had to be devised to select and use only the optimal B-27 lot, so as to maintain consistency between each culture preparations. What worked best was maintaining hippocampal cultures in NGM with various lots of B-27, treating neurons on DIV7 with 55mM KCl for 2 hours to induce continuous membrane depolarization, and verify robust protein expression upregulation of the of the immediate-early transcription factor Npas4 (49). The reserved B-27 lot with the highest satisfactory upregulation was ordered in sufficient supply to last 6 months to a year, kept frozen at -20°C, aliquoted and used as appropriate.

2.5.3 Primary Astroglial Cultures

A modified version of the previously published cortical astrocyte isolation protocol was followed (71). Briefly, 6x post-natal day (P)0 Sprague-Dawley rat pups were sprayed with 70% ethanol and sacrificed. Brains were removed, washed with, and dissected in Dulbecco's Phosphate Buffered Saline (DPBS) (Gibco 14287-080). Cortical tissue was microdissected and cut into small pieces, approximately 1-2mm in size. Then, most of the Ca²⁺ and Mg²⁺-containing DPBS was removed, and tissue was transferred into 37°C-equilibrated Ca²⁺- and Mg²⁺-free DPBS (Gibco 14190-144) with 160U of Papain (Worthington Biochemical LS003126), 5000U of DNase I (Worthington

Biochemical LS002007), and 2mg L-cysteine hydrochloride (Sigma C7477). Tissue was digested at 34°C for 45 minutes, with intermittent gentle agitation. After digestion, tissue was re-suspended in 10X Low-Ovomucoid solution, containing 3g bovine serum albumin (BSA) (Sigma A8806), 3g Trypsin inhibitor (Worthington Biochemicals LS003086) prepared in DPBS. After trituration for about 2 rounds of 10 passes, tissue was centrifuged at 1100 rpm for 11 minutes at room temperature before another round of trituration in High-Ovomucoid solution, containing 6g BSA and Trypsin inhibitor. Once centrifuged, cells were re-suspended in Astrocyte Growth Medium (AGM), which is a modified version of NGM, where 10% heat-inactivated donor equine serum (HyClone SH30074.03) replaced D(+)-glucose and B-27 supplement. After filtering the cell suspension, counting viable cells, centrifuging and re-suspending the cell pellet in AGM, approximately 20 million cells were plated onto a 10µg/mL poly-D-lysine (Sigma P6407) coated 75 cm² flask (TPP TP90075) with 15mL of AGM. After a half media change with fresh AGM on DIV 1, flasks were allowed to reach confluence on about DIV3, during which time flasks were agitated vigorously until holes in the astroglial layer were created. After most contaminating non-astroglial cells were sufficiently shaken off, fresh AGM was added to the flask. On DIV5, another half-media change was carried out, this time with a final concentration of 2µM AraC (Sigma C1768) to inhibit mitotic fibroblast proliferation. Before initiating the collection of ACM, astrocytes were diligently washed with AGM, this time containing only 1% donor equine serum. Later on, ACM was collected every 3-5 days for approximately 1.5 months. Each collection was immediately filtered and stored at -20°C. At the termination point of the astroglial cultures, all

collected and stored ACM were thawed overnight at 4°C, combined, filtered once again, and aliquoted for future use with neuronal cultures.

2.5.4 Pharmacological Treatments

Neuronal cultures were treated with the following pharmacological reagents with reported final concentrations, catalog numbers, and solvents: 55mM potassium chloride (Fisher Scientific P330) [Neurobasal], 5mM EGTA (Sigma E8145) [Neurobasal], 2μM tetrodotoxin citrate (Abcam ab120055) [ddH₂O], 40-50μM (+)-bicuculline (Tocris 0130) [DMSO], 200nM K252a (Calbiochem 420298) [ddH₂O], 10μM AMPA (Sigma) [ddH₂O], 20μM Y27632 [DMSO], 30μM blebbistatin [DMSO], 10μM forskolin (Sigma F6886) [DMSO], 2μM KT5720 (Tocris 1288) [DMSO], 1μM KN-93 (EMD Millipore 422711) [ddH₂O], 10μM nifedipine [DMSO], 20ng/mL rapamycin [Ethanol], 5μM cyclosporin-A (Tocris 1101) [DMSO].

2.5.5 Transient and Sparse Transfection

Primary hippocampal neuronal cultures were transfected on DIV3 for highest survival and transfection efficiency. For each well of a 24-well plate, 0.5μg plasmid amplified and purified in endonuclease-free solutions was mixed with 1μL of Lipofectamine 2000 (Sigma L3000008) and OptiMEM (Gibco 31985070). Following brief incubation at 37°C, this solution was mixed with NGM and used to replace whole media covering the coverslips for 3-4 hours. Lastly, saved NCM and fresh, pre-warmed NGM

were combined 1:1, and replaced the entirety of the media per well. If the transfected plasmid has a fluorescent marker or a molecular tag, transfection efficiency was qualitatively assessed under an epifluorescent microscope prior to fixation and staining, which followed at least 3-4 days after transfection to see full expression. For transient and sparse knockdown of NogoA, we used the GFP-tagged plasmid with shRNA against NogoA, which was received from Dr. Christine Bandtlow, amplified, and purified in-house. The sequence of the previously published shRNA against NogoA is as follows: AAGATTGCTTATGAAAC (24).

2.5.6 Lentiviral Transduction

All lentiviral preparations used in this study were conducted by the University of Michigan Vector Core. If the plasmid packaged into the lentiviral particles contained a fluorescent marker, Vector Core transduced A549 cells with the lentivirus at 1X concentration, and quantified the percentage of fluorescent cells on an epifluorescent microscope. Their reported transduction efficiency ranged from 90-95%. Although a formal fluorescent quantification was never carried out with primary neurons, qualitative assessment reveals ~80% transduction efficiency. Regardless, transduction efficiency was always measured as a function of remaining protein product, as detected by Western blot analysis. Most lentiviral transductions were carried out on DIV3-6, with the exceptions of co-infections of multiple lentiviruses. Importantly, at least 4 days were allowed following any lentiviral transduction before cells were fixed or lysed for analysis. Lentiviral preparations ranged from 10X to 500X stock concentrations in Neurobasal,

depending on the scale of the production. However, the final viral concentration used in this study has always been kept at 1X, since repeated or higher load of viral content could very well change neuronal physiology. All lentiviral transductions were carried out in half media changes with fresh and pre-warmed NGM. If ACM were to be supplemented to a neuronal culture that had received lentiviral transductions on DIV3, at least 2 days were allowed so as to prevent counteracting influence of the donor equine serum on lentiviral transduction efficiency. For knockdown of NogoA, Dr. Christine Bandtlow's shRNA (described above) was cloned into the GFP-tagged pLentilox3.7 plasmid obtained from the UM Vector Core, and packaged into concentrated lentivirus.

2.5.7 Immunofluorescence Labeling

Cells were washed with 1x Phosphate-Buffered Saline (PBS) pH 7.4, and fixed with 4% paraformaldehyde (Sigma 158127), often supplemented with 4% sucrose (Fisher Scientific S5-3) for 15 minutes at room temperature. Following additional PBS washes, cells were permeabilized with 0.3% Triton X-100 (Sigma T8787) prepared in 1x PBS for 5 minutes. For staining with extracellular epitopes of cell surface proteins, this step was omitted. Cells were then blocked with 5% donkey serum (EMD Millipore S30), 0.1% Triton X-100 (omitted for extracellular staining) in PBS for 1 hour at room temperature, and incubated overnight at 4°C with 1:500 dilutions of the following primary antibodies: chicken anti-GFAP (EMD Millipore AB5541), rabbit anti-GFAP (Dako Z033429-2), rabbit anti-CD11b (Abcam ab133357), rabbit anti-Olig2 (EMD

Millipore AB9610), goat anti-NogoAB (R&D Systems AF3098), mouse anti-NogoA (11C7, courtesy of Martin E. Schwab), chicken anti-MAP2 (Abcam ab92434), mouse anti-MAP2 (Abcam ab36447), rabbit anti-Ankryin G (courtesy of Paul Jenkins), rabbit anti-GluA1-CT (EMD Millipore AB1504), mouse anti-GluA1-NT (EMD Millipore MAB2263). Following PBS washes, coverslips were incubated with species-specific, Cy- or Alexa fluorophore-conjugated secondary antibodies (Jackson ImmunoResearch Laboratories and Life Technologies) diluted at 1:500 in blocking buffer for 1 hour at room temperature. Nuclei were counterstained with 1:50000 Hoechst 33342 (Invitrogen) diluted in 1x PBS. Coverslips were washed extensively and mounted in antifade Prolong Gold (Thermo Fisher Scientific P36930) on microscope slides (Fisher 12-550-15). Coverslips were then imaged with a Zeiss Apotome2 microscope equipped with an Axiocam 503 mono camera and Zen software.

2.5.8 Cell Surface Biotinylation

Cell surface biotinylation experiments were performed on primary rat hippocampal neuronal cultures on DIV 13-14. 6-well plates of neuronal cultures were brought to room temperature momentarily before being placed on ice, at which point media were aspirated, and cells were washed three times with ice-cold 1x PBS supplemented with 1mM CaCl_2 and 0.5mM MgCl_2 . At the end of washes, cells were incubated with 1-2mg/mL EZ-LinkTM Sulfo-NHS-LC-Biotin reagent (Thermo Scientific 21335), which was equilibrated to room temperature for at least 30 minutes prior. The reaction was later on quenched with 3x washes of 1x Tris-Buffer Saline (TBS) pH 7.4

following removal of the biotin reagent. Neurons were then lysed for ~30 minutes on ice using ice-cold Brij lysis buffer (BLB): 10mM potassium phosphate pH 7.2 (Sigma P0662), 1mM EDTA (EMD Millipore 4010-OP), 10mM MgCl₂ (Sigma M8266), 50mM β -glycerophosphate (BGP) (Sigma G9422), 1mM Na₃VO₄ (Sigma S6508), 0.5% NP-40 (Fluka Analytical I3021, and 0.1% Brij-35 (Fisher Scientific BP345) containing 1:100 protease inhibitor cocktail (PIC) (Sigma P8340). Lysates were then centrifuged at 15000rpm (Eppendorf 5430R) for 5 minutes at 4°C, and supernatant was tumbled in an end-over-end tube revolver overnight at 4°C with pre-washed high capacity streptavidin agarose resin (Thermo Scientific 20359). Following centrifugation, bead resins were washed 3x times with 1x PBS and once with BLB, boiled in equal volume of 2x Laemmli sample buffer (BioRad 1610737) containing 1:20 β -mercaptoethanol (BME), and stored at -80°C until Western Blot analysis.

2.5.9 Crude Fractionation of Myelin, Synaptosomes, and PSD

Isolation of crude and concomitant fractionation of myelin, synaptosomes, and PSD of adult Sprague-Dawley rats and male C3H mice was performed as described previously with slight modifications (21, 29). Following concurrent CO₂-induced euthanasia, animals were decapitated and kept on ice. Different regions of the CNS tissue were dissected out in ice-cold 1x PBS supplemented with 1 mM CaCl₂ and 0.5mM MgCl₂. Tissue was combined with either 0.32M sucrose homogenization buffers: A. 0.32M sucrose, 0.1mM CaCl₂, 1mM MgCl₂, 25 μ M HEPES pH 7.4 (Sigma H4034), 1:100 PIC, 1mM Na₃VO₄, B. 0.32M sucrose, 10mM HEPES pH 7.4, 1mM EDTA, 5mM

sodium pyrophosphate (Sigma P8010), 1mM Na_3VO_4 , 200nM okadaic acid (EMD Millipore 495604), 1:100 PIC. Tissue was then homogenized with 12 strokes with the loose pestle, followed by another 12 strokes with the tight pestle in the tissue dounce homogenizer (Wheaton 06-435B). Tissue was centrifuged 1000xg for 10 minutes at 4°C, agitated, vortexed, and re-centrifuged at 500xg for 2 minutes at 4°C. Small fraction of homogenates was stored at this point for WB analysis. The remaining was underlaid with 0.80M and 1.20M sucrose solutions. Samples were subjected to an ultracentrifugation step at 100000xg (Beckman Coulter SW-41 Ti rotor, 28000rpm) for 2 hours at 4°C. Following ultracentrifugation, fractions at 0.80M/1.20M and 0.32M/0.80M interfaces were collected as synaptosomes and crude myelin, respectively. Myelin fractions were subjected to osmotic shock with 10mM HEPES pH 7.4 prepared in ddH₂O, and centrifuged at 10000xg (Beckman Coulter SW-41 Ti rotor, 9000rpm) for 10 minutes at 4°C. Pellets were transiently tried and initially reconstituted in PBS for protein concentration assays, diluted appropriately, boiled in equal volume of 2x Laemmli sample buffer containing 1:20 BME, and stored at -80°C until Western Blot analysis. Terminal synaptosome fractions were diluted with 0.1mM CaCl_2 , 1mM MgCl_2 and 0.2mM Na_3VO_4 in ddH₂O, and centrifuged at 17000rpm with SW-41 Ti rotor for 10 minutes at 4°C. Resulting pellet was treated the same way for WB preparation. Repurposed synaptosome fractions were combined with 1% Triton X-100, tumbled for 30 minutes at 4°C, and centrifuged at 14000rpm with SW-41 Ti rotor for 20 minutes. Resulting PSD pellet was treated the same way for WB preparation.

2.5.10 Lambda Phosphatase Treatment

Primary E18.5 rat hippocampal cultures were treated on DIV7 with 55mM KCl for 2 hours with or without 10 minutes of 5mM EGTA. Following treatments, cells were lysed in 100 μ L of RIPA buffer pH 8.0 supplemented only with 1:100 PIC, without any phosphatase inhibitors: 150mM NaCl (Fisher Scientific BP358), 50mM Tris (Fisher Scientific BP152), 1% NP-40, 3.5mM sodium dodecyl sulfate (Fisher Scientific BP166), 12mM sodium deoxycholate (Sigma D6750). Following thorough scraping, cell lysates were centrifuged for 3 minutes at 15000rpm at 4°C, and each tube's supernatant was split into two tubes. While input samples were directly processed by combining 1:1 with 2x Laemmli buffer with BME and boiling at 100°C for 10 minutes, reaction samples were subjected to the instructions followed by the supplier (NEB P0753S). Briefly, lysates were mixed with buffer constituents and active λ -PP, and intermittently shaken at 30°C for 1 hour. At the end of reaction, samples were processed for WB analysis in the same manner as input.

2.5.11 NogoA Immunoprecipitation

Three E18.5 rat embryo whole brains were pooled and lysed in BLB, homogenized using a pestle motor mixer (RPI 299200), vortexed thoroughly, and centrifuged at 15000rpm for 10 minutes at 4°C. Pellets were homogenized similarly for a second round of solubilization. Supernatants were pooled, diluted 5-fold in BLB to reach approximately 1mg/mL protein concentration, and pre-cleared with pre-washed protein

G Plus/protein A-Agarose beads (EMD Millipore IP10) during a 20 minute rotation at 4°C. Lysates were then combined with pre-washed beads, and one of the following: A. 5µg of 11C7 mouse monoclonal anti-NogoA antibody, B. 5µg of mouse monoclonal anti-BrdU antibody (epitope-matched control), C. nothing (negative control). Samples were tumbled in an end-over-end tube revolver overnight at 4°C; beads were washed extensively with PBS and BLB, while precipitating with brief centrifugation in between. Post-immunoprecipitation supernatant of each sample was saved and boiled in equal volume of 2x Laemmli buffer with BME for 10 minutes. Beads were precipitated with brief centrifugation, and prepared for WB in the same fashion. 20µL of input, immunoprecipitate, and post-immunoprecipitate was loaded and analyzed concurrently.

2.5.12 Development of anti-Rat NogoA p-343 Antibody

Phospho-specific polyclonal antibody production package was purchased from GenScript, NJ, USA. Briefly, New Zealand rabbits were immunized with an antigen consisting of a short peptide sequence with phosphorylated rat NogoA (DRVVSPEKTMDIFNC). Pre- and post-immune sera were collected from immunized rabbits, and phospho-specific antibody was affinity-purified. Specificity of the purified polyclonal antibody was tested by ELISA to assess direct binding to small peptide sequences of pan (lot no. U8894CE260-1) and phosphorylated (lot no. U7443CE260-1) rat NogoA at various dilutions. According to the reported ELISA results, at 1:4000 dilution or 250ng/mL final concentration of the purified antibody, binding to the phospho-

NogoA antigen was ~31.6 fold higher than that to the pan-NogoA antigen. This was the only dilution used at this study.

2.5.13 Western Blot Analysis

Primary neuronal and astroglial cultures, whole brains, and subcellular fractions of CNS tissue were solubilized in either BLB or RIPA buffer supplemented with 50mM BGP, 1mM Na₃VO₄, and 1:100 PIC. Briefly, cells were gradually brought to room temperature, extensively washed with ice-cold 1x PBS, lysed in complete lysis buffer for 20-30 minutes on ice, and scraped off the wells. Samples were centrifuged at 15000rpm at 4°C for 10 minutes, supernatant was transferred to a new tube, and protein concentration was measured with a *DC* Protein Assay Kit (Bio-Rad 5000111) using a photospectrometer at 750 nm (Molecular Devices SpectraMax M5e). Supernatant was then diluted with an equal volume of 2x Laemmli sample buffer with BME, boiled for 10 minutes, and stored at -80°C. If nuclear, and especially DNA-bound transcription factors were to be included in investigation, cells were directly lysed on the plate with 1:1 combination of RIPA buffer and Laemmli buffer. The resulting DNA-rich viscous lysate was scraped off and transferred into a fresh tube, boiled for 10 minutes to fully dissociate any forming pellet, and stored at -80°C. For SDS-PAGE, equal amounts of total protein (~5-10µg) for each sample were loaded per lane of a 7.5% gel. Separated proteins were transferred onto PVDF membrane (EMD Millipore IPVH00010) for 2 hours at constant 120V in cold transfer buffer: 25mM Tris, 192mM Glycine (Fisher G48), 10% methanol (Fisher Scientific A412P). Membranes were blocked in 5% blotting-grade

blocker (BioRad 1706404) prepared in 1x TBS-T [TBS pH 7.4 supplemented with 0.1% Tween-20 (Sigma P1379)] for 1 hour at room temperature, and probed overnight at 4°C with the following primary antibodies diluted in 3% BSA (Fisher Scientific BP1600) in 1x TBS-T: rabbit anti-NogoAB Bianca (courtesy of Martin E. Schwab, 1:25000), goat anti-NogoAB (R&D Systems AF3098, 1:5000), mouse anti-NogoA (courtesy of Martin E Schwab, 1:5000), rabbit anti-NogoA p-S343 (custom GenScript, 1:4000), rabbit anti-MAG (homemade serum, 1:1000), mouse anti- β -actin (Sigma A5441, 1:20000), mouse anti- β III-Tubulin (Promega G712A, 1:50000), rabbit anti-GFAP (Dako Z033429-2, 1:10000), mouse anti-GAPDH (Abcam ab8245, 1:5000), mouse anti-Transferrin Receptor (Invitrogen 13-6800, 1:1000), rabbit anti-AKT (CST 4691S, 1:5000), rabbit anti-AKT p-S473 (CST 4060S, 1:2000), rabbit anti-PSD-95 (EMD Millipore AB9708, 1:2000), mouse anti-Homer-1 (SCBT sc-17842, 1:250), rabbit anti-Npas4 (courtesy of Michael E. Greenberg, 1:1000), rabbit anti-GluA1-CT (EMD Millipore AB1504, 1:500), rabbit anti-GluA1 p-S845 (EMD Millipore AB5849, 1:1000), rabbit anti-p70 S6 Kinase (CST 9202S, 1:1000), rabbit anti-p70 S6 Kinase p-Thr389 (CST 9234L, 1:1000). Horseradish peroxide (HRP)-conjugated secondary IgG's were obtained from EMD Millipore with the following catalog numbers: AP136P (α -rat), AP182P (α -rabbit), AQ160P (α -mouse), AP106P (α -goat), AP147P (α -sheep). All HRP-conjugated secondary antibodies were diluted at half the dilution of the corresponding primary antibody in 3% BSA in 1x TBS-T, and the HRP signal was developed with various strengths of chemiluminescent substrates from Thermo-Fisher Scientific (SuperSignal West Pico Plus, 34580 or SuperSignal West Femto. 34095) or Li-COR Biosciences (WesternSure Premium, 926-95000). Protein band intensity was visualized and

quantified in the linear range using LI-COR C-Digit (CDG-001313) and Image Studio Software (Version 5.2.5).

2.5.14 Mass Spectroscopy for Phospho-Proteomics

For proteomic analysis of NogoA post-translation modifications, NogoA was immunoprecipitated with the anti-NogoAB antibody (R&D Systems AF3098) from rat hippocampal cultures on DIV17 either following 24 hours of vehicle or 2 μ M tetrodotoxin treatments. Following solubilization of resin-bound proteome, 70 μ L of supernatant was loaded into a 1.5mm-thick 7.5% gel, and separated by SDS-PAGE. The gel was stained with Imperial Protein Stain (Life Technologies 24615) according to the manufacturers instructions, in a clean StainEase Staining Tray (Life Technologies NI2400). The NogoA band was excised, digested with trypsin, and analyzed by liquid chromatography tandem mass spectrometry (LC-MS/MS) using an Orbitrap Fusion Tribrid Mass Spectrometer (Thermo Scientific). Samples were run in both collision-induced dissociation (CID) and higher-energy collisional dissociation (HCD) fragmentation methods. Data were analyzed using X!Tandem/TPP software suite and Proteome Discoverer 1.4.

2.5.15 Statistical Analysis

There was no experimental prediction of the difference between control and experimental groups when the study was designed. Therefore, we did not use

computational methods or power analysis to determine sample size *a priori*. Instead, we used minimum of three ($n=3$) biological replicates coming from independent experiments, when permitting with technical replicates to increase confidence. Signals derived from technical replicates were averaged and used as one data entry for the purposes of statistical analysis. Unless indicated otherwise, results were reported as mean value \pm SEM. For comparison between two groups, unpaired two-tailed Student's *t*-test was used, where a p -value <0.05 was considered statistically significant. For comparison amongst multiple groups, ordinary one-way ANOVA followed by multiple comparisons tests such as Dunnett's or Tukey's were used. All statistical analyses were carried out using GraphPad Prism Software (version 8.3.0).

2.6 Acknowledgements

We thank Dr. Christine Bandtlow for providing NogoA-shRNA and scrambled control plasmid, Dr. Xiao-Feng Zhao for help with cloning, Dr. Martine E. Schwab for anti-NogoA antibodies, including Bianca, 11C7, and anti-BrdU isotype control, Dr. Michael E. Greenberg for providing anti-Npas4 antibody, and Dr. Yingxi Lin for sharing protocol details for transcription factor solubilization. We acknowledge Dr. Paul Jenkins' help with sharing anti-Ankyrin-G antibody, and helpful discussion. We greatly appreciate Dr. Cagla Eroglu's protocol and guidance with the astroglial culture preparation. We feel indebted to Dr. Michael A. Sutton and his research laboratory specialists J. Christian Althaus and Cinthia Carruthers for sharing perinatal rat offspring and helping us troubleshoot some problems the primary neuronal culture protocol. We also appreciate Dr. Richard Huganir's insights on homeostatic scaling with neuronal cultures. We are grateful for Dr. Katherine T. Baldwin's (KTB) contribution, as they laid the project foundation.

2.7 Author Contribution

The experiments were conceived and designed by Rafi Kohen (RK) and Roman J. Giger (RJG). RK, KTB, and Corey G. Flynn (CGF) collected and analyzed the data. RK wrote the manuscript, together with edits from RJG.

2.8 Figures

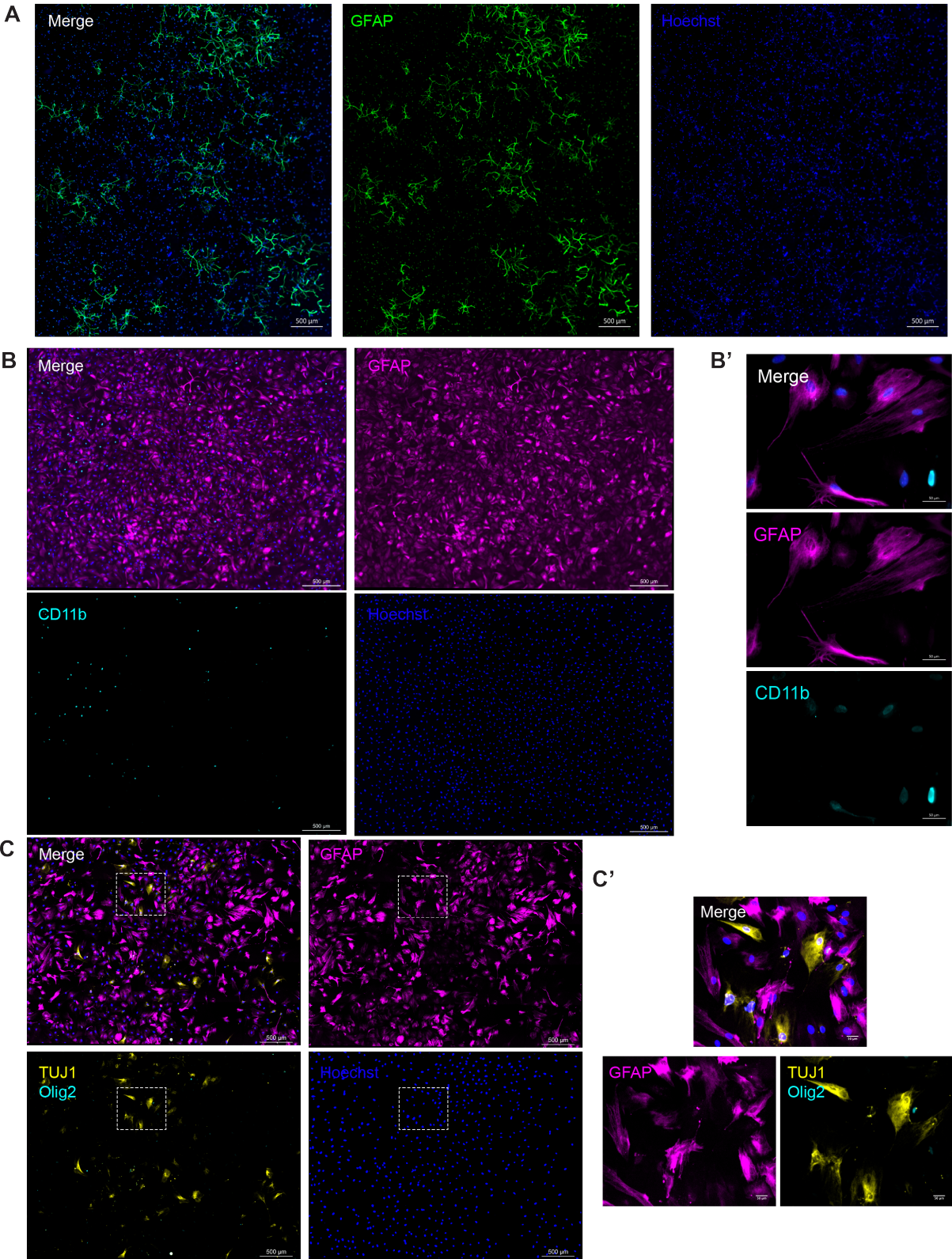


Figure 2-1: *In vitro* primary cultures offer extremely powerful, albeit impure systems to study.

(A) Primary neuronal culture from the E18.5 rat hippocampus was analyzed on DIV11 for abundance of astrocytes. Culture was stained for astrocyte-specific marker GFAP (green), and total number of cells was assessed by were Hoechst nuclear acid counterstain (blue). A tiled image was acquired at 20x magnification to cover a representative area of the center of the 12mm-coverslip. Scale bar=500µm. (B) Primary astroglial culture from the perinatal rat neocortex was analyzed at confluence for the composition of different cell types. The two most prominent cell types found in astroglial cultures, astrocytes and microglia were marked with astrocyte-specific GFAP (magenta) and macrophage/microglia-specific CD11b (cyan). A tiled image was acquired at 20x magnification to cover a representative area of the center of the 25cm²-flask. Scale bar=500µm. (B') A single image acquired from the same flask at 20x magnification to show greater detail. GFAP staining is completely absent from the CD11b^{high}-expressing cells, but there is a faint CD11b^{low} expression derived from the GFAP-expressing astrocytes. Scale bar=50µm. (C) Parallel-prepared and -processed 25cm²-flask of primary astroglial culture was analyzed at confluence for composition of different cell types. Oligodendrocyte-lineage marker Olig2 (cyan) and neuron-specific marker βIII-Tubulin (TUJ1) (yellow) were used to identify contaminating cell types. A tiled image was acquired at 20x magnification to cover a representative area of the center of the flask. Scale bar=500µm. Olig2-expressing cells were in the minority. Numerically more abundant were GFAP-negative, TUJ1-expressing cells, which had non-neuronal cytoskeletal morphology resembling more that of fibroblasts. (C') Zoom-in on the boxed region-of-interest within the tiled image to show greater detail. Scale bar=50µm.

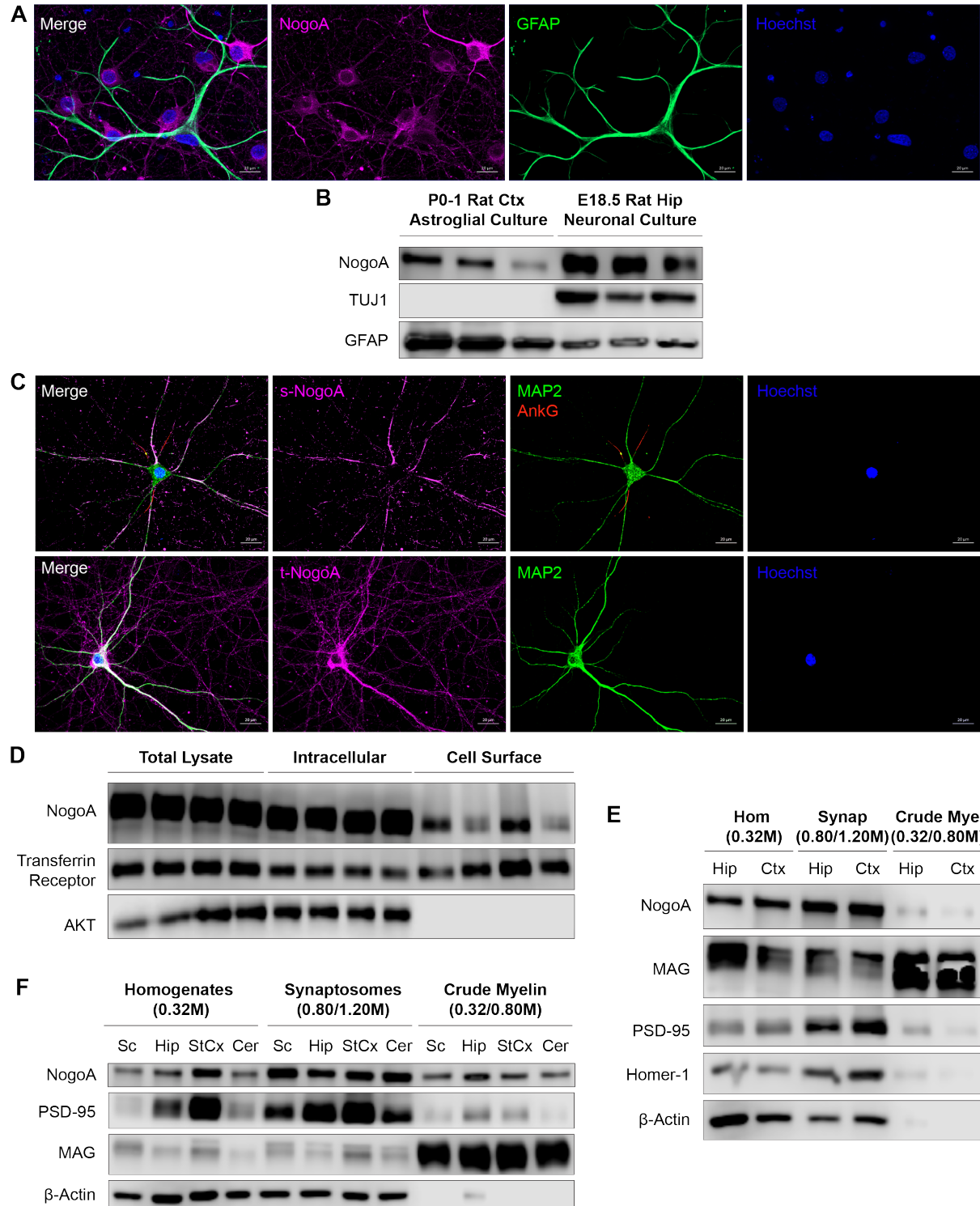


Figure 2-2: NogoA is expressed at the neuronal somatodendritic regions and synaptosomes more strongly than on neuronal cell surface, crude CNS myelin, and astrocytes.

(A) Primary neuronal culture from the E18.5 rat hippocampus was analyzed for NogoA expression. Astrocytes were stained with astrocyte-specific marker GFAP (green), and all cells were non-specifically counterstained with the nuclear acid marker Hoechst (blue). NogoA expression was detected and qualitatively assessed from both cell types (magenta). Neuronal NogoA expression was somatodendritic, and most strongly perinuclear. Astrocytic NogoA expression was significantly weaker, with preferential localization to the cell soma rather than end-feet. Scale bar=20 μ m. (B) Total cell lysates from perinatal rat neocortical astroglial culture and embryonic rat hippocampal neuronal culture were analyzed by Western blotting. Neuron-specific marker β III-Tubulin (TUJ1) was completely absent from the astroglial cultures. Astrocyte-specific marker GFAP showed a drastic enrichment within the astroglial cultures compared to mixed neuronal. NogoA was expressed at higher levels by the neuronal cultures. (C) Neuronal NogoA localization and expression pattern was analyzed with mature embryonic rat hippocampal cultures. Under permeabilized conditions (bottom), NogoA (magenta) is expressed strongest within the MAP2-expressing (green) perinuclear regions of the cell soma and along the dendrites. There is weaker, but considerable NogoA expression derived from the MAP2⁻ axons. Under non-permeabilized conditions (top), NogoA (magenta) is expressed on the cell surface, along the MAP2⁺ (green) dendrites, especially in discrete and discontinuous patches. There is considerably less surface NogoA expression along the axons identified with the axon initial segment marker Ankryin-G⁺ (red). Cell nuclei were counterstained with Hoechst (blue). Scale bar=20 μ m. (D) Following cell surface biotinylation, total lysate, supernatant, and precipitated biotinylated surface proteome were altogether analyzed for NogoA expression by Western blotting. Intracellular signaling protein AKT was absent from the cell surface, and endosomal transferrin receptor was partially depleted from the intracellular pools. NogoA expression was robustly higher in total and intracellular lysates, compared to cell surface. (E) Hippocampus (Hip) and neocortex (Ctx) of adult female Sprague-Dawley rat were subjected to subcellular fractionation by discontinuous sucrose gradient ultracentrifugation. Crude myelin isolation from the 0.32/0.80M interface was confirmed by robust enrichment of MAG. Synaptosomal enrichment within the 0.80/1.20M interface was verified by stronger detection of PSD-95 and Homer-1. NogoA was expressed at the highest level within the synaptosomes compared to whole homogenate and crude myelin. (F) Spinal cord (Sc), hippocampus (Hip), somatosensory cortex (StCx), and cerebellum (Cer) of adult male C3H mice were subjected to the same subcellular fractionation by discontinuous sucrose gradient ultracentrifugation. Isolated fractions were verified similarly by MAG and PSD-95 enrichment. NogoA expression showed similar subcellular expression pattern, with a slight preference to plastic-most regions of the adult CNS, such as hippocampus and neocortex.

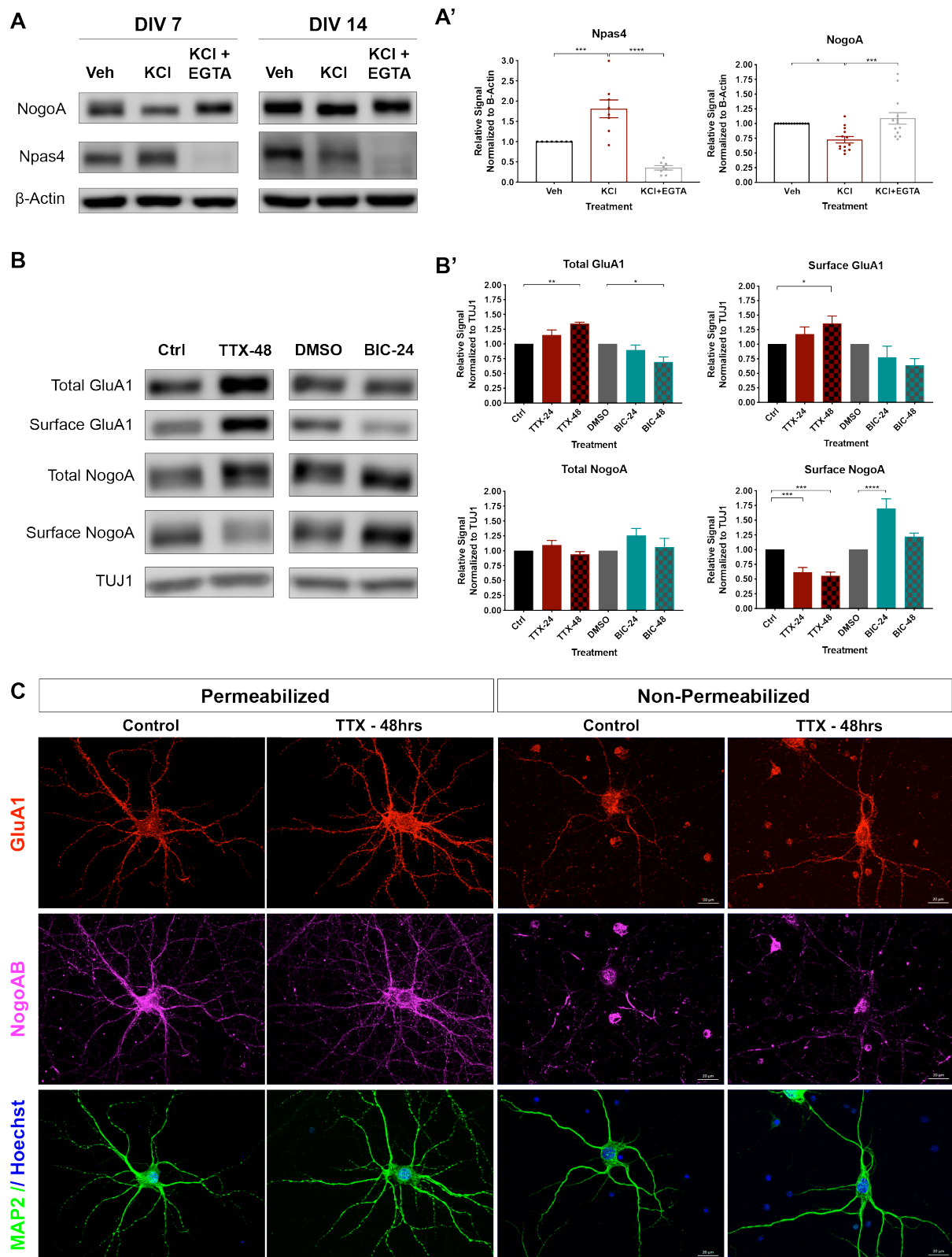


Figure 2-3: Surface expression of neuronal NogoA is under the bidirectional regulation of network activity states.

(A) Primary neuronal cultures from the E18.5 rat hippocampus were continuously depolarized with 55mM KCl for 2 hours with or without extracellular calcium chelation with 5mM EGTA pre-treatment for 10 minutes. Immediate-early transcription factor Npas4 expression showed robust upregulation with KCl treatment and complete depletion with EGTA pre-treatment on DIV7. On DIV14, while calcium chelation showed the same depletion, KCl no longer upregulated Npas4 following synaptic maturation. KCl treatment reversed the baseline NogoA expression, double band separation, and visibly reduced the molecular weight. EGTA pre-treatment was sufficient for partial recovery. (A') Quantification of protein expression following DIV7 experiments with KCl and EGTA. Loading control normalization was against β -Actin. $n=8$ for Npas4, $n=13$ for NogoA quantification. $p_{adj}<0.05$ was deemed statistically significant, as assessed by ordinary one-way Anova followed by Tukey's multiple comparisons test. (B) Primary neuronal cultures were subjected to cell surface biotinylation on DIV13-14 following 2 μ M tetrodotoxin (TTX) or 40 μ M bicuculline (BIC) treatments for 24-48 hours. Total and surface protein expression of GluA1 were assessed as read-out of homeostatic scaling entrainment. TTX induced molecular band separation of NogoA, and reduced surface NogoA expression. BIC only increased surface NogoA expression without apparent post-translational modification. (B') Quantification of total and surface protein expression following chronic TTX and BIC treatments. Loading control normalization for both was against β III-Tubulin (TUJ1) signal from total lysates. $n=5-6$. $p_{adj}<0.05$ was deemed statistically significant, as assessed by ordinary one-way Anova followed by Dunnett's multiple comparisons test. (C) Synaptically mature primary neuronal cultures were treated with 2 μ M TTX for 48 hours to induce homeostatic scaling up. Somatodendritic regions were delineated by MAP2 (green), and nuclei were counterstained with Hoechst (blue). Both total and surface GluA1 expression (red) showed increase with TTX treatment. TTX reduced NogoAB (magenta) slightly for total and significantly for surface expression. Scale bar=20 μ m.

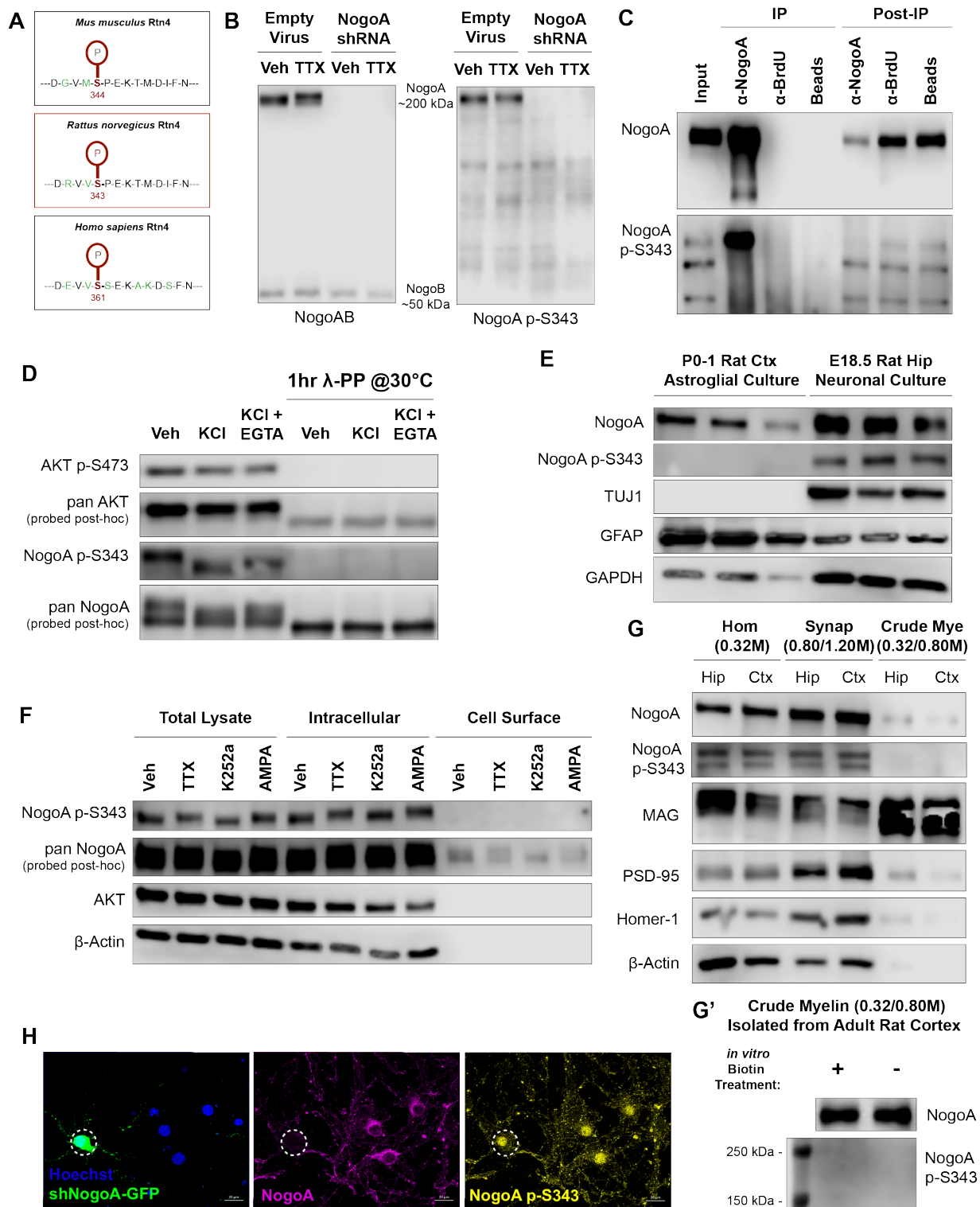


Figure 2-4: Intracellular and synaptosomal neuronal NogoA is phosphorylated at serine 343.

(A) Schematic of mouse, rat, and human NogoA protein sequence with the same conserved phosphorylation site (red). Amino acids that are not conserved are marked in green. (B) Primary neuronal cultures were infected with with LV-EmptyVector or LV-shNogoA, treated with 2 μ M TTX for 48 hours upon synaptic maturity, and lysates were analyzed by Western blotting. Pan-NogoAB was probed with the polyclonal antibody Bianca to verify NogoA-specific knockdown. Same lysates were concurrently probed with the anti-NogoA p-S343 antibody. Higher molecular NogoA band was detected by the phospho-specific antibody, the signal from which completely disappeared upon NogoA loss. (C) NogoA was successfully immunoprecipitated (IP) from the embryonic rat whole brains, using the NogoA-specific monoclonal 11C7 antibody. Epitope-matched anti-BrdU antibody and empty beads were used as negative controls. Supernatants following precipitation (Post-IP) were assessed to confirm NogoA depletion. Same samples were concurrently analyzed with the anti-NogoA p-S343 antibody. Only the band around 200kDa was enriched with NogoA IP, confirming NogoA-specificity. (D) Primary neuronal cultures from the embryonic rat hippocampus were treated with 55mM KCl for 2 hours with or without 10 minute pre-treatment with 5mM EGTA. Lysates were collected, split, and subjected to 1 hour of lambda phosphatase (λ -PP) reaction. Successful and near-complete dephosphorylation of AKT (positive control) and NogoA (experimental group) was verified using phospho-specific antibodies. Retention of unphosphorylated proteins with lower molecular weight was consecutively verified using pan antibodies. (E) Previously described lysates from the astroglial and neuronal cultures were analyzed by Western blotting for NogoA phosphorylation. NogoA p-S343 was completely absent from the astroglial cultures. (F) Previously described cell-surface biotinylated neuronal lysates were analyzed for NogoA phosphorylation. While 48 hours of 2 μ M TTX and 2 hours of 10 μ M AMPA treatments induced phosphorylation of the higher molecular NogoA band, 2 hours of 200nM K252a treatment reduced molecular weight due to dephosphorylation. Phosphorylated NogoA was completely absent from the neuronal cell surface, even though presence of unphosphorylated NogoA was verified by consecutive probing with the pan-NogoAB antibody. (G) Previously described rat hippocampal and cortical subcellular fractions were analyzed for NogoA phosphorylation. NogoA p-S343 was detected from the synaptosomes, but completely absent from the crude myelin. (G') Cortical crude myelin membranes were precipitated and combined with the biotinylation reagent *in vitro*. Biotinylation did not affect NogoA detection, but phosphorylation was still absent despite high input. (H) Primary hippocampal neurons were sparsely and transiently transfected with the GFP-tagged shRNA against NogoA. Perinuclear NogoA signal (magenta) was completely lost from the GFP-expressing neurons (green). However, NogoA p-S343 signal (yellow) overlapped strongly with the Hoechst stain (blue), but not with NogoA, and did not disappear with NogoA loss. Scale bar=20 μ m.

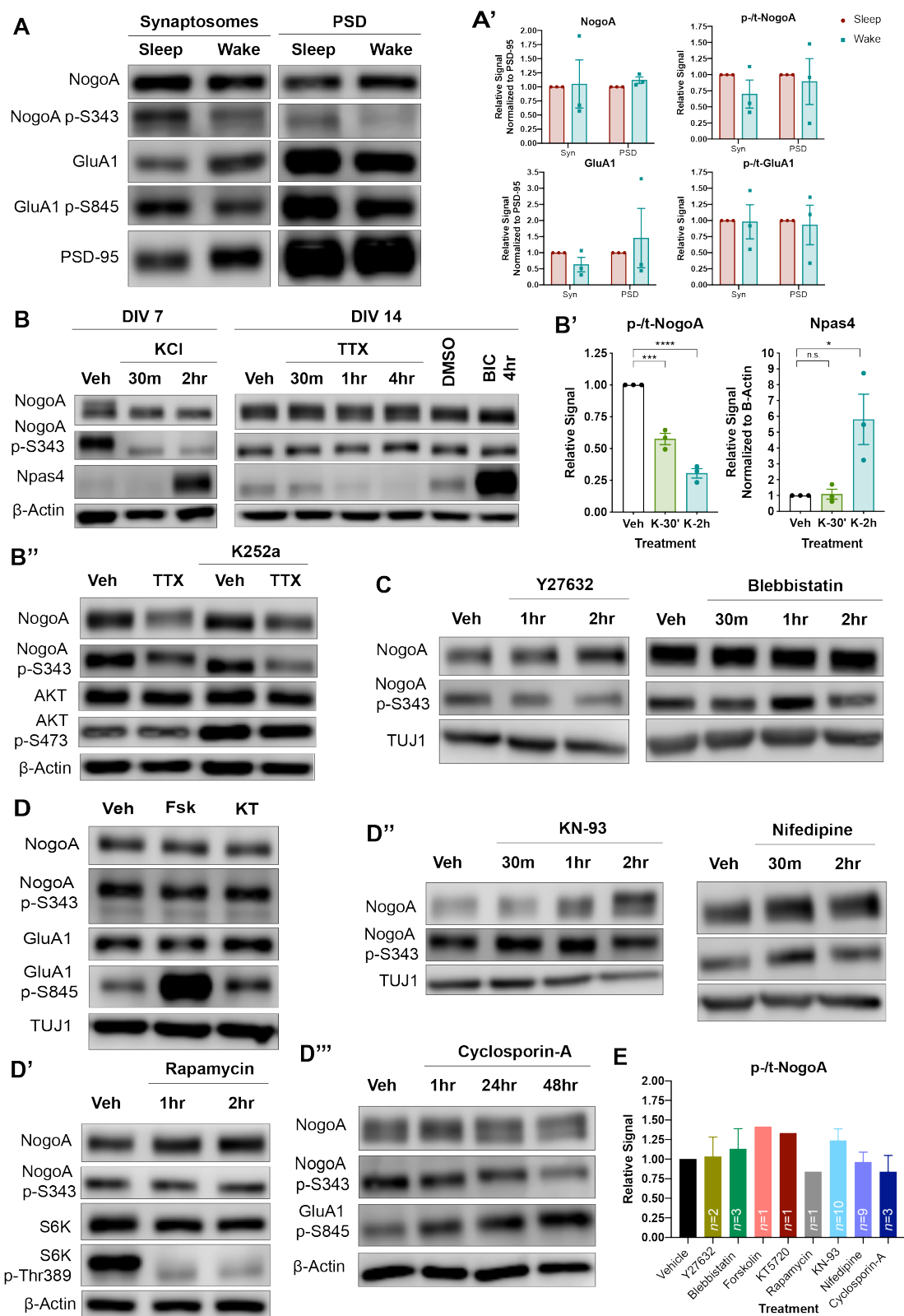


Figure 2-5: NogoA phosphorylation is regulated by network activity *in vitro*, with an unknown physiological relevance and kinase/phosphatase pair.

(A) Rat forebrains were subjected to subcellular fractionation for isolation of synaptosomes and post-synaptic densities (PSD) at sleep (10AM) and wake (10PM) states. Enrichment of PSD-95 was used to verify fractionation. Samples were analyzed for expression and phosphorylation of NogoA and GluA1. (A') Quantification of total and phosphorylated forms of NogoA and GluA1 expression. Loading control normalization was against PSD-95. $n=3$. $p_{adj}<0.05$ was deemed statistically significant, as assessed by unpaired Student's *t*-test. (B) Synaptically immature DIV7 rat neuronal cultures were treated with 30 minutes or 2 hours of 55mM of KCl to induce continuous membrane depolarization. Immediate-early transcription factor Npas4 was strongly upregulated by 2-hour timepoint. Both treatments led to robust loss of NogoA phosphorylation and molecular weight downward shift. Synaptically mature DIV14 rat neuronal cultures were treated with 2 μ M TTX or 50 μ M BIC for different timepoints. After 4 hours of treatment, Npas4 expression was drastically reduced with TTX and upregulated with BIC. Molecular weight shifts of pan- and phosphorylated NogoA were observed, although without any change in expression level. (B') Quantification of DIV7 experiments with 30 minutes or 2 hours of KCl treatment. Loading control normalization was against β -Actin. $n=3$ biological with 2 technical replicates each. $p_{adj}<0.05$ was deemed statistically significant, as assessed by ordinary one-way Anova followed by Dunnett's multiple comparisons test. (B'') Synaptically mature rat hippocampal cultures were treated with 2 μ M TTX with or without 2 hours of 200nM K252a treatment prior to lysis. Lysates were probed for AKT phosphorylation at ser-473 for bioreactivity verification. Acute K252a treatment overrode upward molecular weight shift of NogoA p-S343 induced by chronic TTX treatment. (C-D''') Mature rat hippocampal cultures were treated with the following pharmacological reagents to modulate NogoA-NgR1, PKA, CamKII, L-VGCC, mTOR, and calcineurin signaling in this order: 20 μ M Y27632, 30 μ M blebbistatin, 10 μ M forskolin, 2 μ M KT5720, 1 μ M KN-93, 10 μ M nifedipine, 20ng/mL rapamycin, 5 μ M cyclosporin-A. NogoA expression and phosphorylation were assessed, along with positive controls for drug bioreactivity. (E) Comprehensive quantification of phosphorylated over total expression of NogoA, as assessed by Western blot analysis. Loading control normalization was against either β III-Tubulin (TUJ1) or β -Actin. $n=1-10$ biological replicates, as indicated. Statistical analysis was only conducted for blebbistatin, KN-93, nifedipine, and cyclosporin-A treatments, since prerequisite was $n\geq 3$ biological replicates. Unpaired two-tailed Student's *t*-test revealed no statistical significance, as assessed by $p_{adj}<0.05$ cut-off.

2.9 Tables

Description	Σ Coverage	Σ # PSMs	Coverage A3
Reticulon OS=Rattus norvegicus GN=Rtn4 PE=1 SV=1 - [F1LQN3_RAT]	78.93	2055	71.71
Sequence	# PSMs	Modifications	phosphoRS Site Probabilities
AQIITEK	3		
AQIITEKTSPK	10	S9(Phospho)	T(5): 0.1; T(8): 50.0; S(9): 50.0
ASISPSNVSALEPQTEMGSIVK	8		
ASISPSNVSALEPQTEMGSIVK	23	M17(Oxidation)	
ASISPSNVSALEPQTEMGSIVK	23	S4(Phospho)	S(2): 0.6; S(4): 98.9; S(6): 0.6; S(9): 0.0; T(15): 0.0; S(19): 0.0
ASISPSNVSALEPQTEMGSIVK	25	S2(Phospho); M17(Oxidation)	S(2): 78.4; S(4): 10.8; S(6): 10.8; S(9): 0.0; T(15): 0.0; S(19): 0.0
ATNPFVNR	21		
AYITCASFTSATESTTANTFPLEDHTSENK	8	C5(Carbamidomethyl)	
AYITCASFTSATESTTANTFPLEDHTSENKTDEK	14	C5(Carbamidomethyl)	
AYLESEVAISEELVQK	103		
CLEDSLEQK	5	C1(Carbamidomethyl)	
DAASNDIPTLTK	18		
DAASNDIPTLTK	1	K12(GlyGly)	
DAASNDIPTLTKK	1		
DEVHVSDEFSENK	44		
DKEDLVCSAALHSPQESPVGK	6	C7(Carbamidomethyl)	
DKEDLVCSAALHSPQESPVGK	3	C7(Carbamidomethyl); S13(Phospho)	S(8): 0.0; S(13): 100.0; S(17): 0.0
DKEDLVCSAALHSPQESPVGKEDR	3	C7(Carbamidomethyl)	
DKEDLVCSAALHSPQESPVGKEDR	3	C7(Carbamidomethyl); S13(Phospho); S17(Phospho)	S(8): 3.4; S(13): 96.6; S(17): 100.0
DKEDLVCSAALHSPQESPVGKEDR	1	C7(Carbamidomethyl); S13(Phospho)	S(8): 0.2; S(13): 99.5; S(17): 0.2
DLAEFSELEYSEMGSSEFK	21		
DLAEFSELEYSEMGSSEFK	51	M13(Oxidation)	
DLAEFSELEYSEMGSSEFKGSPK	10	M13(Oxidation); S20(Phospho)	S(6): 0.0; Y(10): 0.0; S(11): 0.0; S(15): 0.0; S(16): 0.0; S(20): 100.0
DSEGRNEDASFPSTPEPVK	7		
DSEGRNEDASFPSTPEPVK	11	T14(Phospho)	S(2): 0.0; S(10): 0.7; S(13): 49.6; T(14): 49.6
DSEGRNEDASFPSTPEPVK	2	S10(Phospho); S13(Phospho)	S(2): 0.1; S(10): 99.3; S(13): 50.3; T(14): 50.3
DSEGRNEDASFPSTPEPVKDSSR	9		
DSEGRNEDASFPSTPEPVKDSSR	15	T14(Phospho)	S(2): 0.0; S(10): 0.0; S(13): 11.7; T(14): 88.3; S(21): 0.0; S(22): 0.0

DSEGRNEDASFPSTPEPVKDSSR	3	S10(Phospho); S13(Phospho)	S(2): 0.1; S(10): 99.8; S(13): 16.8; T(14): 83.4; S(21): 0.0; S(22): 0.0
EEYADFKPFEQAWVEVK	29		
EEYADFKPFEQAWVKDTYEGSR	4		
EGIKEPESFNAAVQETEAPYISACDLIK	34	C25(Carbamidomethyl)	
EHGYLGNLSAVSSSEGTIEETLNEASK	51		
EKISLQMEEFNNTAIYSNDDLSSK	7	M7(Oxidation)	
EKISLQMEEFNNTAIYSNDDLSSK	4		
EKISLQMEEFNNTAIYSNDDLSSKEDK	3	M7(Oxidation)	
EPESFNAAVQETEAPYISACDLIK	9	C21(Carbamidomethyl)	
ESETFSDSSPIEIIDEFPTFVSAK	7		
ESETFSDSSPIEIIDEFPTFVSAK	19	S8(Phospho)	S(2): 0.0; T(4): 0.0; S(6): 8.5; S(8): 82.9; S(9): 8.5; T(19): 0.0; S(22): 0.0
ESETFSDSSPIEIIDEFPTFVSAK	2	S2(Phospho); S6(Phospho)	S(2): 75.4; T(4): 43.9; S(6): 43.9; S(8): 18.3; S(9): 18.3; T(19): 0.2; S(22): 0.1
ESLTEVSETVAQHK	24		
ESLTEVSETVAQHK	11	K14(GlyGly)	
ESLTEVSETVAQHKEER	58		
ESLTEVSETVAQHKEER	3	K14(GlyGly)	
ETKLSTEPSPDFSNYSEIAK	2	S5(Phospho); S9(Phospho)	T(2): 0.1; S(5): 86.7; T(6): 13.2; S(9): 100.0; S(13): 0.0; Y(15): 0.0; S(16): 0.0
ETKLSTEPSPDFSNYSEIAK	3	T6(Phospho)	T(2): 0.3; S(5): 49.8; T(6): 49.8; S(9): 0.1; S(13): 0.0; Y(15): 0.0; S(16): 0.0
ETKLSTEPSPDFSNYSEIAK	1		
EYTDLEVSDK	23		
EYTDLEVSDKSEIANIQSGADSLPCLELPCDLSFK	15	C25(Carbamidomethyl); C30(Carbamidomethyl)	
GESAILVENTK	22		
GESAILVENTK	2	K11(GlyGly)	
GESAILVENTKEEVIVR	113		
GPLPAAPPAAPER	23		
GPLPAAPPAAPERQPSWER	4	S16(Phospho)	S(16): 100.0
GSGSVDETLFALPAASEVPVPSAEK	12	T8(Phospho)	S(2): 33.3; S(4): 33.3; T(8): 33.3; S(16): 0.0; S(22): 0.0; S(23): 0.0
GSGSVDETLFALPAASEVPVPSAEK	2		
GSPKGESAILVENTK	1	S2(Phospho)	S(2): 88.9; S(7): 11.1; T(14): 0.0
GVIQAIQK	6		
HQVQIDHYLGLANK	88		
IKESETFSDSSPIEIIDEFPTFVSAK	13		
IKESETFSDSSPIEIIDEFPTFVSAK	20	S11(Phospho)	S(4): 0.0; T(6): 0.0; S(8): 0.2; S(10): 10.8; S(11): 89.0; T(21): 0.0; S(24):

			0.0
IKESETFSOSSPIEIDEFPTFVSAK	28	S8(Phospho); S10(Phospho)	S(4): 70.5; T(6): 81.9; S(8): 27.1; S(10): 16.0; S(11): 4.6; T(21): 0.0; S(24): 0.0
IMDLMEQPGNTVSSGQEDFPSVLLETAASLPSLSPLSTVSK	12	M2(Oxidation); M5(Oxidation)	
IMDLMEQPGNTVSSGQEDFPSVLLETAASLPSLSPLSTVSK	30	M2(Oxidation)	
IMDLMEQPGNTVSSGQEDFPSVLLETAASLPSLSPLSTVSK	28	M2(Oxidation); S34(Phospho)	T(11): 0.0; S(13): 0.0; S(14): 0.0; S(21): 0.0; T(26): 0.0; S(29): 0.0; S(32): 5.7; S(34): 93.7; S(37): 0.4; T(38): 0.1; S(40): 0.1
IMDLMEQPGNTVSSGQEDFPSVLLETAASLPSLSPLSTVSK	11	M2(Oxidation); M5(Oxidation); S34(Phospho)	T(11): 0.0; S(13): 0.0; S(14): 0.0; S(21): 0.1; T(26): 1.3; S(29): 1.3; S(32): 18.3; S(34): 72.9; S(37): 4.8; T(38): 1.3; S(40): 0.1
IMDLMEQPGNTVSSGQEDFPSVLLETAASLPSLSPLSTVSK	3		
IMDLMEQPGNTVSSGQEDFPSVLLETAASLPSLSPLSTVSK	4	S34(Phospho)	T(11): 0.0; S(13): 0.0; S(14): 0.0; S(21): 0.0; T(26): 0.2; S(29): 0.1; S(32): 0.5; S(34): 1.2; S(37): 32.7; T(38): 32.7; S(40): 32.7
ISLQMEEFNTAIYSNDDLSSK	23	M5(Oxidation)	
ISLQMEEFNTAIYSNDDLSSK	26		
ISLQMEEFNTAIYSNDDLSSKEDK	3		
ISLQMEEFNTAIYSNDDLSSKEDK	2	M5(Oxidation); S20(Phospho)	S(2): 0.0; T(10): 0.0; Y(13): 0.1; S(14): 1.2; S(20): 18.6; S(21): 80.1
KAQITEK	18		
KAQITEKTSPK	16	S10(Phospho)	T(6): 0.0; T(9): 7.1; S(10): 92.9
KCLEDSLEQK	7	C2(Carbamidomethyl)	
KLPSDTEK	1		
KLPSDTEKEDR	14		
KPAAGLSAAVPPAAAAPLDFSSDSVPPAPR	46		
LEPENPPPYEEAMNVALK	10		
LEPENPPPYEEAMNVALK	32	M13(Oxidation)	
LFLVDDLVDLSK	4		
LPEDDEPPARPPPPPPAGASPLAEPAPSTPAAPK	30		
LPEDDEPPARPPPPPPAGASPLAEPAPSTPAAPK	10	S20(Phospho)	S(20): 100.0; S(30): 0.0; T(31): 0.0
LPSDTEKEDR	4		
LSASPQELGKPYLESFQPNLHSTK	41	S4(Phospho)	S(2): 50.0; S(4): 50.0; Y(12): 0.0; S(15): 0.0; S(22): 0.0; T(23): 0.0

LSASPQELGKPYLESFQPNLHSTK	40		
LSTEPSPDFSNYSEIAK	20		
LSTEPSPDFSNYSEIAK	12	S6(Phospho)	S(2): 0.0; T(3): 0.0; S(6): 100.0; S(10): 0.0; Y(12): 0.0; S(13): 0.0
LSTEPSPDFSNYSEIAK	1	K17(GlyGly)	
MEDIDQSSLVSSSTDSPRRPPPAFK	2	M1(Oxidation); S7(Phospho)	S(7): 49.9; S(8): 49.9; S(11): 0.1; S(12): 0.0; S(13): 0.0; T(14): 0.1; S(16): 0.0
NEDASFPSTPEPVK	10		
NEDASFPSTPEPVK	13	S8(Phospho)	S(5): 0.0; S(8): 50.0; T(9): 50.0
NEDASFPSTPEPVK	8	S5(Phospho); S8(Phospho)	S(5): 100.0; S(8): 50.0; T(9): 50.0
NEDASFPSTPEPVKDSSR	21		
NEDASFPSTPEPVKDSSR	22	T9(Phospho)	S(5): 0.0; S(8): 90.4; T(9): 9.6; S(16): 0.0; S(17): 0.0
NEDASFPSTPEPVKDSSR	6	S5(Phospho); S8(Phospho)	S(5): 100.0; S(8): 1.7; T(9): 98.3; S(16): 0.0; S(17): 0.0
NIYPKDEVHVSDEFSENK	7		
QPSWERSPAAPAPSLPPAAAVLPSK	2	S3(Phospho)	S(3): 96.8; S(7): 3.2; S(14): 0.0; S(24): 0.0
QPSWERSPAAPAPSLPPAAAVLPSK	1	S3(Phospho); S7(Phospho)	S(3): 100.0; S(7): 100.0; S(14): 0.0; S(24): 0.0
RGSGSVDETLFALPAASEPVIPSSAEK	11	S3(Phospho)	S(3): 79.6; S(5): 10.2; T(9): 10.2; S(17): 0.0; S(23): 0.0; S(24): 0.0
RRGSGSVDETLFALPAASEPVIPSSAEK	35	S6(Phospho)	S(4): 14.6; S(6): 85.4; T(10): 0.0; S(18): 0.0; S(24): 0.0; S(25): 0.0
SDEGHPFR	11		
SEIANIQSGADSLPCLELPCDLSFK	13	C15(Carbamidomethyl); C20(Carbamidomethyl)	
SKDKEDLVCSAALHSPQESPVGK	11	C9(Carbamidomethyl)	
SKDKEDLVCSAALHSPQESPVGK	7	C9(Carbamidomethyl); S15(Phospho)	S(1): 0.0; S(10): 0.0; S(15): 100.0; S(19): 0.0
SKDKEDLVCSAALHSPQESPVGK	3	C9(Carbamidomethyl); S15(Phospho); S19(Phospho)	S(1): 0.0; S(10): 0.0; S(15): 100.0; S(19): 100.0
SLGKDSEGR	1		
SLSAVLSAELSK	21		
SPAAPAPSLPPAAAVLPSK	19		
SPAAPAPSLPPAAAVLPSK	1	S1(Phospho)	S(1): 100.0; S(8): 0.0; S(18): 0.0
SVPEHAELVEDSSPESEPVDLFSDDSIPEVPQTQEEAVMLMK	2	M39(Oxidation); M41(Oxidation)	
SVPEHAELVEDSSPESEPVDLFSDDSIPEVPQTQEEAVMLMK	3	M39(Oxidation)	
TMDIFNEMQMSVVPVR	28	M2(Oxidation); M8(Oxidation); M10(Oxidation)	

TMDIFNEMQMSVVAPVR	27	M2(Oxidation)	
TMDIFNEMQMSVVAPVR	7		
TMDIFNEMQMSVVAPVR	5	M8(Oxidation); M10(Oxidation)	
TMDIFNEMQMSVVAPVREEYADFKPFEQAWEVK	9	M8(Oxidation); M10(Oxidation)	
TMDIFNEMQMSVVAPVREEYADFKPFEQAWEVK	4	M2(Oxidation); M8(Oxidation); M10(Oxidation)	
TMDIFNEMQMSVVAPVREEYADFKPFEQAWEVK	12	M8(Oxidation)	
TMDIFNEMQMSVVAPVREEYADFKPFEQAWEVK	2		
TSNPFLVAVQDSEADYVTTDTLSK	44		
TSVVDLLYWR	33		
VTEAAVSNMPEGLTPDLVQEACESELNEATGTK	9	M9(Oxidation); C22(Carbamidomethyl)	
VTEAAVSNMPEGLTPDLVQEACESELNEATGTK	6	C22(Carbamidomethyl)	
VTEAAVSNMPEGLTPDLVQEACESELNEATGTK	4	M9(Oxidation); T14(Phospho); C22(Carbamidomethyl)	T(2): 0.0; S(7): 0.0; T(14): 100.0; S(24): 0.0; T(30): 0.0; T(32): 0.0
VVSPEKTMDFNEMQMSVVAPVR	8	S3(Phospho); M8(Oxidation)	S(3): 11.2; T(7): 88.8; S(17): 0.0
VVSPEKTMDFNEMQMSVVAPVR	5	S3(Phospho); M8(Oxidation); M14(Oxidation); M16(Oxidation)	S(3): 99.9; T(7): 0.1; S(17): 0.0
VVSPEKTMDFNEMQMSVVAPVR	6	T7(Phospho); M8(Oxidation); M14(Oxidation)	S(3): 12.0; T(7): 88.0; S(17): 0.0
VVSPEKTMDFNEMQMSVVAPVREEYADFKPFEQAWEVK	5	S3(Phospho); M8(Oxidation); M14(Oxidation); M16(Oxidation)	S(3): 95.5; T(7): 4.5; S(17): 0.0; Y(26): 0.0
YQFVTEPEDEEEDDEEEDDEEDLEEVLER	27		
YSNSALGHVNSTIK	40		
YSNSALGHVNSTIK	1	K14(GlyGly)	

Table 2-1: Neuronal NogoA is post-translationally modified in baseline conditions. NogoA was immunoprecipitated from rat primary hippocampal neurons on DIV17, and subjected to LC-MS/MS. This table summarizes the peptides identified from both CID and HDC fragmentation methods. The column on the right indicates the probability that each serine, threonine, or tyrosine residue is phosphorylated, for a given phosphopeptide.

Description	ΣCoverage	Σ# PSMs	Coverage A3
Reticulon OS=Rattus norvegicus GN=Rtn4 PE=1 SV=1 - [F1LQN3_RAT]	79.02	1888	68.1
Sequence	# PSMs	Modifications	phosphoRS Site Probabilities
EHGYLGNLSAVSSSEGTIEETLNEASK	64		
RRGSGSVDETLFALPAASEPVPSSAEK	36	S4(Phospho)	S(4): 98.3; S(6): 1.7; T(10): 0.0; S(18): 0.0; S(24): 0.0; S(25): 0.0
KPAAGLSAAAVPPAAAAPLDFSSDSVPPAPR	29		
ESLTVSETVAQHKEER	46		
DLAEFSELEYSEMGSSFKGSPK	5	S20(Phospho)	S(6): 0.0; Y(10): 0.0; S(11): 0.0; S(15): 0.0; S(16): 0.0; S(20): 100.0
GESAILVENTKEEVIVR	138		
DLAEFSELEYSEMGSSFKGSPK	12	M13(Oxidation); S20(Phospho)	S(6): 0.0; Y(10): 0.0; S(11): 0.0; S(15): 1.0; S(16): 1.0; S(20): 98.0
LSASPQELGKPYLESFQPNLHSTK	33	S4(Phospho)	S(2): 50.0; S(4): 50.0; Y(12): 0.0; S(15): 0.0; S(22): 0.0; T(23): 0.0
DLAEFSELEYSEMGSSFK	37		
EGIKEPESFNAAVQETEAPYISIACDLIK	21	C25(Carbamidomethyl)	
ISLQMEEFNIAIYSNDDLSSK	31	M5(Oxidation)	
SPAAPAPSLPPAAAVLPSK	22		
LSASPQELGKPYLESFQPNLHSTK	24		
RGSGSVDETLFALPAASEPVPSSAEK	22	S3(Phospho)	S(3): 97.0; S(5): 1.5; T(9): 1.5; S(17): 0.0; S(23): 0.0; S(24): 0.0
TSNPFLVAVQDSEADYVTTDTLSK	68		
SEIANIQSGADSLPCLELPCDLSFK	8	C15(Carbamidomethyl); C20(Carbamidomethyl)	
LPEDDEPPARPPPPPPAGASPLAEPAPSTPAAPK	20		
NEDASFPSTPEPVKDSSR	20		
HQVQIDHYLGLANK	38		
YSNSALGHVNSTIK	22		
AYITCASFTSATESTTANTFPLEDHTSENKTDEK	7	C5(Carbamidomethyl)	
ESLTVSETVAQHK	17		
DAASNDIPTLT	20		
AYLESEVAISEELVQK	115		
DSEGRNEDASFPSTPEPVKDSSR	5		
NEDASFPSTPEPVK	16		
DEVHVSDEFSEN	25		
GESAILVENTK	19		
KAQIITEKTSPK	30	S10(Phospho)	T(6): 0.0; T(9): 6.6; S(10): 93.4
LSTEPSPDFSNYSEIAK	6		
LEPNPPPYEEAMNVALK	30	M13(Oxidation)	
SLSAVLSAELSK	15		
KLPDTEKEDR	19		
LEPNPPPYEEAMNVALK	11		
IKESETFSDSSPIIEFPTFVSAK	12		
ASISPSNVSALEPQTEMGSIVK	15		

DLAEFSELEYSEMGSSEFK	38	M13(Oxidation)	
KAQIITEK	9		
NEDASFPSTPEPVK	7	S8(Phospho)	S(5): 4.0; S(8): 48.0; T(9): 48.0
DSEGRNEDASFPSTPEPVK	10		
GPLPAAPPAAPER	15		
SKDKEDLVCSAALHSPQESPVGK	7	C9(Carbamidomethyl); S15(Phospho)	S(1): 0.0; S(10): 0.0; S(15): 100.0; S(19): 0.0
DSEGRNEDASFPSTPEPVKDSSR	16	T14(Phospho)	S(2): 0.0; S(10): 0.0; S(13): 12.2; T(14): 87.8; S(21): 0.0; S(22): 0.0
ISLQMEEFNNTAIYSNDDLSSKEDK	7		
TSVVDLLYWR	20		
EEYADFKPFEQAWVEVK	21		
ISLQMEEFNNTAIYSNDDLSSK	41		
TMDIFNEMQMSVVPVR	19	M2(Oxidation); M8(Oxidation); M10(Oxidation)	
TMDIFNEMQMSVVPVREEYADFKPFEQAWVEVK	6	M2(Oxidation); M8(Oxidation); M10(Oxidation)	
ASISPSNVSALEPQTEMGSIVK	35	M17(Oxidation)	
NIYPKDEVHVSDEFSENK	9		
LSTEPSPDFSNYSEIAK	4	S6(Phospho)	S(2): 0.0; T(3): 0.0; S(6): 99.2; S(10): 0.8; Y(12): 0.0; S(13): 0.0
EKISLQMEEFNNTAIYSNDDLSSK	5	M7(Oxidation)	
VTEAAVSNMPEGLTPDLVQEACESELNEATGTK	4	M9(Oxidation); C22(Carbamidomethyl)	
ESLTVSETVAQHK	4	K14(GlyGly)	
ESETFSDSSPIIIDEFPTFVSAK	9		
TMDIFNEMQMSVVPVR	24	M2(Oxidation)	
EYTDLEVSDK	24		
CLEDSLEQK	14	C1(Carbamidomethyl)	
NEDASFPSTPEPVKDSSR	14	S8(Phospho)	S(5): 0.0; S(8): 88.6; T(9): 11.3; S(16): 0.0; S(17): 0.0
ATNPFVNR	21		
KCLEDSLEQK	4	C2(Carbamidomethyl)	
EEYADFKPFEQAWVEVKDTYEGSR	3		
TMDIFNEMQMSVVPVR	12	M8(Oxidation); M10(Oxidation)	
YQFVTEPEDEEEDDEEEDDEEDLEEVLER	43		
DKEDLVCSAALHSPQESPVGK	8	C7(Carbamidomethyl)	
LFLVDDLVDLSK	6		
ASISPSNVSALEPQTEMGSIVK	11	S4(Phospho)	S(2): 8.6; S(4): 91.3; S(6): 0.1; S(9): 0.0; T(15): 0.0; S(19): 0.0
LPSDTEKEDR	4		
VVSPEKTMDFNEMQMSVVPVR	12	S3(Phospho); M8(Oxidation); M14(Oxidation); M16(Oxidation)	S(3): 90.1; T(7): 9.9; S(17): 0.0
TMDIFNEMQMSVVPVR	4		

EKISLQMEEFNNTAIYSNDDLSSK	2		
LPEDDEPPARPPPPPPAGASPLAEPAAPSTPAAPK	13	S20(Phospho)	S(20): 100.0; S(30): 0.0; T(31): 0.0
IKESETFSDSSPIEIIDEFPTFVSAK	38	S10(Phospho); S11(Phospho)	S(4): 0.5; T(6): 86.6; S(8): 37.6; S(10): 37.6; S(11): 37.6; T(21): 0.0; S(24): 0.0
SKDKEDLVCSAALHSPQESVVGK	8	C9(Carbamidomethyl)	
ASISPSNVSALEPQTEMGSIVK	45	S4(Phospho); M17(Oxidation)	S(2): 47.4; S(4): 47.4; S(6): 5.3; S(9): 0.0; T(15): 0.0; S(19): 0.0
IKESETFSDSSPIEIIDEFPTFVSAK	28	S11(Phospho)	S(4): 0.0; T(6): 0.0; S(8): 0.1; S(10): 9.4; S(11): 90.5; T(21): 0.0; S(24): 0.0
VVSPEKTMDIFNEMQMSVVAPVR	13	T7(Phospho); M8(Oxidation); M14(Oxidation)	S(3): 2.0; T(7): 98.0; S(17): 0.0
VVSPEKTMDIFNEMQMSVVAPVREEYADFKPFEQAWVEVK	4	S3(Phospho); M8(Oxidation); M14(Oxidation); M16(Oxidation)	S(3): 93.2; T(7): 6.6; S(17): 0.1; Y(26): 0.1
AYITCASFTSATESTTANTFPLLEDHTSENK	6	C5(Carbamidomethyl)	
EYTDLEVSDKSEIANIQSGADSLPCLELPCDLSFK	4	C25(Carbamidomethyl); C30(Carbamidomethyl)	
VTEAAVSNMPEGLTPDLVQEACESELNEATGTK	2	C22(Carbamidomethyl)	
ESETFSDSSPIEIIDEFPTFVSAK	24	S8(Phospho)	S(2): 0.0; T(4): 0.0; S(6): 1.1; S(8): 89.1; S(9): 9.7; T(19): 0.0; S(22): 0.0
VTEAAVSNMPEGLTPDLVQEACESELNEATGTK	5	M9(Oxidation); T14(Phospho); C22(Carbamidomethyl)	T(2): 0.0; S(7): 0.2; T(14): 99.8; S(24): 0.0; T(30): 0.0; T(32): 0.0
GSGSVDETLFALPAASEPVPSSAEK	11	T8(Phospho)	S(2): 10.4; S(4): 10.4; T(8): 79.1; S(16): 0.0; S(22): 0.0; S(23): 0.0
EPESFNAAVQETEAPYISACDLIK	11	C21(Carbamidomethyl)	
DKEDLVCSAALHSPQESVVGK	1	C7(Carbamidomethyl); S13(Phospho)	S(8): 0.0; S(13): 100.0; S(17): 0.0
GSGSVDETLFALPAASEPVPSSAEK	4		
VVSPEKTMDIFNEMQMSVVAPVR	1	S3(Phospho); M8(Oxidation)	S(3): 1.5; T(7): 98.5; S(17): 0.0
IMDLMEQPGNTVSSGQEDFPSVLLETAASLPSLSPLSTVSFK	2	M2(Oxidation); M5(Oxidation)	
SPAAPAPSLPPAAAVLPSK	2	S1(Phospho)	S(1): 100.0; S(8): 0.0; S(18): 0.0
TMDIFNEMQMSVVAPVREEYADFKPFEQAWVEVK	5	M8(Oxidation); M10(Oxidation)	
NEDASFPSTPEPVKDSSR	11	S5(Phospho); S8(Phospho)	S(5): 99.9; S(8): 50.0; T(9): 50.0; S(16): 0.0; S(17): 0.1
IMDLMEQPGNTVSSGQEDFPSVLLETAASLPSLSPLSTVSFK	7	M2(Oxidation); M5(Oxidation); S37(Phospho)	T(11): 0.0; S(13): 0.0; S(14): 0.0; S(21): 0.0; T(26): 0.0; S(29): 0.0; S(32): 0.6; S(34):

			5.5; S(37): 58.6; T(38): 17.6; S(40): 17.6
DKEDLVCSAALHSPQESPVGKEDR	2	C7(Carbamidomethyl); S13(Phospho); S17(Phospho)	S(8): 50.1; S(13): 50.1; S(17): 99.9
DKEDLVCSAALHSPQESPVGKEDR	1	C7(Carbamidomethyl)	
SVPEHAELVEDSSPESEPVDLFSDDSIPEVPQTQEEAVMLMK	2	M39(Oxidation); M41(Oxidation)	
QPSWERSPAAPAPSLPPAAAVLPSK	3	S3(Phospho); S7(Phospho)	S(3): 100.0; S(7): 100.0; S(14): 0.0; S(24): 0.0
QPSWERSPAAPAPSLPPAAAVLPSK	2	S3(Phospho)	S(3): 84.4; S(7): 15.6; S(14): 0.0; S(24): 0.0
DSEGRNEDASFPSTPEPVK	5	S10(Phospho); S13(Phospho)	S(2): 0.0; S(10): 66.7; S(13): 66.7; T(14): 66.7
ETKLSTEPSPDFSNYSEIAK	2	S5(Phospho)	T(2): 0.2; S(5): 49.2; T(6): 49.2; S(9): 1.3; S(13): 0.0; Y(15): 0.0; S(16): 0.0
EKISLQMEEFNIAIYSNDDLSSKEDK	1	M7(Oxidation)	
GPLPAAPPAAPERQPSWER	2	S16(Phospho)	S(16): 100.0
ETKLSTEPSPDFSNYSEIAK	3	S5(Phospho); S9(Phospho)	T(2): 1.1; S(5): 49.5; T(6): 49.5; S(9): 100.0; S(13): 0.0; Y(15): 0.0; S(16): 0.0
TSNPFLVAVQDSEADYVTTDTLSK	2	S2(Phospho)	T(1): 23.0; S(2): 76.8; S(12): 0.1; Y(16): 0.1; T(18): 0.1; T(19): 0.0; T(21): 0.0; S(23): 0.0
SDEGHPFR	12		
AQIITEKTSK	6	S9(Phospho)	T(5): 0.1; T(8): 49.9; S(9): 49.9
SKDKEDLVCSAALHSPQESPVGK	2	C9(Carbamidomethyl); S15(Phospho); S19(Phospho)	S(1): 0.0; S(10): 0.0; S(15): 100.0; S(19): 100.0
ESETFSDSSPIEIIDEFPTFVSAKDDSPK	3	T19(Phospho)	S(2): 0.0; T(4): 0.0; S(6): 0.0; S(8): 0.0; S(9): 0.0; T(19): 78.8; S(22): 17.2; S(27): 4.0
IMDLMEQPGNTVSSGQEDFPSVLLETAASLPSLSPLSTVSFK	7	M2(Oxidation); S34(Phospho)	T(11): 0.7; S(13): 2.8; S(14): 2.8; S(21): 13.3; T(26): 2.8; S(29): 0.7; S(32): 13.3; S(34): 31.0; S(37): 13.3; T(38): 13.3; S(40): 6.0
IMDLMEQPGNTVSSGQEDFPSVLLETAASLPSLSPLSTVSFK	1	M5(Oxidation)	
DAASNDIPTLTK	1	K12(GlyGly)	
GVIQAIQK	3		
DSEGRNEDASFPSTPEPVK	4	T14(Phospho)	S(2): 0.0; S(10): 0.0; S(13): 2.7; T(14): 97.3

ESLTEVSETVAQHKEER	2	K14(GlyGly)	
DSEGRNEDASFPSTPEPVKDSSR	4	S10(Phospho); S13(Phospho)	S(2): 2.6; S(10): 97.3; S(13): 13.8; T(14): 86.3; S(21): 0.0; S(22): 0.0
NEDASFPSTPEPVK	4	S5(Phospho); S8(Phospho)	S(5): 99.9; S(8): 50.0; T(9): 50.0
KLPSDTEK	1		
IKESETFSDSSPIEIDEFPTFVSAKDDSPK	1	T6(Phospho); S29(Phospho)	S(4): 3.9; T(6): 3.9; S(8): 12.1; S(10): 40.0; S(11): 40.0; T(21): 2.9; S(24): 8.6; S(29): 88.5
SVPEHAELVEDSSPESEPVDLFSDDSIPEVPQTQEEAVMLMK	1		
DKEDLVCSAALHSPQESPVGK	2	C7(Carbamidomethyl); S13(Phospho); S17(Phospho)	S(8): 0.0; S(13): 100.0; S(17): 100.0
DAASNDIPTLTCK	2		
AQIITEK	3		
GSPKGESAILVENTK	2	S2(Phospho)	S(2): 100.0; S(7): 0.0; T(14): 0.0
ESETFSDSSPIEIDEFPTFVSAK	1	S6(Phospho); S8(Phospho)	S(2): 12.1; T(4): 27.6; S(6): 69.9; S(8): 81.1; S(9): 8.8; T(19): 0.2; S(22): 0.2
ESETFSDSSPIEIDEFPTFVSAKDDSPK	1	S9(Phospho); S22(Phospho)	S(2): 0.8; T(4): 0.8; S(6): 2.3; S(8): 7.4; S(9): 88.7; T(19): 47.9; S(22): 47.9; S(27): 4.1
YSNSALGHVNSTIK	1	K14(GlyGly)	
MEDIDQSSLVSSSTDSPRPAPAFK	1	M1(Oxidation); S7(Phospho)	S(7): 27.7; S(8): 27.7; S(11): 7.4; S(12): 7.4; S(13): 27.7; T(14): 2.1; S(16): 0.1
SVPEHAELVEDSSPESEPVDLFSDDSIPEVPQTQEEAVMLMK	2	M39(Oxidation)	
LSTEPSPDFSNYSEIAK	1	K17(GlyGly)	

Table 2-2: Post-translationally modifications on neuronal NogoA do not significantly change following chronic TTX treatment.

NogoA was immunoprecipitated from rat primary hippocampal neurons on DIV17 following 24 hours of 2 μ M tetrodotoxin (TTX) treatment, and subjected to LC-MS/MS. This table summarizes the peptides identified from both CID and HDC fragmentation methods. The column on the right indicates the probability that each serine, threonine, or tyrosine residue is phosphorylated, for a given phospho-peptide.

2.10 References

1. M. S. Chen *et al.*, Nogo-A is a myelin-associated neurite outgrowth inhibitor and an antigen for monoclonal antibody IN-1. *Nature* **403**, 434-439 (2000).
2. A. B. Huber, O. Weinmann, C. Brosamle, T. Oertle, M. E. Schwab, Patterns of Nogo mRNA and protein expression in the developing and adult rat and after CNS lesions. *The Journal of neuroscience : the official journal of the Society for Neuroscience* **22**, 3553-3567 (2002).
3. Y. Zhang *et al.*, An RNA-sequencing transcriptome and splicing database of glia, neurons, and vascular cells of the cerebral cortex. *The Journal of neuroscience : the official journal of the Society for Neuroscience* **34**, 11929-11947 (2014).
4. Y. Zhang *et al.*, Purification and Characterization of Progenitor and Mature Human Astrocytes Reveals Transcriptional and Functional Differences with Mouse. *Neuron* **89**, 37-53 (2016).
5. A. E. Fournier, T. GrandPré, S. M. Strittmatter, Identification of a receptor mediating Nogo-66 inhibition of axonal regeneration. *Nature* **409**, 341-346 (2001).
6. F. Hu, S. M. Strittmatter, The N-Terminal Domain of Nogo-A Inhibits Cell Adhesion and Axonal Outgrowth by an Integrin-Specific Mechanism. *The Journal of Neuroscience* **28**, 1262-1269 (2008).
7. T. GrandPré, F. Nakamura, T. Vartanian, S. M. Strittmatter, Identification of the Nogo inhibitor of axon regeneration as a Reticulon protein. *Nature* **403**, 439-444 (2000).
8. R. Prinjha *et al.*, Inhibitor of neurite outgrowth in humans. *Nature* **403**, 383-384 (2000).
9. T. Oertle *et al.*, Nogo-A inhibits neurite outgrowth and cell spreading with three discrete regions. *The Journal of neuroscience : the official journal of the Society for Neuroscience* **23**, 5393-5406 (2003).
10. D. H. Hubel, T. N. Wiesel, S. LeVay, H. B. Barlow, R. M. Gaze, Plasticity of ocular dominance columns in monkey striate cortex. *Philosophical Transactions of the Royal Society of London. B, Biological Sciences* **278**, 377-409 (1977).
11. S. Le Vay, T. N. Wiesel, D. H. Hubel, The development of ocular dominance columns in normal and visually deprived monkeys. *Journal of Comparative Neurology* **191**, 1-51 (1980).

12. A. W. McGee, Y. Yang, Q. S. Fischer, N. W. Daw, S. M. Strittmatter, Experience-driven plasticity of visual cortex limited by myelin and Nogo receptor. *Science (New York, N.Y.)* **309**, 2222-2226 (2005).
13. J. Syken, T. Grandpre, P. O. Kanold, C. J. Shatz, PirB restricts ocular-dominance plasticity in visual cortex. *Science* **313**, 1795-1800 (2006).
14. T. Pizzorusso *et al.*, Reactivation of Ocular Dominance Plasticity in the Adult Visual Cortex. *Science* **298**, 1248-1251 (2002).
15. S. J. Raiker *et al.*, Oligodendrocyte-Myelin Glycoprotein and Nogo Negatively Regulate Activity-Dependent Synaptic Plasticity. *The Journal of Neuroscience* **30**, 12432-12445 (2010).
16. A. Delekate, M. Zagrebelsky, S. Kramer, M. E. Schwab, M. Korte, NogoA restricts synaptic plasticity in the adult hippocampus on a fast time scale. *Proceedings of the National Academy of Sciences* **108**, 2569-2574 (2011).
17. B. Tews *et al.*, Synthetic microRNA-mediated downregulation of Nogo-A in transgenic rats reveals its role as regulator of synaptic plasticity and cognitive function. *Proceedings of the National Academy of Sciences* **110**, 6583-6588 (2013).
18. A. Zemmar *et al.*, Neutralization of Nogo-A Enhances Synaptic Plasticity in the Rodent Motor Cortex and Improves Motor Learning in Vivo. *The Journal of Neuroscience* **34**, 8685-8698 (2014).
19. A. Kempf *et al.*, The Sphingolipid Receptor S1PR2 Is a Receptor for Nogo-A Repressing Synaptic Plasticity. *PLOS Biology* **12**, e1001763 (2014).
20. A. Zemmar *et al.*, Oligodendrocyte- and Neuron-Specific Nogo-A Restrict Dendritic Branching and Spine Density in the Adult Mouse Motor Cortex. *Cereb Cortex*, 1-9 (2017).
21. H. Lee *et al.*, Synaptic function for the Nogo-66 receptor NgR1: regulation of dendritic spine morphology and activity-dependent synaptic strength. *The Journal of neuroscience : the official journal of the Society for Neuroscience* **28**, 2753-2765 (2008).
22. A. Kempf, M. E. Schwab, Nogo-A Represses Anatomical and Synaptic Plasticity in the Central Nervous System. *Physiology* **28**, 151-163 (2013).
23. S. Jitsuki *et al.*, Nogo Receptor Signaling Restricts Adult Neural Plasticity by Limiting Synaptic AMPA Receptor Delivery. *Cerebral Cortex* **26**, 427-439 (2015).
24. M. Zagrebelsky, R. Schweigreiter, C. E. Bandtlow, M. E. Schwab, M. Korte, Nogo-A stabilizes the architecture of hippocampal neurons. *The Journal of*

- neuroscience : the official journal of the Society for Neuroscience* **30**, 13220-13234 (2010).
25. S. Fricke *et al.*, Fast Regulation of GABAAR Diffusion Dynamics by Nogo-A Signaling. *Cell Reports* **29**, 671-684.e676 (2019).
 26. G. G. Turrigiano, K. R. Leslie, N. S. Desai, L. C. Rutherford, S. B. Nelson, Activity-dependent scaling of quantal amplitude in neocortical neurons. *Nature* **391**, 892-896 (1998).
 27. G. G. Turrigiano, S. B. Nelson, Homeostatic plasticity in the developing nervous system. *Nat Rev Neurosci* **5**, 97-107 (2004).
 28. Graham H. Diering, Ahleah S. Gustina, Richard L. Huganir, PKA-GluA1 Coupling via AKAP5 Controls AMPA Receptor Phosphorylation and Cell-Surface Targeting during Bidirectional Homeostatic Plasticity. *Neuron* **84**, 790-805 (2014).
 29. G. H. Diering *et al.*, Homer1a drives homeostatic scaling-down of excitatory synapses during sleep. *Science* **355**, 511-515 (2017).
 30. M. C. Ashby, S. R. Maier, A. Nishimune, J. M. Henley, Lateral diffusion drives constitutive exchange of AMPA receptors at dendritic spines and is regulated by spine morphology. *The Journal of neuroscience : the official journal of the Society for Neuroscience* **26**, 7046-7055 (2006).
 31. Richard L. Huganir, Roger A. Nicoll, AMPARs and Synaptic Plasticity: The Last 25 Years. *Neuron* **80**, 704-717 (2013).
 32. G. H. Diering, R. L. Huganir, The AMPA Receptor Code of Synaptic Plasticity. *Neuron* **100**, 314-329 (2018).
 33. P. Cohen, The regulation of protein function by multisite phosphorylation – a 25 year update. *Trends in Biochemical Sciences* **25**, 596-601 (2000).
 34. W. Lu, K. W. Roche, Posttranslational regulation of AMPA receptor trafficking and function. *Current Opinion in Neurobiology* **22**, 470-479 (2012).
 35. A. Barria, V. Derkach, T. Soderling, Identification of the Ca²⁺/Calmodulin-dependent Protein Kinase II Regulatory Phosphorylation Site in the α -Amino-3-hydroxyl-5-methyl-4-isoxazole-propionate-type Glutamate Receptor. *Journal of Biological Chemistry* **272**, 32727-32730 (1997).
 36. A. L. Mammen, K. Kameyama, K. W. Roche, R. L. Huganir, Phosphorylation of the α -Amino-3-hydroxy-5-methylisoxazole-4-propionic Acid Receptor GluR1 Subunit by Calcium/ Calmodulin-dependent Kinase II. *Journal of Biological Chemistry* **272**, 32528-32533 (1997).

37. A. Barria, D. Muller, V. Derkach, L. C. Griffith, T. R. Soderling, Regulatory Phosphorylation of AMPA-Type Glutamate Receptors by CaM-KII During Long-Term Potentiation. *Science* **276**, 2042-2045 (1997).
38. J. Boehm *et al.*, Synaptic Incorporation of AMPA Receptors during LTP Is Controlled by a PKC Phosphorylation Site on GluR1. *Neuron* **51**, 213-225 (2006).
39. N. J. Allen *et al.*, Astrocyte glypicans 4 and 6 promote formation of excitatory synapses via GluA1 AMPA receptors. *Nature* **486**, 410-414 (2012).
40. L. E. Clarke, B. A. Barres, Emerging roles of astrocytes in neural circuit development. *Nature Reviews Neuroscience* **14**, 311-321 (2013).
41. Ç. Eroglu *et al.*, Gabapentin Receptor $\alpha 2 \delta$ -1 Is a Neuronal Thrombospondin Receptor Responsible for Excitatory CNS Synaptogenesis. *Cell* **139**, 380-392 (2009).
42. C. Eroglu, B. A. Barres, Regulation of synaptic connectivity by glia. *Nature* **468**, 223-231 (2010).
43. M. Simonen *et al.*, Systemic Deletion of the Myelin-Associated Outgrowth Inhibitor Nogo-A Improves Regenerative and Plastic Responses after Spinal Cord Injury. *Neuron* **38**, 201-211 (2003).
44. F. Vajda *et al.*, Cell type-specific Nogo-A gene ablation promotes axonal regeneration in the injured adult optic nerve. *Cell death and differentiation* **22**, 323-335 (2015).
45. D. A. Dodd *et al.*, Nogo-A, -B, and -C Are Found on the Cell Surface and Interact Together in Many Different Cell Types. *Journal of Biological Chemistry* **280**, 12494-12502 (2005).
46. J. C. Tu *et al.*, Coupling of mGluR/Homer and PSD-95 Complexes by the Shank Family of Postsynaptic Density Proteins. *Neuron* **23**, 583-592 (1999).
47. R. H. Quarles, Myelin-associated glycoprotein (MAG): past, present and beyond. *Journal of Neurochemistry* **100**, 1431-1448 (2007).
48. J. Barral, A. D Reyes, Synaptic scaling rule preserves excitatory–inhibitory balance and salient neuronal network dynamics. *Nature Neuroscience* **19**, 1690-1696 (2016).
49. Y. Lin *et al.*, Activity-dependent regulation of inhibitory synapse development by Npas4. *Nature* **455**, 1198 (2008).
50. M. Ichikawa, K. Muramoto, K. Kobayashi, M. Kawahara, Y. Kuroda, Formation and maturation of synapses in primary cultures of rat cerebral cortical cells: an electron microscopic study. *Neurosci Res* **16**, 95-103 (1993).

51. T. A. Basarsky, V. Parpura, P. G. Haydon, Hippocampal synaptogenesis in cell culture: developmental time course of synapse formation, calcium influx, and synaptic protein distribution. *The Journal of neuroscience : the official journal of the Society for Neuroscience* **14**, 6402-6411 (1994).
52. J. D. Sinor *et al.*, NMDA and glutamate evoke excitotoxicity at distinct cellular locations in rat cortical neurons in vitro. *The Journal of neuroscience : the official journal of the Society for Neuroscience* **20**, 8831-8837 (2000).
53. K. T. Baldwin, A. A. University of Michigan, Ed. (Dissertations and Theses (Ph.D. and Master's), Deep Blue, 2015).
54. F. K. Stephan, Circadian rhythms in the rat: constant darkness, entrainment to T cycles and to skeleton photoperiods. *Physiology & behavior* **30**, 451-462 (1983).
55. P. P. Roux *et al.*, K252a and CEP1347 are neuroprotective compounds that inhibit mixed-lineage kinase-3 and induce activation of Akt and ERK. *The Journal of biological chemistry* **277**, 49473-49480 (2002).
56. B. Niederost, T. Oertle, J. Fritsche, R. A. McKinney, C. E. Bandtlow, Nogo-A and myelin-associated glycoprotein mediate neurite growth inhibition by antagonistic regulation of RhoA and Rac1. *The Journal of neuroscience : the official journal of the Society for Neuroscience* **22**, 10368-10376 (2002).
57. M. Kovacs, J. Toth, C. Hetenyi, A. Malnasi-Csizmadia, J. R. Sellers, Mechanism of blebbistatin inhibition of myosin II. *The Journal of biological chemistry* **279**, 35557-35563 (2004).
58. T. Walchli *et al.*, Nogo-A is a negative regulator of CNS angiogenesis. *Proc Natl Acad Sci U S A* **110**, E1943-1952 (2013).
59. M. Sepe *et al.*, Proteolytic control of neurite outgrowth inhibitor NOGO-A by the cAMP/PKA pathway. *Proceedings of the National Academy of Sciences* **111**, 15729-15734 (2014).
60. P. Tsokas *et al.*, Local protein synthesis mediates a rapid increase in dendritic elongation factor 1A after induction of late long-term potentiation. *The Journal of neuroscience : the official journal of the Society for Neuroscience* **25**, 5833-5843 (2005).
61. B. E. Pfeiffer, K. M. Huber, Current Advances in Local Protein Synthesis and Synaptic Plasticity. *The Journal of Neuroscience* **26**, 7147-7150 (2006).
62. M. A. Sutton *et al.*, Miniature Neurotransmission Stabilizes Synaptic Function via Tonic Suppression of Local Dendritic Protein Synthesis. *Cell* **125**, 785-799 (2006).

63. R. S. Zucker, Calcium- and activity-dependent synaptic plasticity. *Current Opinion in Neurobiology* **9**, 305-313 (1999).
64. I. M. Mansuy, S. Shenolikar, Protein serine/threonine phosphatases in neuronal plasticity and disorders of learning and memory. *Trends Neurosci* **29**, 679-686 (2006).
65. H.-K. Lee, Synaptic plasticity and phosphorylation. *Pharmacology & Therapeutics* **112**, 810-832 (2006).
66. K. Okamoto, M. Bosch, Y. Hayashi, The Roles of CaMKII and F-Actin in the Structural Plasticity of Dendritic Spines: A Potential Molecular Identity of a Synaptic Tag? *Physiology* **24**, 357-366 (2009).
67. J. Lisman, R. Yasuda, S. Raghavachari, Mechanisms of CaMKII action in long-term potentiation. *Nat Rev Neurosci* **13**, 169-182 (2012).
68. K. L. Arendt *et al.*, Calcineurin mediates homeostatic synaptic plasticity by regulating retinoic acid synthesis. *Proc Natl Acad Sci U S A* **112**, E5744-5752 (2015).
69. D. Z. Bar *et al.*, Biotinylation by antibody recognition—a method for proximity labeling. *Nature Methods* **15**, 127-133 (2018).
70. K. J. Roux, D. I. Kim, B. Burke, D. G. May, BioID: A Screen for Protein-Protein Interactions. *Curr Protoc Protein Sci* **91**, 19.23.11-19.23.15 (2018).
71. K. D. McCarthy, J. de Vellis, Preparation of separate astroglial and oligodendroglial cell cultures from rat cerebral tissue. *The Journal of Cell Biology* **85**, 890-902 (1980).

CHAPTER 3:

shRNA in Neurons: Robust Synaptic Regulations Independent of Primary Target

3.1 Abstract

NogoA's inhibition on synaptic plasticity has been studied through function neutralization and genomic knockout. Since ER-resident NogoA is largely intracellular, surface neutralization is an inadequate approach to block NogoA signaling and function. Moreover, *NogoA* knockout causes compensation by *NogoB* and other inhibitory genes. Hence, studies used various RNA interference (RNAi) approaches to knock down neuronal NogoA. However, there has not been a consolidatory characterization of the molecular mechanisms underlying reported morphological phenotypes. Here, we use lentiviral vector (LV)-mediated transduction of a small hairpin RNA (shRNA) against NogoA (shNogoA). In shNogoA-transduced neurons, we observe a strong upregulation of the immediate-early gene (IEG) *Npas4*, and downregulation of excitatory (GluA1) and inhibitory (GAD-65/67) synaptic proteins. In stark contrast, both Cre excision of *NogoABC^{fl/fl}* from hippocampal neurons and step-wise mutations in the shNogoA seed region confirm NogoA-independent nature of synaptic regulations. RNA-sequencing experiments investigate shNogoA's off-target effects, dependence on the micro RNA (miRNA) machinery, and participation in regulating synapse generation and strength.

3.2 Introduction

The mammalian *Reticulon-4* (*Rtn4*) gene encodes three different splice isoforms, with corresponding protein products NogoA (190kDa), NogoB (55kDa), and NogoC (25kDa) (1-3). While NogoC is not expressed within the CNS and restricted to muscle tissue, NogoA and NogoB are abundantly found in the developing and adult brain and spinal cord (3). NogoA and NogoB share the Nogo-66 domain, which has been extensively characterized as the principal binding partner of Nogo-66 Receptor 1 (NgR1) and paired immunoglobulin-like receptor B (PirB) to drive growth cone collapse and negatively regulate activity-dependent synaptic strength (2, 4-8). In addition, NogoA harbors another inhibitory transmembrane domain, NogoA- Δ 20, which binds to a poorly characterized set of receptors including sphingosine-1-phosphate receptor 2 (S1PR2) and integrins. NogoA- Δ 20 region signaling has been shown to relay a whole set of inhibitory function, especially on the regulation of activity-dependent synaptic plasticity (2, 9-11).

Most studies used monoclonal function blocking antibodies against the NogoA- Δ 20 region or NgR1 counteract NogoA signaling on the cell surface. As a result, negating the inhibitory function of NogoA yielded a more robust induction of LTP (10, 12, 13). However, the drawback of this method is the expression pattern and unknown intracellular signaling of NogoA: NogoA is an ER-resident protein (14), and expressed only at a small fraction on cell surface (Figure 2-2) (15). Upon binding to the function-blocking antibody, NogoA is endocytosed and therefore can no longer interact with NgR1 or S1PR2 on the cell surface. However, this recycling endosomal NogoA complex's physiological function, degradation, and turnover are still not well understood

(16). To circumvent remaining intracellular NogoA and its unknown function, many groups have generated genomic knockout mouse models, where either gene encoding *Nogo(A)* or *NgR1* was completely removed from the genome. First of all, based on the generation of the knockout mouse model, different groups demonstrated different extents of axonal regeneration following injury to the spinal cord (17-19). Moreover, genomic deletion of *NogoA* or *NgR1* failed to display enhanced LTP induction (10). Upon closer examination, this lack of regenerative or synaptic phenotypes could be explained by compensatory upregulation of the *NogoB* isoform and numerous other inhibitory genes, which might collectively act as homeostatic regulators upon activity-dependent synaptic plasticity mechanisms (17, 20).

Altogether, there is a gap in our knowledge of NogoA function specifically within the context of synaptic formation, maintenance, and plasticity. To address that question, many groups have used various small RNA interference methods to acutely knockdown NogoA (13, 21-23). More recently, studies have shifted to using *Rtn4(a)* conditional knockout mouse models for neuron- or oligodendrocyte-specific deletion (24-26). Many of these investigations successfully release the inhibitory brakes imposed by NogoA, and evaluate structural and morphological changes of the dendritic spine maturity, density, and complexity (6, 7, 12, 13, 23, 25, 27). Although these findings are of significance, our understanding of how neuronal or even synaptic NogoA loss entrains these snapshot observations is still lacking. To date, there is a singular study with some concentration on molecular consequences of NogoA loss. Investigators knocked down NogoA in primary hippocampal neuronal cultures using a small interfering RNA (siRNA), and observed a robust upregulation of glutamatergic AMPA and NMDA receptor subunit

expression in an mTOR-pathway dependent manner (28). However, there has been no significant effort to follow up on and conceptualize these novel findings.

Here, we attempt to bridge the gap in our understanding of physiological function of NogoA as well as consequences of NogoA depletion. We employed a previously published small hairpin RNA (shRNA), which was designed specifically to target NogoA and successfully used in organotypic hippocampal slice cultures (13). Most importantly, we verified stable expression of NogoB, without obvious compensatory upregulation as seen with genomic knockouts. Using this shRNA, we knocked down neuronal NogoA expression in primary neuronal cultures prepared from the rodent hippocampus, and observed robust changes in many genes implicated in synaptic formation and plasticity. Unfortunately, despite use of similar systems, our findings were in opposition to the above-mentioned study (28). To deepen our understanding and consolidate different findings, we conducted and analyzed nascent and stable mRNA transcriptome following NogoA knockdown. This allowed us to identify interesting molecular players, which involved activity-dependent and immediate-early transcription factors, especially important for inhibitory synaptogenesis. However, combining shRNA-mediated NogoA knockdown (13) with recombination-mediated *NogoABC* knockout (26) revealed that the observed phenotypes were due to the presence of non-specific targets that persist with step-wise point mutations within the NogoA shRNA seed region. As such, ongoing work is focused on conceptualizing the analysis of additional total and small RNA sequencing experiments. Further investigations will focus on the identification of shRNA off-targets, dysregulated miRNA processing machinery, and activated interferon response that collectively impair excitatory synaptic transmission and inhibitory synaptogenesis.

3.3 Results

3.3.1 *NogoA shRNA Reduces Baseline Excitatory Synaptic Transmission and Blocks Homeostatic Scaling*

Since there was an account of shRNA-mediated NogoA knockdown robustly upregulating glutamatergic receptor subunits, we were curious about the possible contributing mechanisms (28). We therefore used a NogoA-specific shRNA, previously characterized to increase dendritic branching complexity and spine immaturity of CA3 pyramidal neurons similarly to the function-blocking antibody 11C7 treatment (13). We transduced days *in vitro* (DIV)10 primary hippocampal cultures with this GFP-tagged shRNA (hereafter referred to as shNogoA), and allowed 7DIV before processing and analysis. For most experiments, concomitant lentiviral transduction with an empty vector pLentilox3.7-GFP (hereafter referred to as pLL3.7 or EV) was used as negative control. First of all, we assessed the extent of GFP-expressing cell numbers, and verified that both lentiviral vectors (LVs) had approximately 80% transduction efficiency (data not shown). Total cell lysate analysis by Western blotting replicated initial characterization of the shRNA: LV-shNogoA transduction depleted almost all detectable levels of neuronal NogoA ($\Delta_{\text{mean}} \pm \text{SEM} = -96.26 \pm 1.22\%$, $n=4$, $p<0.0001$), while the NogoB isoform remained unchanged ($n=2$, $p=0.4270$). Then, we looked at some of the proteins important for glutamatergic synaptic transmission and synaptic plasticity. In stark contrast to the previous study's reports (28), both AMPA receptor subunits GluA1 ($\Delta_{\text{mean}} \pm \text{SEM} = -58.39 \pm 2.58\%$, $n=5$, $p<0.0001$) and GluA2 ($\Delta_{\text{mean}} \pm \text{SEM} = -26.03 \pm 3.24\%$,

$n=5$, $p=0.0013$) were robustly downregulated upon LV-shNogoA transduction. Moreover, even within glutamatergic signaling, this was quite specific to AMPA receptors, since neither NMDA receptor subunit GluN2B nor the post-synaptic density scaffolding protein PSD-95 expression showed significant change ($n=2-3$, $p\geq 0.2830$). Lastly, since *Peng et al.* implicated mTOR signaling pathway as the mediator of their siNogoA's effects (28), we investigated the possibility of mTOR signaling pathway activation, and instead discovered a robust downregulation of both total and phosphorylated levels of S6K ($\Delta_{\text{mean}}\pm\text{SEM}=-46.45\pm 5.73\%$, $n=4$, $p=0.0002$) (Figure 3-1A-A'). To answer whether or not these protein expression patterns were downstream of gene regulation, we employed RT² Profiler PCR array plates for GABA/Glutamate in addition to mTOR signaling pathways. Consistent with previous biochemical findings, genes encoding GluA1 (*Gria1*, $\Delta_{\text{mean}}\pm\text{SEM}=-56.20\pm 6.36\%$, $n=4$, $p=0.0001$), GluA2 (*Gria2*, $\Delta_{\text{mean}}\pm\text{SEM}=-37.94\pm 12.59\%$, $n=4$, $p=0.0236$), and S6K (*Rps6kb1*, $\Delta_{\text{mean}}\pm\text{SEM}=-49.62\pm 0.10\%$, $n=4$, $p<0.0001$) were all drastically and significantly downregulated upon shNogoA transduction. On the other hand, gene products encoding NMDA receptor subunits GluN1 (*Grin1*), GluN2B (*Grin2b*), or another post-synaptic density protein Homer1 (*Homer1*) did not change significantly ($n=4$, $p\geq 0.3551$) (Figure 3-1A'). This suggested that there was an upstream downregulation of genes important for excitatory synaptic transmission, albeit in opposition with previous findings (28).

We were then curious whether the delivery of shNogoA transduction within the developmental timeline of the primary hippocampal cultures plays a role in neuronal health or manifestation of observed phenotypes. To investigate the kinetics of NogoA knockdown and regulation of synaptic proteins, we transduced neurons at synaptically

immature (DIV3), intermediate (DIV10), and mature (DIV14) states, and harvested total cell lysates on DIV17 (29). Firstly, morphological assessment by bright field microscopy (data not shown) and detection of comparable neuron-specific β -III Tubulin (TUJ1) signal (Figure 3-1B) collectively indicated lack of significant neuronal toxicity associated with LV-shNogoA transduction, regardless of the developmental timeline of the cultures at the time of infection. Next, Western blot analysis demonstrated two important findings: 1. shNogoA-mediated NogoA depletion requires more than three days to reach near-complete levels. 2. The robust downregulation of GluA1 can be observed regardless of the maturity of the culture at the time of shNogoA infection, so long as NogoA levels are significantly knocked down (Figure 3-1B).

Before we further investigated the mechanisms underlying phenotypes observed following the shNogoA transduction, we wanted to confirm NogoA dependence and target specificity. To that end, we employed the same embryonic rat hippocampal culture system and experimental timeline, but transduced neurons with different commercially available shRNAs against NogoA. We established baseline expression by including three negative controls: no lentiviral vector infection, empty-vector (pLL3.7) that serves as backbone for all LV constructs used in our studies, and a scrambled shRNA designed for the previously published shNogoA (13). Then we compared our characterized shNogoA (13) to commercially available shRNAs against NogoA, one from Open Biosystems and two from Origene. Having observed satisfactory baseline similarity amongst the negative controls, we verified that none of the lentiviral vector transductions showed neuronal toxicity, as assessed by comparable TUJ1 signal (Figure 3-1C) and bright field microscopy (data not shown). Next, we first investigated

NogoA expression following these four shNogoAs. Besides sh-OpenBio, all other shNogoAs robustly reduced NogoA protein expression, even though previously characterized shNogoA was still the most effective (13). Whenever NogoA expression was successfully knocked down, we observed a drastic decrease with GluA1 and p-S6K expression, while NogoB levels remained unchanged (Figure 3-1C). Lastly, we generated an shNogoA-resistant, LV-human-NogoA-myc overexpression construct to conduct phenotype rescue experiments. Despite successful overexpression in non-neuronal (HEK-293T) cells, transduction of primary hippocampal neurons with the same construct failed to overexpress recombinant NogoA or rescue depleted NogoA (data not shown). Taken together, these results still strongly indicate the involvement of NogoA in the regulation of glutamatergic synaptic proteins.

Because GluA1 transcription, translation, and trafficking are important steps within the maintenance of activity-dependent and homeostatic synaptic plasticity (30-39), we became interested in the shNogoA-transduced neurons' ability to dynamically modulate synaptic strength. To investigate this question, we transduced embryonic rat hippocampal neurons with the pLL3.7 or shNogoA lentiviral vectors on DIV10, allowed 6DIV for near-complete NogoA depletion and GluA1 downregulation, and silenced global neuronal activity with 2 μ M of tetrodotoxin (TTX) for 24 hours. Upon chronic silencing, pyramidal neurons are known to increase GluA1 production, trafficking to and stabilization at the post-synaptic sites (31-39), by so doing maintain a stable range of firing rate. In addition to the reduction in GluA1 mRNA and protein expression (Figure 3-1A-A'), we found that shNogoA transduction decreased baseline surface GluA1 levels by about 50% ($n=5$, $p=0.0005$). More interestingly, when neurons were challenged with

chronic TTX treatment, while pLL3.7-transduced neurons could upregulate surface GluA1 expression by ~45% ($n=5$, $p=0.0018$), shNogoA-transduced neurons stalled at baseline levels regardless of treatment ($n=5$, $p=0.3957$) (Figure 3-1C-C'). This was a novel observation, indicating that shNogoA transduction blocks homeostatic mechanisms to upregulate and traffic GluA1 subunits onto the cell surface.

To test true physiological relevance of the modulation of mRNA, total and surface protein expression, we employed electrophysiological recordings of miniature excitatory post-synaptic currents (mEPSCs) from GFP-expressing, pyramidal-like neurons that were sparsely transfected with scrambled shRNA or shNogoA. In line with previous reports of homeostatic scaling, neurons transduced with the scrambled shRNA bidirectionally modulated mEPSC amplitude with 24 hours of 1 μ M TTX (scaling up, $\Delta_{\text{mean}}=+21\%$, $p=0.0124$) and 10 μ M bicuculline (BIC) (scaling down, $\Delta_{\text{mean}}=-22\%$, $p=0.0056$) treatments (Figure 3-1E-E') (38). On the other hand, neurons transduced with the shNogoA had a significantly lower baseline mEPSC amplitude ($\Delta_{\text{mean}}=-23\%$, $p=0.0029$), consistent with our previous biochemical findings. In fact, neurons with shNogoA transduction and vehicle treatment displayed very similar mEPSC amplitudes when compared to neurons with scrambled shRNA transduction and chronic BIC treatment ($\Delta_{\text{mean}}=10\%$, $p=0.8642$). This observation was suggestive of their baseline downscaled state. More interestingly, neurons with shNogoA transduction failed to modulate synaptic drive when chronically treated with TTX to scale up ($p=0.2670$), or with BIC to scale down ($p=0.2060$). In fact, comparison of mEPSC amplitudes between TTX- and BIC-treated states revealed no overall difference ($\Delta_{\text{mean}}=1.13\%$, $p=0.8938$). Lastly, there were no significant differences seen with mEPSC frequencies or decay

times (Figure 3-1E'), collectively implicating regulation of glutamatergic post-synaptic receptor abundance and trafficking. Taken together, these data strongly demonstrate that the shNogoA transduction significantly downregulates expression of AMPA receptor subunits, and permanently lowers baseline excitatory synaptic transmission to a downscaled state. As a result, shNogoA-transduction cell autonomously prevents neurons from bidirectionally modulating synaptic drive in an attempt to maintain steady-state firing against drastic changes in network activity levels.

3.3.2 shNogoA Alters the Landscape of the Immediate-Early Synaptic Gene Expression

Since mTOR signaling pathway is especially important for local protein synthesis, which has been previously implicated in various forms of synaptic plasticity (40-42), we reasoned that the shNogoA-mediated robust reduction in S6K mRNA, protein, and phosphorylation might be a valid candidate to explain some of our observations with biochemical regulations and electrophysiological recordings. However, the drastic regulation of synaptic gene expressions cannot be explained by such mechanism. To deepen our understanding and discover possible signaling candidates in an unbiased assay, we carried out extensive RNA sequencing experiments with rat forebrain cultures transduced with LV-pLL3.7 control vector or LV-shNogoA. We infected these neurons on DIV6 to intervene at a more critical, synaptically immature state, and waited for 4DIV to capture shNogoA's effects in intermediate action, towards the near-complete depletion state. On DIV10, we incubated both groups of neurons with 30 minutes of bromodeoxyuridine (BrdU) in neuronal conditioned medium (NCM), during which any

RNA that was in the process of transcription would incorporate bromo-uridine (BrU). Next, we isolated total RNA from these cultures, and used half of the input RNA to immunoprecipitate BrU-incorporated nascent RNA. We prepared separate RNA libraries, and concomitantly analyzed nascent and total mRNA by next generation sequencing (Figure 3-2A).

Overall, BrU-incorporated, nascent RNA sequencing (BrU-seq) revealed very mild changes induced by shNogoA transduction compared to control, with only ~20% changes in read numbers of differentially expressed genes in either direction. Altogether, we identified 49 upregulated and 28 downregulated genes, nascent RNA of which showed statistically significant change ($p_{adj}<0.05$). Upon closer examination and categorization of some of the candidate genes, we detected many were associated with synaptic components, regulators of axon guidance, and RNA binding (Figure 3-2B). We were particularly interested in *Bdnf*, since its exon-specific transcript expression is heavily regulated by various transcriptional factors binding at different promoter regions depending on behavioral and developmental contexts. Moreover, BDNF protein function has been associated with neuronal development and growth, synaptic plasticity, and inhibitory synaptogenesis (43-49). In our dataset, nascent RNA expression of *Bdnf* was upregulated by ~30% ($p_{adj}=0.0067$), which was relatively high compared to the total change in number of differentially regulated genes (Figure 3-2B).

Next, we analyzed ribosomal RNA (rRNA)-depleted mRNA sequencing (mRNA-seq), which was carried out from the same input RNA isolated from control- vs. shNogoA-transduced forebrain neurons (Figure 3-2A). Compared to nascent transcriptome, mRNA-seq revealed a much greater number of differentially expressed

gene pool: we detected 97 upregulated and 124 downregulated genes with statistical significance ($p_{adj}<0.05$). Even then, the mean fold-change difference in read numbers of mRNA-seq was around 20-30%, quite similar to that of BrU-seq. At an initial glance, we observed that the primary target of the shNogoA, *Rtn4* gene expression, was unequivocally the most heavily downregulated gene product, with a reduction of ~75% in expression ($p_{adj}=8.9\times10^{88}$). On a closer examination, we found the three most well-characterized immediate-early genes (IEGs), *Arc*, *Fos*, and *Npas4*, were all upregulated by more than ~50% upon shNogoA transduction ($p_{adj}=1.0\times10^7$ for *Arc*, $p_{adj}=9.8\times10^8$ for *Fos*, $p_{adj}=9.2\times10^{16}$ for *Npas4*) (Figure 3-2C). We focused particularly on the upregulation of *Npas4*, since many of this transcription factor's established direct DNA-binding partners such as *Nr4a1/2* or *Junb* (50-53) were also upregulated upon shNogoA transduction. Amongst that list was also *Bdnf*, which had come up as one of the prime upregulated candidate genes from our nascent BrU-seq dataset (Figure 3-2B).

Due to poor specificity and affinity of the commercially available antibodies against premature and mature forms of BDNF, we wanted to validate *Bdnf* gene expression upregulation upon shNogoA transduction by quantitative reverse transcription PCR (RT-qPCR). We used previously characterized primer sets (54-56) to detect *Bdnf* gene expression at promoter regions *Bdnf IV* and *Bdnf IX*, since they were both under the regulation of activity-dependent synaptic plasticity, learning and memory (54, 57, 58). Before setting out to assess *Bdnf* upregulation following shNogoA transduction, we wanted to confirm whether expression detection patterns were in line with previous reports. To that end, total RNA was isolated from primary forebrain cultures, treated with 2 μ M TTX (48hrs), 200nM K252a (2hrs), or 10 μ M forskolin (2hrs).

We found that both *Bdnf IV* and *IX* expression were mildly decreased with TTX treatment alone (59), and robustly increased with K252a treatment alone. Moreover, the upregulation induced by K252a could no longer be observed when combined with TTX treatment. Additionally, we observed a significant increase in *Bdnf* expression following acute forskolin treatment (60) (Figure 3-2D). Confident in this system, we isolated total RNA from a separate set of forebrain cultures following the same experimental timeline as depicted in Figure 3-2A. We observed 98.8% and 36.7% increase in *Bdnf IV* and *Bdnf IX* gene expression following shNogoA transduction, respectively ($n=6$; $p=0.0377$ for *IV*, $p=0.0173$ for *IX*) (Figure 3-2D). Here, we demonstrated and confirmed that shNogoA transduction induces upregulation of many immediate-early synaptogenic genes, as well as a number of their direct binding partners. Taken together, these findings render NogoA knockdown an ideal candidate to study regulation synaptic transmission, formation, and modulation.

3.3.3 Global shNogoA Transduction Upregulates *Npas4* via L-Type VGCC Activation

Through our Bru-seq and mRNA-seq experiments, we discovered that *Npas4* and *Bdnf* gene expressions are both upregulated following shNogoA transduction, and the transcription factor *Npas4* was previously shown to directly bind *Bdnf* promoter regions (50, 51). Next, we wanted to explore whether there is a stronger correlation between these two observations. We transduced primary hippocampal cultures with the control vector pLL3.7 or lentiviral shNogoA on DIV3, and allowed for 4DIV to efficiently knock down NogoA to near-complete levels (Figure 3-1B). On DIV7, we treated these

synaptically immature hippocampal neurons with 55mM KCl for 2 hours to induce sustained membrane depolarization, with or without 10 minutes of 5mM EGTA pre-treatment for extracellular calcium chelation (51). We first verified by Western blotting that NogoA protein expression was indeed almost completely depleted (Figure 3-3A). As reported previously and replicated through our studies (Figure 2-3) (51), KCl treatment induced an 81% upregulation of the Npas4 protein expression compared to vehicle-treated baseline ($n=8$, $p=0.0016$). Moreover, EGTA pre-treatment further reduced baseline Npas4 protein expression by an additional 65% ($n=8$, $p=0.0180$) (Figure 3-3A-A'). Next, we examined whether the 86% increase in *Npas4* gene expression we detected with mRNA-seq (Figure 3-2C) translated to the Npas4 protein levels. We found that shNogoA transduction also upregulated baseline Npas4 protein levels by 77% ($n=8$, $p=0.0028$). Strikingly, following shNogoA transduction, KCl treatment failed to cause further upregulation of Npas4 protein expression ($n=8$, $p=0.1660$), possibly due to a ceiling effect. This observation provided the first clue about the involvement of an over-activated calcium influx and/or impaired recycling mechanism (Figure 3-3A-A').

Next, we were curious whether the upregulation of baseline Npas4 persisted well into synaptic maturity, and if so, whether it could be further increased by pharmacological manipulations of synaptic activity. When maintained until DIV14, hippocampal neurons can be synaptically over-activated by acute (2hr) treatment with 50 μ M BIC, which competitively blocks GABA_A receptors, and therefore reduces inhibitory tone. Unlike non-specific membrane depolarizing agent KCl, acute BIC treatment will lead an over-activation of neuronal networks due to pronounced influx of

synaptic calcium through glutamatergic AMPA/NMDA receptors as well as voltage-gated calcium channels (VGCC). In fact, the IEG *Npas4* gets activated by this increase in intracellular calcium concentrations, thereby increasing *Npas4* protein expression, consequent DNA binding, and transcription modulation. For instance, upon such stimulation, direct *Npas4* binding increases at *Bdnf* promoter regions I and IV, which later on plays an important role in driving inhibitory synaptogenesis. In fact, previous reports have shown that complete chelation of extracellular calcium (EGTA), blockade of calcium-permeable glutamate receptors (CNQX, APV), and specific inhibition of L-type VGCCs (nimodipine) drastically negate the BIC-induced upregulation of *Npas4* protein expression (51). As such, we transduced hippocampal neurons with pLL3.7 or shNogoA on DIV3, waited until synaptic maturation on DIV14, and assessed *Npas4* protein expression through different pharmacological treatments. First of all, control neurons transduced with pLL3.7 behaved as previously reported (51): *Npas4* protein expression increased by 5-fold following 2-hour treatment with 50 μ M BIC ($n=8$, $p<0.0001$), and by 8.3-fold following 2-hour treatment with 1 μ M L-type VGCC agonist FPL64176 ($n=8$, $p<0.0001$). This robust induction of *Npas4* expression by BIC treatment was completely reversed to baseline levels with 1-hour pre-treatment with 5 μ M L-type VGCC antagonist nimodipine ($n=8$, $p<0.0001$). Lastly, already low baseline levels of *Npas4* could not be further reduced with 3-hour treatments with 5mM EGTA or 5 μ M nimodipine alone ($n=8$, $p>0.9999$). Following vehicle treatment of shNogoA-transduced neurons, we observed that baseline *Npas4* protein levels increased by 186% ($n=11$, $p=0.0328$) (Figure 3-3A-A''). Compared to DIV7, shNogoA-dependent *Npas4* upregulation was more robust on DIV14, suggestive of an accumulated load or

impairment of the calcium recycling mechanisms of these cultures. Unlike global KCl stimulation on DIV7, however, synaptically mature DIV14 neurons transduced with shNogoA can further upregulate Npas4 expression upon acute BIC ($n=8$, $\Delta_{\text{mean}}=4.15x$, $p=0.0122$) or FPL64176 treatments ($n=8$, $\Delta_{\text{mean}}=6.68x$, $p<0.0001$). As with control neurons, this robust BIC-induced Npas4 upregulation can also be completely depleted by nimodipine pre-treatment ($n=8$, $\Delta_{\text{mean}}=3.39x$, $p<0.0001$). Lastly, we observed that shNogoA-induced upregulation of baseline Npas4 protein expression was reduced by almost 2-fold following acute EGTA ($n=8$, $\Delta_{\text{mean}}=1.4x$, $p_{\text{adj}}=0.4421$) or nimodipine alone ($n=8$, $\Delta_{\text{mean}}=1.6x$, $p_{\text{adj}}=0.2034$) treatments (Figure 3-3A-A''). Taken together, we demonstrated that shNogoA transduction induces robust IEG expression following elevated levels of intracellular calcium, particularly but not exclusively through over-activated L-type VGCCs.

We were then curious about the mechanism(s) behind shNogoA-induced upregulation of Npas4 protein expression, especially upstream of the L-type VGCC activation. To differentiate between cell-autonomous versus network effect, we sparsely transfected hippocampal neurons on DIV3 with the GFP-tagged shNogoA construct, maintained neuronal cultures until synaptic maturity is attained by DIV14, and assessed immunofluorescence signal intensity from nuclear Npas4 expression in comparison to neighboring GFP-negative control cells (Figure 3-3B). Quantification from GFP⁺, NogoA⁻ cells ($n=28$) versus GFP⁻, NogoA⁺ cells ($n=100$) revealed no difference in nuclear Npas4 signal intensity ($p=0.3254$) (Figure 3-3B'). This demonstrated that the cell-autonomous expression of shNogoA does not cause sufficient calcium influx or subsequent Npas4 protein induction. In fact, this observation was in line with the cell-autonomous decrease

in mEPSC amplitude following sparse shNogoA transfection (Figure 3-1D-D'), which would translate to less calcium influx. We then explored the impact of network neuronal activity modulation caused by global LV-shNogoA transduction. Following a similar experimental timeline as DIV3-14 biochemical analysis (Figure 3-3A), we verified robust and global knockdown of NogoA, and assessed nuclear Npas4 protein expression by immunofluorescence analysis. In line with our reported biochemical results (Figure 3A-A''), the percentage of Npas4-expressing Hoechst⁺ nuclei increased by ~50% upon global shNogoA transduction ($n=19-20$ fields of view from $n=3$ biological replicates, $p=0.0001$). Moreover, nuclear Npas4 signal intensity increased by 127% upon global shNogoA transduction, compared to LV-pLL3.7-transduced neurons ($n=76$ neurons from $n=3$ biological replicates, $p<0.0001$). Overall, these data strongly demonstrate that the global shNogoA transduction induces a strong upregulation of Npas4 protein expression through overall increase in neuronal network activity and subsequent influx of extracellular calcium through L-type VGCCs. Future studies should consolidate the interplay between the cell-autonomous decrease in GluA1 expression and mEPSC and network upregulation of calcium influx and Npas4 expression.

3.3.4 NogoA Interacts with and/or Modulates L-type VGCC Auxiliary Subunit Cav α 2 δ 1

In our attempt to decipher the upstream activation of L-type VGCCs following shNogoA transduction, we focused on known calcium channel auxiliary subunits, which can modulate conductance by changing conformation and activation states based on physiological contexts, external stimuli, and intercellular signaling. One such auxiliary

subunit, $\text{Ca}_v\alpha 2\delta 1$ directly interacts with L-type VGCC (61, 62), is the receptor for gabapentin, strongly inhibits excitatory synaptogenesis (63, 64). $\text{Ca}_v\alpha 2\delta 1$ is also the neuronal receptor for thrombospondins, which are astrocyte-secreted growth-promoting molecules that play a role in the excitatory synapse formation and maturation (64, 65). Lastly, hippocampal samples obtained from patients with mesial temporal lobe epileptiform activity showed increased NogoA expression (66), which implicates NogoA in regulating the fine balance between excitation and inhibition.

In order to determine whether NogoA and $\text{Ca}_v\alpha 2\delta 1$ interact *in vivo*, we isolated membrane fractions from post-natal 24 (P24) or adult (\geq P60) mouse brains, and immunoprecipitated NogoA using the NogoA- $\Delta 20$ -specific, mouse monoclonal (11C7) antibody or the isotype-matched anti-FG12 antibody. Despite higher NogoA expression during mid-development, in both young and adult mouse brains, NogoA was strongly detected in the total homogenate (S1), cytosolic fraction (S2), and to a higher extent in the membrane fraction (P2) (Figure 3-4A). The membrane fractions were then solubilized, pre-cleared, and incubated with the above-specified antibodies or empty beads. Using the anti-pan-NogoAB antibody (Bianca), we confirmed that NogoA was specifically enriched in the immunoprecipitated samples. We first checked whether membrane-bound NogoA directly binds GluA1, since shNogoA transduction drastically reduces its expression and surface trafficking. However, no such binding was observed. Our next candidate was the L-type VGCC subunit $\text{Ca}_v 1.2$, which was enriched in brain membrane without NogoA binding. Lastly, we observed a strong co-immunoprecipitation of the membrane-enriched $\text{Ca}_v\alpha 2\delta 1$ auxiliary subunit with anti-NogoA, but not with anti-

FG12 isotype control antibody. This interaction was not as pronounced in the adult brain, perhaps due to the lower input and immunoprecipitation of NogoA (Figure 3-4A).

Next, we immunostained synaptically mature hippocampal neurons with the anti-NogoA (11C7) and anti-Ca_vα2δ1 antibodies under non-permeabilized conditions to detect surface expression patterns, followed by permeabilized anti-MAP2 co-staining to delineate somatodendritic morphology (Figure 3-4B). While overall surface expression patterns were quite distinct from one another, almost all discrete and discontinuous dendritic surface NogoA signal (Figure 2-2C) overlapped with surface Ca_vα2δ1 expression. However, the reverse did not hold true: there was distinguishable surface Ca_vα2δ1 signal that did not overlap with surface NogoA (Figure 3-4B). Overall, immunofluorescence labeling of primary neurons corroborated our biochemical findings, strongly indicating overlapping expression and possible interaction.

Next, we wondered whether shNogoA transduction regulated Npas4 expression through changing Ca_vα2δ1 protein levels. To address that question, we transduced rat hippocampal neurons with shNogoA or control pLL3.7, and probed for total Ca_vα2δ1 by Western blotting. Our initial observation was two distinct bands with different mobility and associated molecular weights: one at the predicted 150kDa (63), and another around 200kDa. shNogoA transduction did not significantly alter the 150kDa band intensity, whereas the band at 200kDa almost completely disappeared (Figure 3-4C). Given NogoA itself is around 200kDa, this was our first suspicion that the commercially available anti-Ca_vα2δ1 antibody also detected rat NogoA. In parallel with consultation with the commercial vendor (Alomone), we aligned the protein sequence of rat NogoA (Uniport # Q9JK11) and the epitope that the anti-Ca_vα2δ1 antibody targets, but at least

algorithmically could not find sufficient homology for cross-detection (data not shown). Finally, we immunostained rat hippocampal neurons for surface NogoA and $\text{Ca}_v\alpha 2\delta 1$ following pLL3.7 or shNogoA transduction. We verified that control-transduced neurons demonstrated similar expression patterns for surface NogoA and $\text{Ca}_v\alpha 2\delta 1$ signal (Figure 3-4B). Upon global knockdown of NogoA, $\text{Ca}_v\alpha 2\delta 1$ surface expression showed a robust reduction along the MAP2^- axons as well as the previously observed discrete and discontinuous patches along the MAP2^+ dendrites (Figure 3-4D). This increased our confidence in cross-reactivity between rat NogoA and $\text{Ca}_v\alpha 2\delta 1$.

To introduce another species and an alternative approach to NogoA depletion, we used a *NogoABC^{fl/fl}* conditional knockout mouse model (Figure 3-7B) (26). Hippocampal cultures were prepared, and one half was transduced with LV-CMV-Cre on DIV3. This would allow for Cre recombinase expression, and subsequent excision of mouse *Rtn4* exons 4 and 5, common to NogoA-C (Figure 3-7B) (26). On DIV6, all cultures were lentivirally co-transduced with either pLL3.7 or shNogoA. We then maintained these cultures until synaptic maturity, and harvested total cell lysates on DIV14 to assess global protein expression by Western blotting. We first verified that NogoA was successfully depleted by either Cre-mediated recombination (~83%) or shNogoA-mediated knockdown (~99%) alone ($n=6$, $p_{adj}<0.0001$). The NogoA-specificity of the shNogoA was once again verified (Figure 3-1) (13, 29), since only the conditional knockout robustly (~90%) depleted NogoB protein expression ($n=3$, $p_{adj}<0.0001$) (Figure 3-7B-B''). When mouse $\text{Ca}_v\alpha 2\delta 1$ protein expression was assessed, observations differed from those with rat hippocampal neurons (Figure 3-4C). First of all, probing for the mouse $\text{Ca}_v\alpha 2\delta 1$ revealed a weak signal at ~100kDa and much stronger, distinct

band around the expected molecular weight ~150kDa (Figure 3-4E). Unlike with rat neurons, we did not observe a non-specific, cross-reactive band around ~200kDa, which had previously disappeared following shNogoA transduction. More interestingly, we show that although the mouse $\text{Ca}_v\alpha 2\delta 1$ levels did not change upon *NogoABC* knockout ($n=3$, $p_{adj}=0.8986$), the protein expression was significantly downregulated following shNogoA knockdown ($n=3$, $\Delta_{\text{mean}}=-31\text{-}35\%$, $p_{adj}=0.0044\text{-}0.0084$) (Figure 3-4E-E'). Taken together, we report a strong functional, biochemical, and colocalizational relationship between the NogoA and $\text{Ca}_v\alpha 2\delta 1$ as a foundation for future investigation of their interconnected regulation. Overall, we demonstrated that rat and mouse protein products could show varying degrees of influence from either shNogoA targeting or antibody reactivity, regardless of highly conserved algorithmic homology.

3.3.5 shNogoA Impairs Homeostatic Scaling Through Immediate-Early Gene Induction

We demonstrated that the shNogoA-transduced neurons not only showed lower baseline synaptic transmission, but also had impaired ability to entrain bidirectional homeostatic scaling (Figure 3-1). We wondered whether these neurons' ability to transcriptionally respond to acute or chronic activity modulators were also impaired. To address this question, we lentivirally transduced hippocampal neurons with pLL3.7 or shNogoA on DIV3, and maintained cultures until synaptic maturity is reached by DIV14. We treated these cultures with 2 μM TTX for 3, 24, and 48 hours, where only the last two chronic treatments will induce homeostatic scaling up (38). On DIV14, 2 hours prior to lysate collection, we challenged these TTX-treated neurons with 50 μM BIC to decrease

spontaneous inhibitory synaptic transmission, which would normally induce Npas4 and c-Fos protein expression. Control neurons behaved as expected: acute BIC treatment induced robust Npas4 and c-Fos protein expression ($n=4$; $p<0.0001$ for Npas4, $p=0.0007$ for c-Fos). Moreover, 1 hour of TTX pre-treatment (totaling 3 hours) sufficiently blocked action potential propagation and prevented BIC-induced upregulation of Npas4 and c-Fos ($n=4-9$; $p=0.0002$ for Npas4, $p=0.0034$ for c-Fos). In contrast, when action potentials were still blocked in the continuous presence of TTX for 48 hours, neuronal cultures still responded to acute BIC treatment possibly by way of blocked miniature inhibitory postsynaptic currents (mIPSCs), and robustly induced Npas4 and c-Fos expression ($n=8-11$; $p=0.0077$ for Npas4, $p=0.0831$ for c-Fos). On the other hand, shNogoA-transduced neurons behaved similarly following acute TTX treatment, but failed to drive scaling up following chronic TTX treatment. First of all, Npas4, but not c-Fos, protein expression was elevated at baseline ($n=10-12$; $p=0.0017$ for Npas4, $p=0.8329$ for c-Fos). As previously reported, acute BIC treatment was able to induce Npas4 and c-Fos upregulation ($n=4-12$; $p=0.2605$ for Npas4, $p=0.0036$ for c-Fos). Like control neurons, 1 hour TTX pre-treatment abolished the BIC-induced IEG expression ($n=4-9$; $p=0.0022$ for Npas4, $p=0.0291$ for c-Fos). In stark contrast, there was no significant difference in the BIC-induced Npas4 or c-Fos protein expression between 3 hours and 48 hours of TTX treatment ($n=8-10$; $p=0.1193$ for Npas4, $p=0.3734$ for c-Fos) (Figure 3-5). These data strongly implicated the induction and regulation of calcium- and activity-dependent IEGs as possible candidates responsible for shNogoA-mediated impaired entrainment of homeostatic synaptic scaling.

3.3.6 *shNogoA Transduction Impairs Inhibitory Synaptogenesis*

One functional and cell-autonomous outcome of post-synaptic Npas4 activation is proper inhibitory synapse formation and strength by way of direct binding to and driving *Bdnf* expression (51). Inspired by this set of findings, we wanted to test whether the Npas4 and *Bdnf* upregulation caused by shNogoA transduction leads to a consequent increase in inhibitory synapse density and/or strength. We sparsely transfected DIV3 hippocampal neurons with the GFP-tagged shNogoA, and qualitatively assessed inhibitory synapse number by immunofluorescence staining against the presynaptic marker GAD-65. We did not detect any noticeable change in peri-somatic or dendritic GAD-65⁺ puncta density between GFP⁺ transduced neurons and GFP⁻ neighboring neurons (Figure 3-6A). Since we had previously demonstrated that shNogoA-mediated Npas4 induction was a network effect rather than a cell autonomous regulation (Figure 3-3), we globally transduced hippocampal neurons following the same timeline, and immunostained for the presynaptic marker GAD-65. Qualitative assessment revealed that global shNogoA transduction robustly decreased presynaptic GAD-65⁺ puncta density, even with similar numbers of somatostatin⁺ inhibitory interneurons (Figure 3-6B). As an alternative verification, we subjected hippocampal neurons to the same experimental paradigm, and quantitatively assessed protein expression by Western blotting. In contrast to previous studies (50, 51, 53), ~3-fold upregulation of Npas4 protein expression ($n=33$, $p<0.0001$) did not lead to an upregulation of inhibitory synaptogenesis. In fact, both GAD-65 and GAD-67 protein expression were consistently reduced by ~50% ($p<0.0001$; $n=35$ for GAD-65, $n=6$ for

GAD-67) (Figure 3-6C-C'). Taken together, we suspected these observations would lead to decreased inhibitory synapse formation following shNogoA transduction.

To test functional relevance of these robust reductions in the GABAergic pre-synaptic markers GAD-65 and GAD-67, we globally transduced primary rat hippocampal neurons with LV-pLL3.7 or LV-shNogoA on DIV7, compared miniature inhibitory post-synaptic current (mIPSC) events on DIV14. Unlike our observations with mEPSC recordings (Figure 3-1E-E'), mIPSC amplitude did not significantly change between pLL3.7- and shNogoA-transduced neurons ($n=8-9$, $\Delta_{\text{mean}}=+21.56\pm14.66\%$, $p=0.1614$). This ruled out possible differences in inhibitory synaptic transmission due to the regulation of post-synaptic receptor clustering or abundance. Next, we assessed mIPSC frequency between these two groups, and discovered a drastic decrease in the shNogoA-transduced neurons ($n=8$, $\Delta_{\text{mean}}=-75.13\pm18.80\%$, $p=0.0013$). This was in line with the robust decline in pre-synaptic GAD-65 and GAD-67 protein expression by both qualitative immunofluorescence staining and semi-quantitative Western blot analysis. Lastly, we detected no change in the mIPSC decay time ($n=8-9$, $\Delta_{\text{mean}}=-8.17\pm17.03\%$, $p=0.6383$), indicating similar temporal kinetics between the two groups. These data collectively demonstrate a reduction in inhibitory synaptogenesis in shNogoA-transduced neurons, independent of global *Npas4* and *Bdnf* upregulation. While the molecular mechanisms currently remain elusive, these results can be explained by concurrent – instead of unilateral – *Npas4* increase in both pre- and post-synaptic neurons (51), maintenance of excitatory-inhibitory balance (53), and compensatory mechanisms to ensure synaptic homeostasis (30).

3.3.7 Observed Synaptic Phenotypes are NogoA-Independent

Since our observations so far depended on an established primary rat hippocampal neuronal culture system, here we describe some additional controls we carried out to verify the inter-species and target specificity of the shNogoA (13). Due to the inconsistent observations with mouse and rat NogoA-Ca α 2 δ 1 interactions (Figure 3-4), we used primary hippocampal neurons from E15.5-18.5 Crl:CD1(ICR) (hereafter referred to as CD1) mouse (67, 68), transduced cultures similarly with control pLL3.7 or shNogoA on DIV3, treated with the same pharmacological reagents on DIV7 or DIV14, and assessed for expression patterns of target proteins by Western blotting. Before any experimentation, we aligned NogoA amino acid sequence for *Rattus norvegicus* (accession number Q9JK11.1) and *Mus musculus* (accession number Q99P72.2), and found 100% coverage with 89.39% identity. Similar to experiments with rat neurons (Figures 2-3A-A' and 3-3A), we found that at a synaptically immature state on DIV7, 2 hours of 55mM KCl treatment decreased mouse NogoA expression by ~30% ($n=12$, $p=0.0009$), and 10 minutes of extracellular calcium chelation with 5mM EGTA pre-treatment could effectively negate this decrease ($n=12$, $p=0.0087$) (Figure 3-7A-A'). Worthy of note here is that anti-pan-NogoAB antibodies, including homemade (Bianca) or the commercially available alternative (R&D), failed to detect a mouse NogoA band separation (compare Figure 3-7A to Figure 2-3A). This possible epitope unavailability was also evident by lack of detection using the serine-343 phospho-specific anti-NogoA antibody (Figure 2-4) (data not shown). As such, we could only observe a slight decrease in mouse NogoA molecular weight following KCl treatment (Figure 3-7A).

Following synaptic maturation, mouse NogoA protein remained stably expressed regardless of pharmacological treatments, in complete accord with previous biochemical findings on the regulation of rat NogoA (Figure 3-3A).

Next, we assessed expression of proteins that showed significant regulation following shNogoA transduction of rat hippocampal neurons. In control-transduced mouse neurons, Npas4 protein expression showed similar induction patterns with various pharmacological treatments, and at baseline was upregulated by ~2.5-fold upon shNogoA transduction on both DIV 7 and 14 ($n=12$; $p=0.0336$ for DIV7, $p=0.0022$ for DIV14). Similarly, mouse GAD-65 levels were downregulated by 56% and 70% upon shNogoA transduction on both developmental stages, respectively ($n=12$, $p<0.0001$). By synaptic maturation on DIV14, both GluA1 and S6K protein levels were reduced by 45% and 64% ($n=12$; $p=0.0005$ for GluA1, $p<0.0001$ for S6K) (Figure 3-7A''). Collectively, these data strongly suggest that unlike our observations with Cav α 2 δ 1 (Figure 3-4), most other gene and protein regulation was highly conserved between mouse and rat neurons, resulting in greatly similar observations following shNogoA transduction.

To conclusively test the target-specificity of shNogoA and confirm NogoA's regulatory role in manifesting these phenomena, we employed an independent strategy as described before (Figure 3-4). Briefly, we prepared primary hippocampal cultures from perinatal (P0-1) *NogoABC^{fl/fl}* mice, where exons 4 and 5 common to *NogoA-C* are flanked by *loxP* sites (Figure 3-7B) (26). We infected half of the cultures with LV-CMV-Cre on DIV3, and co-infected both cultures with LV-pLL3.7 or LV-shNogoA on DIV6. Cells were maintained until DIV14, and total cell lysates were analyzed by Western blotting. We first demonstrated that efficiency of Cre-mediated recombination of

NogoABC by assessing NogoA protein expression by using commercial (R&D) and homemade (11C7) antibodies for Western blotting. As seen qualitatively with 1/4th sample loading and quantitatively following normalization with β -actin, NogoA levels were reduced by 83% upon Cre-recombination only ($n=6$, $p<0.0001$). In contrast, NogoA protein expression decreased beyond detection following shNogoA transduction, regardless of Cre-recombination ($n=6$, $p<0.0001$). Western Blot analysis revealed that the Cre-mediated recombination of *NogoABC*^{fl/fl} alone does not lead to upregulation of Npas4 or downregulation of GAD-65, GluA1, or S6K expression. On the other hand, infection of shNogoA alone, or co-infection of shNogoA following Cre-recombination recapitulated all of these previously characterized bidirectional regulations (Figure 3-7B-B''). Despite small fraction of leftover NogoA protein expression (17%), these data collectively demonstrate for the first time that the observed regulations in synaptic proteins are independent of NogoA depletion, but might instead be artifacts of non-specific targeting of the previously published and characterized shNogoA.

3.3.8 Step-wise Mutated shNogoA Still Replicates Regulation of Excitatory and Inhibitory Synapse Formation and Strength

We demonstrated that the robust regulation of synaptic proteins following LV-sh-NogoA transduction is independent of NogoA expression (Figure 3-7), and therefore likely the result of off-target effects of the shNogoA construct. Here, we carried out additional studies in order to identify the molecular targets of the shNogoA responsible for driving such drastic synaptogenic phenotypes. We used the original shNogoA

construct (13) in the pLL3.7 vector backbone; but introduced two (shNogoA-2pMt) or five point mutations (shNogoA-5pMt) within the seed region of the shNogoA stem loop (Figure 3-8). We anticipated that additive point mutations of the seed sequence would incrementally reduce the efficacy of shRNA-mediated knockdown of NogoA, while retaining regulatory elements and their target binding activities within the shNogoA.

We prepared primary hippocampal cultures from embryonically age-matched Sprague-Dawley and C57BL/6 mice, and lentivirally transduced neurons on DIV4-6 with the following plasmids: pLL3.7 (empty vector) control plasmid, characterized shNogoA, shNogoA-2pMt, and shNogoA-5pMt. We maintained cultures until synaptic maturity, collected whole cell lysates on DIV14, and analyzed protein expression by Western blotting. We first assessed NogoA protein expression with these four plasmids. As expected, shNogoA reduced NogoA protein levels by ~97% for both species ($p < 0.0001$; $n=3$ for rat, $n=6$ for mouse). Neuronal transduction with of two point mutations to the LV-shNogoA (shNogoA-2pMt) caused an incomplete (~80-90%) knockdown of the NogoA compared to pLL3.7 transduced cultures ($n=3$, $p=0.0004$ for rat; $n=6$, $p < 0.0001$ for mouse). Transduction of hippocampal neurons with the shNogoA with five point mutations (shNogoA-5pMt) did not result in a significant (~13-17%) reduction of NogoA compared to the control cultures ($n=3$, $p=0.4281$ for rat; $n=6$, $p=0.1467$ for mouse) (Figure 3-9A-A'). Together, these results show that the seed region of the shNogoA stem loop is important for NogoA targeting, and that introduction of mismatch mutations leads to a stepwise reduction in NogoA knockdown efficiency. Worthy of note here is that transduction with shNogoA-2pMt (Figure 3-9A-A') revealed similar NogoA expression as that of *NogoABC^{fl/fl}* mouse neurons infected with LV-CMV-Cre (Figure 3-

7B-B"). Therefore, comparison between the previously described and following phenotypes should dispel the possibility of regulation entrained by remaining NogoA.

As demonstrated before, shNogoA transduction of mouse hippocampal neurons robustly upregulated Npas4 protein expression ($n=6$, $\Delta_{\text{mean}}=2.5x$, $p=0.0042$). However, transduction with neither shNogoA-2pMt nor shNogoA-5pMt induced Npas4 upregulation in mouse neurons ($n=6$; $p=0.9964$ for shNogoA-2pMt, $p>0.9999$ for shNogoA-5pMt), suggesting the need for a robust, near-complete depletion of NogoA protein expression. Worthy of note here is that in rat neurons, Npas4 protein expression was strikingly upregulated to a significantly greater extent with shNogoA-5pMt transduction, even when compared to shNogoA ($n=3$, $\Delta_{\text{mean}}=7.3x$, $p=0.0013$) (Figure 3-9A). Beyond Npas4, the molecular targets we had identified in our previous efforts were regulated in a similar fashion: upon lentiviral transduction with shNogoA, shNogoA-2pMt, or shNogoA-5pMt, protein expression of GluA1, S6K, GAD-65, and GAD-67 was significantly downregulated as assessed by Western blotting (Figure 3-9A-A'). Most of these reductions were also observed with rat neurons (quantification not shown) (Figure 3-9A). Collectively, experiments with stepwise-mutated shNogoAs revealed that the previously observed regulations of synaptic proteins occur independently of NogoA, and are in fact due to shNogoA-mediated off-target effects.

Curiously, step-wise mutations within the seed-region of the shNogoA also revealed some *de novo* phenotypes. In rat, but not mouse, neurons, protein expression of ser-133 phosphorylated CREB was downregulated by 40-50%, only following transduction with shNogoA-2pMt and shNogoA-5pMt but not shNogoA ($n=3$; $p=0.9818$ for shNogoA, $p=0.0355$ for shNogoA-2pMt, $p=0.0214$ for shNogoA-5pMt). Moreover, in

both rat and mouse neurons, the expression of the presynaptic protein synapsinIIa remained at comparable levels with shNogoA transduction ($n=3$, $p=0.8150$ for rat; $n=6$, $p=0.6309$ for mouse), but showed a dramatic reduction following transduction with shNogoA-2pMt and shNogoA-5pMt ($n=3$, $p=0.0032$, 0.0315 for rat; $n=6$, $p\leq 0.0001$ for mouse). In fact, this decrease in synapsinIIa showed a step-wise effect, intensifying with additive introduction of mismatch basepairs ($n=3$, $p=0.3512$ for rat; $n=6$, $p=0.1898$ for mouse) (Figure 3-9A-A'). These *de novo* phenotypes observed with shNogoA mutations were both interesting and alarming at the same time. We will attempt to explore the significance, ramifications, and mechanism of such phenomenon in greater detail.

To increase our confidence in afore-mentioned biochemical findings, we subjected mouse hippocampal cultures to a similar experimental timeline, followed by immunofluorescence staining against synaptic markers. First, we verified the near-complete knockdown of NogoA protein expression following shNogoA transduction. Qualitative assessment revealed that transduction of neurons with the shNogoA-2pMt recovered some faint NogoA signal, whereas shNogoA-5pMt almost completely restored NogoA expression (Figure 3-9B). We then explored the density of excitatory, glutamatergic synapses, by assessing puncta and signal intensity of presynaptic synapsinIIa and postsynaptic GluA1. Following a similar pattern to our Western blot analysis (Figure 3-9A-A'), qualitative assessment of immunostaining showed that total GluA1 signal dramatically decreased with shNogoA transduction, and remained low with either shNogoA-2pMt or shNogoA-5pMt transduction. On the other hand, synapsinIIa remained unchanged following shNogoA transduction, but was significantly downregulated following transduction with either shNogoA-2pMt or shNogoA-5pMt

(Figure 3-9B). Next, we explored inhibitory synapses as assessed by immunostaining against the presynaptic GAD-65 and postsynaptic GABA_AR γ 2. Compared to the control pLL3.7, qualitative assessment revealed a robust reduction in GAD-65 puncta density following transduction with all three constructs, while GABA_AR γ 2 density and/or intensity remained unchanged (Figure 3-9B). Overall, albeit qualitative, these observations complemented our biochemical findings, and implicated the role of off-target regulatory elements within the shNogoA, rather than varying levels of NogoA expression.

3.3.9 mRNA Sequencing Experiments with Step-wise Mutated shNogoA Constructs Shed Light onto NogoA-Independent Regulations

We showed that even though shNogoA transduction of hippocampal neurons leads to highly efficient depletion of NogoA expression, some unknown regulatory element(s) within the rest of the shNogoA plasmid interact(s) with secondary, unspecific targets. As a result, the signaling cascade dysregulates excitatory synaptic strength and impairs inhibitory synapse formation, altogether shifting the fine balance between excitation and inhibitory. So far, we attempted to distinguish NogoA-dependent versus NogoA-independent gene regulation by using RT-qPCR arrays (Figure 3.1A') or RNA-seq experiments (Figure 3-2). In order to investigate on a deeper level, we transduced mouse forebrain neurons on DIV4 with the control empty vector pLL3.7 (EV), the characterized shNogoA, as well as shNogoA that was mutated with two (shNogoA-2pMt) or five (shNogoA-5pMt) basepairs (Figure 3-8). Unlike our previous RNA-seq studies (Figure 3-2), we maintained cultures for 10 DIV following LV-transduction for two

main reasons: we wanted these cultures to reach synaptic maturity (DIV14), while allowing a chronic phase following, instead of an intermediate snapshot during, depletion of NogoA. Finally, we isolated all RNA from cultures, split the RNA input for concurrent total and small RNA library preparations, and analyzed mRNA and micro RNA (miRNA) transcriptomes by next-generation sequencing (Figure 3-10A).

We first examined mRNA and long-noncoding RNA (lncRNA) transcriptome of these cultures following transduction with four different lentiviral plasmids. Principal component analysis (PCA) revealed highly reproducible, but global transcriptional changes amongst cultures transduced with different LV constructs. We found that the transcriptomes of LV-EV- and LV-shNogoA-transduced cultures were more similar, than those of LV-shNogoA-2pMt- or LV-shNogoA-5pMt-transduced cultures (Figure 3-10B). We then studied the differentially expressed genes (DEGs) amongst these four groups of lentivirally-transduced cultures. Due to high level of reproducibility between biological replicates, even the smallest changes in a plethora of genes were deemed statistically significant ($p_{adj} < 0.05$). To capture only biologically relevant as opposed to statistically significant changes, we focused on DEGs with ≥ 2 -fold change compared to EV-transduced cultures. Even then, we found that shNogoA transduction alone significantly changed expression of 827 genes, when compared to pLL3.7-transduced control neurons. In parallel with the PCA, transduction with either shNogoA-2pMt or shNogoA-5pMt greatly diverged from the transcriptome of shNogoA-transduced neurons, and altered expression of as many as 2884 or 2143 genes, respectively. Moreover, all three plasmids significantly changed expression of the same 185 transcripts when compared to EV-transduced neurons, regardless of varying extents of NogoA expression. Finally,

we also detected a great number of DEGs, which changed significantly upon combinatorial comparison between transcriptomes of neuronal cultures transduced with any two shNogoA constructs. (Figure 3-10B).

Plotting differentially expressed genes between LV-pLL3.7 and LV-shNogoA-transduced neurons once again demonstrated that *Rtn4* was once again the most robustly and statistically significantly downregulated gene, as the primary target of the shNogoA (Figure 3-10C). To confirm the intended regulation dictated by shNogoA and step-wise point mutations, we showed that shNogoA reduced *Rtn4* gene expression by 96% ($n=4$, $p_{adj}=4.8 \times 10^{-24}$). Introduction of only two point mutations within the shNogoA (shNogoA-2pMt) led to an incomplete knockdown of the *Rtn4* expression, corresponding to a %85 decrease ($n=4$, $p_{adj}=4.6 \times 10^{-21}$) compared to the LV-pLL3.7-transduced neurons. Introduction of three more point mutations (shNogoA-5pMt) only downregulated *Rtn4* gene expression by 4%, thereby making it indistinguishable from EV-transduced cultures ($n=4$, $p_{adj}=0.1516$) (Figure 3-11A). These findings confirmed that our shNogoA mutations behaved as intended, resulting in stepwise loss of *NogoA* mRNA knockdown efficiency. We then started by going after the DEGs we had identified in our previous RNA-seq following shNogoA transduction (Figure 3-2). For instance, both *Gad1* and *Gad2*, encoding for GAD-67 and GAD-65 respectively, were downregulated by ~60-80% upon shNogoA transduction ($n=4$; $p_{adj}=4.1 \times 10^{-8}$ for *Gad1*, $p_{adj}=5.9 \times 10^{-7}$ for *Gad2*). The transcript downregulation for both genes also remained low following either of the two step-wise mutated shNogoA transduction, albeit to varying extents (Figure 3-11A). This indicated that the reduction in GAD-65/67 expression was indeed not NogoA-dependent. Looking more closely onto inhibitory synaptogenesis, we

found that expression of two inhibitory interneuron subtype-specific genes, *somatostatin* (*Sst*) and *parvalbumin* (*Pvalb*), was reduced by ~60-80% following shNogoA transduction ($n=4$; $p_{adj}=1.4\times 10^{-10}$ for *Sst*, $p_{adj}=5.0\times 10^{-7}$ for *Pvalb*) (Figure 3-10C). Curiously, while *Sst* transcript expression seemed to be downregulated only following transduction with shNogoA constructs causing successful NogoA depletion, *Pvalb* remained downregulated upon transduction with any of the three shNogoA constructs regardless of differential NogoA expression. This was our first indication that unlike results gathered from previous immunofluorescence staining (Figure 3-6B), the reduction in GAD-65/67⁺ presynaptic puncta might in fact be due to the downregulation of parvalbumin, alternatively interpreted as loss of parvalbumin-expressing cells.

Since the most prominent DEGs from our previous RNA-seq were IEGs (Figure 3-2), we shifted our attention to the same three implicated genes: *Npas4*, *Bdnf*, and *Arc*. Whereas the 2-fold *Npas4* upregulation following shNogoA transduction was not statistically significant ($n=4$, $p_{adj}=0.05935$), gene induction of *Arc* and *Bdnf* were more than 2.5-fold ($n=4$; $p_{adj}=4.6\times 10^{-5}$ for *Arc*, $p_{adj}=1.8\times 10^{-7}$ for *Bdnf*) (Figure 3-11B). Based on the WB images and quantification with mouse neurons (Figure 3-9A-A'), we expected baseline expression with either shNogoA-2pMt or shNogoA-5pMt transduction. However, *Bdnf*, and to a lesser extent *Npas4*, transcript expression bounced back and forth between shNogoA, shNogoA-2pMt, and shNogoA-5pMt transductions (Figure 3-11B), reminiscent of the *Npas4* protein expression seen with rat neurons (Figure 3-9A). On the other hand, *Arc* transcript expression remained high with all three forms of shNogoA transductions when compared to control pLL3.7 (Figure 3-11B). The inconsistency of expression patterns continued with genes encoding for

GluA1 (*Gria1*) and S6K (*Rps6kb1*). Consistent with our initial RT-qPCR findings (Figure 3-1A'), both *Gria1* and *Rps6kb1* transcript levels decreased by ~50% following the original shNogoA transduction ($n=4$; $p_{adj}=3.3\times10^{-11}$ for *Gria1*, $p_{adj}=1.9\times10^{-11}$ for *Rps6kb1*) (Figure 3-11A). However, the regulation of these two genes diverged following transduction with stepwise-mutated shNogoA constructs. For example, shNogoA-2pMt-transduced neurons had only ~30% downregulation of *Gria1* expression ($n=4$, $p_{adj}=6.8\times10^{-8}$), while transduction with shNogoA-5pMt reduced *Gria1* expression (47%) just as efficiently as shNogoA, despite control levels of *NogoA* ($n=4$, $p_{adj}=3.1\times10^{-12}$). In stark contrast, shNogoA-2pMt-transduced neurons showed 56% reduction in *Rps6kb1* expression ($n=4$, $p_{adj}=3.9\times10^{-13}$), while transduction with shNogoA-5pMt did not change *Rps6kb1* when compared to control neurons ($n=4$, $p_{adj}=0.6081$) (Figure 3-11A). Taken together, these data demonstrated that the regulation of IEGs and *Gria1* was due to off-target regulatory elements, whereas that of *Rps6kb1* was in fact NogoA-dependent.

Next, we explored DEGs implicated in excitatory synaptogenesis, regulation of which could reinstitute excitatory-inhibitory homeostasis. We first explored *Syn2*, since the corresponding protein product synapsinIIa was downregulated *de novo* with shNogoA-2pMt or shNogoA-5pMt transduction (Figure 3-9). Similar to protein expression, we found that *Syn2* remained unchanged with shNogoA or shNogoA-2pMt transductions, but was downregulated by 27% following shNogoA-5pMt ($n=4$, $p_{adj}=2.3\times10^{-6}$) (Figure 3-10C). This was a NogoA-independent regulation, emerging due to the introduced novel binding partner(s) of the mutated shNogoA seed region. Another gene we identified was *Syt2*, encoding for the calcium-dependent synaptic vesicle membrane protein synaptotagmin2. mRNA-seq analysis revealed 90% reduction in *Syt2*

gene expression following shNogoA transduction ($n=4$, $p_{adj}=3.4\times10^{-9}$). Moreover, *Syt2* expression remained downregulated by 59-69% upon transduction with either shNogoA-2pMt or shNogoA-5pMt ($n=4$; $p_{adj}=5.7\times10^{-7}$ for shNogoA-2pMt, $p_{adj}=6.0\times10^{-8}$ for shNogoA-5pMt) (Figure 3-10C). This was the first indication that neuronal transduction with shNogoA might cause impaired vesicle priming, fusion, and subsequent neurotransmitter release, all regulated in a NogoA-independent manner.

Lastly, we wanted to investigate the NogoA-independent, off-target transcriptional regulation of the shNogoA-5pMt construct in a larger biological framework. To that end, we subjected top 300 DEGs detected following lentiviral transduction with LV-shNogoA-5pMt compared to LV-pLL3.7 to STRING analysis (69) (Figure 3-12). At initial glance, we observed a major cluster of DEGs, all strongly regulated despite the near-endogenous levels of NogoA. In fact, STRING analysis revealed that this network of corresponding proteins has more statistically significant interactions than expected amongst size-matched proteins randomly drawn from the genome (protein-protein interaction (PPI) enrichment p -value= 1.52×10^{-7}). Upon closer investigation, we identified many biological processes and pathways that could summarize the observed phenotypes with the dysregulation of synapse formation and strength. To name just a few at the core of the major-most cluster, we are interested in further studying DEGs participating in the regulation of ion transport (*Prkcb*, *Calm1*, *Cacna2d2*), chemical synaptic transmission (*Mef2c*), synaptic vesicle cycle (*Syt11*, *Dnm1/3*, *Vamp2*, *Slc17a7*), and mTOR signaling pathway (*Nras*, *Map2k1*, *Pik3r3*) (Figure 3-12). Taken together, with deeper bioinformatic data-mining and

complementary biochemical studies, these datasets hold the potential of elucidating key mechanisms involved in the regulation of synapse formation and strength.

3.3.10 Small RNA Sequencing Identifies shNogoA-Regulated miRNA Expression

To deepen our understanding of the regulatory elements within shNogoA, we concurrently investigated small RNA transcriptome following the same experimental paradigm (Figure 3-10A). Since microRNAs (miRNAs) are known to be powerful regulators of mRNA expression, stability, and translation (70, 71), we hypothesized that the shNogoA might somehow influence miRNA production, transport, or processing machinery. To address this possibility, we first looked at all differentially expressed small RNAs expressed following transductions with the same lentiviral vectors. Similar to the global mRNA transcriptome association (Figure 3-10B), PCA revealed that the small RNAs expressed following EV and shNogoA transductions were the most similar. Also consistently, shNogoA-2pMt or shNogoA-5pMt showed great deviation from this pair, onto opposite ends (Figure 3-13A). When we looked more closely to the spread of differentially expressed miRNAs upon shNogoA transduction, we came across 37 upregulated and 22 downregulated miRNAs with statistical significance (Figure 3-13B). If we filtered this list based on the highest fold-change of regulation and greatest read counts per million (CPM), we were left with select miRNAs that satisfied these two criteria (Figure 3-13C). For instance, two of the highest upregulated miRNAs with the greatest CPM was *mmu-miR-181a-5p* and *mmu-miR-132-3p* (Figure 3-13B). These miRNAs were upregulated by 68% and 95% upon shNogoA transduction ($n=4$;

$p_{adj}=4.3\times10^{-9}$ for *mmu-miR-181a-5p*, $p_{adj}=9.2\times10^{-11}$ for *mmu-miR-132-3p*), and remained consistently upregulated upon shNogoA-2pMt or shNogoA-5pMt transduction ($n=4$; $p_{adj}<10^{-5}$) (Figure 3-14B). Two other miRNAs that were robustly regulated following shNogoA transduction were *mmu-miR-1a-3p* and *mmu-miR-7b-5p*, which were downregulated by 76% and upregulated 4-fold, respectively ($n=4$; $p_{adj}=7.4\times10^{-10}$ for *mmu-miR-1a-3p*, $p_{adj}=3.1\times10^{-18}$ for *mmu-miR-7b-5p*) (Figure 3-13B). Strikingly these miRNAs' regulation patterns (Figure 3-14) were reminiscent of the IEG mRNA expression that bounced back and forth between different LV transduction (Figure 3-11B). We reasoned that NogoA expression played no role in regulating these four miRNAs, since the expression profiles following EV and shNogoA-5pMt transductions bore no resemblance. On the other hand, for example, *mmu-miR-210-3p* expression was downregulated by 69% and 50% following shNogoA and shNogoA-2pMt transduction, respectively ($n=4$; $p_{adj}=1.8\times10^{-5}$ for shNogoA, $p_{adj}=0.0113$ for shNogoA-2pMt). However, upon shNogoA-5pMt transduction, *mmu-miR-210-3p* expression was completely indistinguishable from EV levels ($n=4$, $p_{adj}=0.8909$) (Figure 3-14A). This observation strongly suggested that there were also some miRNAs, expression of which was regulated following shNogoA transduction in a NogoA-dependent manner.

To initiate a preliminary overview of the correlative link between miRNA expression and mRNA regulation, we characterized differentially expressed miRNAs with two different calculations. For instance, the strongly and steadily upregulated *mmu-miR-7b-5p* has 22 known targets that were significant in the top 250 DEGs. In other words, 8.9% of the DEGs have validated interactions with *mmu-miR-181a-5p*. On the flip side, we used a complementary calculation, where *mmu-miR-181a-5p* is known to

target 30.98% of the differentially expressed mRNAs that have an identified miRNA in this analysis (Figure 3-13C). In fact, *Rtn4* was one of these 22 differentially regulated mRNAs targeted by *mmu-miR-181a-5p*, even when their expression patterns are vastly different (compare Figures 3-11A and 3-14B). Following similar calculations, we found that the strongly but inconsistently downregulated *mmu-miR-7b-5p* has 19 known targets, making 7.7% of the top 250 DEGs. Moreover, *mmu-miR-7b-5p* itself is known to target 26.8% of the significantly regulated mRNAs that have a known miRNA in this analysis (Figure 3-13C). Moreover, *Gria1* was one of the 19 established targets of *mmu-miR-7b-5p*, where the regulation of both showed complementary expression patterns (compare Figures 3-11A and 3-14B).

Lastly, we explored known protein-protein interactions amongst the 72 DEGs that were regulated in conjunction with their known miRNA targets following neuronal transduction with shNogoA constructs. To that end, we subjected this gene set to STRING analysis to investigate implicated biological processes and pathways (Figure 3-13D) (69). The resulting interactome of miRNA-dependent mRNA regulation was less strongly correlated compared to the analysis with overall DEGs (Figure 3-12), but was nonetheless more statistically significant than random selection (PPI enrichment p -value=0.0498). At an initial glance, we failed to detect visibly associated protein clusters with more than 5 DEGs. However, upon closer examination, we identified genes participating in many key biological processes and pathways. In fact, we noticed that some of the DEGs targeted by miRNAs identified by our sequencing experiments participate in synaptogenic biological processes such as learning or memory (*Gria1*, *Hif1a*), modulation of chemical synapses (*Mef2c*, *ErbB4*), and mTOR signaling pathway

(*Rps6kb1*, *Map2k1*). Overall, future investigations should focus on the complementary and overlapping analyses of mRNA and miRNA regulation following shRNA constructs in an attempt to elucidate some of the secondary targets underlying the observed robust synaptic phenotypes.

3.4 Discussion

NogoA's negative regulation of activity-dependent synaptic plasticity was studied by two key accounts that laid the foundation of our work. Zagrebelsky *et al.* used a powerful shRNA to specifically knock down NogoA, which led to an increase in proximal apical dendritic complexity within the CA3 region of the hippocampus (13). Peng *et al.* used an siRNA that partially knock down NogoA to demonstrate that the transduced hippocampal neurons express increased levels of excitatory GluA1/2, GluN1/2AB, and PSD-95, under the regulation of the mTOR signaling pathway (28). As these studies used different knockdown approaches (shRNA versus siRNA) and systems (organotypic slice versus dissociated neuronal cultures), and looked at different aspects of synaptic plasticity (dendritic morphology versus glutamate receptor expression), they do not complement one another, or deepen our understanding of NogoA's regulation of synaptic plasticity. To fill this gap, we combined Zagrebelsky *et al.*'s NogoA-specific shRNA and Peng *et al.*'s culture system, analyzed, and compared results.

To our surprise, when NogoA was specifically and almost completely knocked down from hippocampal neurons via lentiviral transduction with this shNogoA at any developmental stage (Figure 3-1B), AMPA receptor subunits GluA1 and GluA2 were drastically downregulated, while GluN2B or PSD-95 protein expression remained unchanged (Figure 3-1A-A''). In fact, the reduction in total GluA1 expression and surface trafficking (Figure 3-1D-D') correlated with cell-autonomously and permanently reduced baseline synaptic strength, as assessed by mEPSC amplitude (Figure 3-1E-E'). Because these results were in direct opposition with Peng *et al.*'s work, we

reasoned a more detailed investigation was warranted. We showed that unlike germline knockout models (17, 20), NogoB was not compensatorily upregulated (Figure 3-1A-A'), these downregulated proteins were also regulated on an mRNA level (Figure 3-1A'), and various commercially available shRNAs against NogoA manifested similar results (Figure 3-1C). More importantly, our unbiased mRNA-seq experiments reproducibly corroborated the fact that *Rtn4* was the most strongly downregulated gene, separated from other DEGs in terms of fold-change, statistical significance, and RCM (Figures 3-2, 3-9). These mRNA-seq experiments also revealed a robust increase in expression of well-characterized IEGs (*Arc*, *Fos*, *Npas4*), their established binding partners (*Nr4a1/2*, *Bdnf*, *Junb*) (Figures 3-2, 3-9). We went one step further and demonstrated that the protein expression of these synaptogenic genes also increase, at least in part due to an elevated calcium influx through activation of L-type VGCC (Figure 3-3).

If these transcriptional and molecular observations were indeed due to the complete knockdown of NogoA protein levels, we reasoned that other forms of NogoA depletion should at least partially reproduce these changes. After demonstrating high level of homology and reproducibility between rat and mouse neurons (Figure 3-7A-A''), we were curious whether acute, Cre recombination-mediated deletion of *NogoABC*^{fl/fl} (26) would manifest a similar set of phenotypes. If synaptic phenotypes observed with shNogoA-mediated NogoA knockdown could be replicated with *NogoABC* conditional knockout, this would be an important entryway to studying outcomes of spatiotemporally controlled NogoA depletion *in vivo* as well. Whereas protein expression of candidate genes was indistinguishable between wildtype and NogoABC-depleted cultures, shNogoA alone or co-transduction was sufficient to manifest all of the observed

phenotypes (Figure 3-7B-B''). Even though extensive bioinformatic analyses, mRNA-seq results (Figure 3-2), and commercially available shNogoAs (Figure 3-1C) collectively had revealed shNogoA target specificity against *Rtn4*, this was our first indication that shNogoA had secondary, non-specific targets that were at least partially responsible for these molecular changes. To distinguish between the NogoA-dependent and shNogoA-linked phenotypes, we mutated two or five base pairs within the seed region of the shNogoA to create an alternative scrambled shRNA, while keeping intact all the promoter/enhancer and regulatory elements within the pLL3.7 lentiviral expression backbone (Figure 3-8). We transduced rat and mouse hippocampal neurons with the pLL3.7 empty vector, the original shNogoA (13), or the mutated versions shNogoA-2pMt and shNogoA-5pMt. Upon close examination, we discovered that many of the observed synaptogenic phenotypes were replicated even with the shNogoA-5pMt, despite near-control levels of NogoA expression. Even more strikingly, there were phenotypic differences between rat and mouse neurons, as well as *de novo* regulations that were not observed with either EV or shNogoA itself (Figure 3-9). Considering how prevalent the use of scrambled shRNA as a negative control is in the field (72), we were alarmed by the fact that our newly generated alternative scrambled shRNA could replicate as well as create many non-specific changes in protein expression. However, we are confident this was not an isolated account, since a similar observation was previously reported for another characterized shRNA against *doublecortin* family. In this study, investigators generated nine scrambled shRNAs, and demonstrated that four showed statistically significant differences in neuronal migration in a sequence-dependent, but not sequence-specific manner (73). In other words, if we had originally

used this shNogoA-5pMt as our scrambled control, we would have concluded that reduction in NogoA protein expression following shNogoA transduction would have caused a downregulation of Npas4 and S6K, and an upregulation of p-CREB and synapsinIIa (Figure 3-9).

Deeply alarmed by these alternative and opposite interpretations, we decided to undertake comprehensive total and small RNA sequencing experiments using all four lentiviral constructs, with hopes of elucidating the intricate mechanisms underlying observed differential gene expression associated with altered synapse density and strength (Figures 3-10-14). Upon confirming the reproducibility of results derived from the previous mRNA-seq experiments (Figure 3-2), we attempted to identify genes regulations that were solely differentially expressed following shNogoA transduction, and returned to baseline with five point mutations (shNogoA-5pMt). These would be key candidates, since the off-targeting regulatory shNogoA elements would be shared, and the observed gene expression changes could be more easily correlated with unchanged NogoA protein expression. We were surprised that many of the genes that we had identified before were regulated independently of NogoA expression, and more so in striking patterns. In fact, there were cases where *Bdnf* gene expression, for example, was differentially upregulated following transduction with shNogoA or shNogoA-5pMt, but returned to control-like baseline upon shNogoA-2pMt transduction (Figure 3-11B). Overall, we had expected to see closest correlation to be between shNogoA and shNogoA-2pMt, since the only difference was two point mutations that did not drastically impact NogoA knockdown efficiency. In stark contrast, PCA revealed greatest association between global transcriptomes following EV and shNogoA transductions,

despite the near-complete depletion of NogoA expression (Figure 3-10B). This suggested that synaptically implicated genes were more vulnerable than overall transcriptome to show diverged regulation between EV- and shNogoA-transduced neurons. Last but not least, STRING analysis (69) of the top 300 DEGs between pLL3.7- and shNogoA-5pMt-transduced cultures corroborated this hypothesis, and revealed that the inter-connected, multi-faceted regulations were in fact observed within key biological processes such as chemical synaptic transmission, synaptic vesicle cycle, and mTOR signaling pathway were all NogoA-independent (Figure 3-12).

Since gene expression can be epigenetically and post-transcriptionally regulated, we reasoned that shNogoA could be manifesting these phenotypes due to regulation of small, non-coding RNAs called micro RNAs (miRNAs) (70, 71, 74). Processed in multiple, highly regulated steps with the involvement of key enzymes such as Drosha/Dgcr8 and Dicer (70, 75-77), miRNAs offer a fine-tuned, master regulation of local and dynamic expression of numerous mRNAs even within highly specialized dendritic spines (71, 78-80), especially under the regulation of activity-dependent synaptic plasticity (71, 80-82). We were additionally interested in investigating the possibility of shNogoA transduction mediating its regulation through miRNA targeting or machinery for three reasons: 1. miRNAs can bind to the 3' untranslated regions (UTRs) of as many as 100 mRNAs, and therefore have the power of regulating expression of multiple genes at the same time (74). 2. miRNA copy numbers are drastically outweighed by the abundance of mRNAs (79, 83, 84), raising the possibility of a more fine-tuned and dynamic spatiotemporal regulation of gene expression (81). 3. shRNA overexpression may choke the miRNA pathway by modulating expression of exportin-5

and/or argonaute-2, where the former is involved in transporting shRNAs and pre-miRNAs from the nucleus into the cytoplasm, and the latter is involved in miRNA biogenesis and cleavage of the bound target mRNA (85). Even though shNogoA transduction did not significantly change *Xpo5* and *Ago2* expression on an mRNA level, future studies should investigate protein levels and possible interplay.

Taken together, we carried out a concurrent small RNA sequencing with the same samples in an attempt to identify miRNAs responsible for gene regulation driving changes in synapse formation and strength. At an initial look, PCA revealed that the overall small RNA expression profile (Figure 3-13A) was highly similar to that of global transcriptome (Figure 3-10B). Upon a closer inspection, we identified 37 upregulated and 22 downregulated miRNAs with statistical significance (Figure 3-13B). In fact, some of the most differentially expressed (fold change) and abundant (CPM) miRNAs demonstrated highly alternating expression patterns (Figure 3-14), and implicated key biological processes such as modulation of chemical synaptic transmission and learning or memory (Figure 3-13D). Cross-reference between mRNA and miRNA sequencing data (Figure 3-13C) helped us to narrow our focus on a subset of miRNAs, since it revealed that *mmu-miR-181a-5p* was shown to regulate *Rtn4* gene expression, whereas *mmu-miR-7b-5p* was shown to regulate *Gria1* gene expression. More strikingly, our dataset identified miRNAs that were previously characterized and linked to activity-dependent and homeostatic synaptic plasticity. For example, Sambandan *et al.* identified miR-181a as the most abundantly expressed miRNA at dendritic spines of hippocampal neurons. Moreover, expression of the mature form of miR-181a within dendritic spines was induced as soon as 10 seconds following local stimulation (81).

Another activity-dependent miRNA that was upregulated following shNogoA transduction was miR-132, which is processed into the mature form in a Dicer-dependent manner following BIC-induced activation of CREB (86). Last but not least, shNogoA transduction was shown to significantly downregulate miR-485, which Cohen *et al.* characterized as a developmentally expressed miRNA that dynamically modulates dendritic spine number and synapse formation in an activity-dependent and homeostatic fashion (87). The list also includes miR-129 (88), miR-132 (89, 90), and miR-212 (89), all of which were characterized as participating in or regulating some form of synaptic plasticity. Inspired by these findings, we are curious whether or not the shNogoA-driven molecular phenotypes are results of dysregulation of the miRNA processing machinery. Hence, ongoing investigations are focusing on studies with primary hippocampal neurons prepared from *Dgcr8^{fl/fl}* (91-93) and *Dicer^{fl/fl}* (94-96) mice, where miRNA processing can be interrupted at a pri- or pre-miRNA stage, respectively (70, 71). By co-transducing neurons with LV-Cre and LV-EV or LV-shNogoA, we hope to elucidate whether disruption of the miRNA processing machinery alone causes similar synaptic phenotypes as observed with LV-shNogoA transduction. We are also curious to entertain the possibility of shNogoA depending on functional miRNA machinery to relay transcriptional regulations and signaling that underlie observed molecular phenotypes.

In conclusion, although we had set out to conciliate two previous bodies of work (13, 28) using different approaches and models into one platform and shared mechanism, we now know a lot more about the complicated and non-specific physiology of shRNA-mediated knockdown. Whereas our report had started off addressing only those working on the physiological role of NogoA within the regulatory

context of synaptic formation, maintenance, and strength, our findings should concern biologists of all domains that integrate RNA interference as an approach of studying a singular gene's or protein's function. Our findings clearly demonstrate that a concurrent use of empty vector (pLL3.7) or a scrambled shNogoA (shNogoA-5pMt) cannot be sufficient and adequate negative control to confirm the specificity of shRNAs. In fact, even reversal of phenotypes by way of rescue experiments with ectopic overexpression constructs should not surpass the need to rigorously control for target specificity either (97). We hereby propose that any shRNA must be thoroughly tested against null cells or tissue, before it can be deemed, at least preliminarily, target-specific. This control is particularly important when working with primary neurons, where dynamic trafficking, maturation, and regulation of miRNAs are known to play a key role in synapse development and function (71, 80). Even then, possible non-specific effects caused by off-target binding should be explored with extensive and unbiased RNA-seq studies. Our datasets should, therefore, lay a strong foundation for future investigations interested in studying non-specific gene regulation by shRNAs.

3.5 Materials and Methods

3.5.1 *Animals*

All procedures and experiments were approved by the University of Michigan Institutional Committee on the Use and Care of Animals (ICUCA) and were performed in accordance with guidelines developed by the National Institutes of Health (NIH). Time-pregnant adult Sprague-Dawley rats or C57BL/6J mice were purchased from Charles River Laboratories, MA, USA. Time-pregnant CD1 and adult *NogoABC^{fl/fl}* mice were contributions of Catherine Collins (U-M) and Binhai Zheng (UCSD) (26), respectively.

3.5.2 *Primary Neuronal Cultures*

The protocol followed for the preparation and maintenance of neuronal cultures used in experiments described in this chapter was the same as that for Chapter 2. Briefly, brain tissue was isolated, digested, and thoroughly triturated for single cell suspension. Cells were seeded onto PDL-coated plastic plates or PLL-coated glass coverslips. For electrophysiological recordings, cells were seeded onto PLL-coated MatTek dishes (MatTek P35G-0-14-C). Cells were supplemented with half-media changes every 2-3 days with a mix of ACM, NCM, and fresh NGM. Cultures were maintained until DIV7 for immature, but polarized state, and DIV14 for synaptically fully mature state. For these experiments, we prepared neuronal cultures from either embryonic (E15.5-E18.5) or perinatal (P0-1) staged rat or mouse pups. To increase

yield and depth for RNA-seq experiments, we used the whole rodent forebrain, comprised of the hippocampus and the neocortex. For all other experiments, only the hippocampi were used for culture preparation.

2.5.3 Pharmacological Treatments

For biochemical and immunofluorescence experiments, neuronal cultures were treated with the following pharmacological reagents in reported final concentrations, catalog numbers, and solvents: 55mM potassium chloride (Fisher Scientific P330) [Neurobasal], 5mM EGTA (Sigma E8145) [Neurobasal], 2 μ M tetrodotoxin citrate (Abcam ab120055) [ddH₂O], 40-50 μ M (+)- bicuculline (Tocris 0130) [DMSO], 200nM K252a (Calbiochem 420298) [ddH₂O], 10 μ M forskolin (Sigma F6886) [DMSO], 1 μ M FPL64176 (Tocris 1403) [DMSO], 5 μ M nimodipine (Tocris 0600) [DMSO]. For electrophysiological recordings, neuronal cultures were treated with 1 μ M tetrodotoxin (Tocris 1078) [ddH₂O] or 10 μ M 1(S),9(R)-(-)-Bicuculline methiodide (Sigma 14343) [ddH₂O]. For BrU-seq experiments, neuronal cultures were incubated with 2mM 5-Bromouridine (Sigma 850187) [ddH₂O].

3.5.4 Transient and Sparse Transfection

For immunofluorescence studies, embryonic rat hippocampal neurons were transfected with the GFP-tagged scrambled shRNA or the shNogoA on DIV3 following the same protocol described in Chapter 2. For electrophysiological studies, perinatal rat

hippocampal neurons were transfected on DIV12, however slightly differently: neuronal cultures were first supplemented with a half-media change with transfection media (BrainBits TM500), while keeping the conditioned media for after transfection. 100 μ L transfection reagent was mixed with 1-2 μ L Lipofectamine 2000 (Sigma L3000008). At the same time 100 μ L transfection reagent was mixed with 1 μ g of plasmid DNA. These two mixes were combined by gentle inversion, incubated for 20 minutes at room temperature, mixed again. 200 μ L of the solution was gently placed directly on the neurons plated on the glass portion of the MatTek dishes. Cultures were returned to the incubator for 1-2 hours, and supplemented with the saved neuronal conditioned media until DIV14. shRNA constructs were expressed under the transcriptional control of the Histone H1 promoter. Targeting sequences were identical to the sequences of the previously published shNogoA and its scrambled (mismatch) control (13):

- Scrambled shRNA: GATATGAAACCCCACTTA
- shNogoA: AAGATTGCTTATGAAAC.

3.5.5 Lentiviral Transduction

Primary neuronal cultures were transduced with plasmids packaged into pLL3.7 lentiviral particles by the U-M Vector core, following the same protocol as described in Chapter 2. Briefly, most lentiviral transductions were carried on DIV3-6, primarily depending on the time of the lysate collection. With co-infections, half the neurons were first transduced with the lentiviral construct expressing Cre recombinase on DIV1 in fresh, pre-warmed NGM. On DIV3, half the neurons were transduced with empty vector

(pLL3.7) or shNogoA cloned into pLL3.7 lentiviral expression construct. Sequences and/or catalog numbers of the plasmids used are as follows:

- pLentilox 3.7 GFP: Addgene 11795, obtained from U-M Vector Core
- shNogoA: AAGATTGCTTATGAAAC (13)
- shNogoA-2pMT: AAGATTGCTTATGACAAA
- shNogoA-5pMT: AAGATTGCTTCTAACCA
- shNogoA Open Biosystems (V2LMM_33110): TCTCTTCCTAGTTTATGTG
- shNogoA (Origene TL711619B): CAGCAGTGTCATCCTCAGAAGGAACAATT
- shNogoA (Origene TL711619C): GATACCTTGGTAACTTATCAGCAGTGTCA
- LV-CMV-NLS-Cre: Addgene 12106

3.5.6 Immunofluorescence Labeling

Neurons seeded and maintained on PLL-coated glass coverslips were subjected to the same immunofluorescence labeling protocol as described in Chapter 2. Briefly, cells were washed, permeabilized (skipped for surface staining), blocked, and stained overnight with 1:500 dilution of the following primary antibodies: mouse anti-NogoA (11C7, courtesy of Martin E. Schwab), rabbit anti-Npas4 (courtesy of Michael Greenberg), rabbit anti-Ca_vα2δ1 (Alomone ACC-015), chicken anti-MAP2 (Abcam ab92434), mouse anti-GAD-65 (Santa Cruz sc-377145), rabbit anti-Somatostatin-14 (Peninsula T-4103), rabbit anti-GluA1-CT (EMD Millipore AB1504), mouse anti-SynapsinIIa (BD Pharmingen 610666), chicken anti-GABA_ARγ2 (SySy 224-006). Next day, coverslips were washed, incubated in species-appropriate fluorophore-conjugated

secondary antibodies, counterstained with Hoechst, and mounted as described. Coverslips were imaged using Zeiss Apotome2 microscope equipped with an AxioCam 503 mono camera and Zen software.

For quantification of Npas4 signal intensity, acquired CZI images were Apotome processed, z-stacked, and exported as high-resolution TIFF images. Images were then imported into ImageJ v1.52a (NIH Bethesda, USA) (98), where merged channels were split into separate 8-bit images. Using the DAPI channel, dimensions of neuronal-like, Hoechst-labeled nuclei were outlined using the freehand drawing tool, approximating to $\sim 3\text{-}4\mu\text{m}^2$ in area. The same outlined shapes were transposed onto the dsRed channel, where Npas4 signal was acquired and stored. For each field of view, a randomly determined and placed box was used for background signal quantification. This background signal was subtracted from calculated mean value, where the resulting product was then multiplied by the nuclear area for final signal intensity value. Signal intensities collected from multiple fields of view from each coverslip, experimental and biological replicates were pooled together for statistical analysis.

For quantification of percentage of Npas4-expressing nuclei, similar image processing was carried out. Single channel, 8-bit images were uploaded onto Cell Profiler v3.1.9 (99). Using the DAPI channel, Hoechst-labeled neuronal-like nuclear area was subjected to a filter based on a singular and consistent threshold. On the dsRed channel, Npas4 signal intensity was accepted as positive signal, if and when it fell within the standard threshold range, which was determined by the mean background and signal values derived from the above-mentioned signal intensity analysis. Following streamlined analysis of multiple fields of view from each coverslip, experimental and

biological replicates, percentages of Npas4-expressing, Hoechst-labeled nuclei were pooled together for statistical analysis.

3.5.7 Crude Brain Membrane Isolation

Isolation of crude brain membrane fractions was conducted similarly to as described in Chapter 2. Briefly, whole brains were dissected and homogenized in 10mL of 0.32M sucrose-based homogenization buffer following 12 strokes with first loose, then tight pestles (S0). Homogenates were subjected to tabletop centrifugation at 1000xg for 15 minutes. The insoluble nuclear pellet (P1) was stored, and the soluble supernatant (S1) was subjected to ultracentrifugation with Beckman Coulter SW-41Ti rotor at 200000xg for 30 minutes. The soluble cytosolic supernatant (S2) was stored, and the formed pellet was resuspended in homogenization buffer, and subjected to the same ultracentrifugation step. Along with previously stored fractions, crude brain membranes in the final pellet (P2) were solubilized in RIPA buffer with protease and phosphatase inhibitors, following vigorous trituration and vortexing.

3.5.8 NogoA Immunoprecipitation

NogoA Immunoprecipitation was conducted following the same protocol as described in Chapter 2. Briefly, solubilized crude membrane fractions were diluted accordingly to scale down to 1mg/mL protein concentration for optimized binding probability. Lysates were split into three tubes, where approximately 1mg of protein was

combined with pre-washed A/G beads. While one tube received no additional reagent (negative control), the others were combined with either 10 μ g of mouse monoclonal anti-NogoA (11C7) antibody or epitope-matched anti-FG12 antibody control. Following overnight tumbling, post-immunoprecipitation supernatant (post-IP) was saved, beads were gently precipitated, extensively washed, and boiled 1:1 by volume in 2x Laemmli Buffer supplemented with β -ME to fully dissociate and linearize bound proteins. Samples were analyzed by Western blotting in equal volume and/or protein loading.

3.5.9 Western Blot Analysis

Primary neuronal cultures, whole brains, and subcellular fractions of CNS tissue were solubilized in RIPA buffer, as described in Chapter 2. Also as described previously for experiments requiring analysis of transcription factor expression, cells were directly lysed on-plate with 1:1 by volume combination of RIPA buffer supplemented with the protease and phosphatase inhibitors and 2x Laemmli Buffer supplemented with β -ME. Briefly, proteins were separated by 7.5% SDS-PAGE and transferred onto PVDF membranes, which were then blocked and incubated overnight with the following primary antibodies: rabbit anti-NogoAB Bianca (courtesy of Martin E. Schwab, 1:25000), goat anti-NogoAB (R&D Systems AF3098, 1:5000), mouse anti-NogoA (courtesy of Martin E Schwab, 1:5000), mouse anti- β -actin (Sigma A5441, 1:20000), mouse anti- β III-Tubulin (Promega G712A, 1:50000), mouse anti-Transferrin Receptor (Invitrogen 13-6800, 1:1000), rabbit anti-PSD-95 (EMD Millipore AB9708, 1:2000), mouse anti-SynapsinIIa (BD Pharmingen 610666, 1:5000), rabbit anti-Npas4 (courtesy of Michael

E. Greenberg, 1:1000), rabbit anti-c-Fos (CST 2250S, 1:1000), rabbit anti-CREB p-S133 (CST 9198, 1:2000), rabbit anti-GluA1-CT (EMD Millipore AB1504, 1:500), mouse anti-GluA2 (EMD Millipore MABN71, 1:1000), rabbit anti-GluN2B (EMD Millipore 06-600, 1:1000), rabbit anti-p70 S6 Kinase (CST 9202S, 1:1000), rabbit anti-p70 S6 Kinase p-Thr389 (CST 9234L, 1:1000), rabbit anti-Ca_v1.2 (Alomone ACC-003, 1:500), rabbit anti-Ca_vα2δ1 (Alomone ACC-015, 1:500), mouse anti-GAD-65 (Santa Cruz sc-377145, 1:2000), mouse anti-GAD-67 (EMD Millipore MAB5406, 1:1000). PVDF membranes were then washed extensively, incubated in species-appropriate HRP-conjugated secondary antibodies, and developed with ECL substrates. Protein band intensity was visualized and quantified in linear range with LiCor c-Digit and Image Studio Software.

3.5.10 Electrophysiological Recordings

Hippocampal neuronal cultures were prepared from P1-3 Sprague-Dawley rats, and seeded on PDL-coated MatTek dishes as previously described (100). Cultures were maintained for at least 14 DIV for synaptic maturation. Glial and cortical conditioned media were supplemented to the neuronal growth medium for the initial plating. Neurons were sparsely transfected on DIV12 as described above or globally transduced with LV-pLL3.7 or LV-shNogoA on DIV7, and electrophysiological recordings were acquired on DIV14.

Whole-cell patch-clamp recordings were made with an Axopatch 200B amplifier for mEPSCs and with a Multiclamp 700B amplifier for mIPSCs from cultured hippocampal neurons bathed in HEPES-buffered saline (HBS) containing 119mM NaCl,

5mM KCl, 2mM CaCl₂, 2mM MgCl₂, 30mM Glucose, 10mM HEPES, pH 7.35. Whole-cell pipettes had resistance ranging 3-6 MΩ. Internal solution contained 100mM cesium gluconate, 0.2mM EGTA, 5mM MgCl₂, 2mM adenosine triphosphate, 0.3mM guanosine triphosphate, 40mM HEPES, pH 7.2. mEPSCs were recorded at -70mV from neurons with a pyramidal-like morphology in the presence of 1M TTX and 10M bicuculline, whereas mIPSCs were recorded at 0mV holding potential in the presence of 1μM TTX, 10μM CNQX, and 50μM DL-APV. All acquired traces were analyzed off-line using Synaptosoft MiniAnalysis software.

3.5.11 Reverse Transcription PCR (RT-qPCR)

Primary embryonic rat hippocampal cultures were infected on DIV9 with lentiviral constructs, and maintained until DIV16. RNA was isolated using the RNeasy Mini Kit (Qiagen 74204), QiaShredder Kit (Qiagen 79654), and on-column DNase I digestion (Qiagen 79254). 1μg of RNA was used for first-strand cDNA using the SuperScript III First Strand Synthesis System (Invitrogen 18080-051). Target gene expression was assessed using RT² Profiler PCR Arrays according to the manufacturer's instructions: Rat mTOR Signaling (Qiagen PARN-098Z) and GABA & Glutamate (Qiagen PARN-152Z). Data were acquired using Applied Biosystems StepOne Plus RT-PCR Thermocycler and analyzed with StepOne Software (v.2.2.3). Cycle thresholds for each sample were normalized to *β-actin* levels. Relative mRNA expression following shNogoA transduction was compared to that of cultures with pLL3.7 control transduction. Four independent experiments were performed.

For verification of mRNA-seq by RT-qPCR, primary embryonic rat forebrain neurons were infected with pLL3.7 or shNogoA on DIV6, and maintained until DIV10. RNA was extracted and purified in TRIzol reagent (Invitrogen 15596-018), following manufacturer's instructions. DNase treatment, reverse transcription, and qPCR reaction were carried out as mentioned above. Cycle thresholds for each sample were normalized first to its *Gapdh* expression, then to the internally normalized level of pLL3.7-transduced cultures. Six biological replicates derived from two independent experiments were performed. Previously published primer sequences were selected following drug treatments known to regulate *Bdnf* expression:

- *Gapdh*: 5'-GTGGACCTCATGGCCTACAT-3' (Fw)
5'-TGTGAGGGAGATGCTCAGTG-3' (Rv) (55)
- *Bdnf IV*: 5'-ACTGAAGGCGTGCGAGTATT-3' (Fw)
5'-TGGTGGCCGATATGTACTCC-3' (Rv) (56)
- *Bdnf IX*: 5'-GGGTGAAACAAAGTGGCTGT-3' (Fw)
5'-ATGTTGTCAAACGGCACAAA-3' (Rv) (55).

3.5.12 RNA Sequencing

For BrU-seq (Figure 3-2B), 2mM 5-Bromouridine (Sigma 850187) was added to neuronal cultures for 30 minutes, after which lysates were collected in Tri-Reagent BD (Sigma T3809) and frozen immediately. Purification and enrichment of BrU-containing RNA and library preparation were performed as previously described with minor modifications (101-103). Custom designed adaptors were directly ligated to the 3' ends

of RNA using RNA ligase 1 (NEB M0437), and truncated RNA ligase KQ (NEB M0373). BrU-labeled RNAs were immunoprecipitated using anti-BrdU antibody (SCBT sc-32323). Enriched RNAs were reverse transcribed using a primer complementary to the RNA adaptor. Adaptor duplexes with 5- or 6-base pair random nucleotide overhangs were ligated to the 3' end of the cDNA. The cDNA libraries were amplified using primers that carry Illumina indices; 180-400nt DNA libraries were isolated through 2% agarose gel electrophoresis and sequenced on the Illumina HiSeq 2500, as V2 rapid paired-end 50nt reads, according to manufacturer's recommended protocols.

For mRNA-seq (Figure 3-2C), RNA was assessed for quality using the TapeStation (Agilent, Santa Clara, CA) using manufacturer's recommended protocols. Samples were prepared using the Illumina TruSeq Stranded Total RNA Library Prep kit (Illumina, San Diego, CA) using manufacturer's recommended protocols. 100ng of total RNA was rRNA-depleted using Ribo-Zero (Illumina, San Diego, CA). The rRNA-depleted RNA was then fragmented and copied into first strand cDNA using reverse transcriptase and random primers. The 3' ends of the cDNA were adenylated, and uniquely barcoded adapters were ligated. Products were purified and enriched by PCR to create the final cDNA library. Final libraries were checked for quality and quantity by TapeStation and qPCR following manufacturer's instructions for Kapa's library quantification kit for Illumina Sequencing platforms (Kapa Biosystems, Wilmington MA). Samples were pooled and sequenced on the Illumina NextSeq, as 75 cycle High Output read, according to manufacturer's recommended protocols.

For both BrU- and mRNA-seq (Figure 3-2), the quality of the sequencing data was confirmed by FastQC (<http://www.bioinformatics.babraham.ac.uk/projects/fastqc/>).

Reads were mapped onto the RGSC 6.0/Rn6 reference genome using Bowtie2 (104) and annotated with Tophat2 (105). Adaptors were trimmed using BBDUK (<http://jgi.doe.gov/data-and-tools/bb-tools/>) (k=30, minlength=20, hdist=1). sSeq signals were quantified by FeatureCounts (106), excluding overrepresented ribosomal RNAs (Rn18s, Rn28s, Rn45s, Rn5s, Rn5-8s, Rn4.5s, LOC310928, LOC102723236, Lars2, Cdk8, and Zc3h7a) and the mitochondrial genome. DE-genes were identified using DESeq2 (107) with an adjusted *p*-value <0.05.

For total RNA-seq (Figure 3-9), RNA was assessed for quality using the TapeStation (Agilent, Santa Clara, CA). Samples were prepared using the NEBNext Ultra II Directional RNA Library Prep Kit for Illumina (E7760L), Ribo depletion Module NEBNext rRNA Human/Mouse/Rat (E6310X), and NEBNext Multiplex Oligos for Illumina Unique dual (E6440L) (NEB, Ipswich, MA). The rRNA-depleted RNA is then fragmented 10 minutes determined by RIN (RNA Integrity Number) of input RNA as per protocol, and copied into first strand cDNA using reverse transcriptase and dUTP mix. Samples underwent end-repair and dA-tailing step followed by ligation of NEBNext adapters. Products were purified and enriched by PCR to create the final cDNA library. Final libraries were checked for quality and quantity by TapeStation (Agilent) and qPCR using Kapa's library quantification kit for Illumina Sequencing platforms (KK4835) (Kapa Biosystems, Wilmington MA). Samples were pooled and sequenced on the Illumina NovaSeq S4 Paired-end 150bp, according to manufacturer's recommended protocols.

53-82 million reads were obtained for each sample. Trim_galore 0.6.0 (github.com/FelixKrueger/TrimGalore, a wrapper around, Cutadapt version 1.15) (108) was used to trim the Illumina standard adapter and low quality bases (Phred score 20).

Both reads of the pair were removed if either read had fewer than 20bp remaining. Fewer than 5% of bases were lost. STAR version 2.7.2 (109) was used with the standard ENCODE options to align reads to the GRCm38 reference sequence; all samples had greater than 83% alignment. RSeQC (110) was used to calculate read distributions across genome features; greater than 75% of mapped reads were in an exon or 3' region. featureCounts from the Rsubread Bioconductor (111) package was used along with the comprehensive genecode.vM23.annotation GTF to summarize reads. Multimapped reads were ignored per featureCounts defaults. Counts were preprocessed using the Bioconductor package edgeR (112), normalized and scaled using the weighted trimmed mean (TMM) technique (113) and further prepared for linear modeling using the Voom method from the limma package (114). Linear models are then fit to Log counts per million (CPM) values using the standard limma empirical Bayes method and contrasts of interest are extracted.

For small RNA-seq (Figure 3-10), RNA was assessed for quality using the TapeStation (Agilent, Santa Clara, CA) using manufacturer's recommended protocols. Samples were prepared using the NEBNext Multiplex Small RNA Library Prep Set for Illumina (E7300L). Adapters were ligated to 100ng of total RNA, which then underwent First Strand Synthesis and PCR amplification. Products are purified and size selected by Pippin Prep according to NEB protocol recommendations. Final libraries were checked for quality and quantity by TapeStation (Agilent) and qPCR using Kapa's library quantification kit for Illumina Sequencing platforms (catalog # KK4835) (Kapa Biosystems, Wilmington MA). Samples were pooled and sequenced on the Illumina NovaSeq S4 Paired-end 150bp, according to manufacturer's recommendations.

Single end small RNA fastq files were trimmed similarly to the mRNA files except a minimum length of 18 bases was used. Trimmed fastq files were then aligned using Bowtie (115) through the miRDeep2 software package (116). miRNA's were annotated using mirbase version 22 (117). Counts produced by miRDeep2 were then processed through the same limma pipeline as the mRNA data to find differentially expressed miRNAs. The down-regulated mRNAs and up-regulated miRNAs were used as input into the multiMiR R package (118, 119) to map miRNAs and mRNA interactions. The miRmapper package was used to summarize these interactions and find miRNAs with the greatest impact (120). miRNAs with a large impact were defined as those that regulate the greatest number of targets. In the same sense, mRNAs regulated by the greatest number of miRNAs were also of interest.

3.5.13 Statistical Analysis

There was no experimental prediction of the difference between control and experimental groups when the study was designed. Therefore, we did not use computational methods or power analysis to determine sample size *a priori*. Instead, we used minimum of three ($n=3$) biological replicates coming from independent experiments, when permitting with technical replicates to increase confidence. Signals derived from technical replicates were averaged and used as one data entry for the purposes of statistical analysis. Unless indicated otherwise, results were reported as mean value \pm SEM. For comparison between two groups, unpaired two-tailed Student's *t*-test was used, where a p -value <0.05 was considered statistically significant. For

comparison amongst multiple groups, ordinary one-way ANOVA followed by multiple comparisons tests such as Dunnett's, Tukey's, or uncorrected Fisher's LSD were used. All statistical analyses were carried out using GraphPad Prism Software (version 8.3.0).

3.6 Acknowledgements

We thank Dr. Christine Bandtlow for providing shNogoA and scrambled control plasmid. We appreciate Dr. Xiao-Feng Zhao's help with cloning, step-wise site-directed mutagenesis, and plasmid preparation. We thank Dr. Martine E. Schwab for his generosity with anti-NogoA antibodies, including Bianca and 11C7, as well as anti-FG12, epitope-matched antibody. We also thank Dr. Michael E. Greenberg for providing the anti-Npas4 antibody, and Dr. Yingxi Lin for sharing protocol details for transcription factor solubilization. We recognize Dr. Binhai Zheng's generosity with sharing *NogoABC^{fl/fl}* mouse breeders. We acknowledge Dr. Ashley L. Kalinski's input in RT-qPCR and immunofluorescence quantification. We feel indebted to Alex Chen (AC) and Dr. Michael A. Sutton for carrying out and analyzing the mEPSC electrophysiological recordings. We especially appreciate Patricia M. Garay (PMG.), Dr. Shigeki Iwase, and the U-M Advanced Genomics Core for their insights and contributions for cDNA library preparations. We could not have analyzed extensive RNA-seq data without the expertise of PMG and Craig N. Johnson (CNJ). Last, but not least, we are grateful for Dr. Katherine T. Baldwin's (KTB) contribution, as they laid the project foundation.

3.7 Author Contribution

Experiments were conceived and designed by Rafi Kohen (RK) and Roman J. Giger (RJG). RK, KTB, AC and Corey G. Flynn (CGF) both collected and analyzed data. PMG and CNG analyzed data. RK wrote the manuscript, together with edits from RJG.

3.8 Figures

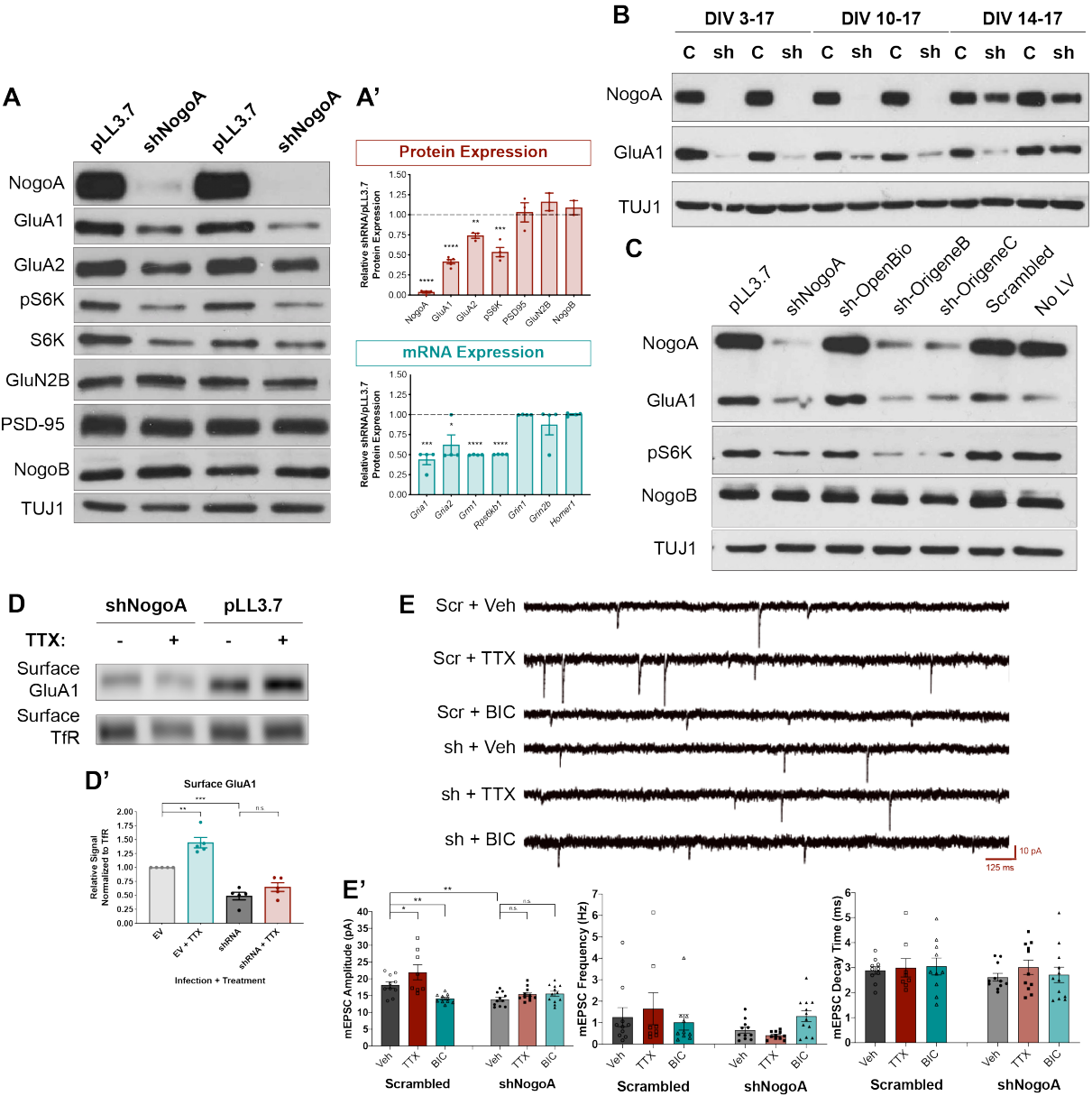


Figure 3-1: NogoA shRNA reduces baseline excitatory synaptic transmission and blocks homeostatic scaling.

(A) Western blot analysis of primary rat hippocampal neurons transduced on DIV10 with LV-pLL3.7-GFP empty vector (EV) control or LV-shNogoA, and lysed on DIV17. (A') Quantification of protein levels, normalized first to TUJ1, then to the EV control. $n=2-5$ biological with 3 technical replicates each. mRNA expression for the same proteins were analyzed by RT² PCR Profiler Array (Qiagen). Cycle threshold was normalized first to *Gapdh*, then to the EV control. $n=4$ independent biological replicates. For both quantification, $p<0.05$ was deemed statistically significant, as assessed by unpaired two-tailed Student's *t*-test. (B) Western blot analysis of rat hippocampal neurons transduced with EV or shNogoA on DIV3, 10, and 14, and harvested on DIV17. Internal loading control was neuron-specific marker TUJ1. (C) Western blot analysis of rat embryonic hippocampal neurons transduced with different lentiviral constructs on DIV10, and harvested on DIV17. pLL3.7 empty vector, scrambled shRNA, and no lentiviral infection served as negative controls. Loading control was TUJ1. (D) Western blot analysis of primary rat hippocampal neurons transduced with the same lentiviral constructs on DIV10, treated with 2 μ M tetrodotoxin (TTX) on DIV16, and subjected to cell surface biotinylation on DIV17. (D') Quantification of surface GluA1 expression, normalized first to the transferrin receptor (TfR), then to the EV+veh control. $n=5$ biological with 3 technical replicates each. $p_{adj}<0.05$ was deemed statistically significant, as assessed by ordinary one-way Anova followed by Tukey's multiple comparisons test. (E) Representative traces of mEPSC electrophysiological recordings on DIV14, following sparse transfection with scrambled or shNogoA plasmids on DIV12, as well as vehicle, 1 μ M TTX or 10 μ M bicuculline (BIC) treatments on DIV13. Scale bars= 10pA (vertical), 125ms (horizontal). (E') Quantification of mEPSC amplitude (pA), frequency (Hz), and decay time (ms) from $n=8-10$ GFP⁺, pyramidal-like neurons per group. $p_{adj}<0.05$ was deemed statistically significant, as assessed by ordinary one-way Anova followed by uncorrected Fisher's LSD multiple comparisons test. All data are presented as mean \pm SEM.

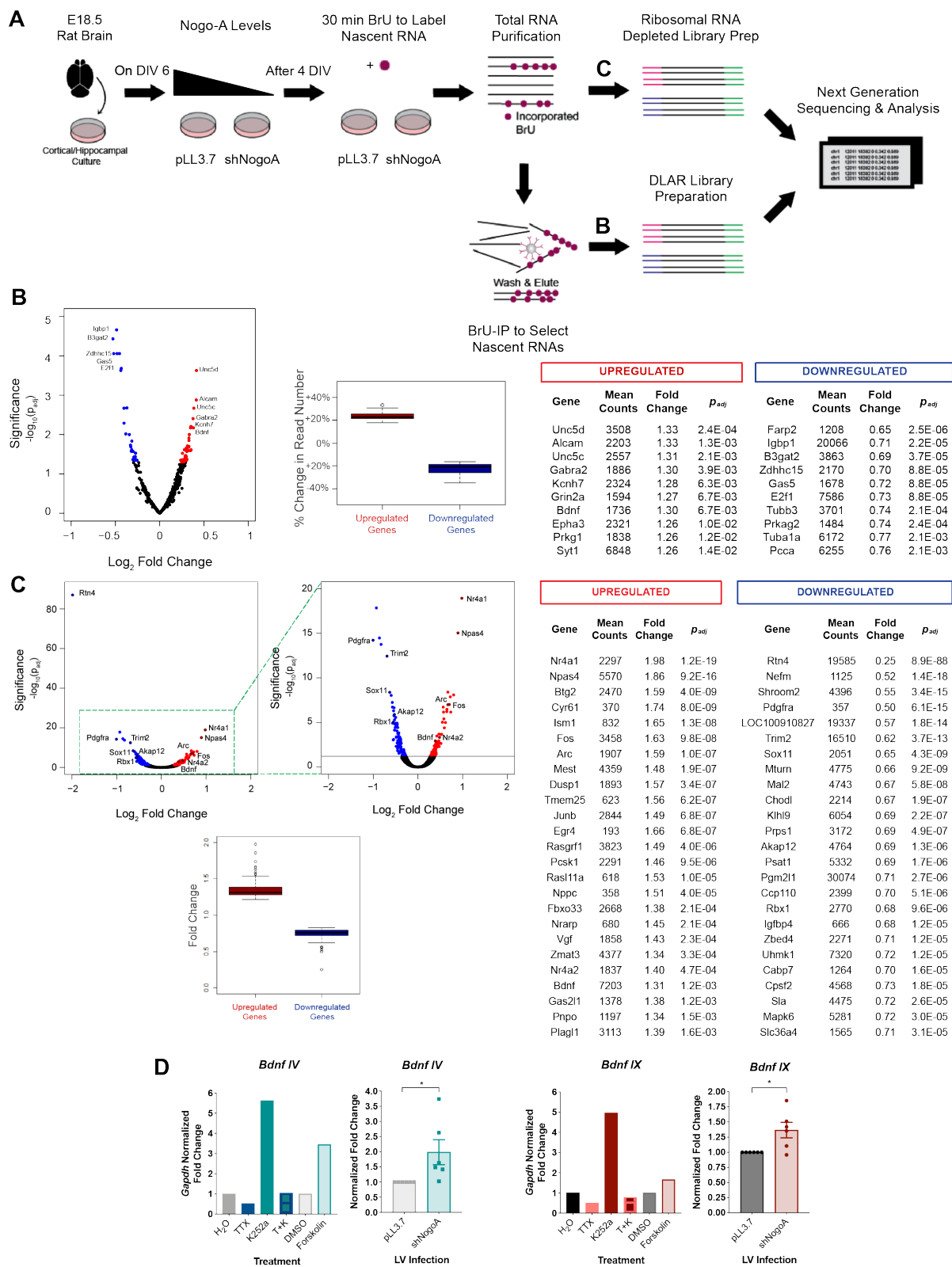


Figure 3-2: shNogoA alters the landscape of the immediate-early synaptic gene expression.

(A) Schematic of experimental design and timeline. Rat primary forebrain cultures were transduced with pLL3.7 and shNogoA on DIV6, treated with 2mM BrU for 30 minutes, and harvested for total RNA isolation. Split into two groups, this input RNA was used for cDNA libraries from BrU-incorporated, nascent RNA (B), or rRNA-depleted mRNA (C). Both libraries were subjected to next generation sequencing and analysis. (B) Volcano plot of BrU-seq data marks upregulated (red) and downregulated (blue) genes with $p_{adj} < 0.05$ are marked (left). Analysis shows the extent of differentially expressed gene regulation (right). Table displays 10 genes with such bidirectional regulation. (C) Overall (left) and zoomed in (right) volcano plots of mRNA-seq data from the same input RNA mark upregulated (red) and downregulated (blue with $p_{adj} < 0.05$). Analysis shows the extent of differentially expressed gene regulation (bottom). Table displays 25 genes with such regulation. (D) Quantification of *Bdnf* IV and IX mRNA expression by first strand RT-qPCR. *Bdnf* expression was normalized first to *Gapdh*, then to pLL3.7 or vehicle control groups. Primary rat forebrain cultures were treated with 2 μ M TTX (48hrs), 200nM K252a (2hrs), or 10 μ M forskolin (2hrs) or lentivirally transduced following same experimental paradigm. For primer verification experiments following drug treatments, $n=1$ biological with 3 technical replicates. For experiments following lentiviral transduction, $n=6$ biological with 2 technical replicates, derived from 2 independent experiments. All data are presented as mean \pm SEM, where $p < 0.05$ was deemed statistically significant, as assessed by unpaired two-tailed Student's *t*-test.

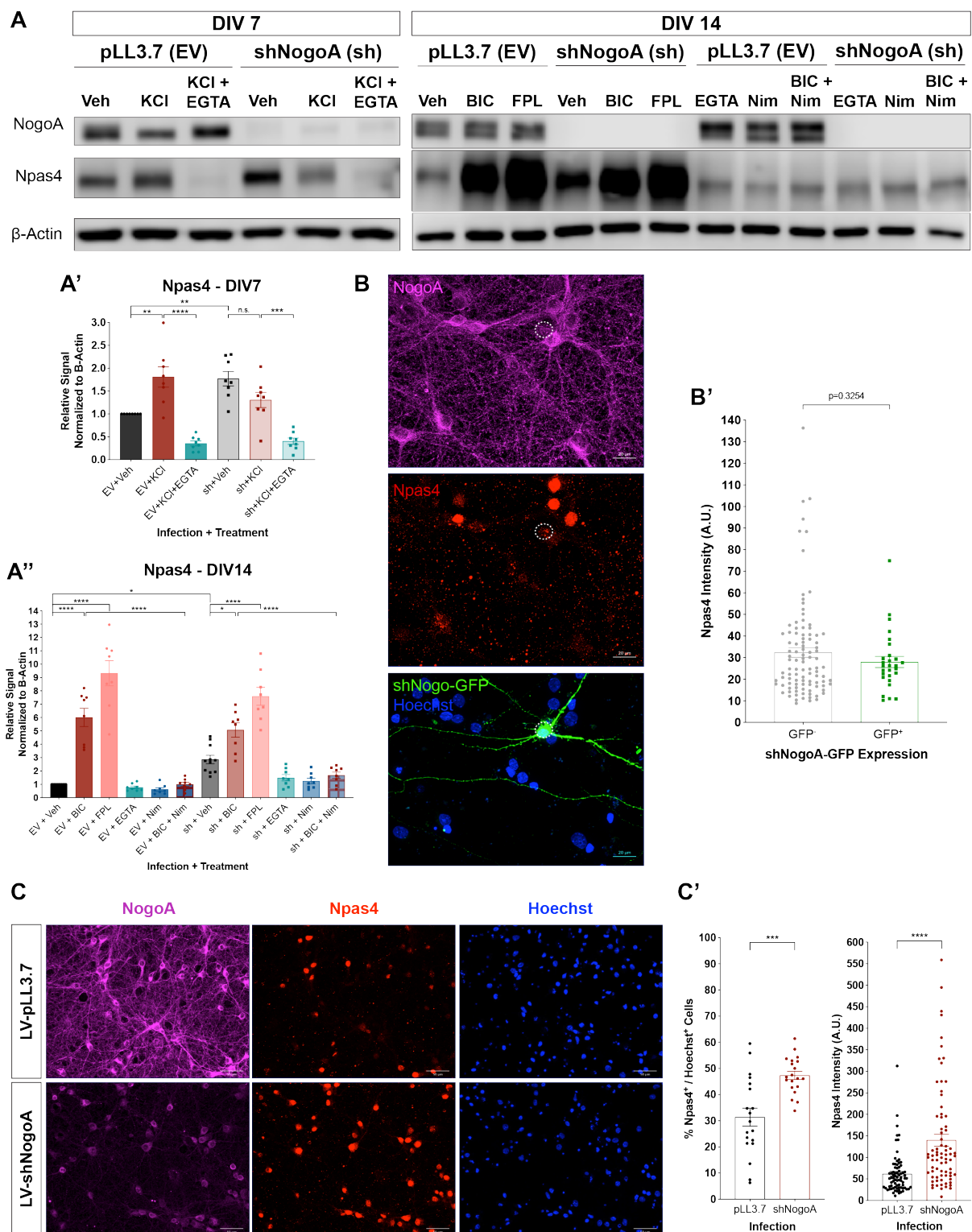


Figure 3-3: Global shNogoA transduction upregulates Npas4 via L-Type VGCC activation.

(A) Western blot analysis of primary hippocampal neurons transduced with pLL3.7 or shNogoA on DIV3, and maintained until DIV7 or DIV14. On DIV7, neurons were treated with 55mM KCl (2hrs) with or without 5mM EGTA (10mins) pretreatment. On DIV14, neurons were treated with 50 μ M BIC (2hrs) or 1 μ M FPL64176 (2hrs) with or without 5mM EGTA (10mins) or 5 μ M nimodipine (1hr) pre-treatment. (A'-A'') Quantification of experiments with DIV7 (A') and DIV14 (A'') cultures. Signal intensity was first normalized to the loading control β -Actin, then to the normalized EV+Veh control levels. Data are presented as mean \pm SEM from $n\geq 8$ biological replicates. $p_{adj}<0.05$ was deemed statistically significant, as assessed by ordinary one-way ANOVA followed by Tukey's multiple comparisons test. (B) Immunofluorescence images of primary hippocampal neurons sparsely transfected with the GFP-tagged shNogoA (green) on DIV3, and maintained until DIV14. Neurons were stained for NogoA (magenta), Npas4 (red), and Hoechst (blue). Scale bar=20 μ m. (B') Quantification of nuclear (Hoechst⁺) Npas4 signal intensity from GFP⁺ cells with shNogoA transduction ($n=28$) compared to GFP⁻ neighboring ($n=100$), NogoA-expressing cells. $p=0.3254$, deemed statistically not significant as assessed by unpaired two-tailed Student's t -test. (C) Immunofluorescence images of primary hippocampal neurons lentivirally transduced with pLL3.7 or shNogoA on DIV3, and maintained until DIV14. Neurons were stained for NogoA (magenta), Npas4 (red), and Hoechst (blue). Scale bar=50 μ m. (C') Quantifications of Npas4-expressing cell percentage as well as nuclear Npas4 signal intensity. For percentage quantification, $n=19-20$ FOVs from 3 biological replicates, $p=0.0001$ as assessed by unpaired two-tailed Student's t -test. For intensity quantification, $n=76$ neurons from 3 biological replicates, $p<0.0001$ as assessed by unpaired two-tailed Student's t -test.

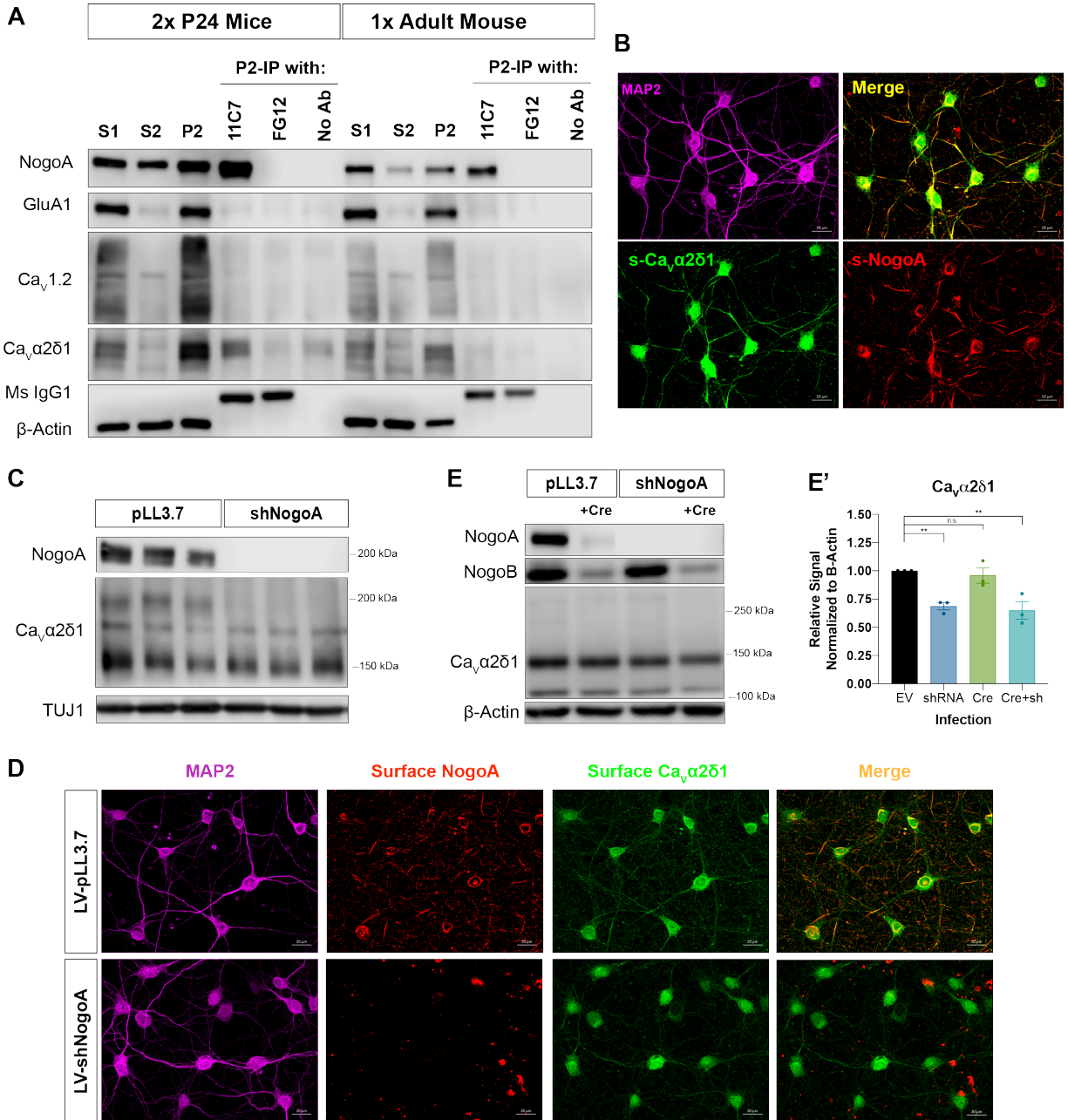


Figure 3-4: NogoA interacts with and/or modulates L-type VGCC auxiliary subunit $\text{Ca}_v\alpha 2\delta 1$.

(A) Western blot analysis of homogenate (S1), cytosol (S2), and membrane (P2) fractions from the early postnatal or adult mouse brains. NogoA was immunoprecipitated with the mouse monoclonal 11C7 antibody from solubilized membrane fractions. Similar mouse IgG1 signals (~50kDa) indicate equal input of 11C7 and isotype control anti-FG12 antibody. Additional negative control was omission of antibodies (beads only). Loading control was β -Actin. (B) Immunofluorescence images of hippocampal neurons stained for surface NogoA (red) and $\text{Ca}_v\alpha 2\delta 1$ (green) expression under non-permeabilized conditions. Consecutive permeabilization allowed for neuronal MAP2 (magenta) staining for somatodendritic morphology delineation. Scale bar=20 μm . (C) Western blot analysis of hippocampal cultures transduced with pLL3.7 or shNogoA on DIV3, and harvested on DIV14. Loading control was TUJ1. (D) Immunofluorescence images of primary hippocampal neurons subjected to a similar experimental timeline. Neurons were stained for surface NogoA (red) and $\text{Ca}_v\alpha 2\delta 1$ (green) expression under non-permeabilized conditions. Neuronal somatodendritic morphology was delineated by immunostaining for MAP2 (magenta) under consecutively permeabilized conditions. Scale bar=20 μm . (E) Western blot analysis of *NogoABC^{fl/fl}* mouse neurons co-infected with LV-CMV-Cre (DIV3) and LV-EV or LV-shNogoA (DIV6). (E') Quantification of $\text{Ca}_v\alpha 2\delta 1$ protein expression from $n=3$ biological replicates. Signal intensity was first normalized to the loading control β -Actin, then to EV control. Data are presented as mean \pm SEM, where statistical significance was based on $p_{\text{adj}} < 0.05$ as assessed by ordinary one-way ANOVA, followed by Dunnett's multiple comparisons test.

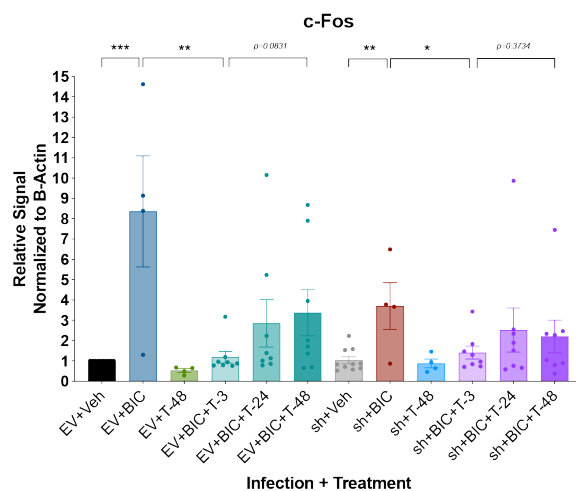
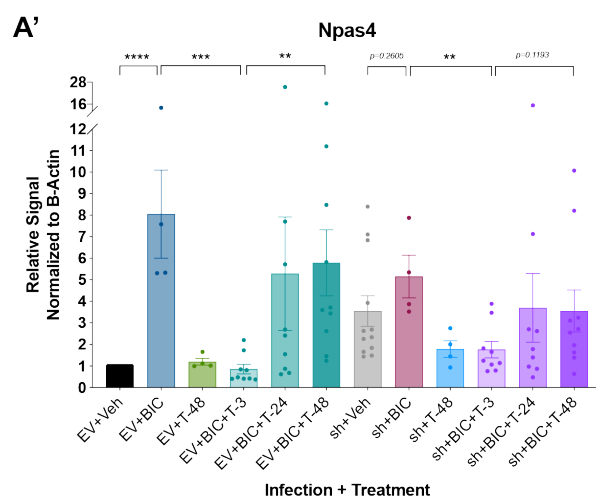
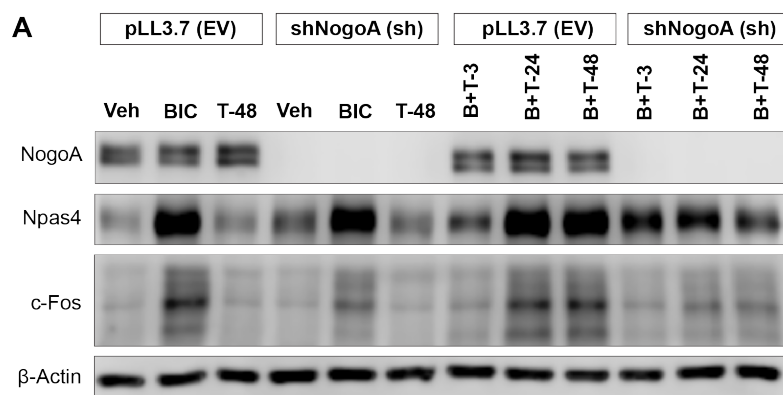


Figure 3-5: shNogoA impairs homeostatic scaling through immediate-early gene induction.

(A) Western blot analysis of hippocampal neurons transduced with pLL3.7 or shNogoA on DIV3, and harvested on DIV14. Cultures were treated with 2 μ M TTX for 3, 24, and 48 hours before lysis. All 50 μ M BIC treatments were for 2 hours. (A) Quantification of Npas4 and c-Fos from $n=4-12$ biological replicates. Signal intensity was first normalized to the loading control β -Actin, then to the EV+Veh control. Data are presented as mean \pm SEM, where statistical significance was based on $p<0.05$ as assessed by unpaired two-tailed Student's t -test.

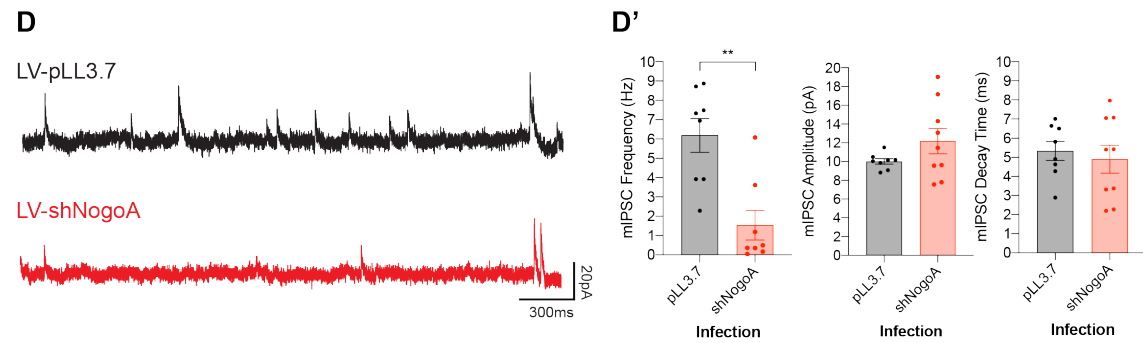
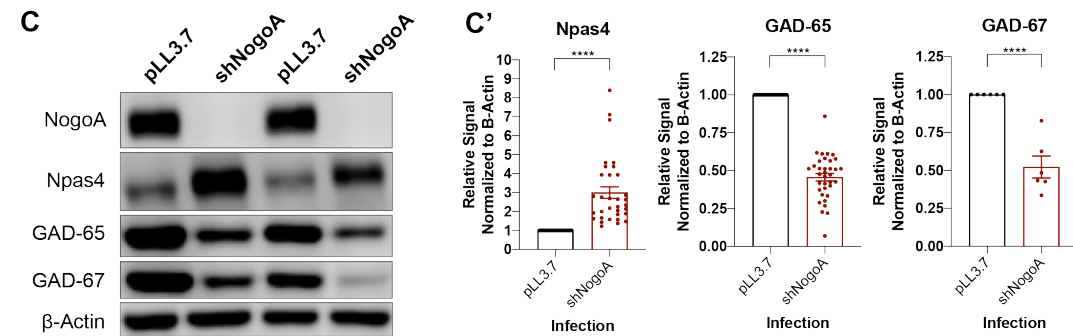
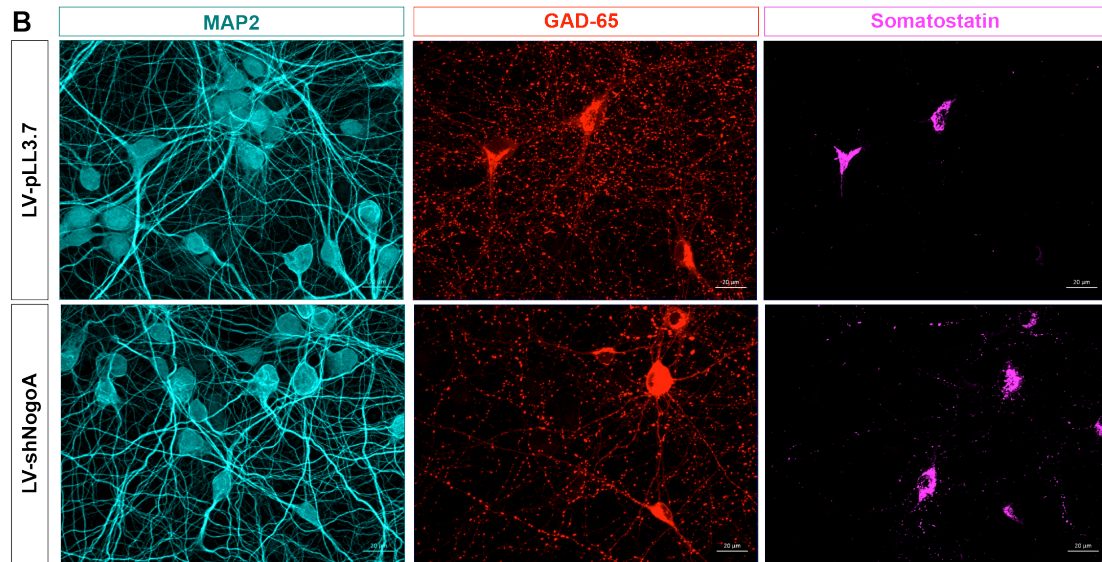
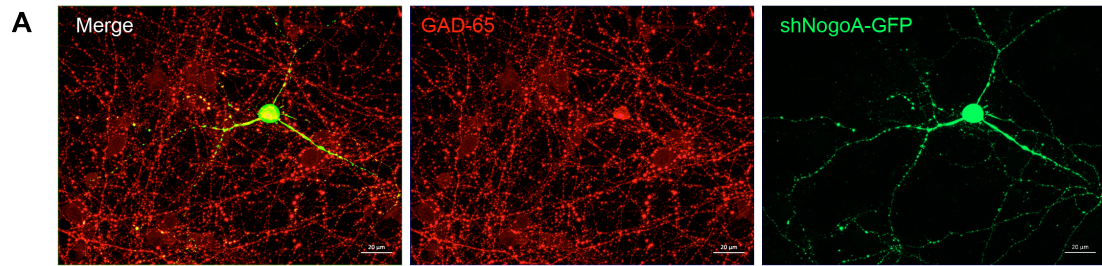


Figure 3-6: shNogoA transduction impairs inhibitory synaptogenesis.

(A) Immunofluorescence images of hippocampal neurons sparsely transfected with the GFP-tagged shNogoA (green) on DIV3, and maintained until DIV14. Neurons were stained for the inhibitory pre-synaptic protein GAD-65 (red). (B) Immunofluorescence images of hippocampal cultures globally transduced with the lentiviral constructs pLL3.7 and shNogoA on DIV3, and maintained until DIV14. GAD-65 (red) marks inhibitory presynaptic sites, somatostatin (magenta) identifies an inhibitory interneuron subtype, and MAP2 (cyan) delineates somatodendritic morphology. (C) Western blot analysis of hippocampal cultures subjected to the same experimental timeline. (C') Npas4, GAD-65 and GAD-67 protein expression were normalized first to the loading control β -Actin, then to the pLL3.7 control. Data are presented as mean \pm SEM from $n=33,35,6$ biological replicates for Npas4, GAD-65, and GAD-67, where $p<0.0001$ as assessed by unpaired two-tailed Student's t -test. (D) Representative traces of miniature inhibitory post-synaptic current (mIPSC) recordings from primary hippocampal neurons globally transduced with LV-pLL3.7 or LV-shNogoA. Scale bars=300ms(horizontal), 20pA(vertical). (D') Quantification of mIPSC frequency, amplitude, and decay time. Data from $n=8-9$ neurons are presented as mean \pm SEM, where statistical significance was based on $p<0.05$ as assessed by unpaired two-tailed Student's t -test.

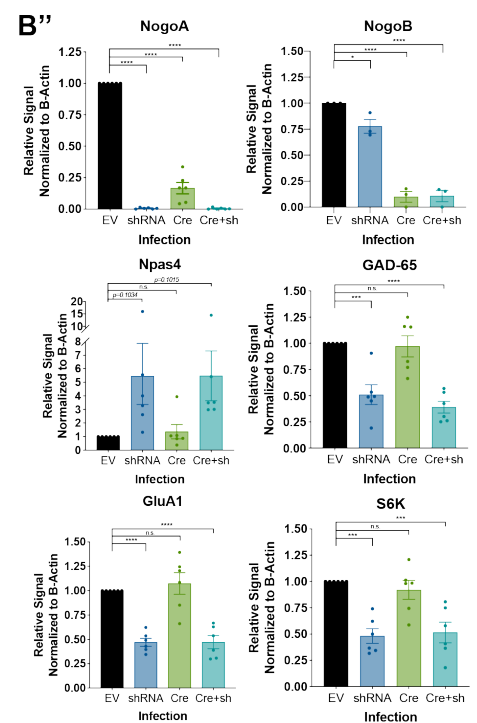
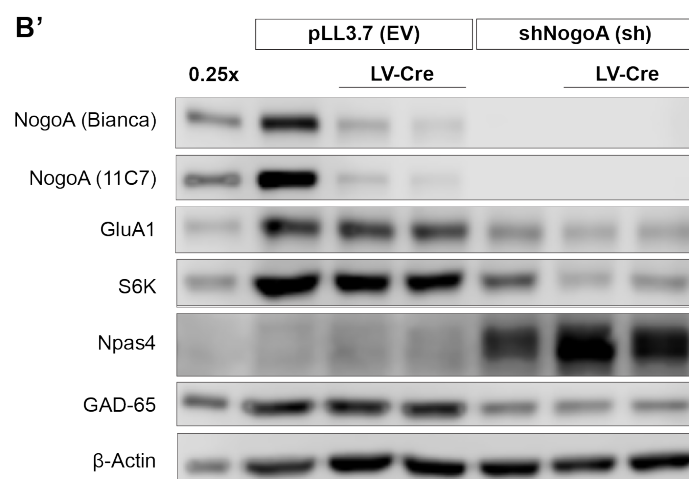
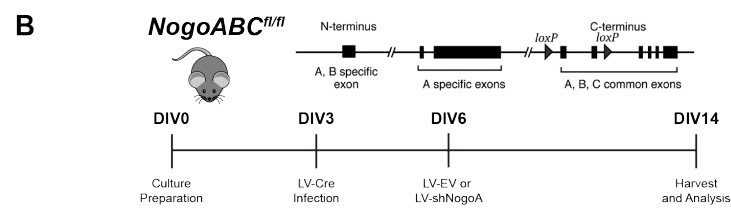
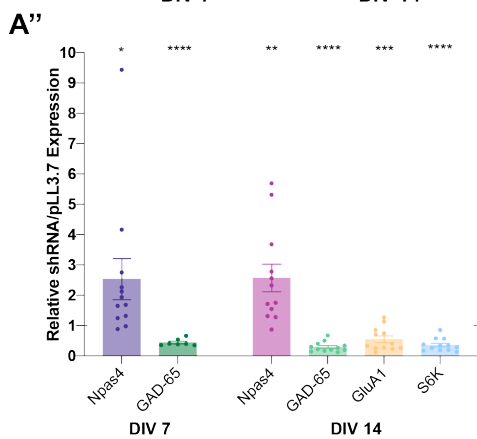
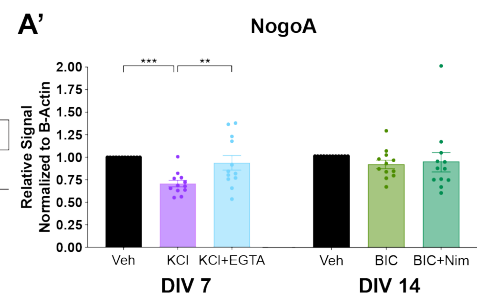
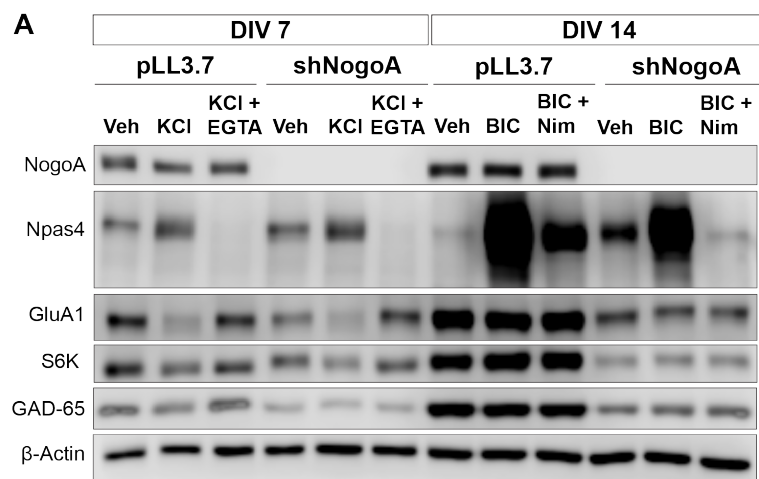
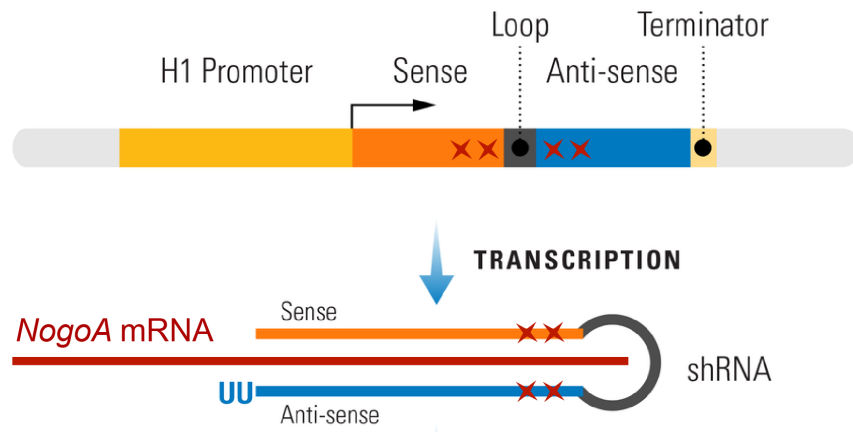


Figure 3-7: Observed synaptic phenotypes are NogoA-independent.

(A) Western blot analysis of CD1 mouse hippocampal cultures transduced on DIV3 with pLL3.7 or shNogoA, and harvested on DIV7 and DIV14. On DIV7, neurons were treated with 55mM KCl (2hrs) with or without 5mM EGTA (10mins) pretreatment. On DIV14, neurons were treated with 50μM BIC (2hrs) with or without 5μM nimodipine (1hr) pretreatment. (A') Quantification of NogoA protein expression. Data are presented as mean±SEM from $n=12$ biological replicates, where $p_{adj}<0.05$ was deemed statistically significant as assessed by ordinary one-way ANOVA followed by Tukey's multiple comparisons test. (A'') Quantification of Npas4, GAD-65, GluA1 and S6K from DIV7 or DIV14 neurons. Data are presented as mean±SEM from $n=7-12$ biological replicates, where $p<0.05$ was deemed statistically significant as assessed by unpaired two-tailed Student's t -test. (B) Diagram of the *NogoABC^{fl/fl}* conditional knockout mouse model and experimental timeline. (B') Western blot analysis of perinatal (P0-1) *NogoABC^{fl/fl}* mouse hippocampal cultures, which were transduced with LV-CMV-Cre on DIV3 and with EV or shNogoA on DIV6, and maintained until DIV14. (B'') Quantification of protein expression, where signal intensity was normalized first to the loading control β-Actin, then to EV only. Data are presented as mean±SEM from $n=3-6$ biological replicates, where $p_{adj}<0.05$ was deemed statistically significant as assessed by ordinary one-way ANOVA followed by Dunnett's multiple comparisons test.

A

shNogoA-2pMt



B

shNogoA-5pMt

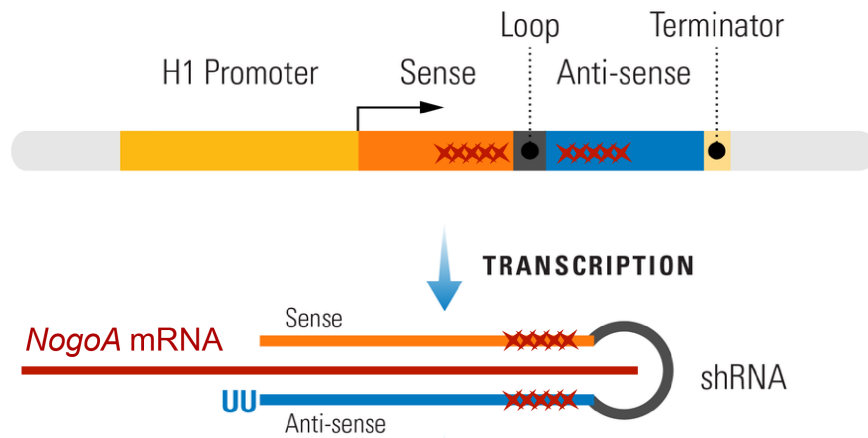


Figure 3-8: shNogoA seed region was mutated with two or five basepairs to study the target-specificity of observed regulations.

Schematic of how the seed sequence of the shNogoA was mutated with two (A) or five (B) basepairs in both sense and anti-sense strands. Once expressed under the weak histone (H1) promoter, shNogoA construct is originally designed to target and repress expression of *NogoA* mRNA. Images adapted with permission from systembio.com.

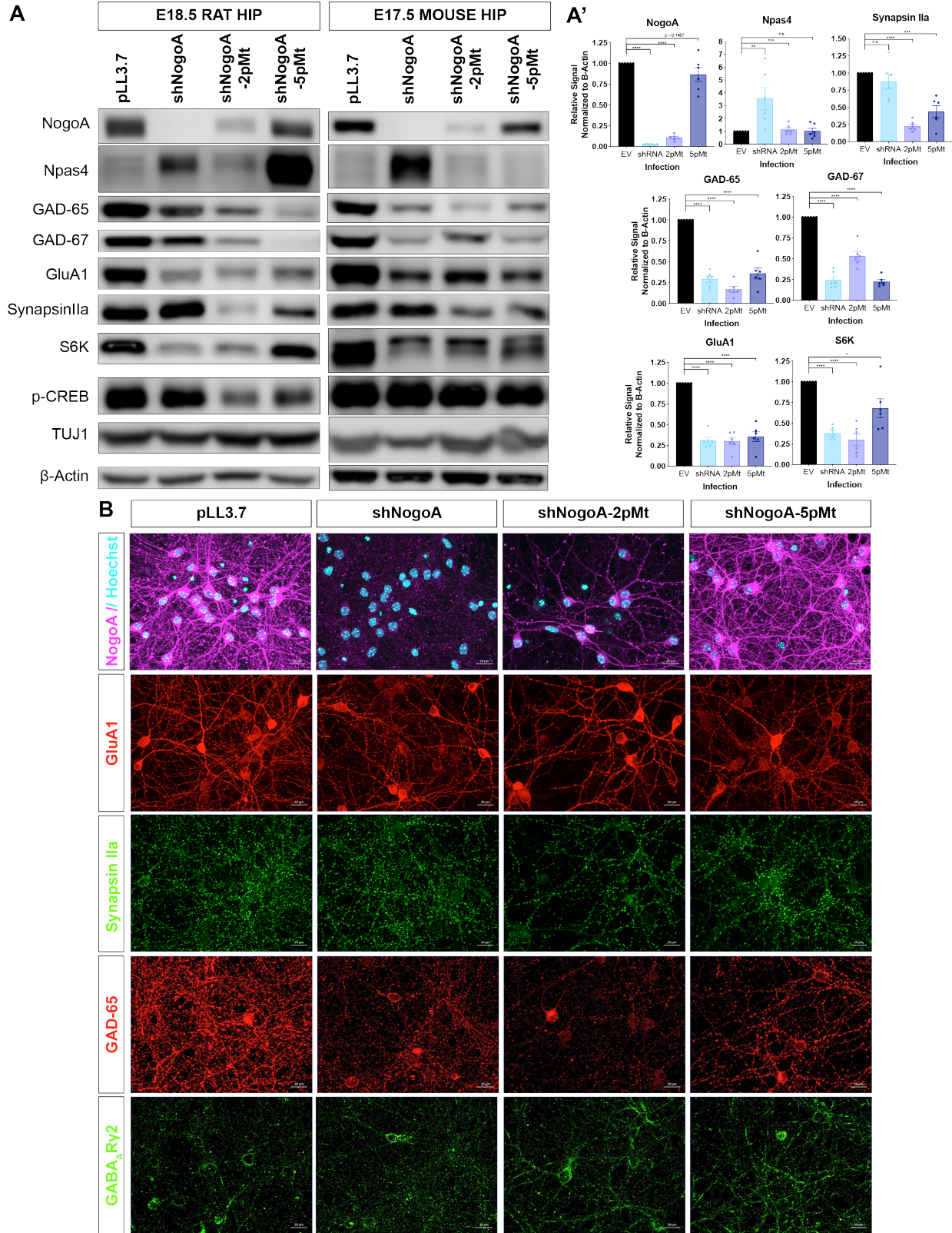


Figure 3-9: Step-wise mutated shNogoA still replicates regulation of excitatory and inhibitory synapse formation and strength.

(A) Western blot analysis of DIV14 hippocampal cultures prepared from E18.5 rat or E17.5 mouse, transduced on DIV4-6 with pLL3.7, shNogoA, shNogoA-2pMt, shNogoA-5pMt. (A') Quantification of protein expression from experiments with mouse hippocampal cultures only. Signal intensity was normalized first to the loading control β -Actin, then to the normalized pLL3.7 value. Data are reported as mean \pm SEM, from $n=6$ biological replicates. $p_{adj}<0.05$ was deemed statistically significant as assessed by ordinary one-way ANOVA followed by Tukey's multiple comparisons test. (B) Immunofluorescence images of mouse hippocampal cultures following similar experimental timeline. Neurons were immunostained for NogoA (magenta) and Hoechst (cyan). Glutamatergic synapses were marked with post-synaptic GluA1 (red) and pre-synaptic SynapsinIIa (green). GABAergic synapses were marked with pre-synaptic GAD-65 (red) and post-synaptic GABA_AR γ 2 (green). Scale bar=20 μ m.

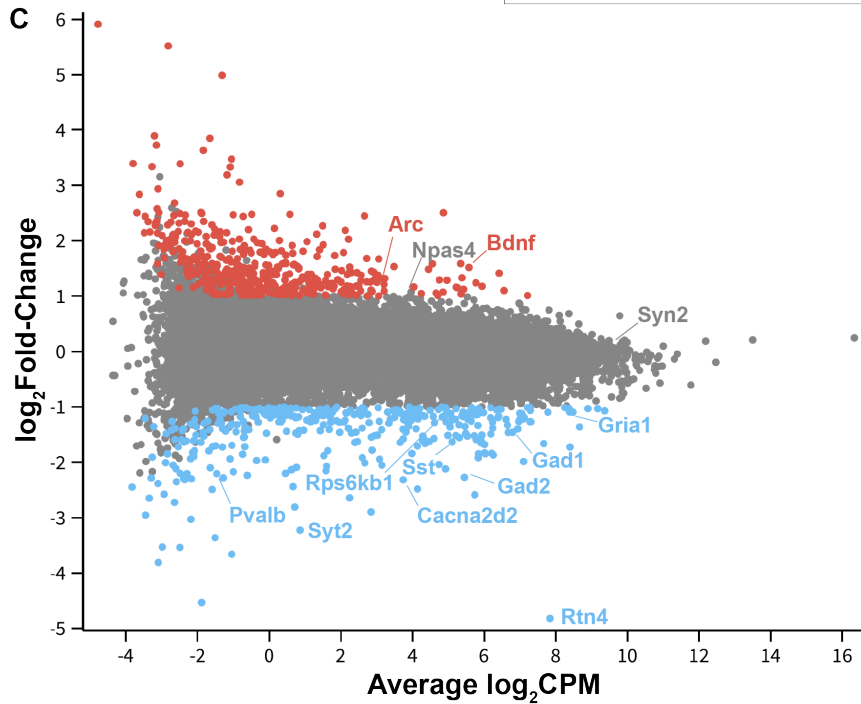
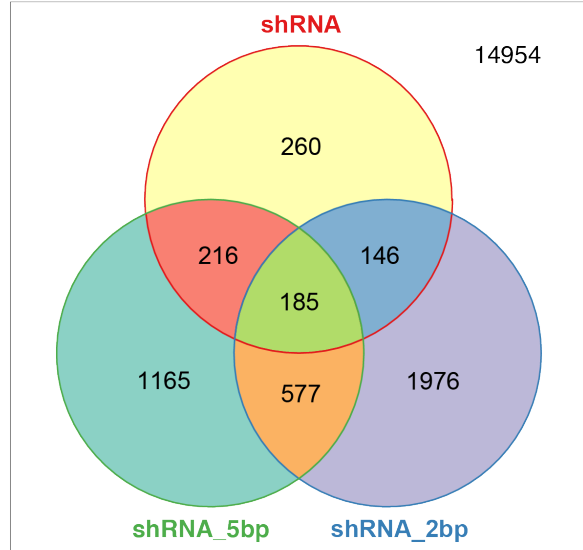
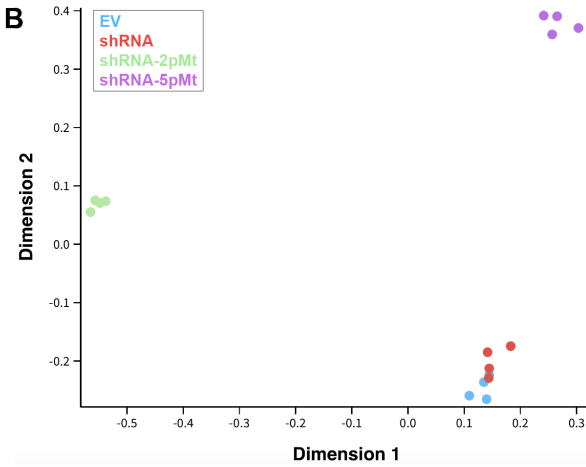
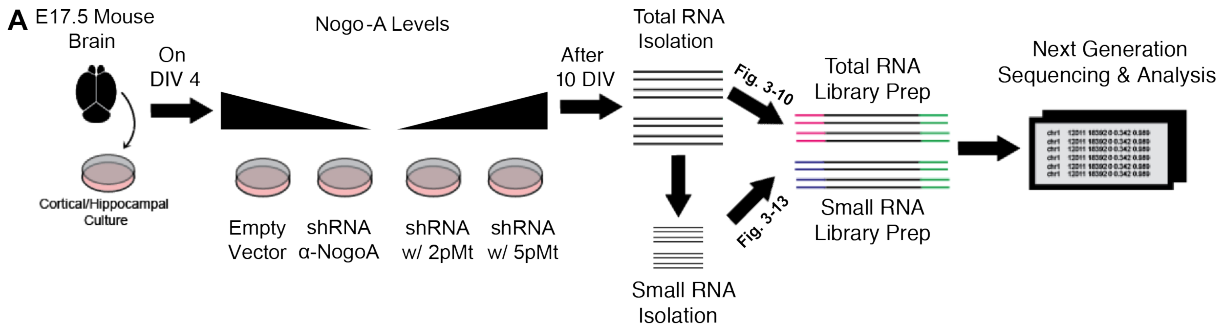


Figure 3-10: mRNA sequencing experiments with step-wise mutated shNogoA constructs demonstrate robust transcript regulation.

(A) Schematic of experimental design and timeline. Neuronal cultures were prepared from E17.5 mouse forebrain, transduced with the four lentiviral constructs on DIV4, and harvested on DIV14. Total RNA was isolated, purified, and split into two groups for separate cDNA library preparations from total and small RNAs. Both libraries were analyzed following next generation sequencing. (B) Principal component analysis (PCA) displays global transcriptome association (left). Venn diagram shows overlap of differentially expressed genes (DEGs) with ≥ 2 -fold regulation (right). (C) Dot-plot displays comparison of individual gene expressions between EV and shNogoA. DEGs with ≥ 2 -fold regulation are marked: upregulated (red) and downregulated (blue). Some candidate genes of interest are annotated.

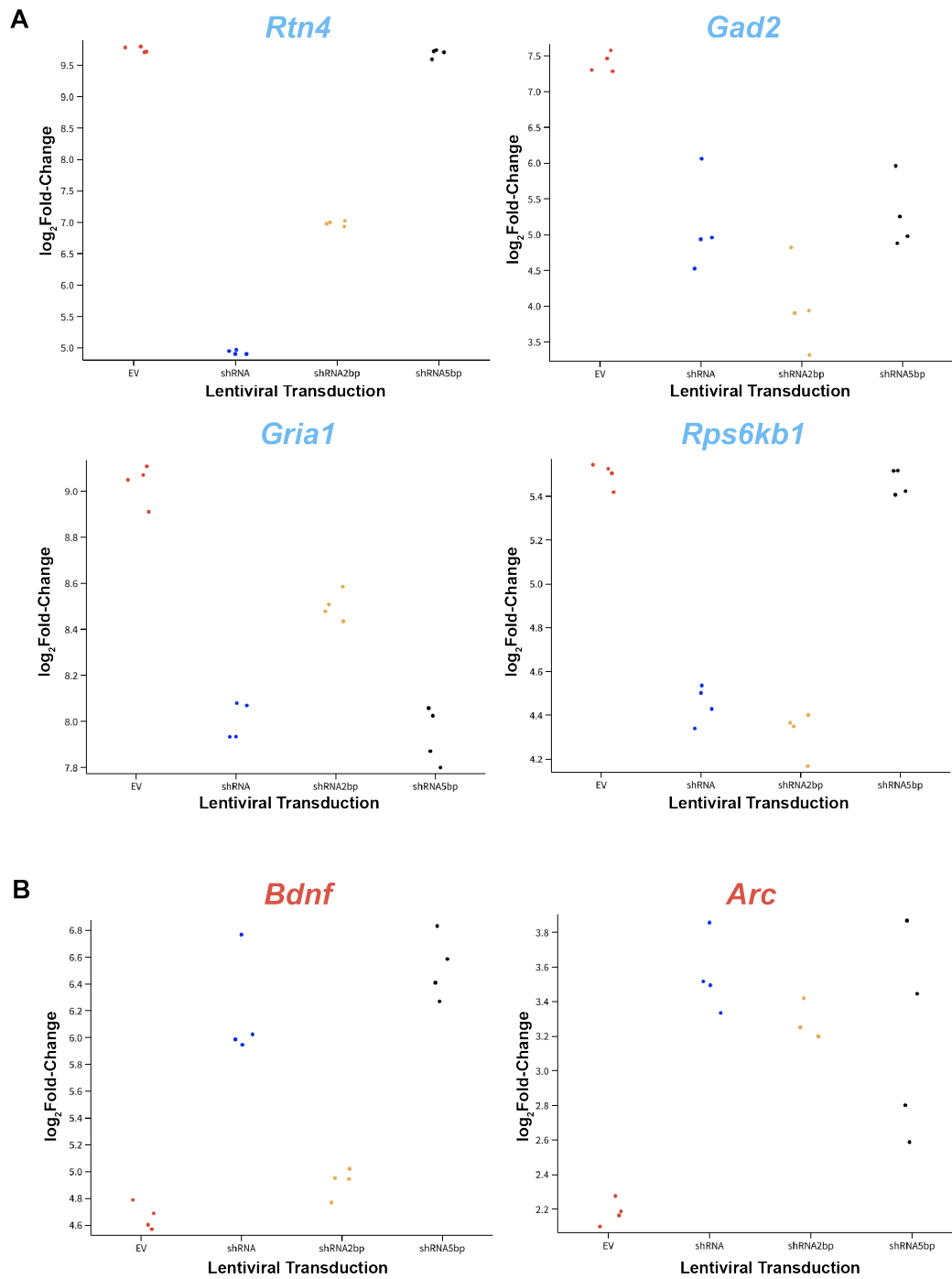







Figure 3-11: mRNA sequencing reveals NogoA-independent regulation of synaptically important gene products.

Individual data points showing expression profiles of selected downregulated (A) or upregulated (B) genes following four different lentiviral transductions.

-  Regulation of Ion Transport
-  Chemical Synaptic Transmission
-  Regulation of Synaptic Vesicle Cycle
-  Axon Guidance
-  mTOR Signaling Pathway

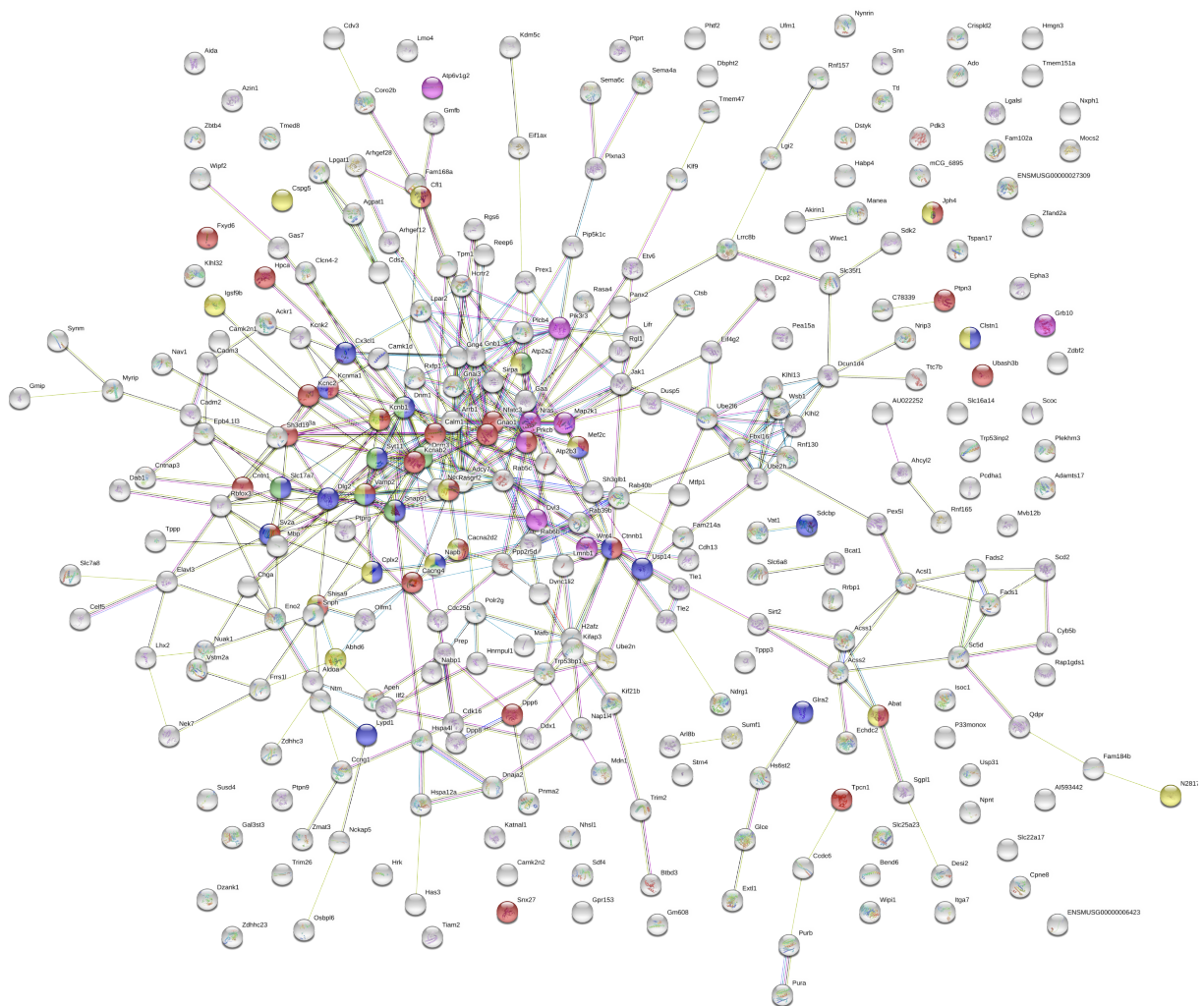


Figure 3-12: Analysis of NogoA-independent differentially expressed genes reveals synaptic protein-protein interactions.

STRING analysis of the top 300 DEGs following lentiviral transduction of primary neuronal cultures with LV-pLL3.7 and LV-shNogoA-5pMt. Lines indicate known protein-protein interactions. Proteins encoded by identified DEGs were categorized by implicated biological processes or signaling pathways.

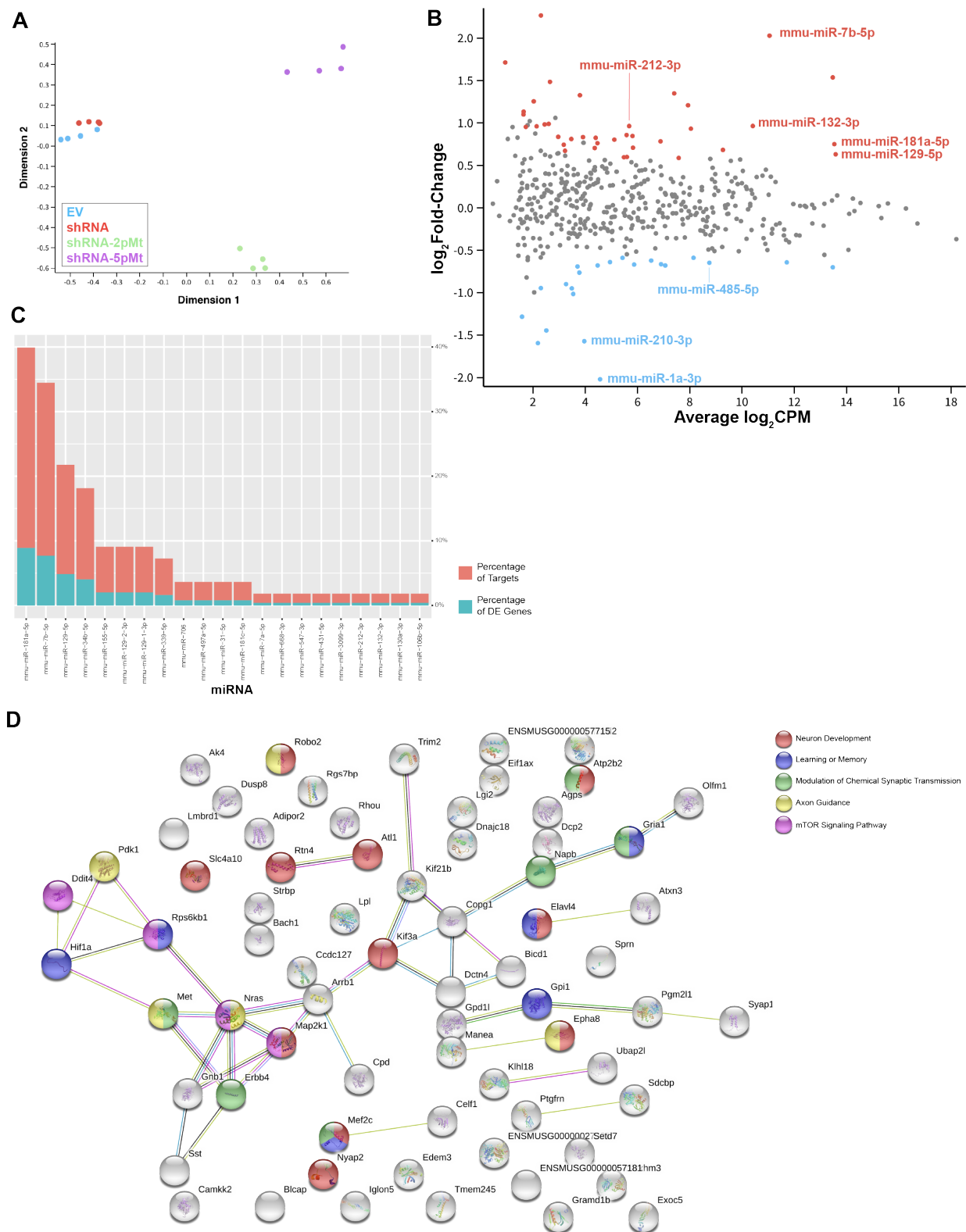


Figure 3-13: Small RNA sequencing identifies shNogoA-regulated miRNA expression.

(A) Principal component analysis (PCA) of the concurrent small RNA-seq displays global transcriptome association. (B) Dot-plot graph displays comparison of individual miRNA expressions between EV and shNogoA. miRNAs with ≥ 2 -fold regulation are marked as upregulated (red) and downregulated (blue). Some candidate miRNAs of interest are annotated. (C) Graphs show the correlative nature of identified miRNAs and their known target mRNAs, as detected by concurrent mRNA sequencing experiments. (D) STRING analysis of the 72 DEGs with known binding by the miRNAs regulated by LV-shNogoA transduction.

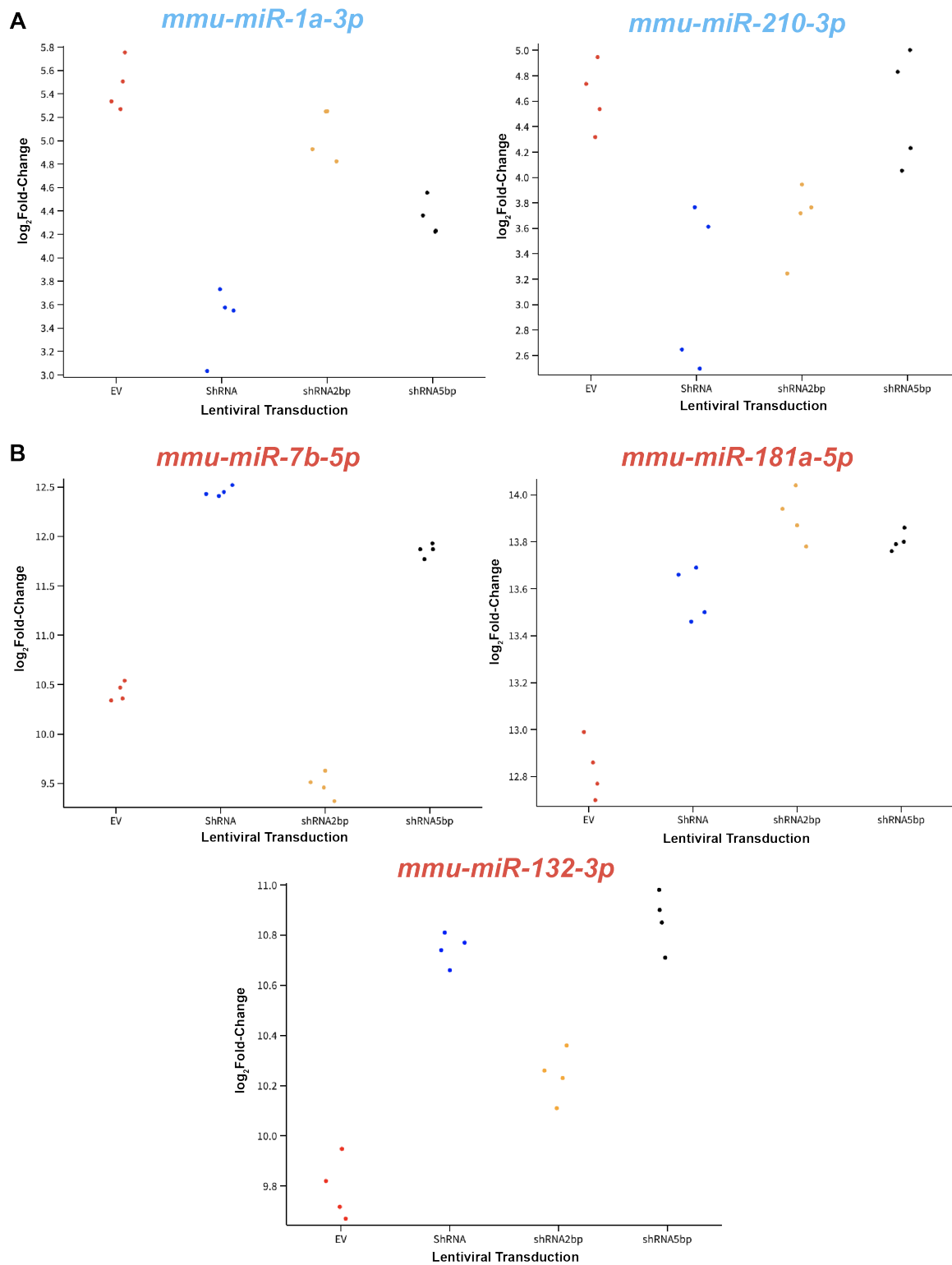


Figure 3-14: Small RNA sequencing reveals NogoA-independent regulation of activity-dependent miRNAs.

Individual data points showing expression profiles of selected downregulated (A) or upregulated (B) miRNAs following four different lentiviral transductions.

3.9 References

1. M. S. Chen *et al.*, Nogo-A is a myelin-associated neurite outgrowth inhibitor and an antigen for monoclonal antibody IN-1. *Nature* **403**, 434-439 (2000).
2. T. Oertle *et al.*, Nogo-A inhibits neurite outgrowth and cell spreading with three discrete regions. *The Journal of neuroscience : the official journal of the Society for Neuroscience* **23**, 5393-5406 (2003).
3. A. B. Huber, O. Weinmann, C. Brosamle, T. Oertle, M. E. Schwab, Patterns of Nogo mRNA and protein expression in the developing and adult rat and after CNS lesions. *The Journal of neuroscience : the official journal of the Society for Neuroscience* **22**, 3553-3567 (2002).
4. A. E. Fournier, T. GrandPre, S. M. Strittmatter, Identification of a receptor mediating Nogo-66 inhibition of axonal regeneration. *Nature* **409**, 341-346 (2001).
5. B. Niederost, T. Oertle, J. Fritsche, R. A. McKinney, C. E. Bandtlow, Nogo-A and myelin-associated glycoprotein mediate neurite growth inhibition by antagonistic regulation of RhoA and Rac1. *The Journal of neuroscience : the official journal of the Society for Neuroscience* **22**, 10368-10376 (2002).
6. H. Lee *et al.*, Synaptic function for the Nogo-66 receptor NgR1: regulation of dendritic spine morphology and activity-dependent synaptic strength. *The Journal of neuroscience : the official journal of the Society for Neuroscience* **28**, 2753-2765 (2008).
7. S. J. Raiker *et al.*, Oligodendrocyte-Myelin Glycoprotein and Nogo Negatively Regulate Activity-Dependent Synaptic Plasticity. *The Journal of Neuroscience* **30**, 12432-12445 (2010).
8. J. K. Atwal *et al.*, PirB is a Functional Receptor for Myelin Inhibitors of Axonal Regeneration. *Science* **322**, 967-970 (2008).
9. A. Kempf *et al.*, The Sphingolipid Receptor S1PR2 Is a Receptor for Nogo-A Repressing Synaptic Plasticity. *PLOS Biology* **12**, e1001763 (2014).
10. A. Delekate, M. Zagrebelsky, S. Kramer, M. E. Schwab, M. Korte, NogoA restricts synaptic plasticity in the adult hippocampus on a fast time scale. *Proceedings of the National Academy of Sciences* **108**, 2569-2574 (2011).
11. F. Hu, S. M. Strittmatter, The N-Terminal Domain of Nogo-A Inhibits Cell Adhesion and Axonal Outgrowth by an Integrin-Specific Mechanism. *The Journal of Neuroscience* **28**, 1262-1269 (2008).

12. A. Zemmar *et al.*, Neutralization of Nogo-A Enhances Synaptic Plasticity in the Rodent Motor Cortex and Improves Motor Learning in Vivo. *The Journal of Neuroscience* **34**, 8685-8698 (2014).
13. M. Zagrebelsky, R. Schweigreiter, C. E. Bandtlow, M. E. Schwab, M. Korte, Nogo-A stabilizes the architecture of hippocampal neurons. *The Journal of neuroscience : the official journal of the Society for Neuroscience* **30**, 13220-13234 (2010).
14. T. GrandPré, F. Nakamura, T. Vartanian, S. M. Strittmatter, Identification of the Nogo inhibitor of axon regeneration as a Reticulon protein. *Nature* **403**, 439-444 (2000).
15. D. A. Dodd *et al.*, Nogo-A, -B, and -C Are Found on the Cell Surface and Interact Together in Many Different Cell Types. *Journal of Biological Chemistry* **280**, 12494-12502 (2005).
16. A. Joset, D. A. Dodd, S. Halegoua, M. E. Schwab, Pincher-generated Nogo-A endosomes mediate growth cone collapse and retrograde signaling. *The Journal of cell biology* **188**, 271-285 (2010).
17. M. Simonen *et al.*, Systemic Deletion of the Myelin-Associated Outgrowth Inhibitor Nogo-A Improves Regenerative and Plastic Responses after Spinal Cord Injury. *Neuron* **38**, 201-211 (2003).
18. B. Zheng *et al.*, Genetic deletion of the Nogo receptor does not reduce neurite inhibition in vitro or promote corticospinal tract regeneration in vivo. *Proceedings of the National Academy of Sciences of the United States of America* **102**, 1205-1210 (2005).
19. J. K. Lee *et al.*, Reassessment of Corticospinal Tract Regeneration in Nogo-Deficient Mice. *The Journal of Neuroscience* **29**, 8649-8654 (2009).
20. A. Kempf *et al.*, Upregulation of axon guidance molecules in the adult central nervous system of Nogo-A knockout mice restricts neuronal growth and regeneration. *European Journal of Neuroscience* **38**, 3567-3579 (2013).
21. B. Tews *et al.*, Synthetic microRNA-mediated downregulation of Nogo-A in transgenic rats reveals its role as regulator of synaptic plasticity and cognitive function. *Proceedings of the National Academy of Sciences* **110**, 6583-6588 (2013).
22. V. Pernet *et al.*, Neuronal Nogo-A upregulation does not contribute to ER stress-associated apoptosis but participates in the regenerative response in the axotomized adult retina. *Cell death and differentiation* **19**, 1096-1108 (2012).

23. A. D. Pradhan *et al.*, Dendritic spine alterations in neocortical pyramidal neurons following postnatal neuronal Nogo-A knockdown. *Developmental neuroscience* **32**, 313-320 (2010).
24. F. Vajda *et al.*, Cell type-specific Nogo-A gene ablation promotes axonal regeneration in the injured adult optic nerve. *Cell death and differentiation* **22**, 323-335 (2015).
25. A. Zemmar *et al.*, Oligodendrocyte- and Neuron-Specific Nogo-A Restrict Dendritic Branching and Spine Density in the Adult Mouse Motor Cortex. *Cereb Cortex*, 1-9 (2017).
26. J. M. Meves, C. G. Geoffroy, N. D. Kim, J. J. Kim, B. Zheng, Oligodendrocytic but not neuronal Nogo restricts corticospinal axon sprouting after CNS injury. *Experimental Neurology* **309**, 32-43 (2018).
27. A. Kempf, M. E. Schwab, Nogo-A Represses Anatomical and Synaptic Plasticity in the Central Nervous System. *Physiology* **28**, 151-163 (2013).
28. X. Peng, J. Kim, Z. Zhou, D. J. Fink, M. Mata, Neuronal Nogo-A regulates glutamate receptor subunit expression in hippocampal neurons. *Journal of Neurochemistry* **119**, 1183-1193 (2011).
29. K. T. Baldwin, A. A. University of Michigan, Ed. (Dissertations and Theses (Ph.D. and Master's), Deep Blue, 2015).
30. G. G. Turrigiano, S. B. Nelson, Homeostatic plasticity in the developing nervous system. *Nat Rev Neurosci* **5**, 97-107 (2004).
31. J. D. Shepherd *et al.*, Arc/Arg3.1 Mediates Homeostatic Synaptic Scaling of AMPA Receptors. *Neuron* **52**, 475-484 (2006).
32. H.-K. Lee, Synaptic plasticity and phosphorylation. *Pharmacology & Therapeutics* **112**, 810-832 (2006).
33. G. Wang, B. Grone, D. Colas, L. Appelbaum, P. Mourrain, Synaptic plasticity in sleep: learning, homeostasis and disease. *Trends in Neurosciences* **34**, 452-463 (2011).
34. M. C. Guzman-Karlsson, J. P. Meadows, C. F. Gavin, J. J. Hablitz, J. D. Sweatt, Transcriptional and epigenetic regulation of Hebbian and non-Hebbian plasticity. *Neuropharmacology* **80**, 3-17 (2014).
35. T. E. Chater, Y. Goda, The role of AMPA receptors in postsynaptic mechanisms of synaptic plasticity. *Frontiers in Cellular Neuroscience* **8**, (2014).

36. Graham H. Diering, Ahleah S. Gustina, Richard L. Huganir, PKA-GluA1 Coupling via AKAP5 Controls AMPA Receptor Phosphorylation and Cell-Surface Targeting during Bidirectional Homeostatic Plasticity. *Neuron* **84**, 790-805 (2014).
37. G. H. Diering, R. L. Huganir, The AMPA Receptor Code of Synaptic Plasticity. *Neuron* **100**, 314-329 (2018).
38. G. G. Turrigiano, K. R. Leslie, N. S. Desai, L. C. Rutherford, S. B. Nelson, Activity-dependent scaling of quantal amplitude in neocortical neurons. *Nature* **391**, 892-896 (1998).
39. J. Barral, A. D Reyes, Synaptic scaling rule preserves excitatory–inhibitory balance and salient neuronal network dynamics. *Nature Neuroscience* **19**, 1690-1696 (2016).
40. P. Tsokas *et al.*, Local protein synthesis mediates a rapid increase in dendritic elongation factor 1A after induction of late long-term potentiation. *The Journal of neuroscience : the official journal of the Society for Neuroscience* **25**, 5833-5843 (2005).
41. M. A. Sutton *et al.*, Miniature Neurotransmission Stabilizes Synaptic Function via Tonic Suppression of Local Dendritic Protein Synthesis. *Cell* **125**, 785-799 (2006).
42. B. E. Pfeiffer, K. M. Huber, Current Advances in Local Protein Synthesis and Synaptic Plasticity. *The Journal of Neuroscience* **26**, 7147-7150 (2006).
43. C. R. Bramham, E. Messaoudi, BDNF function in adult synaptic plasticity: The synaptic consolidation hypothesis. *Progress in Neurobiology* **76**, 99-125 (2005).
44. F. Zheng, Y. Luo, H. Wang, Regulation of brain-derived neurotrophic factor-mediated transcription of the immediate early gene Arc by intracellular calcium and calmodulin. *Journal of Neuroscience Research* **87**, 380-392 (2009).
45. N. Kuzumaki *et al.*, Hippocampal epigenetic modification at the brain-derived neurotrophic factor gene induced by an enriched environment. *Hippocampus* **21**, 127-132 (2011).
46. K. R. Jones, I. Fariñas, C. Backus, L. F. Reichardt, Targeted disruption of the BDNF gene perturbs brain and sensory neuron development but not motor neuron development. *Cell* **76**, 989-999 (1994).
47. P. M. Schwartz, P. R. Borghesani, R. L. Levy, S. L. Pomeroy, R. A. Segal, Abnormal Cerebellar Development and Foliation in BDNF^{-/-} Mice Reveals a Role for Neurotrophins in CNS Patterning. *Neuron* **19**, 269-281 (1997).

48. S. Marty, R. Wehrlé, C. Sotelo, Neuronal Activity and Brain-Derived Neurotrophic Factor Regulate the Density of Inhibitory Synapses in Organotypic Slice Cultures of Postnatal Hippocampus. *The Journal of Neuroscience* **20**, 8087-8095 (2000).
49. L. C. Rutherford, A. DeWan, H. M. Lauer, G. G. Turrigiano, Brain-Derived Neurotrophic Factor Mediates the Activity-Dependent Regulation of Inhibition in Neocortical Cultures. *The Journal of Neuroscience* **17**, 4527-4535 (1997).
50. B. L. Bloodgood, N. Sharma, H. A. Browne, A. Z. Trepman, M. E. Greenberg, The activity-dependent transcription factor NPAS4 regulates domain-specific inhibition. *Nature* **503**, 121-125 (2013).
51. Y. Lin *et al.*, Activity-dependent regulation of inhibitory synapse development by Npas4. *Nature* **455**, 1198 (2008).
52. K. Ramamoorthi *et al.*, Npas4 regulates a transcriptional program in CA3 required for contextual memory formation. *Science* **334**, 1669-1675 (2011).
53. I. Spiegel *et al.*, Npas4 Regulates Excitatory-Inhibitory Balance within Neural Circuits through Cell-Type-Specific Gene Programs. *Cell* **157**, 1216-1229 (2014).
54. F. D. Lubin, T. L. Roth, J. D. Sweatt, Epigenetic Regulation of bdnf Gene Transcription in the Consolidation of Fear Memory. *The Journal of Neuroscience* **28**, 10576-10586 (2008).
55. J. W. Koo *et al.*, Epigenetic basis of opiate suppression of Bdnf gene expression in the ventral tegmental area. *Nature Neuroscience* **18**, 415-422 (2015).
56. B. Nair, M. T. T. Wong-Riley, Transcriptional Regulation of Brain-derived Neurotrophic Factor Coding Exon IX: ROLE OF NUCLEAR RESPIRATORY FACTOR 2. *Journal of Biological Chemistry* **291**, 22583-22593 (2016).
57. X. Tao, S. Finkbeiner, D. B. Arnold, A. J. Shaywitz, M. E. Greenberg, Ca²⁺ Influx Regulates BDNF Transcription by a CREB Family Transcription Factor-Dependent Mechanism. *Neuron* **20**, 709-726 (1998).
58. F. Zheng *et al.*, Regulation of brain-derived neurotrophic factor exon IV transcription through calcium responsive elements in cortical neurons. *PloS one* **6**, e28441-e28441 (2011).
59. J.-M. Jia *et al.*, Brain-derived neurotrophic factor-tropomyosin-related kinase B signaling contributes to activity-dependent changes in synaptic proteins. *The Journal of biological chemistry* **283**, 21242-21250 (2008).
60. S. Morinobu, K. Fujimaki, N. Okuyama, M. Takahashi, R. S. Duman, Stimulation of Adenylyl Cyclase and Induction of Brain - Derived Neurotrophic Factor and TrkB mRNA by NKH477, a Novel and Potent Forskolin Derivative. *Journal of Neurochemistry* **72**, 2198-2205 (1999).

61. A. C. Dolphin, Calcium channel auxiliary $\alpha 2\delta$ and β subunits: trafficking and one step beyond. *Nature Reviews Neuroscience* **13**, 542-555 (2012).
62. M. Campiglio, B. E. Flucher, The role of auxiliary subunits for the functional diversity of voltage-gated calcium channels. *J Cell Physiol* **230**, 2019-2031 (2015).
63. Ç. Eroglu *et al.*, Gabapentin Receptor $\alpha 2\delta$ -1 Is a Neuronal Thrombospondin Receptor Responsible for Excitatory CNS Synaptogenesis. *Cell* **139**, 380-392 (2009).
64. C. Eroglu, The role of astrocyte-secreted extracellular proteins in central nervous system development and function. *Journal of Cell Communication and Signaling* **3**, 167-176 (2009).
65. K. S. Christopherson *et al.*, Thrombospondins Are Astrocyte-Secreted Proteins that Promote CNS Synaptogenesis. *Cell* **120**, 421-433 (2005).
66. C. E. Bandtlow *et al.*, Increased expression of Nogo-A in hippocampal neurons of patients with temporal lobe epilepsy. *European Journal of Neuroscience* **20**, 195-206 (2004).
67. L. S. Hsieh, J. H. Wen, L. Miyares, P. J. Lombroso, A. Bordey, Outbred CD1 mice are as suitable as inbred C57BL/6J mice in performing social tasks. *Neuroscience letters* **637**, 142-147 (2017).
68. K. A. Aldinger, G. Sokoloff, D. M. Rosenberg, A. A. Palmer, K. J. Millen, Genetic variation and population substructure in outbred CD-1 mice: implications for genome-wide association studies. *PloS one* **4**, e4729-e4729 (2009).
69. D. Szklarczyk *et al.*, STRING v11: protein-protein association networks with increased coverage, supporting functional discovery in genome-wide experimental datasets. *Nucleic Acids Res* **47**, D607-d613 (2019).
70. L. He, G. J. Hannon, MicroRNAs: small RNAs with a big role in gene regulation. *Nature Reviews Genetics* **5**, 522-531 (2004).
71. Z. Hu, Z. Li, miRNAs in synapse development and synaptic plasticity. *Current Opinion in Neurobiology* **45**, 24-31 (2017).
72. C. B. Moore, E. H. Guthrie, M. T.-H. Huang, D. J. Taxman, Short hairpin RNA (shRNA): design, delivery, and assessment of gene knockdown. *Methods Mol Biol* **629**, 141-158 (2010).
73. Seung T. Baek *et al.*, Off-Target Effect of doublecortin Family shRNA on Neuronal Migration Associated with Endogenous MicroRNA Dysregulation. *Neuron* **82**, 1255-1262 (2014).

74. L. P. Lim *et al.*, Microarray analysis shows that some microRNAs downregulate large numbers of target mRNAs. *Nature* **433**, 769-773 (2005).
75. E. Bernstein, A. A. Caudy, S. M. Hammond, G. J. Hannon, Role for a bidentate ribonuclease in the initiation step of RNA interference. *Nature* **409**, 363-366 (2001).
76. Y. Lee *et al.*, The nuclear RNase III Drosha initiates microRNA processing. *Nature* **425**, 415-419 (2003).
77. J. Han *et al.*, The Drosha-DGCR8 complex in primary microRNA processing. *Genes & Development* **18**, 3016-3027 (2004).
78. G. Lugli, V. I. Torvik, J. Larson, N. R. Smalheiser, Expression of microRNAs and their precursors in synaptic fractions of adult mouse forebrain. *Journal of Neurochemistry* **106**, 650-661 (2008).
79. M. J. Kye *et al.*, Somatodendritic microRNAs identified by laser capture and multiplex RT-PCR. *RNA (New York, N.Y.)* **13**, 1224-1234 (2007).
80. G. Schratt, microRNAs at the synapse. *Nat Rev Neurosci* **10**, 842-849 (2009).
81. S. Sambandan *et al.*, Activity-dependent spatially localized miRNA maturation in neuronal dendrites. *Science* **355**, 634-637 (2017).
82. M. van Spronsen *et al.*, Developmental and Activity-Dependent miRNA Expression Profiling in Primary Hippocampal Neuron Cultures. *PLOS ONE* **8**, e74907 (2013).
83. U. Bissels *et al.*, Absolute quantification of microRNAs by using a universal reference. *RNA (New York, N.Y.)* **15**, 2375-2384 (2009).
84. B. Schwanhauser *et al.*, Global quantification of mammalian gene expression control. *Nature* **473**, 337-342 (2011).
85. M. A. van Gestel *et al.*, shRNA-induced saturation of the microRNA pathway in the rat brain. *Gene therapy* **21**, 205-211 (2014).
86. G. A. Wayman *et al.*, An activity-regulated microRNA controls dendritic plasticity by down-regulating p250GAP. *Proceedings of the National Academy of Sciences* **105**, 9093-9098 (2008).
87. J. E. Cohen, P. R. Lee, S. Chen, W. Li, R. D. Fields, MicroRNA regulation of homeostatic synaptic plasticity. *Proceedings of the National Academy of Sciences* **108**, 11650-11655 (2011).

88. N. M. Sosanya *et al.*, Degradation of high affinity HuD targets releases Kv1.1 mRNA from miR-129 repression by mTORC1. *Journal of Cell Biology* **202**, 53-69 (2013).
89. J. Remenyi *et al.*, miR-132/212 Knockout Mice Reveal Roles for These miRNAs in Regulating Cortical Synaptic Transmission and Plasticity. *PLOS ONE* **8**, e62509 (2013).
90. H. L. Scott *et al.*, MicroRNA-132 regulates recognition memory and synaptic plasticity in the perirhinal cortex. *European Journal of Neuroscience* **36**, 2941-2948 (2012).
91. K. Fénelon *et al.*, Deficiency of *Dgcr8*, a gene disrupted by the 22q11.2 microdeletion, results in altered short-term plasticity in the prefrontal cortex. *Proceedings of the National Academy of Sciences* **108**, 4447-4452 (2011).
92. L. R. Earls *et al.*, Age-Dependent MicroRNA Control of Synaptic Plasticity in 22q11 Deletion Syndrome and Schizophrenia. *The Journal of Neuroscience* **32**, 14132-14144 (2012).
93. R. Hsu *et al.*, Loss of microRNAs in pyramidal neurons leads to specific changes in inhibitory synaptic transmission in the prefrontal cortex. *Molecular and Cellular Neuroscience* **50**, 283-292 (2012).
94. T. H. Davis *et al.*, Conditional Loss of Dicer Disrupts Cellular and Tissue Morphogenesis in the Cortex and Hippocampus. *The Journal of Neuroscience* **28**, 4322-4330 (2008).
95. A. Fiorenza *et al.*, Blocking miRNA Biogenesis in Adult Forebrain Neurons Enhances Seizure Susceptibility, Fear Memory, and Food Intake by Increasing Neuronal Responsiveness. *Cerebral Cortex* **26**, 1619-1633 (2015).
96. W. Konopka *et al.*, MicroRNA Loss Enhances Learning and Memory in Mice. *The Journal of Neuroscience* **30**, 14835-14842 (2010).
97. T. C. Südhof, Towards an Understanding of Synapse Formation. *Neuron* **100**, 276-293 (2018).
98. C. A. Schneider, W. S. Rasband, K. W. Eliceiri, NIH Image to ImageJ: 25 years of image analysis. *Nature Methods* **9**, 671-675 (2012).
99. C. McQuin *et al.*, CellProfiler 3.0: Next-generation image processing for biology. *PLOS Biology* **16**, e2005970 (2018).
100. F. E. Henry *et al.*, A Unique Homeostatic Signaling Pathway Links Synaptic Inactivity to Postsynaptic mTORC1. *The Journal of Neuroscience* **38**, 2207-2225 (2018).

101. M. T. Paulsen *et al.*, Coordinated regulation of synthesis and stability of RNA during the acute TNF-induced proinflammatory response. *Proceedings of the National Academy of Sciences* **110**, 2240-2245 (2013).
102. M. T. Paulsen *et al.*, Use of Bru-Seq and BruChase-Seq for genome-wide assessment of the synthesis and stability of RNA. *Methods* **67**, 45-54 (2014).
103. P. M. Garay *et al.*, RAI1 Regulates Activity-Dependent Nascent Transcription and Synaptic Scaling. *bioRxiv*, 523456 (2019).
104. B. Langmead, S. L. Salzberg, Fast gapped-read alignment with Bowtie 2. *Nat. Methods* **9**, 357 (2012).
105. D. Kim *et al.*, TopHat2: accurate alignment of transcriptomes in the presence of insertions, deletions and gene fusions. *Genome Biol.* **14**, R36 (2013).
106. Y. Liao, G. K. Smyth, W. Shi, featureCounts: an efficient general purpose program for assigning sequence reads to genomic features. *Bioinformatics* **30**, 923-930 (2014).
107. M. I. Love, W. Huber, S. Anders, Moderated estimation of fold change and dispersion for RNA-seq data with DESeq2. *Genome Biol.* **15**, 550 (2014).
108. M. Martin, Cutadapt removes adapter sequences from high-throughput sequencing reads. *2011* **17**, 3 (2011).
109. A. Dobin *et al.*, STAR: ultrafast universal RNA-seq aligner. *Bioinformatics* **29**, 15-21 (2012).
110. L. Wang, S. Wang, W. Li, RSeQC: quality control of RNA-seq experiments. *Bioinformatics* **28**, 2184-2185 (2012).
111. Y. Liao, G. K. Smyth, W. Shi, The R package Rsubread is easier, faster, cheaper and better for alignment and quantification of RNA sequencing reads. *Nucleic Acids Research* **47**, e47-e47 (2019).
112. D. J. McCarthy, Y. Chen, G. K. Smyth, Differential expression analysis of multifactor RNA-Seq experiments with respect to biological variation. *Nucleic Acids Res* **40**, 4288-4297 (2012).
113. M. D. Robinson, A. Oshlack, A scaling normalization method for differential expression analysis of RNA-seq data. *Genome Biology* **11**, R25 (2010).
114. C. W. Law, Y. Chen, W. Shi, G. K. Smyth, voom: Precision weights unlock linear model analysis tools for RNA-seq read counts. *Genome Biol* **15**, R29 (2014).

115. B. Langmead, C. Trapnell, M. Pop, S. L. Salzberg, Ultrafast and memory-efficient alignment of short DNA sequences to the human genome. *Genome Biology* **10**, R25 (2009).
116. M. R. Friedländer, S. D. Mackowiak, N. Li, W. Chen, N. Rajewsky, miRDeep2 accurately identifies known and hundreds of novel microRNA genes in seven animal clades. *Nucleic Acids Research* **40**, 37-52 (2011).
117. S. Griffiths-Jones, H. K. Saini, S. van Dongen, A. J. Enright, miRBase: tools for microRNA genomics. *Nucleic Acids Research* **36**, D154-D158 (2007).
118. D. Betel, M. Wilson, A. Gabow, D. S. Marks, C. Sander, The microRNA.org resource: targets and expression. *Nucleic Acids Res* **36**, D149-153 (2008).
119. Y. Ru *et al.*, The multiMiR R package and database: integration of microRNA-target interactions along with their disease and drug associations. *Nucleic Acids Res* **42**, e133 (2014).
120. W. A. da Silveira *et al.*, miRmapper: A Tool for Interpretation of miRNA(-)mRNA Interaction Networks. *Genes* **9**, (2018).

CHAPTER 4:

Discussion and Future Directions

4.1 Abstract

The body of work communicated in this dissertation provides novel insights to the neuronal NogoA physiology. Through characterization of a published shRNA against NogoA (shNogoA), we study mechanisms underlying synaptogenesis and synaptic plasticity. Taken together, my work contributes the following to the general knowledge:

1. Neuronal NogoA expression is regulated by membrane depolarization in synaptically immature neurons.
2. Forebrain neurons bidirectionally modulate surface, but not total, NogoA under the regulation of homeostatic synaptic plasticity.
3. Intracellular NogoA pools are phosphorylated at the ser-343 residue, an event that contributes to context-dependent molecular weight changes of neuronal NogoA.
4. Global transduction of forebrain neurons with the shNogoA alters synaptic protein and gene expression as well as disrupts inhibitory synaptogenesis independently of NogoA expression.
5. Differential mRNA regulation seen with the shNogoA transduction is accompanied by changes in miRNA expression implicated in activity-dependent synaptic plasticity.

Here we discuss the significance of our findings and propose future experiments that will elucidate the role of NogoA depletion and/or proper miRNA machinery in observed phenotypes.

4.2 Key Findings and Future Directions for the Regulation of NogoA

4.2.1 Neuronal NogoA Expression is Regulated by Membrane Depolarization

Studies with neutralization of surface NogoA signaling with function-blocking antibodies (1-3) or bath application of the soluble Nogo-66 recombinant protein (4) demonstrated that NogoA exerts a strong inhibition on activity-dependent synaptic plasticity. When this negative regulatory brake is released, forebrain slices entrained stronger induction of long-term potentiation (2, 3), dendritic complexity increased, and dendritic spine morphology became more dynamic and immature (1). As a result, neutralization of NogoA signaling and function led to increased dendritic spine density and enhanced motor learning *in vivo* (3). However, until recently, there was no account of activity-dependent regulation of endogenous neuronal NogoA expression.

Both Fricke *et al.* (5) and our work presented in this dissertation consistently show for the first time that continuous neuronal membrane depolarization causes robust downregulation of NogoA protein levels. The reported study treated acute mouse hippocampal slices with 55mM KCl for 10 minutes, isolated synaptosomal fractions, and demonstrated that NogoA protein levels were drastically reduced (5). In our studies, we treated synaptically immature (DIV7) neurons from the rat or mouse hippocampus with 55mM KCl for 2 hours, and showed robust reduction in total NogoA protein expression (Figures 2-3, 3-7). In fact, NogoA downregulation was seen as soon as 30 minutes of KCl treatment, even before the induction of the immediate-early, activity-dependent transcription factor Npas4 (6) (Figure 2-5). Moreover, we established a strong link

between NogoA downregulation and depolarization-induced influx of extracellular calcium, since 10 minute pre-treatment with the chelating agent EGTA completely reversed these effects (Figures 2-3, 3-7). Curiously, when synaptically mature (DIV14) neurons were similarly treated, no such NogoA regulation was observed (Figures 2-3, 3-7). We therefore hypothesize that once neurons reach synaptic maturity, total NogoA levels get much more tightly regulated. This differs from, but does not contradict, Fricke *et al.*'s findings, since they assessed synaptosomal NogoA expression following depolarization of neuronal networks while still in physical and metabolic interaction with over-populated and physiologically-relevant glial cells (5). In our studies we examined total, but not synaptosomal, NogoA expression in primary hippocampal cultures. While, neurons are still the principal constituents, the existing outnumbered astrocytes assume a different morphological state when compared to that seen with primary astroglial cultures (Figure 2-1). Taken together, we are amongst the first to demonstrate that neuronal NogoA protein levels are rapidly reduced following chemically induced, continuous membrane depolarization.

4.2.2 Surface NogoA is Bidirectionally Regulated by Homeostatic Synaptic Plasticity

Because synaptically mature (DIV14) neurons failed to respond to global membrane depolarization of neuronal networks, we decided to specifically manipulate synaptic activity of primary hippocampal cultures. We induced homeostatic synaptic upscaling with chronic (≥ 24 hr) treatments with tetrodotoxin (TTX), which competitively inactivates voltage-gated sodium channels, and halts action potential propagation.

When neuronal networks are silenced for long periods of times, complex intracellular signaling mechanisms increase individual neuron's synaptic drive by producing, trafficking, and anchoring AMPA receptor subunit GluA1 onto the cell surface and synaptic sites (7, 8). We first verified that total NogoA expression does not change (Figure 2-3), similar to lack of regulation following membrane depolarization of mature neurons (Figures 2-3, 3-7). More importantly, through quantitative biochemical and qualitative immunofluorescence labeling studies, we found that surface NogoA expression was significantly and robustly reduced, while surface GluA1 expression increased (Figure 2-3). This was an interesting and novel finding, since endogenous neuronal NogoA expression itself had never been shown to be regulated within the context of synaptic plasticity. We then induced homeostatic downscaling with chronic (≥ 24 hr) treatment with bicuculline, which competitively antagonizes GABA_A receptors, and reduces inhibitory tone. When neuronal networks are over-activated for long periods of time, signaling mechanisms decrease neuronal synaptic drive by removing the post-translational modifications (PTMs) responsible for better anchoring of GluA1 onto the post-synaptic densities, which causes endocytosis and/or lateral diffusion (7-9). We found that even though total NogoA protein levels did not change, surface NogoA expression robustly increased in this homeostatic downscaled state (Figure 2-3).

Taken together, these data demonstrated for the first time that unlike total expression, NogoA protein levels at the neuronal surface are under the regulation of activity-dependent synaptic plasticity. It is conceivable that the site of regulation of NogoA expression is indeed neuronal cell surface, since NogoA was shown to prominently with membrane-bound Nogo-66 Receptor 1 (NgR1) (10, 11) and

transmembrane paired immunoglobulin-like receptor B (PirB) (4, 12). Our observations were also in line with previous studies, which depend on treatments with the anti-NogoA function-blocking antibodies that specifically target the extracellular NogoA- Δ 20 region to alleviate the inhibitory signaling and function of NogoA (1-3). Lastly, Joset *et al.* showed that neuronal NogoA- Δ 20 is internalized in a pincher- and rac-dependent, but clathrin- and dynamin-independent manner (13), which could be one way of dynamically modulating NogoA signal and function.

4.2.3 Neuronal NogoA is Intracellularly Phosphorylated in a Context-Dependent Manner

Synaptic proteins, such as the AMPA receptor subunit GluA1, undergo various PTMs as they are directed to and from synaptic sites in an activity-dependent manner (8, 14-25). In 2014, Diering *et al.* reported that bidirectional homeostatic synaptic scaling depends on PKA-encoded phosphorylation mark at GluA1 serine-845 residue. When neuronal networks are upscaling following prolonged silencing, for example, GluA1 gets increasingly phosphorylated at this site, and consequently remains anchored at the post-synaptic density (PSD) (8). As circadian rhythmicity is entrained by combined influences including sensory stimulus processing, learning, memory formation, and sleep, the same group isolated forebrain PSDs from the mouse brain at wake and sleep states, and analyzed both total and phosphorylated protein expression. In addition to increased GluA1 and CaMKII α phosphorylation within the wake forebrain PSDs, Diering *et al.* also detected ≥ 4 -fold increase in NogoA phosphorylation at serine-344 residue (24). Since this phosphorylation site was identified in our previous phospho-proteomics

studies with NogoA isolated from primary rat hippocampal cultures (Tables 2-1, 2-2), we became interested in the possibility of this phosphorylation site regulating NogoA expression, surface trafficking, and physiological function.

We generated a polyclonal antibody specifically against the rat NogoA phosphoserine-343 residue, rigorously verified its specificity, and tested this phosphorylation site's expression pattern (Figure 2-4) and physiological role (Figure 2-5). Interestingly, our data strongly suggests that NogoA p-S343 is restricted to neuronal expression, absent from primary astroglial cultures as well as the crude myelin fractions isolated from rat brains. Moreover, we found that neuronal NogoA is phosphorylated at this site only within the intracellular pools, but not on the cell surface. In fact, we detected a strong NogoA p-s343 signal from rat forebrain synaptosomes (Figures 2-4). Next we asked whether NogoA ser-343 phosphorylation changes in rat forebrain synaptosomes and PSDs between sleep and wake states *in vivo*. Despite strong signal detection, we did not find any change in total or phosphorylated expression of GluA1 or NogoA (Figure 2-5). These negative data suggest that animals maintained at our shared housing facilities on a 6AM/6PM, lights on/off schedule failed to entrain a tightly regulated circadian rhythm sufficient to change protein expression and phosphorylation in adult male Sprague-Dawley rats (24, 26). Alternatively, the sleep/wake state of the animals at the time of euthanasia might play a greater role in regulating NogoA phosphorylation, as it relates to neuronal activity better than circadian rhythmicity.

We then wanted to study NogoA phosphorylation *in vitro* using primary hippocampal cultures due to the availability of versatile pharmacological manipulations. We found that in synaptically immature (DIV7) neurons KCl-induced membrane

depolarization reduces expression and molecular weight of phosphorylated NogoA as soon as 30 minutes of KCl treatment. Interestingly, the immediate-early activity-dependent transcription factor Npas4 was only strongly expressed following 2 hours of continuous KCl-mediated membrane depolarization. This suggests that reduction in total and phosphorylated NogoA expression precedes Npas4 induction. However, just like Npas4 induction or total NogoA expression, NogoA phosphorylation is mostly recovered following EGTA pre-treatment (Figure 2-4), indicating an intracellular calcium-dependent mechanism. Moreover, we found that upon synaptic maturation (DIV14), neuronal networks stabilize both total and phosphorylated NogoA expression, regardless of synaptic activity states. We show that increased durations of TTX treatment create a visible NogoA band separation, and phosphorylated NogoA additively decreases in mobility (Figure 2-5). While phosphorylation event specifically at serine-343 is detected in TTX-mediated increase in NogoA molecular weight, the lack of change in expression signal intensity implicates presence of other phosphorylation events. In fact, lambda phosphatase treatment of neuronal lysates strongly increases NogoA mobility even farther than baseline, suggestive of combinatorial phosphate deposition (Figure 2-4). Interestingly, we further showed that this increase in molecular weight via collective phosphorylation marks could be overcome by selective inhibition of Trk receptors. Conversely, BIC treatment causes a small reduction in phosphorylated NogoA molecular weight (Figure 2-5). The duality of lack of difference in abundance and molecular weight shifts still remain elusive, but can be explained by the possibility that serine-343 phosphorylation mark initiating other sets of PTMs on NogoA.

To elucidate the kinase/phosphatase pairs behind the regulation of NogoA phosphorylation we conducted a series of pharmacological treatments of primary hippocampal cultures. We first explored molecular players implicated in intracellular signaling downstream of NogoA-NgR1-PiRB interaction (10, 12, 27). Upon inhibition of neuronal growth-inhibitory molecules, such as ROCK and myosin II ATPase, we failed to see a robust regulation of NogoA expression or phosphorylation. Next, we studied growth-promoting molecules, such as PKA, CaMKII, L-type voltage-gated calcium channels (VGCCs), or the mTOR pathway. Although band separation was still visible with inhibition of CaMKII, L-type VGCC, and calcineurin, expression remained unchanged. Similarly, robust inhibition of phosphorylated S6K did not elicit a noticeable change (Figure 2-5). Taken together, the physiological role or the upstream regulators of NogoA phosphorylation remains elusive.

4.2.4 Future Directions

Our work is amongst the first to demonstrate that NogoA protein expression is regulated under the control of activity-dependent synaptic plasticity. We are also the first to identify NogoA as a phospho-protein, expression of which can be modulated based on neuronal developmental stage and network activity states. However, our findings open doors to many outstanding questions, which should be investigated further.

We demonstrate that upon synaptic maturity, only surface expression of NogoA changes with different network activity states (Figure 2-3). We reasoned NogoA PTMs or more specifically phosphorylation events, could elucidate the mechanism(s) by which

NogoA is trafficked to the cell surface, to and from the synaptic sites, or internalized to modulate its inhibitory signaling. Although phospho-proteomics of NogoA isolated from primary rat hippocampal cultures treated with vehicle or TTX revealed no overall change (Table 2-2), we identified rat NogoA phospho-site at serine-343, which was not expressed at the neuronal cell surface, but was detected in synaptosomes and PSDs (Figure 2-4). Future studies should therefore investigate whether the phosphorylation of NogoA directly causes its internalization, or removal of baseline phosphorylation is the initial signal for NogoA trafficking. Furthermore, complementary protein-protein interactome studies should elucidate the specific kinase/phosphatase pairs responsible for deposition and removal of phosphorylation marks on NogoA to regulate its subcellular localization and function.

We generated a polyclonal phospho-specific antibody against rat NogoA. We later found out that despite inter-species homology, our antibody does not cross-react with mouse NogoA or work with immunofluorescence staining. This necessitates generation of additional antibodies in order to study phosphorylated NogoA's physiological relevance in various genetic knockout models, regulation under circadian rhythmicity, and subcellular localization. Finally, because investigation of the intricate balance between sleep and circadian rhythm presents conceptual and technical challenges, we propose that future studies entrain contextual fear conditioning or induce kainic-acid mediated seizures to robustly elevate hippocampal activity, immediate-early gene expression, and study total and phosphorylated NogoA levels in different subcellular fractions (6, 28-31). This approach would dissociate sleep-mediated regulation from intrinsic circadian rhythmicity, and focus solely on heightened neuronal

activity. Additionally, investigation of NogoA expression in membrane, synaptosome or PSD fractions isolated from these animal models will elucidate the differential trafficking and physiological function of NogoA in an activity-dependent manner.

4.3 Key Findings and Future Directions for the shNogoA-Mediated Regulation of Synapse Formation and Strength

4.3.1 shNogoA Permanently Downscales Baseline Excitatory Synaptic Transmission

When we employed Zagrebelsky *et al.*'s shNogoA (1) with primary hippocampal neurons, we were expecting to recapitulate and build up on Peng *et al.*'s results to add mechanistic insight into how NogoA knockdown drives the mTOR signaling pathway and causes upregulation of AMPA and NMDA receptor subunits (32). Instead, we observed a robust downregulation of GluA1 and GluA2 protein and gene expression. When we verified that neither the developmental stage at the time of LV transduction nor the commercially available shNogoA we used made any difference in these observations: GluA1 expression was reproducibly and reliably downregulated whenever NogoA expression was sufficiently knocked down. Next we discovered that not only total GluA1 production, but also its surface trafficking was drastically downregulated, even in TTX-treated, normally homeostatic upscaling hippocampal cultures. Lastly, we demonstrated that pyramidal-like neurons sparsely transduced with shNogoA showed a permanently and cell-autonomously entrained downscaling of miniature excitatory post-synaptic current (mEPSC) amplitude, regardless of the pharmacologically induced synaptic activity states (Figure 3-1). The reductions in mEPSC amplitude and GluA1/2 expression collectively point to a post-synaptic regulation of synaptic drive, since we found that neither mEPSC frequency (Figure 3-1) nor the presynaptic terminals marked with synapsinIIa changed following global LV-shNogoA transduction (Figure 3-9).

Moreover, we saw a robust downregulation of both phosphorylated and total S6K protein expression following global transduction of primary hippocampal cultures with the shNogoA (Figure 3-1). Since S6K and its activation within the mTOR signaling pathway play an important role for local protein synthesis important for the maintenance of activity-dependent synaptic plasticity (33-36), this provided a preliminary mechanistic insight into how post-synaptic densities failed to keep up with the physiological needs of differential network activity states. Since Peng *et al.* implicated activation of the mTOR signaling pathway in shNogoA-mediated upregulation of GluA1 and GluA2 expression (32), we initially reasoned there might be a link between the concurrent reduction in GluA1 and S6K. However, we then found out that the mRNA transcripts for *Gria1* (GluA1), *Gria2* (GluA2) and *Rps6kb1* (S6K) were drastically downregulated following shNogoA transduction (Figure 3-1). Then we reasoned there must be a higher up, transcriptional regulation that drove these observed phenotypes.

To address this open question, we transduced primary forebrain cultures with LV-shNogoA, isolated nascent and fully processed mRNA, and analyzed transcriptome via next-generation sequencing. At an intermediate time-window following incomplete NogoA depletion, we did not observe any statistically significant change in *Gria1*, *Gria2*, or *Rps6kb1* expression. However, we found striking and robust upregulation of immediate-early genes (IEGs) such as *Npas4*, *Arc*, and *Fos*, and some of the binding targets such as *Bdnf*, *Nr4a1/2*, and *Junb* (6, 29) (Figure 3-2). Curiously, gene expression of these candidates is induced by synaptic activity-dependent intracellular calcium influx, mostly through activated AMPA and NMDA receptors as well as heavily studied L-type VGCCs (6, 28). This was surprising since we demonstrated a reduced

baseline excitatory transmission by both biochemical and electrophysiological analyses (Figure 3-1). Since our observed reduction in mEPSC amplitude correlates with less abundant glutamatergic receptors (7, 8), which would normally be expected to cause a reduction in calcium influx and signaling, we directed our attention to the selective activation of L-type VGCCs. In fact, pharmacological inhibition of these channels was shown to prevent any induction in the activity-dependent transcription factor Npas4 (6). We found that DIV3 shNogoA transduction increased Npas4 protein expression both by DIV7 and DIV14 in an extracellular calcium-dependent manner (Figure 3-3). Unlike our findings with cell-autonomous GluA1 downregulation and consequent decrease in mEPSC amplitude (Figure 3-1), Npas4 upregulation was seen only following global transduction with LV-shNogoA, suggesting dependence on differential network activity states. Interestingly, shNogoA-induced baseline Npas4 upregulation could be significantly reduced following prior inhibition of the L-type VGCCs (Figure 3-3). Taken together, our data strongly suggest that global shNogoA transduction of hippocampal neurons leads to a selective activation of L-type VGCCs, and despite reduced levels of GluA1/2 expression, this causes elevated intracellular calcium concentrations and a consequent induction of activity-dependent IEGs.

Lastly, we entertained the possibility of NogoA directly binding to L-type VGCC subunits or auxiliary subunits to modulate its function. Despite possible antibody cross-reactivity issues, NogoA seems to co-immunoprecipitate not with the L-type VGCC subunit $\text{Ca}_v1.2$, but instead with the auxiliary subunit $\text{Ca}_v\alpha2\delta1$ in the rat brain membrane fractions. This binding event, coupled with these known functions of $\text{Ca}_v\alpha2\delta1$ render it a prime candidate of investigation: 1. $\text{Ca}_v\alpha2\delta1$ is the known receptor

for the anti-epileptic and analgesic pharmacological reagent gabapentin, which antagonizes $\text{Ca}_v\alpha 2\delta 1$ and excitatory synaptic transmission and formation (37, 38). 2. $\text{Ca}_v\alpha 2\delta 1$ was also reported to be the target neuronal receptor of thrombospondins, which are factors secreted by astrocytes to facilitate excitatory synaptogenesis (39, 40). Because of the cross-reactivity between rat NogoA and $\text{Ca}_v\alpha 2\delta 1$, we switched to using primary hippocampal neurons isolated from the *NogoABC^{fl/fl}* mouse (41), where there was no longer a cross-detection issue. Interestingly, Cre recombination-mediated deletion of *NogoABC* did not change protein expression of $\text{Ca}_v\alpha 2\delta 1$. Contrary to our expectation, shNogoA transduction significantly lowered $\text{Ca}_v\alpha 2\delta 1$ protein levels (Figure 3-4). Curiously, mRNA sequencing experiments identified *Cacna2d2*, but not *Cacna2d1*, gene as significantly downregulated following shNogoA transduction (Figure 3-9). While this begs the question of gene homology and functional redundancy or compensation between auxiliary subunits, these data lead to two possible and currently untested hypotheses: 1. LV-shNogoA transduction reduces total $\text{Ca}_v\alpha 2\delta 1$ protein expression. This could alleviate the inhibitory regulation of endogenous antagonists, which would then lead to the activation of L-type VGCCs. 2. LV-shNogoA transduction leads to an immediate and prolonged activation of L-type VGCCs, which would cause an over-excitation due to elevated intracellular calcium concentrations. As such, neuronal networks would maintain homeostasis by downregulating expression of positive modulators such as $\text{Ca}_v\alpha 2\delta 1$. Either way, the interaction between NogoA and $\text{Ca}_v\alpha 2\delta 1$ poses an interesting mechanism, through which LV-shNogoA transduction modulates VGCC activity, calcium influx, and excitatory synaptic transmission.

4.3.2 *shNogoA Transduction Causes a Robust Reduction in Inhibitory Synaptogenesis*

Npas4 upregulation has been shown to induce BDNF production, drive and modulate inhibitory synaptogenesis (6, 28-31). Since global LV-shNogoA transduction causes upregulation in baseline Npas4 gene and protein expression (Figures 3-2, 3-3), we reasoned that the reduction in excitatory synaptic transmission (Figure 3-1) might also be explained by an increase in inhibitory synapse formation and strength. Contrary to our expectations, we found that pre- but not post-synaptic GABAergic markers were robustly downregulated following global shNogoA transduction (Figures 3-6, 3-9). Moreover, our mRNA sequencing data also demonstrated that genes encoding these proteins, *Gad1* and *Gad2*, were also downregulated following shNogoA transduction (Figure 3-10-11). Lastly, we also showed that global shNogoA transduction leads to a drastic decrease in miniature inhibitory postsynaptic current (mIPSC) frequency, while both amplitude and decay time remain unchanged (Figure 3-6). This selective decrease corroborated our biochemical and immunofluorescence analyses of GAD-65/67 expression, and implicated reduced abundance of GABAergic presynaptic terminals following global shNogoA transduction. Taken together, we demonstrate that shNogoA-transduced cultures robustly downregulate inhibitory tone and GABAergic synapse density, despite elevated activation of Npas4-driven signaling mechanisms (6). Although we do not currently know which event occurred first, it is conceivable that the reduction in excitatory synaptic transmission was compensated by homeostatic mechanisms that downscale inhibitory synaptogenesis. By so doing, neuronal networks could still maintain excitatory-inhibitory balance, and return to target firing rate (7, 42, 43).

4.3.3 *shNogoA* Transduction Manifests Synaptic Phenotypes Independently of *NogoA*

In our studies we used Zagrebelsky *et al.*'s *shNogoA*, which was tested in acute hippocampal slices against control shRNA to demonstrate *NogoA*'s inhibitory regulation on the dynamic regulation of complex dendritic architecture (1). Even early on, we tested *NogoA*-dependence of robust GluA1 and S6K downregulation by transducing primary hippocampal neurons with the LV-*shNogoA* at different *in vitro* developmental stages as well as with various commercially available shRNAs targeting different sequences of the *NogoA*-specific exon 3 (Figure 3-1). Next, we attempted to drive overexpression of *NogoA* in un-transduced hippocampal neurons or rescue the depleted *NogoA* pool following *shNogoA* transduction. Transduction of non-neuronal (HEK-293T) cells with the *shNogoA*-resistant, LV-human-*NogoA*-myc construct worked successfully and drove overexpression of myc-tagged *NogoA*. However, once primary hippocampal cultures were transduced with the same lentiviral construct, we detected exogenous myc expression, without an overall change in *NogoA* protein levels (data not shown). Although these RNA interference (RNAi) rescue experiments are commonly used in the field, they pose additional problems stemming from ectopic expression levels typically under the control of strong promoters (44). Since rescue experiments with an *shNogoA*-resistant construct were not feasible, we employed an even more unbiased and stringent approach, and analyzed nascent and mature mRNA isolated from *shNogoA*-transduced neurons by next-generation sequencing (Figure 3-2). As expected, *NogoA* was the most robustly downregulated gene product, easily distinguishable from the rest by fold change, read counts, and statistical significance

(Figures 3-2, 3-10-11). These findings initially increased our confidence in the target-specificity of the previously published shNogoA construct (1), and incentivized us to further study the molecular mechanisms underlying observed phenotypes.

Given how NogoA neutralization, knockdown, and genomic knockout manifested different observations (see Chapter 1), we wondered whether or not conditional knockout of *NogoABC* could reproduce the same phenotypes as shNogoA-mediated knockdown of NogoA. If successful, we reasoned that this experimental paradigm could also provide a highly informative conditional knockout animal model to study the acute and spatiotemporally controlled depletion of NogoABC *in vivo*. We found that LV-CMV-Cre transduction of *NogoABC^{f/f}* hippocampal neurons depleted majority of NogoA and NogoB (41), but did not cause any of our previously observed synaptic phenotypes. On the other hand, when these neurons were co-transduced with the LV-shNogoA, we could recapitulate all of the robust phenotypes (Figure 3-7). There are three arguments that could be raised based on our reported results: 1. One could argue that although *Rattus norvegicus* and *Mus musculus* share evolutionary conserved transcriptomic homology, mRNA sequences might be just different enough to entrain distinguishable shRNA targeting, or protein-protein interactions might diverge between two species. To address this concern, we verified that rat and mouse *NogoA* sequences shared satisfactory homology *in silico*, and that LV-shNogoA transduction alone could successfully reproduce all observed synaptic phenotypes in mouse hippocampal neurons (Figure 3-7). 2. Because LV-CMV-Cre transduction does not lead to complete depletion of NogoA, one could argue that the remaining levels of NogoA protein could still act as an inhibitory brake on intracellular signaling. This incomplete depletion could

then explain why we could recapture observed phenotypes following shNogoA co-transduction (Figure 3-7). We addressed this concern by mutating the seed region of the shNogoA with two (shNogoA-2pMt) or five (shNogoA-5pMt) basepairs (Figure 3-8), recovered NogoA protein expression in a stepwise fashion, and assessed NogoA and synaptic protein expression profiles (Figure 3-9). 3. LV-CMV-Cre transduction equally depleted both *NogoA* and *NogoB* gene and protein products, whereas LV-shNogoA transduction specifically targets the NogoA isoform. Therefore, it is conceivable that combinatorial knockout of both inhibitory *Nogo* isoforms could potentially cause compensatory regulations in genomic and/or protein expression levels. This possibility has not yet been tested by our studies, hence offers a platform for further investigations.

When we transduced rat or mouse hippocampal neurons with shNogoA-2pMt, we saw that NogoA protein expression was very similar to that after conditional knockout of *NogoABC* (compare Figures 3-7 to 3-9). Whereas *NogoABC* conditional knockout did not cause any observable changes in synaptic protein expression (Figure 3-7), shNogoA-2pMt transduction retained a small fraction of NogoA protein expression while recapitulating robust reductions in GluA1, S6K, and GAD-65 levels (Figure 3-9). This strongly suggested that the comparable extents of remaining NogoA protein expression following conditional knockout cannot be deemed sufficient to justify persistent inhibitory actions that were later on alleviated by shNogoA co-transduction. We then assessed NogoA expression and synaptic phenotypes following shNogoA-5pMt transduction. As expected, this alternative form of scrambled shRNA did not change NogoA protein expression. However, the reductions in GluA1, S6K, and GAD-65 protein expression were still present at indistinguishable levels when compared to shNogoA-transduced

cultures (Figure 3-9). Taken together, these data corroborated the NogoA-independent nature of observed regulations of synaptic gene and protein expressions.

4.3.4 shNogoA Transduction Concurrently Regulates mRNA and miRNA Expression Important for Synapse Formation and Strength

Our biochemical and immunofluorescence analyses demonstrated that step-wise mutations within the seed region of the shNogoA recapitulated regulation of the same synaptic proteins independent of NogoA expression, and even created *de novo* phenotypes. To understand the mechanism behind such consistent dysregulation regardless of abundance of the primary target, we employed next-generation sequencing analysis of mRNA expression of cultures transduced with LV-shNogoA, LV-shNogoA-2pMt, and LV-shNogoA-5pMt constructs. Principal component analysis (PCA) revealed that neurons transduced with the LV-pLL3.7 control construct had the highest extent of transcriptomic similarity with those transduced with the LV-shNogoA (Figure 3-10). This was most surprising, since *NogoA* expression was robustly depleted in shNogoA-transduced cultures. Moreover cultures transduced with LV-shNogoA-5pMt had indistinguishable levels of *NogoA* with those transduced with LV-pLL3.7. This led to the hypothesis that robust depletion of *NogoA* expression does not significantly affect global transcriptome of primary forebrain cultures. When we examined some of the differentially expressed genes (DEGs), we found that expression of our candidate synaptically relevant genes was generally comparable amongst primary forebrain cultures transduced with LV-shNogoA, LV-shNogoA-2pMt, and LV-shNogoA-5pMt

(Figure 3-10). These unbiased findings further increased our confidence in concluding the NogoA-independent regulation of the shNogoA construct.

Next, we wanted to understand how transductions with the original and step-wise mutated shNogoA constructs could elicit such robust and similar regulation of synaptically important gene expressions. Since micro RNAs (miRNAs) are known to be master regulators of dynamic and local mRNA stability and translation, especially important in dendritic spine synapses where they regulate synaptic structure and function (45-51), we concurrently analyzed small RNA expression profiles using next-generation sequencing. We identified several miRNAs (Figure 3-13), which were differentially expressed following shNogoA transduction and a subset that remained unchanged following step-wise mutations (Figure 3-14). Curiously, some of the mRNA expression patterns (Figure 3-11) following transduction with the three versions of the LV-shNogoA constructs matched corresponding miRNA expression patterns (Figure 3-14), indicative of a miRNA-mediated mRNA regulation. More interestingly, some of the miRNAs we identified to be differentially regulated following LV-shNogoA transduction were known regulators of activity-dependent and homeostatic synaptic plasticity as well as synaptogenesis (Figure 3-14) (52-57). Taken together, transduction of forebrain neurons with the LV-shNogoA and its step-wise mutated forms appears to relay its NogoA-independent off-target effects by dysregulating miRNA expression profiles, possibly due to altered miRNA synthesis, processing or export machinery (58, 59).

This hypothesis is certainly not derived from a stand-alone, isolated observation specific to our shNogoA. shRNA-mediated exogenous overexpression has been previously observed to cause adverse effects due to the induction of an interferon

response, cell toxicity and organismal fatality, and significant off-target effects and saturation of the miRNA machinery (60-66). In fact, van Gestel *et al.* reported that when rat ventromedial hypothalamus was transduced with adeno-associated 2 (AAV2) viral vectors containing five different shRNAs targeting the *fat mass and obesity-associated protein (FTO)*, infected regions manifested a reduction in NeuN-expressing neuron numbers as well as noticeable degenerative changes in tissue morphology. Moreover, transduced GFP-expressing neurons were found to express decreased levels of the neuronal miRNA miR-124, indicating saturation of the miRNA pathway (58). Similarly to our observations with scrambled LV-shNogoA-5pMt transduction, van Gestel *et al.* also found a similar loss in miR-124 levels in neurons transduced with AAV2-control-shRNA, indicating a higher up regulation of the miRNA processing machinery independent of target gene expression (58).

Since shRNAs are structurally and functionally similar to precursors to mature miRNA called pre-miRNAs, overexpression of shRNAs might be competing for the machinery that would otherwise be processing intermediates of the endogenously expressed miRNAs. As such, Yi *et al.* used easily transduced cell lines to demonstrate that the saturation of the miRNA machinery caused by shRNA overexpression could be reversed by concurrent overexpression of exportin-5 (67), which is responsible for nuclear export of both shRNAs and pre-miRNAs (68). Moreover, they found that the efficiency of the shRNA-mediated knockdown of the targeted gene significantly increased with the simultaneous overexpression of exportin-5. This suggested that shRNA overexpression can significantly hijack existing miRNA processing machinery at the expense of compromising targeted knockdown (67). Taken together, these previous

reports could help reveal a miRNA-dependent component of our observed phenotypes and gene expression regulations.

In conclusion, we hypothesize that neuronal transduction with the LV-shNogoA and its mutated versions might impair the miRNA processing machinery, and cause off-target effects independent of the seed sequence or primary target. However, if this were the sole mechanism by which we observed changes in synaptic formation and strength, PCA would reveal closer transcriptomic association amongst shNogoA lentiviral constructs (Figure 3-10). The fact that LV-shNogoA-5pMt could introduce *de novo* synaptic phenotypes, such as the robust downregulation of synapsinIIa (Figure 3-9), suggests that there must be other physiological targets of the shNogoA currently unidentified by our work. Given how Alvarez *et al.* demonstrated that transducing rat hippocampal neurons with an shRNA targeting a coding region absent from the rat genome can still show reductions in dendritic branching complexity and spine density, we recognize how shRNAs can have sequence-dependent and widespread off-target effects particularly in complex cell types such as neurons (69). Hence, taking into account that intricate processes such as regulation of synapse formation and strength are especially vulnerable to shRNA-mediated off-target effects, we acknowledge the need for further investigations to describe how additive point mutations within the seed sequence of the shNogoA stem loop could modulate gene expression in a different way from commonly generated and employed scrambled shRNAs (44, 70, 71)

4.3.5 Future Directions

The work we reported here address a lot of unanswered questions, but more importantly opens up the doors to exciting future directions. Based on some of the conceptual gaps in our studies, we identify five main sets of experiments that need to be followed up on by further investigation.

Firstly, the binding interaction between NogoA and $\text{Ca}_v\alpha 2\delta 1$ needs to be verified. In our studies, we determined that the rat NogoA and $\text{Ca}_v\alpha 2\delta 1$ showed antibody cross-reactivity issues by both biochemical co-immunoprecipitation and immunofluorescence co-localization. However, mouse NogoA and $\text{Ca}_v\alpha 2\delta 1$ do not seem to show the same cross-reactivity problem (Figure 3-4). Hence, these experiments need to be repeated and expanded upon using the *Cacna2d1* conditional knockout mouse tissue (72), an alternative and knockout-verified anti- $\text{Ca}_v\alpha 2\delta 1$ antibody, and greater input of membrane fractions isolated from embryonic mouse forebrains. Alternatively *in vitro* binding assays could be used to verify direct binding of NogoA and $\text{Ca}_v\alpha 2\delta 1$, while determining necessary binding-supportive domains on each protein. Lastly, ultrastructure studies could be employed to determine whether or not NogoA directly binds $\text{Ca}_v\alpha 2\delta 1$ at the same spot as gabapentin and thrombospondins (39).

Secondly, we would like to get a deeper understanding of why and how shNogoA transduction relays a robust regulation of synaptically relevant mRNA and miRNA expression. To test if these NogoA-independent, off-target effects depend on proper miRNA synthesis and processing machinery, we suggest that future studies employ *Dgcr8* (73-77) and *Dicer* (78-82) conditional knockout mouse models. Once

synthesized, pri-miRNAs are processed by Drosha/Dgcr8 enzyme complex in the nucleus, exported into the cytoplasm by exportin-5 as pre-miRNAs, processed by Dicer into miRNA complexes, and assembled into RNA-induced silencing complexes (RISCs) by association with argonaute proteins (59). As such, studying the synaptic phenotypes following Cre-mediated deletion of *Dgcr8* or *Dicer* alone or in conjunction with the LV-shNogoA transduction would be extremely informative. By so doing, future studies could elucidate the shNogoA's dependence on proper miRNA processing to relay its off-target effects, especially on excitatory synaptic transmission and inhibitory synaptogenesis.

Along similar lines, we entertained the possibility that shNogoA transduction might be causing observed regulations of synaptic mRNA and miRNA expression through induction of an interferon response. In fact, shRNA overexpression was shown to induce expression of interferon genes in a construct-, promoter-, and dose-dependent manner. Moreover, these observations become relevant to our studies since interferon response was shown to extend to mammalian cells, including neurons. A classic interferon target gene that is robustly upregulated by various RNAi approaches is 2',5'-oligoadenylate synthetase (*Oas1*) (60, 61, 66). Another well-established phenomenon is how introduction of double stranded RNA (dsRNA) or even small interfering RNA (siRNA) induces an interferon response in mammalian cells through activation of dsRNA-dependent protein kinase R (PKR), which could eventually result in global shutdown of protein synthesis (64, 65, 83). Informed by these observations, we checked back our datasets, and found that LV-shNogoA transduction does not significantly upregulate either *Oas1b* or *Oas1c* mRNA expression. Moreover, the gene product encoding for PKR, *eukaryotic translation initiation factor 2-alpha kinase 2* (*Eif2ak2*), also

remained unchanged in all three LV-shNogoA constructs. This at least preliminarily rules out a major contribution of interferon response in manifesting observed synaptic regulations. Curiously enough, however, shNogoA-2pMt-transduced neurons displayed elevated levels of *Oas1b* mRNA, while transduction with either LV-shNogoA-2pMt or LV-shNogoA-5pMt was sufficient to induce a robust upregulation of *Oas1c* mRNA. Given how shNogoA-2pMt and shNogoA-5pMt produced *de novo* synaptic phenotypes and greatly diverged from shNogoA as revealed by PCA of both mRNA and miRNA transcriptomes, we suspect that a neuronal interferon response might at least be partially responsible. Hence, future investigations should employ manipulations to bidirectionally regulate the interferon target gene expression to either accentuate or alleviate the off-target effects seen with the original and step-wise mutated versions of the shNogoA construct.

We demonstrated that the synaptic phenotypes observed upon shNogoA transductions were independent of NogoA expression (Figures 3-7, 3-8, 3-9). Although we might be able to identify the molecular targets and mechanisms through which synapse formation and strength are regulated, the question of how NogoA or NgR1 function neutralization alleviates the negative regulation on activity-dependent synaptic plasticity remains elusive (2, 3, 84-86). Even though multiple constructs of RNAi-mediated NogoA-specific knockdown exist in the literature (1, 32, 87-89), we propose that future studies employ an alternative route of acute depletion, and avoid off-target effects of shRNAs (58, 70), deceptive scrambled controls, and ectopic overexpression of rescue experiments (44). One such example would be the CRISPR-Cas9-mediated excision of *NogoA*, using single guide RNAs (sgRNAs) targeting NogoA-specific exon 3.

We empirically learned that algorithmic predictions of sgRNA target efficiency do not always match reality. However, future investigations could verify successful *NogoA* excision by testing the efficiency of multiple sgRNA transductions of primary neurons prepared from the same constitutively active *CRISPR-Cas9* knock-in mouse forebrain (90). This would also enable testing of cell-autonomy and *NogoA*-dependence of observed phenotypes in sparsely transfected neurons.

Last but not least, we propose that future studies study the *NogoA*'s negative regulation on activity-dependent synaptic plasticity by driving acute and cell-type specific *NogoA* depletion in *NogoA* (91, 92) or *NogoABC* (41) conditional knockout mouse models. As we demonstrated (Figure 3-8), LV-Cre transduction of primary forebrain neurons prepared from *NogoABC^{fl/fl}* mouse will deplete majority of *NogoA/B* protein expression. Next-generation RNA sequencing experiments with acute *NogoA* or *NogoABC* deletion would help elucidate the *NogoA*-dependent changes in gene expression in an unbiased and stringent manner. These experiments could also be complemented by co-transduction of the sh*NogoA*, in an attempt to identify the *NogoA*-independent changes in neuronal transcriptome with more certainty than point mutations within the seed region of the sh*NogoA* (Figure 3-9). Collectively, these experiments have the potential of describing *NogoA*'s physiological function in forebrain neurons as well as higher up mechanisms regulating synapse formation and strength.

4.4 Concluding Remarks

The work communicated in this dissertation advances the field by characterizing neuronal and glial NogoA expression patterns, identifying neuronal NogoA as a novel phospho-protein, and demonstrating activity-dependent regulation of NogoA in rodent forebrain neurons. Our consolidatory efforts revealed lack of single target specificity of a previously published shRNA initially directed against NogoA (1). More importantly, our work transcends the audiences of myelin-associated inhibitors, CNS regeneration, or synaptic plasticity, and advises devoted caution when employing models of RNA interference as an approach to knock down targeted gene expression. We hope the scientific rigor and transparency shown in our studies will serve not to deter or discourage passionate and curious scientists, but to encourage and motivate them to carefully validate their tools early on in their studies.

4.5 References

1. M. Zagrebelsky, R. Schweigreiter, C. E. Bandtlow, M. E. Schwab, M. Korte, Nogo-A stabilizes the architecture of hippocampal neurons. *The Journal of neuroscience : the official journal of the Society for Neuroscience* **30**, 13220-13234 (2010).
2. A. Delekate, M. Zagrebelsky, S. Kramer, M. E. Schwab, M. Korte, NogoA restricts synaptic plasticity in the adult hippocampus on a fast time scale. *Proceedings of the National Academy of Sciences* **108**, 2569-2574 (2011).
3. A. Zemmar *et al.*, Neutralization of Nogo-A Enhances Synaptic Plasticity in the Rodent Motor Cortex and Improves Motor Learning in Vivo. *The Journal of Neuroscience* **34**, 8685-8698 (2014).
4. S. J. Raiker *et al.*, Oligodendrocyte-Myelin Glycoprotein and Nogo Negatively Regulate Activity-Dependent Synaptic Plasticity. *The Journal of Neuroscience* **30**, 12432-12445 (2010).
5. S. Fricke *et al.*, Fast Regulation of GABAAR Diffusion Dynamics by Nogo-A Signaling. *Cell Reports* **29**, 671-684.e676 (2019).
6. Y. Lin *et al.*, Activity-dependent regulation of inhibitory synapse development by Npas4. *Nature* **455**, 1198 (2008).
7. G. G. Turrigiano, K. R. Leslie, N. S. Desai, L. C. Rutherford, S. B. Nelson, Activity-dependent scaling of quantal amplitude in neocortical neurons. *Nature* **391**, 892-896 (1998).
8. Graham H. Diering, Ahleah S. Gustina, Richard L. Huganir, PKA-GluA1 Coupling via AKAP5 Controls AMPA Receptor Phosphorylation and Cell-Surface Targeting during Bidirectional Homeostatic Plasticity. *Neuron* **84**, 790-805 (2014).
9. M. C. Ashby, S. R. Maier, A. Nishimune, J. M. Henley, Lateral diffusion drives constitutive exchange of AMPA receptors at dendritic spines and is regulated by spine morphology. *The Journal of neuroscience : the official journal of the Society for Neuroscience* **26**, 7046-7055 (2006).
10. A. E. Fournier, T. GrandPre, S. M. Strittmatter, Identification of a receptor mediating Nogo-66 inhibition of axonal regeneration. *Nature* **409**, 341-346 (2001).
11. H. Lee *et al.*, Synaptic function for the Nogo-66 receptor NgR1: regulation of dendritic spine morphology and activity-dependent synaptic strength. *The Journal of neuroscience : the official journal of the Society for Neuroscience* **28**, 2753-2765 (2008).

12. J. K. Atwal *et al.*, PirB is a Functional Receptor for Myelin Inhibitors of Axonal Regeneration. *Science* **322**, 967-970 (2008).
13. A. Joset, D. A. Dodd, S. Halegoua, M. E. Schwab, Pincher-generated Nogo-A endosomes mediate growth cone collapse and retrograde signaling. *The Journal of cell biology* **188**, 271-285 (2010).
14. A. Barria, D. Muller, V. Derkach, L. C. Griffith, T. R. Soderling, Regulatory Phosphorylation of AMPA-Type Glutamate Receptors by CaM-KII During Long-Term Potentiation. *Science* **276**, 2042-2045 (1997).
15. A. Barria, V. Derkach, T. Soderling, Identification of the Ca²⁺/Calmodulin-dependent Protein Kinase II Regulatory Phosphorylation Site in the α -Amino-3-hydroxyl-5-methyl-4-isoxazole-propionate-type Glutamate Receptor. *Journal of Biological Chemistry* **272**, 32727-32730 (1997).
16. A. L. Mammen, K. Kameyama, K. W. Roche, R. L. Huganir, Phosphorylation of the α -Amino-3-hydroxy-5-methylisoxazole-4-propionic Acid Receptor GluR1 Subunit by Calcium/ Calmodulin-dependent Kinase II. *Journal of Biological Chemistry* **272**, 32528-32533 (1997).
17. J. Boehm *et al.*, Synaptic Incorporation of AMPA Receptors during LTP Is Controlled by a PKC Phosphorylation Site on GluR1. *Neuron* **51**, 213-225 (2006).
18. I. M. Mansuy, S. Shenolikar, Protein serine/threonine phosphatases in neuronal plasticity and disorders of learning and memory. *Trends Neurosci* **29**, 679-686 (2006).
19. H.-K. Lee, Synaptic plasticity and phosphorylation. *Pharmacology & Therapeutics* **112**, 810-832 (2006).
20. T. Saneyoshi *et al.*, Activity-Dependent Synaptogenesis: Regulation by a CaM-Kinase Kinase/CaM-Kinase I/ β PIX Signaling Complex. *Neuron* **57**, 94-107 (2008).
21. W. Lu, K. W. Roche, Posttranslational regulation of AMPA receptor trafficking and function. *Current Opinion in Neurobiology* **22**, 470-479 (2012).
22. J. Lisman, R. Yasuda, S. Raghavachari, Mechanisms of CaMKII action in long-term potentiation. *Nat Rev Neurosci* **13**, 169-182 (2012).
23. T. E. Chater, Y. Goda, The role of AMPA receptors in postsynaptic mechanisms of synaptic plasticity. *Frontiers in Cellular Neuroscience* **8**, (2014).
24. G. H. Diering *et al.*, Homer1a drives homeostatic scaling-down of excitatory synapses during sleep. *Science* **355**, 511-515 (2017).

25. G. H. Diering, R. L. Huganir, The AMPA Receptor Code of Synaptic Plasticity. *Neuron* **100**, 314-329 (2018).
26. F. K. Stephan, Circadian rhythms in the rat: constant darkness, entrainment to T cycles and to skeleton photoperiods. *Physiology & behavior* **30**, 451-462 (1983).
27. B. Niederost, T. Oertle, J. Fritsche, R. A. McKinney, C. E. Bandtlow, Nogo-A and myelin-associated glycoprotein mediate neurite growth inhibition by antagonistic regulation of RhoA and Rac1. *The Journal of neuroscience : the official journal of the Society for Neuroscience* **22**, 10368-10376 (2002).
28. K. Ramamoorthi *et al.*, Npas4 regulates a transcriptional program in CA3 required for contextual memory formation. *Science* **334**, 1669-1675 (2011).
29. B. L. Bloodgood, N. Sharma, H. A. Browne, A. Z. Trepman, M. E. Greenberg, The activity-dependent transcription factor NPAS4 regulates domain-specific inhibition. *Nature* **503**, 121-125 (2013).
30. I. Spiegel *et al.*, Npas4 Regulates Excitatory-Inhibitory Balance within Neural Circuits through Cell-Type-Specific Gene Programs. *Cell* **157**, 1216-1229 (2014).
31. W. Shan *et al.*, Neuronal PAS domain protein 4 (Npas4) controls neuronal homeostasis in pentylenetetrazole-induced epilepsy through the induction of Homer1a. *Journal of Neurochemistry* **145**, 19-33 (2018).
32. X. Peng, J. Kim, Z. Zhou, D. J. Fink, M. Mata, Neuronal Nogo-A regulates glutamate receptor subunit expression in hippocampal neurons. *Journal of Neurochemistry* **119**, 1183-1193 (2011).
33. P. Tsokas *et al.*, Local protein synthesis mediates a rapid increase in dendritic elongation factor 1A after induction of late long-term potentiation. *The Journal of neuroscience : the official journal of the Society for Neuroscience* **25**, 5833-5843 (2005).
34. B. E. Pfeiffer, K. M. Huber, Current Advances in Local Protein Synthesis and Synaptic Plasticity. *The Journal of Neuroscience* **26**, 7147-7150 (2006).
35. M. A. Sutton *et al.*, Miniature Neurotransmission Stabilizes Synaptic Function via Tonic Suppression of Local Dendritic Protein Synthesis. *Cell* **125**, 785-799 (2006).
36. M. A. Sutton, E. M. Schuman, Dendritic Protein Synthesis, Synaptic Plasticity, and Memory. *Cell* **127**, 49-58 (2006).
37. A. C. Dolphin, Calcium channel auxiliary $\alpha 2\delta$ and β subunits: trafficking and one step beyond. *Nature Reviews Neuroscience* **13**, 542-555 (2012).

38. M. Campiglio, B. E. Flucher, The role of auxiliary subunits for the functional diversity of voltage-gated calcium channels. *J Cell Physiol* **230**, 2019-2031 (2015).
39. Ç. Eroglu *et al.*, Gabapentin Receptor $\alpha 2\delta$ -1 Is a Neuronal Thrombospondin Receptor Responsible for Excitatory CNS Synaptogenesis. *Cell* **139**, 380-392 (2009).
40. C. Eroglu, The role of astrocyte-secreted matricellular proteins in central nervous system development and function. *Journal of Cell Communication and Signaling* **3**, 167-176 (2009).
41. J. M. Meves, C. G. Geoffroy, N. D. Kim, J. J. Kim, B. Zheng, Oligodendrocytic but not neuronal Nogo restricts corticospinal axon sprouting after CNS injury. *Experimental Neurology* **309**, 32-43 (2018).
42. G. G. Turrigiano, S. B. Nelson, Homeostatic plasticity in the developing nervous system. *Nat Rev Neurosci* **5**, 97-107 (2004).
43. J. Barral, A. D. Reyes, Synaptic scaling rule preserves excitatory–inhibitory balance and salient neuronal network dynamics. *Nature Neuroscience* **19**, 1690-1696 (2016).
44. T. C. Südhof, Towards an Understanding of Synapse Formation. *Neuron* **100**, 276-293 (2018).
45. L. He, G. J. Hannon, MicroRNAs: small RNAs with a big role in gene regulation. *Nature Reviews Genetics* **5**, 522-531 (2004).
46. L. P. Lim *et al.*, Microarray analysis shows that some microRNAs downregulate large numbers of target mRNAs. *Nature* **433**, 769-773 (2005).
47. M. J. Kye *et al.*, Somatodendritic microRNAs identified by laser capture and multiplex RT-PCR. *RNA (New York, N.Y.)* **13**, 1224-1234 (2007).
48. D. P. Bartel, MicroRNAs: target recognition and regulatory functions. *Cell* **136**, 215-233 (2009).
49. G. Schratt, microRNAs at the synapse. *Nat Rev Neurosci* **10**, 842-849 (2009).
50. M. van Spronsen *et al.*, Developmental and Activity-Dependent miRNA Expression Profiling in Primary Hippocampal Neuron Cultures. *PLOS ONE* **8**, e74907 (2013).
51. Z. Hu, Z. Li, miRNAs in synapse development and synaptic plasticity. *Current Opinion in Neurobiology* **45**, 24-31 (2017).

52. J. E. Cohen, P. R. Lee, S. Chen, W. Li, R. D. Fields, MicroRNA regulation of homeostatic synaptic plasticity. *Proceedings of the National Academy of Sciences* **108**, 11650-11655 (2011).
53. R. Saba *et al.*, Dopamine-Regulated MicroRNA MiR-181a Controls GluA2 Surface Expression in Hippocampal Neurons. *Molecular and Cellular Biology* **32**, 619-632 (2012).
54. J. Remenyi *et al.*, miR-132/212 Knockout Mice Reveal Roles for These miRNAs in Regulating Cortical Synaptic Transmission and Plasticity. *PLOS ONE* **8**, e62509 (2013).
55. S. Bicker *et al.*, The DEAH-box helicase DHX36 mediates dendritic localization of the neuronal precursor-microRNA-134. *Genes & Development* **27**, 991-996 (2013).
56. G. A. Wayman *et al.*, An activity-regulated microRNA controls dendritic plasticity by down-regulating p250GAP. *Proceedings of the National Academy of Sciences* **105**, 9093-9098 (2008).
57. S. Sambandan *et al.*, Activity-dependent spatially localized miRNA maturation in neuronal dendrites. *Science* **355**, 634-637 (2017).
58. M. A. van Gestel *et al.*, shRNA-induced saturation of the microRNA pathway in the rat brain. *Gene therapy* **21**, 205-211 (2014).
59. H. Matsuyama, H. I. Suzuki, Systems and Synthetic microRNA Biology: From Biogenesis to Disease Pathogenesis. *International Journal of Molecular Sciences* **21**, 132 (2019).
60. C. A. Sledz, M. Holko, M. J. de Veer, R. H. Silverman, B. R. G. Williams, Activation of the interferon system by short-interfering RNAs. *Nature Cell Biology* **5**, 834-839 (2003).
61. A. J. Bridge, S. Pebernard, A. Ducraux, A.-L. Nicoulaz, R. Iggo, Induction of an interferon response by RNAi vectors in mammalian cells. *Nature Genetics* **34**, 263-264 (2003).
62. A. L. Jackson *et al.*, Expression profiling reveals off-target gene regulation by RNAi. *Nature Biotechnology* **21**, 635-637 (2003).
63. D. Grimm *et al.*, Fatality in mice due to oversaturation of cellular microRNA/short hairpin RNA pathways. *Nature* **441**, 537-541 (2006).
64. M. J. Clemens, A. Elia, The Double-Stranded RNA-Dependent Protein Kinase PKR: Structure and Function. *Journal of Interferon & Cytokine Research* **17**, 503-524 (1997).

65. G. R. Stark, I. M. Kerr, B. R. G. Williams, R. H. Silverman, R. D. Schreiber, How Cells Respond to Interferons. *Annual Review of Biochemistry* **67**, 227-264 (1998).
66. S. Pebernard, R. D. Iggo, Determinants of interferon-stimulated gene induction by RNAi vectors. *Differentiation* **72**, 103-111 (2004).
67. R. Yi, B. P. Doehle, Y. Qin, I. G. Macara, B. R. Cullen, Overexpression of exportin 5 enhances RNA interference mediated by short hairpin RNAs and microRNAs. *RNA (New York, N.Y.)* **11**, 220-226 (2005).
68. R. Yi, Y. Qin, I. G. Macara, B. R. Cullen, Exportin-5 mediates the nuclear export of pre-microRNAs and short hairpin RNAs. *Genes & development* **17**, 3011-3016 (2003).
69. V. A. Alvarez, D. A. Ridenour, B. L. Sabatini, Retraction of Synapses and Dendritic Spines Induced by Off-Target Effects of RNA Interference. *The Journal of Neuroscience* **26**, 7820-7825 (2006).
70. Seung T. Baek *et al.*, Off-Target Effect of doublecortin Family shRNA on Neuronal Migration Associated with Endogenous MicroRNA Dysregulation. *Neuron* **82**, 1255-1262 (2014).
71. C. B. Moore, E. H. Guthrie, M. T.-H. Huang, D. J. Taxman, Short hairpin RNA (shRNA): design, delivery, and assessment of gene knockdown. *Methods Mol Biol* **629**, 141-158 (2010).
72. J. Park *et al.*, Central Mechanisms Mediating Thrombospondin-4-induced Pain States. *The Journal of biological chemistry* **291**, 13335-13348 (2016).
73. J. Han *et al.*, The Drosha-DGCR8 complex in primary microRNA processing. *Genes & Development* **18**, 3016-3027 (2004).
74. K. Fénelon *et al.*, Deficiency of *Dgcr8*, a gene disrupted by the 22q11.2 microdeletion, results in altered short-term plasticity in the prefrontal cortex. *Proceedings of the National Academy of Sciences* **108**, 4447-4452 (2011).
75. L. R. Earls *et al.*, Age-Dependent MicroRNA Control of Synaptic Plasticity in 22q11 Deletion Syndrome and Schizophrenia. *The Journal of Neuroscience* **32**, 14132-14144 (2012).
76. R. Hsu *et al.*, Loss of microRNAs in pyramidal neurons leads to specific changes in inhibitory synaptic transmission in the prefrontal cortex. *Molecular and Cellular Neuroscience* **50**, 283-292 (2012).
77. P. K. Rao *et al.*, Loss of cardiac microRNA-mediated regulation leads to dilated cardiomyopathy and heart failure. *Circulation research* **105**, 585-594 (2009).

78. E. Bernstein, A. A. Caudy, S. M. Hammond, G. J. Hannon, Role for a bidentate ribonuclease in the initiation step of RNA interference. *Nature* **409**, 363-366 (2001).
79. G. Lugli, J. Larson, M. E. Martone, Y. Jones, N. R. Smalheiser, Dicer and eIF2c are enriched at postsynaptic densities in adult mouse brain and are modified by neuronal activity in a calpain-dependent manner. *J Neurochem* **94**, 896-905 (2005).
80. T. H. Davis *et al.*, Conditional Loss of Dicer Disrupts Cellular and Tissue Morphogenesis in the Cortex and Hippocampus. *The Journal of Neuroscience* **28**, 4322-4330 (2008).
81. A. Fiorenza *et al.*, Blocking miRNA Biogenesis in Adult Forebrain Neurons Enhances Seizure Susceptibility, Fear Memory, and Food Intake by Increasing Neuronal Responsiveness. *Cerebral Cortex* **26**, 1619-1633 (2015).
82. B. D. Harfe, M. T. McManus, J. H. Mansfield, E. Hornstein, C. J. Tabin, The RNaseIII enzyme Dicer is required for morphogenesis but not patterning of the vertebrate limb. *Proc Natl Acad Sci U S A* **102**, 10898-10903 (2005).
83. P. Lingor, U. Michel, U. Schöll, M. Bähr, S. Kügler, Transfection of “naked” siRNA results in endosomal uptake and metabolic impairment in cultured neurons. *Biochemical and Biophysical Research Communications* **315**, 1126-1133 (2004).
84. A. Kempf, M. E. Schwab, Nogo-A Represses Anatomical and Synaptic Plasticity in the Central Nervous System. *Physiology* **28**, 151-163 (2013).
85. A. Kempf *et al.*, The Sphingolipid Receptor S1PR2 Is a Receptor for Nogo-A Repressing Synaptic Plasticity. *PLOS Biology* **12**, e1001763 (2014).
86. S. Jitsuki *et al.*, Nogo Receptor Signaling Restricts Adult Neural Plasticity by Limiting Synaptic AMPA Receptor Delivery. *Cerebral Cortex* **26**, 427-439 (2015).
87. A. D. Pradhan *et al.*, Dendritic spine alterations in neocortical pyramidal neurons following postnatal neuronal Nogo-A knockdown. *Developmental neuroscience* **32**, 313-320 (2010).
88. V. Pernet *et al.*, Neuronal Nogo-A upregulation does not contribute to ER stress-associated apoptosis but participates in the regenerative response in the axotomized adult retina. *Cell death and differentiation* **19**, 1096-1108 (2012).
89. B. Tews *et al.*, Synthetic microRNA-mediated downregulation of Nogo-A in transgenic rats reveals its role as regulator of synaptic plasticity and cognitive function. *Proceedings of the National Academy of Sciences* **110**, 6583-6588 (2013).

90. R. J. Platt *et al.*, CRISPR-Cas9 knockin mice for genome editing and cancer modeling. *Cell* **159**, 440-455 (2014).
91. F. Vajda *et al.*, Cell type-specific Nogo-A gene ablation promotes axonal regeneration in the injured adult optic nerve. *Cell death and differentiation* **22**, 323-335 (2015).
92. A. Zemmar *et al.*, Oligodendrocyte- and Neuron-Specific Nogo-A Restrict Dendritic Branching and Spine Density in the Adult Mouse Motor Cortex. *Cereb Cortex*, 1-9 (2017).